MAPPING RANGELAND VEGETATION

IN

NORTHERN KENYA

FROM

LANDSAT DATA

Being a thesis presented by Geoffrey Hugh Griffiths, in accordance with the regulations governing the award of the degree Doctor of Philosophy of the University of Aston in Birmingham.

May, 1985

MAPPING RANGELAND VEGETATION IN NORTHERN KENYA

FROM LANDSAT DATA

Geoffrey Hugh Griffiths Ph.D. 1985.

SUMMARY

In this thesis the potential usefulness of multispectral imagery and digital data obtained from the Landsat series of Earth resource satellites for monitoring rangeland vegetation resources in a semi-arid region of northern Kenya, is examined.

In the first part of the study the effectiveness of a visual interpretation of Landsat false colour imagery is evaluated by comparing the results obtained, with reference data derived from fieldwork and air photography. Various digital image processing techniques, including multispectral classification, principal components analysis and an index of green vegetation cover, are evaluated in the second part of the study.

Rangeland vegetation could not be mapped successfully from an interpretation of the Landsat false colour imagery due to the sparse nature of the semi-arid vegetation cover and its spectral similarity to bare soil. The results indicated that further progress would only be made by a quantitative analysis of the reflectance of the major spectral components of the semi-arid environment.

A simple model describing the reflectance properties of bare soil, non-green and green vegetation was established. From the improved understanding of the spectral behaviour of rangeland vegetation gained from the model, a vegetation index based upon a linear combination of the visible red (MSS5) and near-infrared (MSS7) Landsat wavebands was developed. The index, which is an orthogonal measure of green vegetation cover, was designed to minimise the effect of variations in soils reflectance, whilst maximising the spectral contrast between bare soil and green vegetation.

The index was applied within the Study Area to monitor the changing distribution of green vegetation cover from Landsat scenes acquired at two different dates. Results showed that the methodology could potentially be used to monitor rangeland vegetation resources in semi-arid regions but that further research will be required to establish the relationship between indices of green vegetation cover derived from Landsat, and rangeland production.

The images resulting from the application of the vegetation index showed that digitally processed Landsat MSS imagery can be used to monitor changes in the productivity of semi-arid vegetation within the Study Area and potentially, within other environmentally similar regions of Africa.

Key Words

Landsat
Remote sensing
Northern Kenya
Rangeland production
Monitoring

ACKNOWLEDGEMENTS

There are many people whom I would like to thank in connection with the preparation of this thesis and without whose help and advice much of this work would not have been possible.

In particular I would like to thank Dr. W.G. Collins of the Remote Sensing Unit, University of Aston, in his capacity of research supervisor, for his continued help and guidance, and Dr. H. Lamprey of the Integrated Project for Arid Lands (IPAL) for his early interest and encouragement in the study.

I would like to thank the members of the Cambridge Northern Kenya Expedition, Miss J.E.M. Corbett and Miss M. Biddle, and numerous IPAL support staff for their assistance during fieldwork in northern Kenya.

For assistance with the preparation of this thesis I would like to thank Hunting Technical Services Limited, and in particular Mr N.G. Schofield, Mr A.J. Lonslow, Mrs D. Godfrey, Miss A Thwaite and Mr G. Knight. Much general advice and assistance was also given by Miss G. Thomas of the Remote Sensing Unit, University of Aston.

I am indebted to the Overseas Development Administration (ODA), The Integrated Project for Arid Lands (IPAL) and the University of Aston for financial support towards the study. Data processing was undertaken at the Natural Environment Research Council (NERC), the National Remote Sensing Centre (NRSC) and Hunting Technical Services Limited (HTS).

Finanlly, I should like to thank my parents for their continued patience and encouragement.

CONTENTS

LIST OF TABLES

LIST OF FIGURES

CHAPTER 1

INTRODUCTION

The background and objectives to the project are presented and the general environmental characteristics of the Study Area are described.

1.1 GENERAL BACKGROUND

In many semi-arid regions of Africa, desertification[1] is destroying the productivity of the rangeland vegetation cover and reducing the capacity of the land to sustain the largely nomadic population. A continuing pattern of low rainfall in the Sudano-Sahel zone following the severe drought of 1968-73 combined with a large increase in livestock numbers is causing widespread overgrazing in many areas and endangering the livelihood of the pastoralists.

The United Nations Conference on Desertification (U.N., 1976), which was convened in Nairobi to discuss the consequences of the Sahel drought and to suggest possible remedies, emphasied the potential role of satellite remote sensing for monitoring the effects of desertification on the general productivity of rangeland vegetation. The Conference recognised that the synoptic and repetitive view of global resources provided by the Landsat series of earth resource satellites, could be used to monitor the condition of rangeland vegetation and thereby provide information for the more efficient management of rangeland vegetation resources.

The first satellite in the series, ERTS 1 (Earth Resources Technology Satellite - renamed Landsat), was launched in July, 1972. Since that date a further four satellites have been launched providing sequential multi-spectral scanner (MSS) data from 1972 to the present. In the early years of the Landsat programme the analysis of the imagery for basic resource mapping was mostly restricted to visual interpretation techniques. With the introduction of digital processing of Landsat data, it has been possible to obtain more detailed and precise information from the data, thus expanding the range of applications for which Landsat data could potentially be used, including rangeland monitoring. In

[1]. Desertification takes many forms, but in general the term is used to describe a severe reduction in the potential of semi-arid land to sustain various forms of agriculture or pastoralism resulting from over-exploitation of the resource base (Rapp, 1978).

agricultural applications however, much of the research effort into the characteristics of Landsat data and the development of new image processing techniques has been undertaken in temperate and humid tropical regions where the vegetation cover is high. At the spatial resolution of Landsat MSS data mapping rangeland vegetation of sparse canopy cover in semi-arid regions from Landsat MSS imagery presents difficult research problems, and until recently this area of research had been neglected.

The objectives of the study therefore, are to develop and evaluate a technique for mapping semi-arid rangeland vegetation resources and for monitoring annual and, if possible seasonal changes in their distribution from Landsat MSS imagery. Rangeland vegetation resources are defined as those characteristics of the vegetation, including species composition, per cent canopy cover and productivity, which are important indicators of rangeland condition.

The approach has been to analyse the reflectance properties of the major spectral components of the semi-arid landscape within a selected Study Area, and to apply the knowledge gained from this analysis to develop a technique for monitoring rangeland vegetation. Although the study has been restricted to the analysis of a relatively small area of northern Kenya, it is anticipated that the results could be applied within other semi-arid regions of Kenya and subsequently in other environmentally similar regions of Africa.

1.2 THE STUDY AREA

The Study Area chosen for the investigation lies within a larger region (23,000 km^2) (Figure 1.1) at present being studied by the Integrated Project for Arid Lands (IPAL), whose research is aimed at; "finding direct solutions to the most urgent environmental problems associated with desert encroachment and ecological degradation of arid lands" (Lamprey, 1978).

More than six years of field work and data analysis have been undertaken in northern Kenya by IPAL research staff within the framework of the Kenyan contribution to the Man and Biosphere Programme (MAB) with support from UNEP (United Nations Environmental Programme), UNESCO and various governments. Following the submission of an earlier report to IPAL (Griffiths, 1980), which formed the basis of an undergraduate dissertation submitted as part of the Geography Tripos at the University of Cambridge, IPAL agreed that an evaluation of Landsat imagery for mapping vegetation resources in northern Kenya would be a useful contribution to their research programme.

Fieldwork and image analysis has been concentrated within two differently sized

Figure 1.1 **Location of the IPAL Study Area**

study areas of similar environmental type (Figure 1.2):

(a) Hedad subscene (1024 x 1024 Landsat pixels: approximately 6600 km^2)

(b) Kargi subscene (512 x 512[2] Landsat pixels; approximately 1650 km^2)

The purpose of selecting two study areas was do develop a technique for mapping range resources within the smaller area for which detailed soil and vegetation data had been obtained. The effectiveness of the technique could then be evaluated by applying it within the larger Study Area. The Kargi subscene was selected for detailed investigation because it contains a range of vegetation and soil types which are representative of large areas of semi-arid thorn savanna rangeland in Kenya. Additionally the Rendille settlement at Kargi (Figure 1.2) was a suitable base for fieldwork and provided easy access by motorable roads into the surrounding country for field sampling. In the following sections of this chapter the environmental influences, both natural and man-made, which explain the nature and distribution of the vegetation cover within the Study Area are described.

1.3 SOILS AND GEOLOGY

There is little published information about the soils and geology of the area at a scale suitable for a study of this kind. Only a small percentage (11 per cent) of the IPAL study area has been geologically surveyed to date (Dodson, 1963; Randel, 1970). A more extensive survey is at present being undertaken by the British Geological Survey (BGS). Two major rock types dominate the area; Pleistocene flood basalts associated with the tectonic activity of the Kenya Rift Valley, and alluvial Quarternary sediments derived from Precambrian gneissic basement rocks.

These two lithologies are clearly visible on the single channel MSS 5 Landsat scene illustrated in Figure 1.3. The dark flood basalts from Kulal (2335 m) in the west and Marsabit (1865 m) in the east, contrast sharply with the bright sandy-loam sediments which lie at a much lower elevation (700 m) within an extensive basin. The two study areas are located almost entirely within this sedimentary basin.

1.4 CLIMATE

There exists a close link between mean annual rainfall and average range production which determines the livestock carrying capacity of the rangeland. Le Houerou and Hoste (1977) estimate that in the Sudano-Sahel Zone each millimetre of rainfall produces 1 kg ha^{-1}

(2) The picture resolution of a standard image analysis monitor.

Figure 1.2 **Location of Subscenes within the IPAL Study Area**

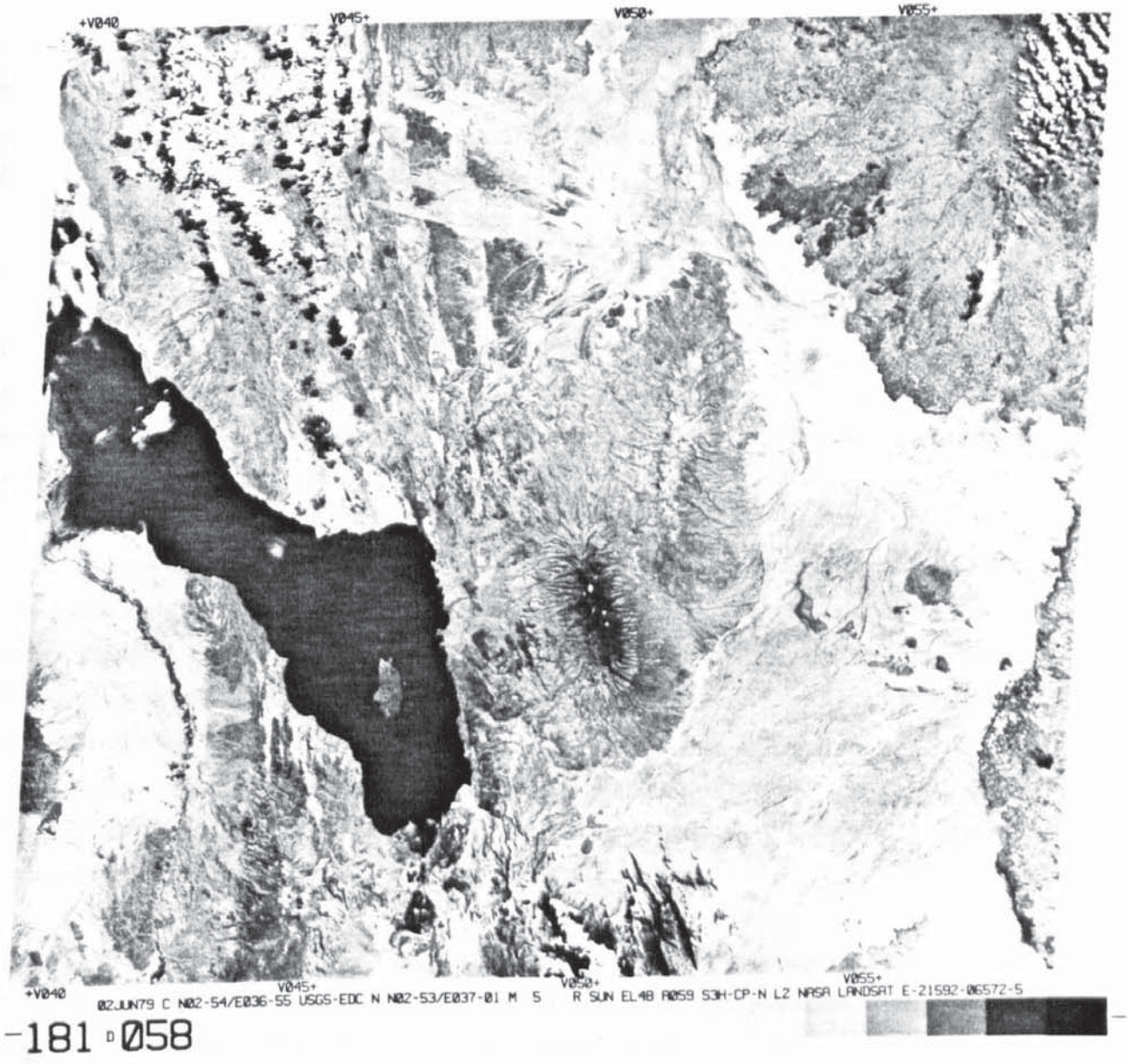

Figure 1.3 A single waveband MSS5 Landsat scene of the IPAL Study Area, Marsabit District (Path 181/Row 058, June 1979). Flood basalts appear in dark tones and basin sediments in light tones.

of consumable (herbaceous) dry matter. Human livestock husbandry is thus highly dependent on climate conditions and, in a region where drought is a frequent occurrence, animal husbandry is particularly influenced by rainfall variability.

Studies of rangeland productivity therefore require detailed climatic data but, until the establishment of IPAL in 1976 only three rain gauges were in operation within the region and rainfall records prior to 1976 are few. Since 1976 IPAL have operated twenty four monthly-read storage rain gauges and twelve daily-read gauges, a number of which are within or close to the Hedad study area. The mean monthly rainfall for North Horr is given in Figure 1.4 (a), and shows that annual rainfall is low (200 mm/annum) and bimodal, with peaks in April and November (Edwards et al., 1979). Annual rainfall amounts are also highly variable and Figure 1.4 (b) shows the deviation in annual rainfall totals from the mean between 1959 - 1981 at North Horr. The severe drought between 1970 - 76 and the exceptionally wet years from 1977 - 79 are clearly visible from the histogram. During this severe drought six years had less rainfall than the mean, and in four of those years, rainfall was less than 50 per cent of the mean with an extreme deficit in 1973 with only 5 per cent of the mean being recorded (Edwards et al., 1979).

This extreme variability in mean annual rainfall is a characteristic of the Sudano-Sahel zone and appears to be related to fluctuations in the latitudinal position of the Intercontinental Tropical Convergance Zone (ITCZ) and associated weather zones (Musk, 1983). In northern Kenya during exceptional years (1977), the equatorial low-pressure trough associated with the ITCZ may be displaced northwards and rain may occur in the region at any time between Ootober and April. Conversely, during the dry years of the early seventies there was little penetration of the northern equatorial trough into northern Kenya, and severe drought conditions were widespread.

Rainfall totals also vary locally within any one wet season over quite small areas. Detailed data on localised variations in rainfall totals are not available given the small number of rain gauges which IPAL is able to operate, and the short time over which records have been kept. However, some indication of this variability can be gained from the data in Table 1.1. Rainfall data from seven rain-gauges located within or close to the Hedad study area show that totals varied considerably between stations, with the highest mean deviation (94.0) occurring in 1978. Such localised micro-climatic variations in rainfall, which are thought to be related to small scale relief features (M.D. Gwynne, pers. comm.) have profound effects upon the spatial distribution of plant growth during a wet season.

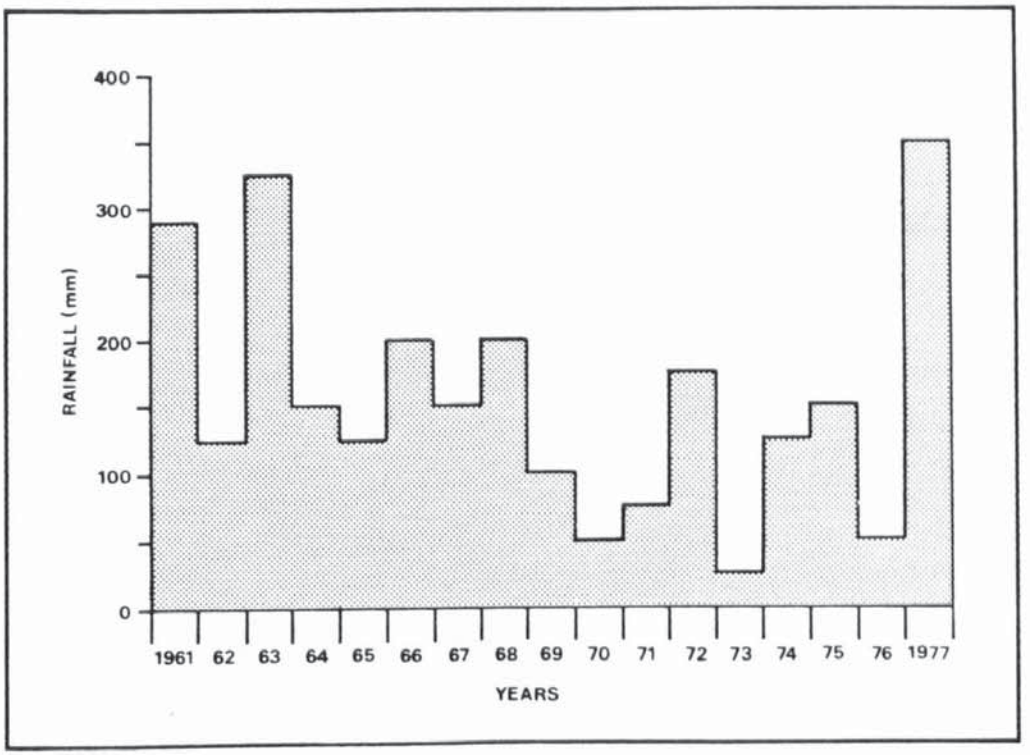

Figure 1.4 (a) Mean Monthly Rainfall for North Horr

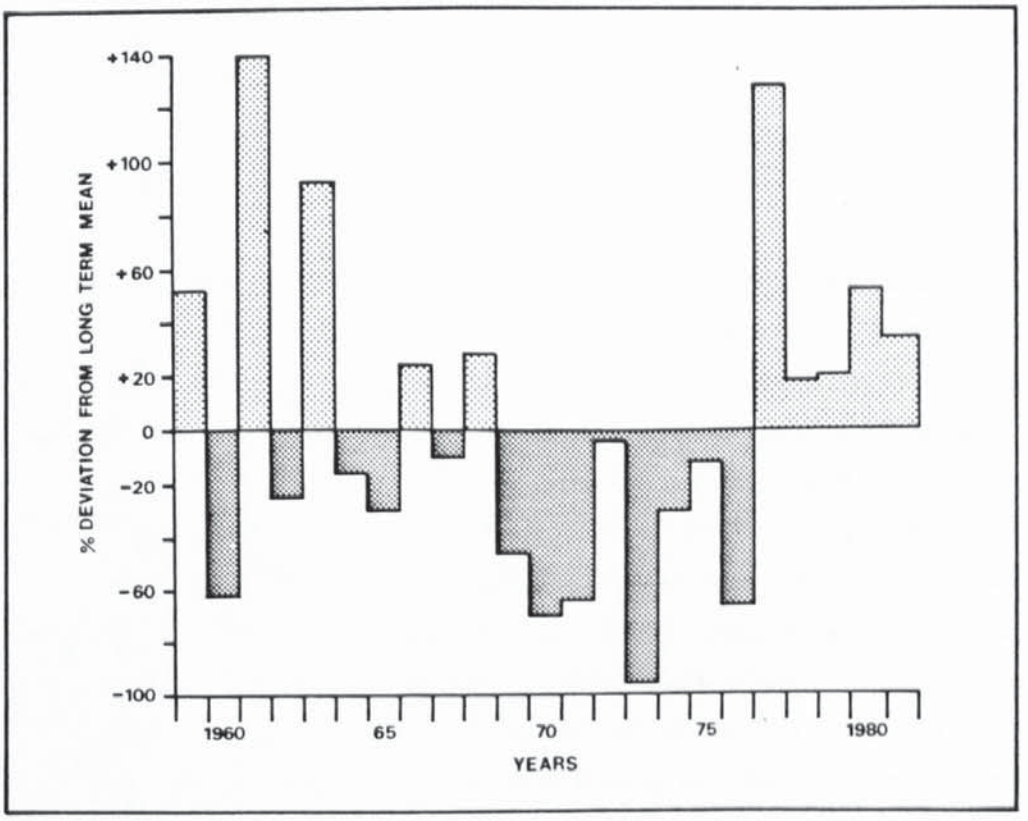

Figure 1.4 (b) The Deviation in Annual Rainfall Totals from the Mean of North Horr (1959-1981)

TABLE 1.1 MEAN ANNUAL RAINFALL (mm) FOR FIVE RAIN GAUGES LOCATED WITHIN THE KARGI AND HEDAD STUDY AREAS

	1977	1978	1979	1980
Kargi	282.3	415.0	254.4	137.2
Kurkum	373.0	404.4	279.0	78.0
Balesa Kulal	350.0	299.7	272.9	172.4
Maikona	352.0	485.9	-	57.2
Falam	355.0	300.0	129.0	187.0
Kalacha	-	388.5	124.5	63.8
North Horr	33.8	95.0	141.8	227.0
Mean	340.5	341.2	200.3	131.8
Mean Deviation	22.6	94.0	70.6	36.1

1.5 DESERTIFICATION

Man-made factors have also had an important effect upon the nature and distribution of the vegetation cover, particularly over the last 15 years. Drought in the early seventies, a doubling of the local Rendille population to 13,000 in 40 years (Lusigi, 1981) and a transition from a largely nomadic to a sedentary lifestyle, has lead to severe desertification at some locations and a general loss of rangeland productivity over more extensive areas.

Traditionally the nomadic Rendille tribe who inhabit much of the Marsabit District of northern Kenya, have been able to travel with their livestock across a very wide area stretching from the Chalbi desert in the north, Lake Turkana in the west, Mount Marsabit in the east, and the Ndoto mountains in the south (Dolan, 1980). This traditional pattern of movement whereby family groups travel across the rangeland in search of good grazing, began to break down during the colonial period and especially following independence in 1963 (Walther and Herlocker, 1980). Settlement became more sedentary as Catholic missions and schools were built, and trading posts ('dukas') became established. With the sinking of wells and the installation of pumps a reliable supply of water further encouraged permanent settlement, particularly at Kargi and Korr which are now important centres of Rendille population. Tribal insecurity due to cattle raiding has also encouraged settlement with the promise of a more secure lifestyle.

The environmental consequences of the concentration of people and their livestock

at Kargi and Korr are twofold and visibly evident. Firstly, woody vegetation has been cut for fuel and to build the stock-proof fence ('boma') surrounding the family habitation ('manyatta'). This has resulted in a dramatic loss of woodland (*Acacia tortilis*) and large shrub (*A. reficiens*) species within a radius of several kilometres from the village centre (Griffiths, 1980). Wood for fuel and building material in the vicinity of Kargi is now extremely scarce. This not only leads to considerable hardship for the local people, but has also created a barren and generally inhospitable landscape at Kargi (Figure 1.5). Secondly, intensive grazing by livestock has denuded the herbaceous cover (grasses and forbs) and dwarf shrub layer, and lead to changes in species composition in favour of unpalatable species such as *Calotropis*. A comparison between Figure 1.6 taken 60 km south west of Kargi and Figure 1.5 which was taken within 1 km of Kargi village centre, illustrates the devastating combined effects of wood removal and overgrazing on the vegetation cover.

1.6 VEGETATION

The rangeland vegetation classification of Gwynne et al., (1966) assigns the Study Area to a semi-desert eco-climatic zone;

> 'Rangeland of low potential, the vegetation being dwarf shrub grassland or a very dry form of bushed grassland, in which *Acacia reficiens* is a characteristic species.'

Herlocker (1979) adapted the classification system in Gwynne et al. (1966) to produce a vegetation map of the IPAL study area at 1:500 000 scale from air photography and field-checking. A part of this map is illustrated in Figure 1.7 and shows the distribution of primary vegetation strata within the Hedad study area. The majority of the vegetation is composed of low (<2 m), *Acacia reficiens* deciduous shrubland with an understorey of dwarf shrub species in some areas. This widespread vegetation type is illustrated in Figure 1.8 and from the air in Figure 1.9, and shows the dry-season, non-green nature and open canopy of the dominant *Acacia reficiens* shrub cover. Large areas of bare soil are visible and annual grasses and dwarf shrubs can also be seen growing between the taller shrubs.

In the north-east section of the Study Area close to the saline soils of the Chalbi desert and in the east on stabilised paleo sand-dunes near Kargi, extensive areas of dominant dwarf shrubland are found (Figure 1.7). This vegetation type survives under extremely dry conditions and is composed of small shrubs not exceeding one metre in height with a herbaceous layer of annual grasses. Much of the type has a scattered to open (<20 per cent canopy cover) overstorey of larger woody plants, mostly shrubs (Figure 1.10). Other, smaller areas of primary vegetation type growing in areas of increased water availability near the base of the Marsabit lava and along the course of the Balesa Kulal 'lugga' (ephemeral

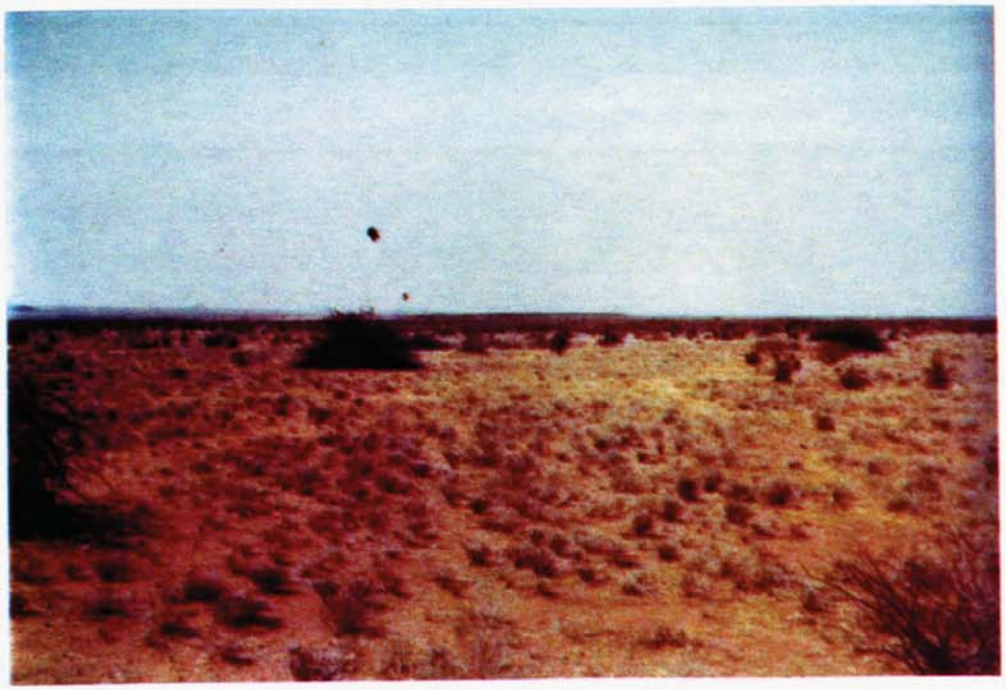

Figure 1.5 Denuded vegetation cover close to the Rendille settlement of Kargi

Figure 1.6 Dense *Acacia* bushland in the Hedad

Figure 1.7 **A Part of the IPAL Vegetation Map (Herlocker, 1979) Covering the Hedad Subscene**

Figure 1.8 *Acacia reficiens* shrub with a ground layer of *Indigofera spinosa* and *Duosperma eromophilum* dwarf shrub on sandy-loam soils

Figure 1.9 An oblique aerial view of the typical *Acacia reficiens* shrub cover found within the study area

Figure 1.10 A sparse cover of *Indigofera spinosa* dwarf shrub associated with *Aristida* spp. annual grassland

Figure 1.11 Mature *Acacia Tortilis* woodland on the Balesa Kulal

TABLE 1.2 DOMINANT SPECIES AND CHARACTERISTICS OF FOUR VEGETATION TYPES FOUND WITHIN THE STUDY AREA

Vegetation class	Dominant species	Characteristics
1. Shrubland	*Acacia reficiens* subsp. *misera* shrub dominant, with *Aristida* spp. annual grassland ground layer. Sometimes associated with dwarf shrub understorey.	Generally open canopy (20-40 per cent) cover of low deciduous shrubs; height <2m.
2. Dwarf Shrub	Dominant or co-dominant *Indigofera spinosa* and *Duosperma eremophilum* with *Aristida* spp. annual grassland ground layer.	Found on drier sites than larger shrub species; sparse cover (<20 per cent); deciduous; height <1 m.
3. Woodland	*Acacia tortilis* dominant with understorey of dwarf shrub.	Tall, mature, mostly deciduous trees found in areas of increased water availability; dense canopy cover; associated with some evergreen species eg. *Salvadora persica*; height 5-15 m.
4. Grassland	*Aristida adscensionis* and *A. mutabilis* dominant with associated herb communities.	Ephemeral, sparse vegetation cover only dominant on shallow, poorly developed, stoney, loam to clay-loam soils. Important ground layer in shrub and dwarf shrub communities.

river), are classified as mature *Acacia* woodland (Figure 1.11). Finally, small areas of annual grassland are found on the less permeable clayey soils on outcrops of flood basalt. The dominant species and important characteristics of these four vegetation types are described in Table 1.2. Further information on the vegetation cover with reference to fieldwork is given in Chapter 3, and a list of commonly occurring species is given in Appendix A.

1.7 THESIS STRUCTURE

In this first chapter the location and evironmental characteristics of the study area have been described. In the second chapter general models of vegetation reflectance are described and their relevance to the present study is assessed. The third chapter describes the collection of field data and the compilation of soil and vegetation maps from air photography. In the fourth chapter Landsat false colour composite imagery is evaluated as a tool for vegetation mapping in semi-arid areas. Reflectance data derived from Landsat computer compatible tapes (CCTs) for different soil and vegetation types within the Study Area are analysed in Chapter 5, prior to the establishment of a model of rangeland reflectance in Chapter 6. This model forms the basis for the development of an effective technique for mapping rangeland vegetation resources and productivity in Chapter 7. The potential benefits and the problems associated with the technique are discussed in the concluding chapter of this thesis, which also includes suggestions for further work.

CHAPTER 2

THE ANALYSIS OF VEGETATION REFLECTANCE

A number of models of vegetation reflectance and analytical techniques for mapping vegetation characteristics from LANDSAT MSS data are described.

2.1 INTRODUCTION

The data obtained by multispectral remote sensors can only be processed and meaningfully interpreted if the fundamental energy-matter interactions at the earth's surface that account for variations in the quality and quantity of the recorded radiation, are fully understood. This chapter presents a number of models that describe the interaction of incident light with vegetation, and attempts to show how these models have formed the basis for the development of various analytical techniques. Emphasis is given to theoretical developments in multispectral remote sensing of vegetation quantity as the basis for measuring the productivity of rangeland vegetation.

2.2 MODELS OF VEGETATION REFLECTANCE

Reflectance is an integrated response from various live and dead plant structures, shadow and soil background components. The contribution of each of these components to the total measured reflectance is a function of their individual reflectances and ground area. An important consideration in the remote sensing of vegetation is to determine the spectral contribution of each cover component to the total composite reflectance. In this way subtle differences in reflectance can be related to causative effects such as variations in vegetation species composition and other non-vegetative factors, particularly soil reflectance. Both theoretical and empirical models have been developed that attempt to predict the transmission, absorption and reflectance properties of the individual components of a canopy, in order to identify those variables which are important determinants of reflectance.

The most important of these models are reviewed by Gates et al. (1965), Allen and Richardson (1968), Gates (1970), Knipling (1970), Gausman et al. (1976), Deering (1978) and Curran (1980). A number of workers (Woolley, 1971, Gausman, 1977) have concentrated upon modelling the spectral properties of a single green leaf. Other workers (Smith and Oliver, 1972, Suits, 1972 and Colwell, 1974) have attempted to model the more complex situation of a closed vegetation canopy in order to understand the effect of

variations in plant canopy geometry, live and dead vegetation amount, soil reflectance, and the geometry of sun and sensor angle to the composite vegetation reflectance.

2.3 SPECTRAL PROPERTIES OF GREEN LEAVES

A typical reflectance curve for a green leaf is given in Figure 2.1 after Swain and Davis (1978). The spectral curve shows the per cent reflectance of the energy incident to the leaf as a function of the wavelength of incident energy over the spectral range 0.4 to 1.1 μm. Only a proportion of the incident energy at any wavelength is reflected from a green leaf, the remainder is either absorbed or transmitted. The amount of reflectance, transmittance and absorption at a given wavelength is affected by the physiological characteristics of the leaf. The very sharp peaks and dips displayed by the green leaf spectral curve in Figure 2.1 are indicative of energy/matter interactions controlled by particular physiological characteristics of the leaf that operate within a narrow wavelength range.

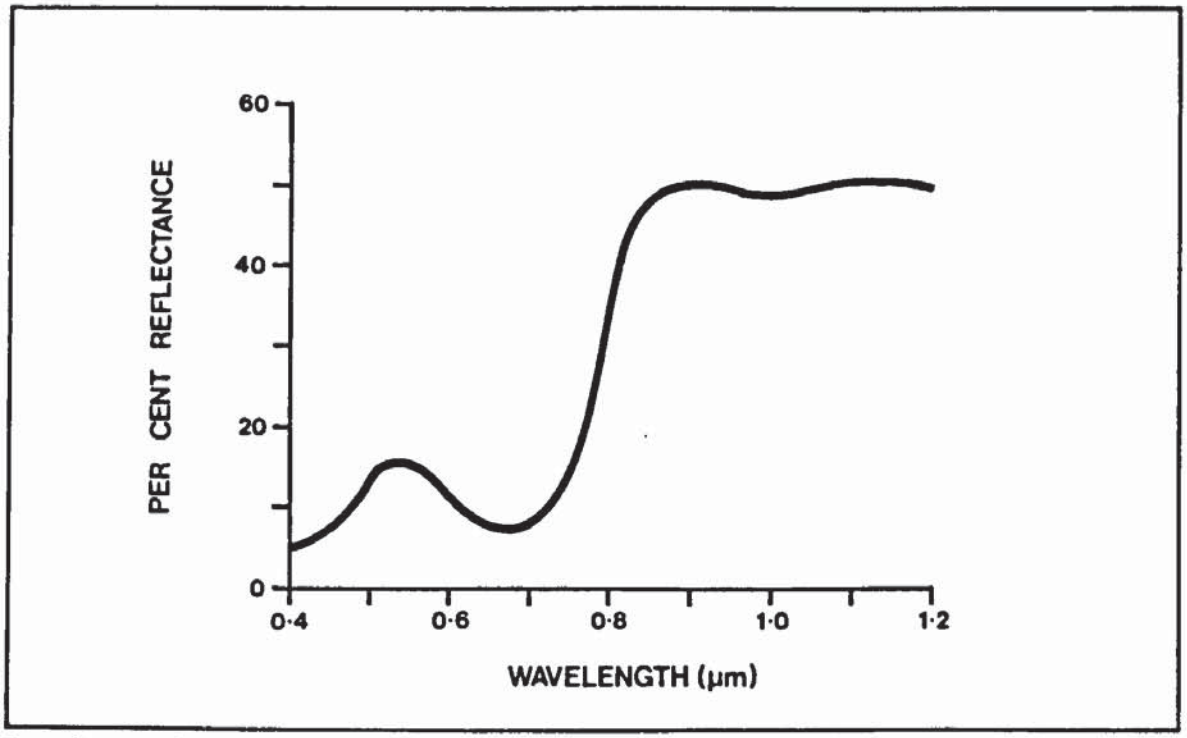

Source: Swain and Davis, 1978

Figure 2.1 Typical Green Leaf Spectral Curve

Visible wavelength light is absorbed by chlorophyll in the outer chloroplast cell walls of the leaf with the strongest absorption in the blue wavelengths (0.47 μm) and a secondary dip in the red (0.68 μm). The remaining near-infrared wavelength light is scattered back through the transparent leaf surface as it undergoes multiple reflection and refraction within

the spongy mesophyll layer, where refractive index differences between air and cell walls occur. Reflectance is reduced when these plant cell-wall air interfaces are eliminated, but usually increases with an increase in the number of intercellular air spaces which occurs with plant maturity and moisture (Gausman, 1977). It is estimated (Knipling, 1970) that between 80-90 per cent of visible light is absorbed by chloroplasts and other pigments and between 40-60 per cent of infrared light is reflected by the spongy mesophyll layer. Thus, as a plant grows and matures the near-infrared reflectance and visible red absorption from the green leaves will increase as the plant takes up water and absorbs light for photosynthesis. The phenological stage of productivity of a green leaf is therefore an important determinant of reflectance (Carneggie and De Gloria, 1973), in addition to canopy cover.

Although this laboratory based research on green leaf reflectance established an understanding of light interaction with single leaves, it was not until researchers began to measure in situ reflectance of vegetation canopies in the field under widely varying environmental conditions that this experimental work could be incorporated into a practical application of satellite and aircraft MSS sensors for the remote sensing of vegetation characteristics.

An analysis of the reflectivity of a vegatation canopy follows in the next section.

2.4 REFLECTIVITY OF VEGETATION CANOPIES

Although the reflectance properties of a single leaf are basic to understanding the reflectivity of a vegetation canopy, there are both qualitative and quantitative differences between the two spectra (Knipling, 1970). Additional factors, including leaf transmittance, the area and geometry of leaves, the characteristics of other components of the canopy e.g. senescent vegetation and plant stalks, and the characteristics of the background, particularly soil reflectance and shadow, must also be considered. Other important factors which influence canopy reflectance are external, and include atmospheric and topographic effects, solar zenith and azimuth angle and sensor look angle. Some of these effects are briefly considered in the following sub-sections:

2.4.1 Reflectance from Multi-Layered Vegetation Canopies

Allen and Richardson (1968) found no difference in the reflectance of visible light from more than one leaf layer, but a dramatic increase in near-infrared reflectance. This is due to the transmission of near-infrared light through separate multiple leaf layers and the subsequent increase in reflectance from each leaf layer in the canopy. With the addition of each leaf layer near-infrared reflectance increases until a stable or asymptotic reflectance is obtained (Gausman et al. 1976; Tucker, 1977). In semi-arid regions similar to the Study

Area where the amount of green vegetation within the canopy is low, the near-infrared asymptote is unlikely to be reached.

2.4.2 Reflectance of Substrate

Substrate is generally composed of soil, plant litter and shadow. In semi-arid regions where green leaf cover is low the effect of soil, shadow, senescent vegetation and non-foliage surfaces on composite reflectance is more pronounced than for regions where green leaf cover is high.

Colwell (1974) showed that if the reflectance of the soil is similar to the reflectance of vegetation in a particular waveband then the relationship between reflectance and vegetation amount will be weak in that waveband. Thus Colwell (1974) found that the red reflectance of a grass canopy had a high negative correlation with per cent vegetation cover for a grass canopy on a light-toned soil background, but was virtually insensitive to changes in per cent canopy cover for a grass canopy on a dark-toned soil background. Conversely, since near-infrared reflectance from vegetation is considerably greater than reflectance from the soil background, there is generally a positive correlation between vegetation amount and near-infrared reflectance making this wavelength particularly suitable for monitoring vegetation amount. However, on a light coloured soil with strong near-infrared reflectance, the relationship between near-infrared reflectance and vegetation amount is less than on a dark soil with a low near-infrared reflectance. This can be a problem in semi-arid regions where near-infrared refletance from the soil is frequently higher than from the vegetation cover.

The amount of shadow in a canopy is a function of the per cent cover of vegetation, sun angle and sensor look angle. As the per cent cover of vegetation increases the area of soil shaded by plant material also increases, thus reducing composite reflectance. A dense thicket composed of semi-arid shrub species is likely to have a higher shadow component and lower reflectance than an open canopy of the same shrub species.

The effect of shadow on reflectance does not operate equally in all wavebands as shadow is darker in the visible wavelengths where most of the incident light is absorbed by leaf layers, and lighter in the near-infrared wavelengths where incident light is transmitted through leaves (Colwell, 1974). In fact Vinogradov (1969) found a negative correlation between reflectance and per cent vegetation cover for grasses in the visible spectral region, which he attributed to an increasing amount of shadow in the canopy as the per cent vegetation cover increased.

At some sun angles the amount of the shadow in the canopy significantly increases.

Graetz and Gentle (1982) used simulated reflectance data to show that as the solar elevation decreased from 50° to 20° between summer and winter for semi-arid shrubland in Central Australia, the percentage of the soil covered by shadow increased from 10 to 45 per cent. In northern Kenya, which is only 2°N of the equator, the range of solar elevations is smaller than for higher latitudes, and seasonal fluctuations in the shadow component will be correspondingly smaller.

The amount of plant litter viewed by the sensor is higher for a canopy of low vegetation cover than for a canopy of high vegetation cover. Otterman and Fraser (1976) found that in the Negev desert it was the character of the surface in the interstices between live plants which controlled the reflectance. The Negev desert was found to be darker than the overgrazed Sinai desert in all Landsat wavebands due to the presence of dead plant material which was masking and therefore reducing an otherwise very bright soil reflectance from the ungrazed Negev. Otterman's results suggest that plant litter is an important contribution to composite reflectance in semi-arid regions.

2.4.3 Reflectance from Senescent and Non-foliage Vegetation

In semi-arid areas the amount of non-foliage vegetation visible to a sensor is much higher than for areas of high canopy cover, particularly during the dry season.

As vegetation senesces the near-infrared reflectance does not significantly decrease (Woolley, 1971) but the breakdown of pigments causes a rise in the visible blue and red reflectance. There is therefore a positive relationship between non-green vegetation amount and reflectance in all wavelengths. This means that in areas of mixed green and non-green vegetation cover it is difficult to discriminate between the live and sensescent or non-foliar components of the cover in only one Landsat waveband.

Despite the complexity of the relationship between the characteristics of a green vegetation canopy and reflectance, Tucker (1978) and others have shown that the basic relationships between the physiological properties of a single leaf reflectance in the near-infrared and visible wavelengths are also valid for the more complex case of a full vegetation canopy. Tucker (1976, 1978) regressed narrow bandwidths in the 0.35 to 1.00 μm spectral range against canopy cover variables, including wet total biomass, dry total biomass, leaf water and chlorophyll content. This statistical analysis identified five specific regions of the spectrum where different biological and physical properties of green vegetation result in different relationships between canopy reflectance and the amount of vegetation present.

The various models which have been established to explain the interaction of incident

visible and near-infrared light within a vegetation canopy, have formed the basis for the development of analytical techniques designed to measure the characteristics of the vegetation cover. Results from these techniques indicate that multispectral reflectance data can be used to measure the amount of vigorously growing, green vegetation within a canopy.

The most important of these analytical techniques are reviewed in the final section of this chapter, and their relevance to the present study is assessed.

2.5 ANALYTICAL TECHNIQUES FOR MEASURING VEGETATION CHARACTERISTICS FROM LANDSAT MSS DATA

Since the mid 1970s powerful computer-based image analysis systems have been widely used for the manipulation and display of digital multispectral data. The use of specialised computer hardware has enabled the very large volumes of data generated by multispectral scanners to be rapidly processed and displayed. Concurrently with the introduction of digital image analysis systems, advanced statistical techniques have been applied to remotely sensed data for performing tasks such as radiometric and geometric corrections, contrast enhancement, multispectral classification and principal components analysis. Such techniques, some of which are described in the following paragraphs have greatly improved the interpretability of MSS image data thus expanding the range of potential applications.

2.5.1 Multispectral Classification

The principles governing the computer-assisted classification of multispectral image data are well reviewed in the literature (Gonzalez and Wintz, 1977; Pratt, 1977; Swain and Davis, 1978; Lillesand and Kiefer, 1979). There are a number of different classification procedures, including cluster analysis, minimum distance to means, parallelpiped and maximum likelihood. Each of these has advantages and disadvantages in terms of computational speed and final accuracy. Only the maximum likelihood classifier was used in the classification of image data in this study, for the reasons given below.

During classification the interpreter visually examines an enhanced false colour display of a Landsat scene and selects training areas which appear to include most of the range of spectral tones displayed on the image. The pixels contained within each training area define the probability density function or 'pattern' which will be used to classify all unknown pixels within the scene. The probability density function for a specified number of wavebands is calculated from the covariance matrix of the training statistics and delineates ellipsoid equiprobability contours in the feature space. Thus, unlike the less

sophisticated minimum distance to means and parallelpiped classifiers, the maximum likelihood algorithm is sensitive to category variance such that the density function for each class more closely approximates the shape of the data cluster in the feature space.

The final classification is strongly influenced by the spectral properties of the training areas selected by the interpreter. In semi-arid regions where differences in ground cover are spatially variable, it is often difficult to delineate training areas of homogeneous spectral response representing distinct land cover classes in the feature space. This may lead to misclassification between different land cover types and a reduced overall classification accuracy. The final result can also be influenced by a technique called 'thresholding'. The standard deviation associated with each probability density function determines the probability of including an unknown pixel within a particular class or placing it in a reject class. By setting the standard deviation at a specified threshold, the probability of assigning a pixel to a particular class can be modified until a satisfactory classification is achieved.

Once the training statistics for the classification have been calculated for selected training areas, the statistics can be used to produce a computer assisted thematic map of land cover classes within a whole Landsat scene. The results from a supervised maximum likelihood classification of the Study Area are presented and analysed in Chapter 7.

2.5.2 Multi-Dimensional Vegetation Indices

Numerous vegetation indices have been used to make quantitative estimates of leaf area index, per cent ground cover, plant height, plant biomass, plant population and other parameters. Most formulae are based on ratios or linear combinations of Landsat wavebands, and exploit differences in the reflectance properties of green vegetation and soils.

Principal components analysis has been widely used in multispectral remote sensing, principally because of its data compression and decorrelation properties. A principal components transform consists of a linear transform of N original variables (wavebands) to N new variables (principal components), where each new variable is a linear combination of the old.

The process is performed in such a fashion that each new variable accounts for, successively, as much of the total remaining variance in the original data-set as possible. When N new variable (principal components) have been computed, all of the original variance will be accounted for.

Starting from a variance/covariance matrix of the original data-set, eigenvalues and

eigenvectors are computed. An eigenvalue is a measure of the amplitude of a component, and an eigenvector is a direction cosine which signifies the angle which each component in N dimensional space subtends with the original, untransformed axes. Hence a principal components transform is equivalent to a rotation of spectral axes, with each orthogonal component accounting for successively less variance within the original data-set. Figure 2.2 shows that the orientation of the first principal component containing most of the variance in the data-set, coincides with the main axis of an elliptical cluster. The second component at right angles to the first, coincides with the second major axis of the ellipse and accounts for correspondingly less of the variance in the original data-set. In Landsat data space it is generally found that the first two components (PC_1 and PC_2) account for more than 90 per cent of the variance in the data-set, whilst the third and fourth components (PC_3 and PC_4) contain very little further information which is not already expressed in PC_1 and PC_2. By decorrelating the data in this way the original, four dimensional data space is reduced to only two dimensions, thus effecting a remarkable compression of the data. Figure 2.2 shows that the box surrounding the original data-set (a) needs to be much larger than the box required to enclose the transformed data (b).

Each principal component corresponds to a principal component image which can potentially be related to a particular land cover type. The first component is generally found to correspond to soil brightness, whilst the second component, orthogonal to the first, corresponds to vegetation greenness. In semi-arid regions of sparse vegetation cover a principal components transformation can be used to separate a green vegetation response from background soil reflectance. In Figure 2.2 (b) the reflectance of green vegetation and soil is plotted in principal components transformed space. Line AB represents the first principal component of maximum variance which corresponds to a mean soil line. Line OD, orthogonal to the first component, represents the second component which in this case corresponds to a 'green vegetation line'. Equal divisions of this line are a measure of green vegetation cover.

A principal components transform is completely determined by the choice of the sample set on which the covariance matrix will be computed (Mulder and Donker, 1976). The amplitude and orientation of the components are purely a function of the spectral properties of the image data. Thus, while principal components analysis can provide insight into the dimensionality of data with more than two dimensions, it may fail to define the actual planes into which the data are dispersed (Crist and Cicone, 1984). In Figure 2.3 data are distributed into two perpendicular planes. The three principal components of the distribution shown on the figure do not provide definiton of those planes; the first component is parallel to the line of intersection of the two planes, the second forms a right

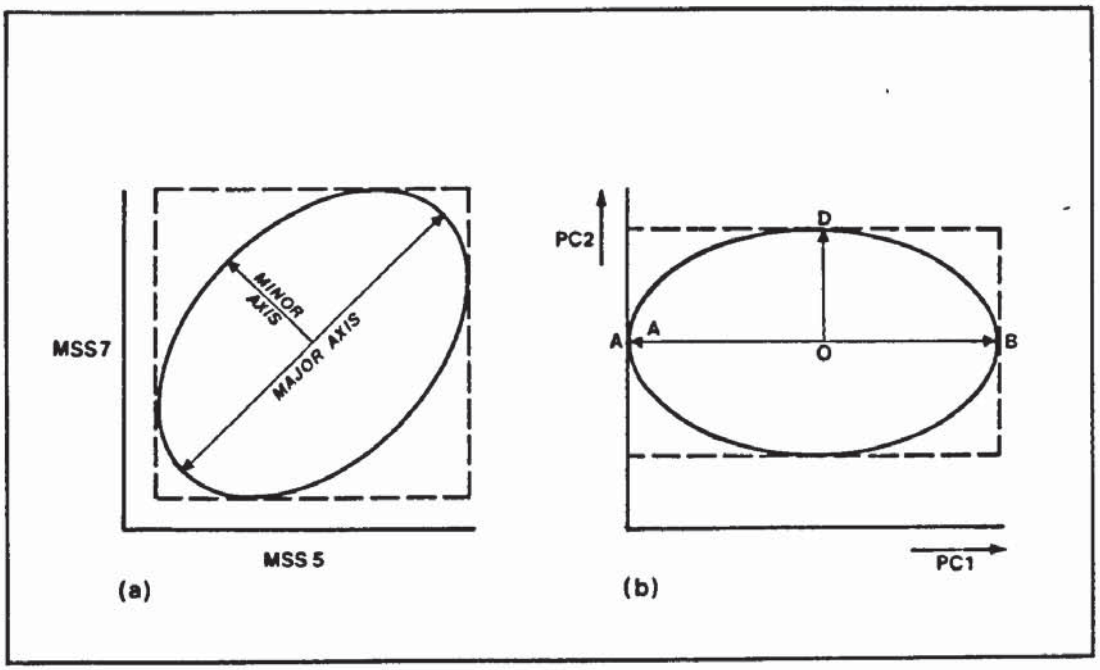

Figure 2.2 The Concept of a Principal Components Transformation

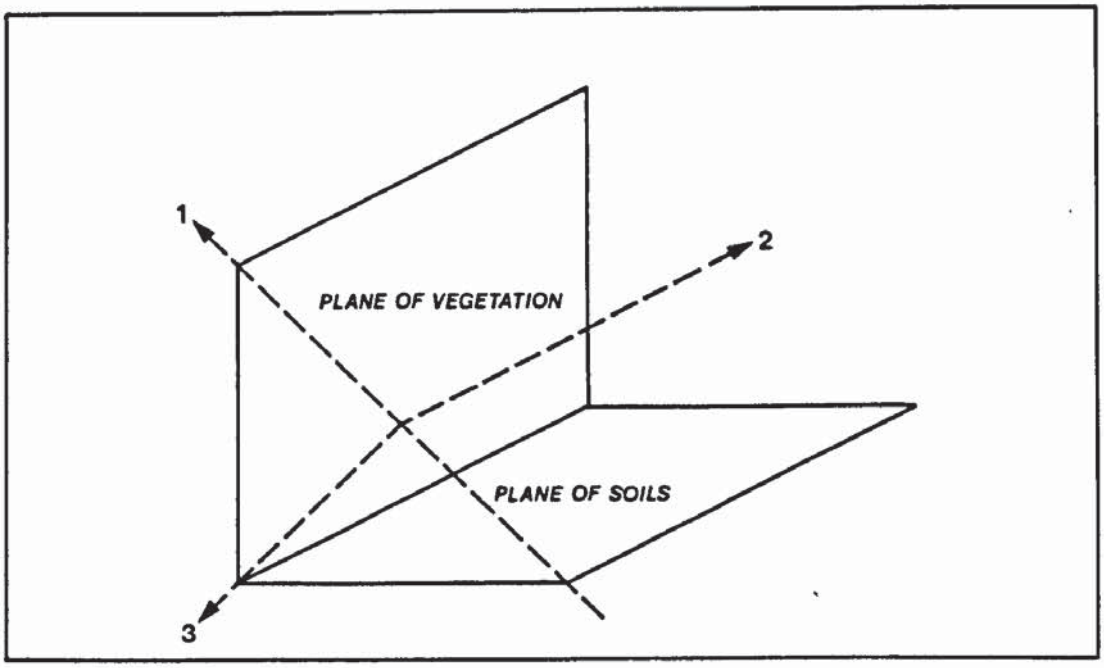

Figure 2.3 Principal Components of Data Dispersed in Two Planes

angle with the edges of the two planes and a third component divides that right angle into two. Thus, no prior order or physical interpretation on the principal directions is imposed on the data-set by a principal components transformation. In practical terms this means that a component cannot necessarily be related to a particular land cover type.

Kauth and Thomas (1976) and Jackson (1983) have used the Gramm-Schmidt orthogonalisation procedure which, unlike principal components analysis, constrains the transformation of the data by ordering the sequence in which the calculations are performed (Perry and Lautenschlager, 1984). Kauth and Thomas (1976) developed a 'tasselled cap' transformation that used linear combinations of Landsat wavebands. An analysis of two-dimensional scatterplots for agricultural MSS data suggested that the structure of agricultural MSS data can be likened to a 'tasselled cap' (Figure 2.4). The spectra of an emerging green crop starts on the plane of soils and, as the crop develops, the spectra progresses outwards roughly normal to the plane of soils on a curving trajectory towards the region of 'green-stuff'. As the crop matures and senesces the trajectories fold over and converge on the region of 'yellow stuff', before finally returning to the soil line.

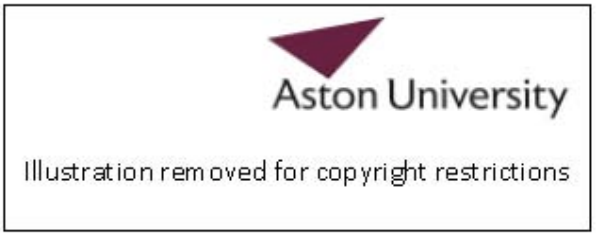

Figure 2.4 The 'Tasselled-Cap' Transformation of Kauth and Thomas (1976)

Vegetation and soil related information fall primarily within a single plane defined by the triangular shape of the 'tasselled cap'. This fact enabled Kauth and Thomas (1976) to

define a specific rotation of the spectral axes in four dimensional space using the following coefficients:

Green vegetation index = 0.29 MSS 4-0.56 MSS5+ 0.60 MSS 6 + 0.49 MSS 7
(Kauth and Thomas, 1976).

The major axis of the transformed distribution which corresponded to soil was termed brightness; greenness was chosen orthogonal to brightness and points towards the green cluster; yellowness was chosen orthogonal to both brightness and greenness and points towards a 'yellow-stuff' point. Finally, 'non-such' was chosen orthogonal to brightness, greenness and yellowness. Unlike principal components analysis the Kauth and Thomas (1976) transformation of spectral axes defines the orientation of components in multi-dimensional space a priori, such that each component is constrained to represent a physically significant land cover class.

2.5.3 Two Dimensional Vegetation Indices

Two dimensional vegetation indices include various ratios of Landsat wavebands and perpendicular vegetation indices (PVI). Both techniques exploit the spectral contrast between soil and green vegetation in the visible and near-infrared wavebands as shown in Figure 2.1.

A simple vegetation ratio is a division of the amplitude of near-infrared radiance which is positively correlated with green vegetation, by the amplitude of visible red radiance, which is negatively correlated with green vegetation. With an increase in green vegetation cover the ratio value will increase to give a measure of relative changes in green vegetation amount (Figure 2.5). The lines of equal ratio value illustrated on Figure 2.5 radiate outwards from the origin and are not parallel to the soil line. As a result, ratio measures of green vegetation amount will vary with variations in soil background reflectance. From Figure 2.5 vegetation with the same greenness cover will display a higher ratio value (1:0.5) at point B on a dark soil, but a much lower ratio value (1:0.75) at point A on a bright soil. Various ratio transformations which were reviewed by Curran (1980), have been developed to reduce the effect of differences in soil background reflectance on the ratio value. Some of these transformations are described in the following paragraphs.

The use of near-infrared ratio or simple vegetation index for estimating vegetation biomass was first reported by Jordan (1969). Pearson and Miller (1972) successfully employed the ratio technique to estimate grass canopy biomass using a two channel hand-held radiometer and airborne multispectral

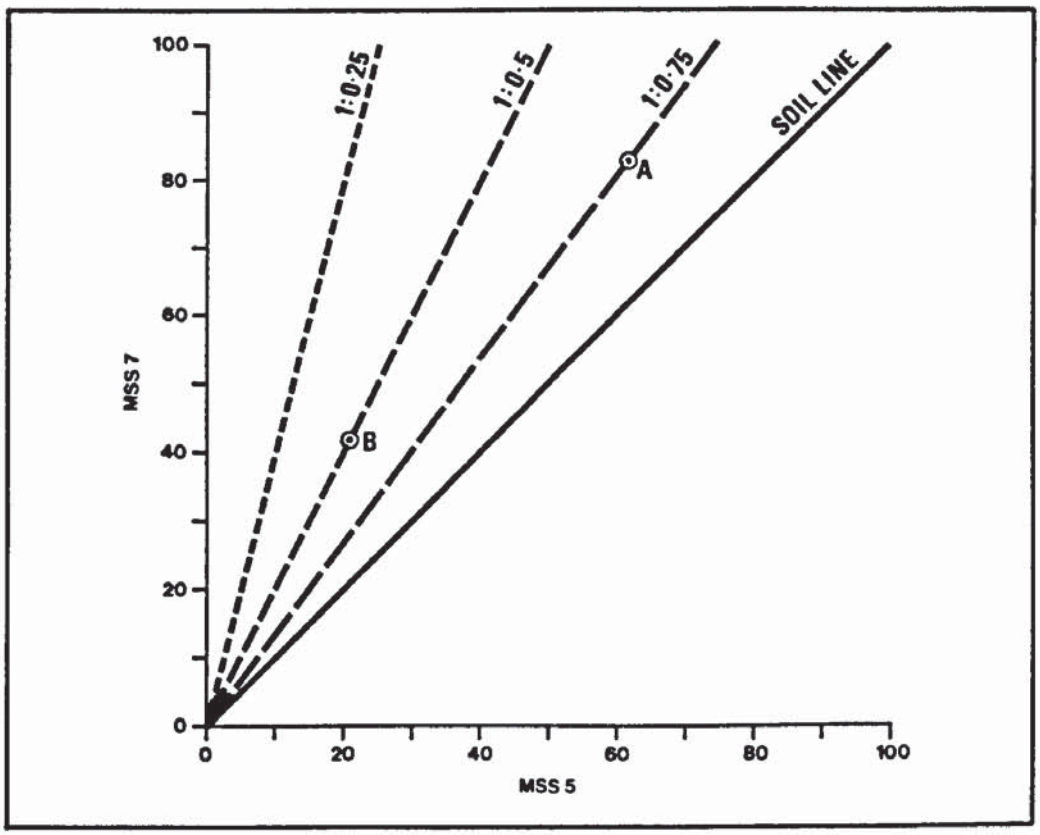

Figure 2.5 Lines of Equal Ratio Value in MSS7/5 Landsat Space

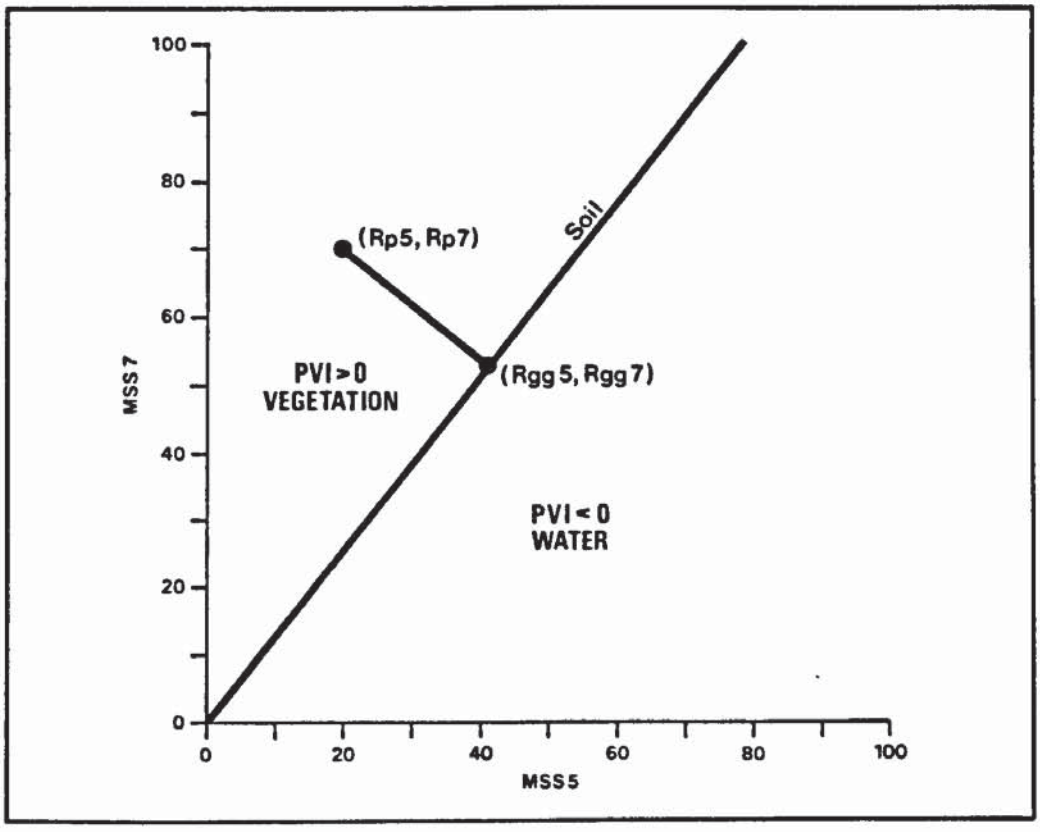

Figure 2.6 The Perpendicular Vegetation Index (PVI) of Richardson and Wiegand (1977)

scanner data. This research showed that simple linear relationships existed between the ratio value and grass biomass over a range of 0-700 g/m^2. Colwell (1974) also found that the simple vegetation index was useful for estimating biomass and was capable of reducing variations in background reflectance. The simple ratio of Landsat MSS data can be expressed:

$$\text{Simple Vegetation Index} = \frac{\text{MSS7}}{\text{MSS5}}$$

Carneggie and De Gloria, 1973) used a ratio of Landsat MSS7/MSS5 and found that the ratio values plotted as a function of time, peaked during the period of greatest forage production and then fell away, signalling the period of drying following the maximum growth period. Thus it was shown that a ratio of Landsat wavebands could be used to monitor critical growth stages in rangeland biomass, both spatially and temporally. Rouse et al, (1974) found that although a simple ratio of MSS7/MSS5 could be used as a measure of relative greenness, spatial differences in brightness within a scene and temporal differences in brightness between scenes introduced a large error component. A division of MSS7 - MSS5 radiance values normalised over the sum of MSS7 + MSS5 was used as an index value and called the vegetation index (VI):

$$\text{Vegetation Index} = \frac{\text{MSS7} - \text{MSS5}}{\text{MSS7} + \text{MSS5}}$$

The VI was found to reduce though not eliminate multiplicative atmospheric effects which cause temporal and spatial variations in average scene brightness. Deering (1978) found that the radiance sum of MSS7 and MSS5 is insensitive to green biomass but closely related to scene brightness, whilst the radiance difference of MSS 7 - MSS 5 is a good indicator of green biomass. However, the radiance sum is poorly related to the radiance difference, and therefore, a division of MSS7 - MSS5 by MSS7 + MSS5 produces a vegetation index with inherent adjustment for scene brightness variations.

Richardson and Wiegand (1977) used the perpendicular distance from the soil line as an indicator of plant development. The technique, which they called the perpendicular vegetation index (PVI), is illustrated in Figure 2.6. A PVI of more than unity denotes the presence of green vetetation. A PVI equal to unity represents soil and a negative PVI value denotes water. The PVI is calculated from the following expression:

$$PVI = (S_R - V_R)^2 + (S_{IR} - V_{IR})^2$$

Where S = Soil Reflectance
V = Vegetation Reflectance
R = Red Reflectance
IR = Near Infrared Reflectance

The soil background reflectance is interpreted as the intersection on the soil background line (S_R and S_{IR}) with a perpendicular drawn from a candidate green vegetation point (V_R, V_{IR}). When the soil background reflectance changes, the point of perpendicular intersection between the vegetation point and soil line must be recalculated, thus restricting the effectiveness of the PVI to a soil of uniform reflectance.

The Richardson and Wiegand (1977) formulae for the perpendicular distance from a point are computationally inefficient. A computationally simpler method of achieving the same result by subtracting MSS5 from MSS7 was therefore proposed by them.

$$DVI = 2.40\ MSS7 - MSS5$$

where DVI is the difference vegetation index, and MSS7 is multiplied by the slope of the linear equation for the soil background line defined by MSS wavebands 7 and 5. The disadvantage of this method is that soil background reflectance cannot be determined.

An index similar to the PVI of Richardson and Wiegand (1977) was developed for this study to calculate both distance along the soil line as a measure of soil reflectance/non-green vegetation cover, and perpendicular distance away from the soil line as a measure of green vegetation cover in MSS7/5 space:

$$S_D = MSS5 \cos \theta + MSS7 \sin \theta$$
$$G_D = MSS7 \cos \theta - MSS5 \sin \theta$$

Where S_D is distance along the soil line, G_D is perpendicular distance along the green vegetation line and θ is the angle between the soil line and the x axis (MSS5). Calculation of the index is based upon standard analytical geometry (Appendix 1).

This is equivalent to a rotation of axes, such that in the new coordinate system the soil line becomes the abiscca and the perpendicular vegetation line the ordinate. Unlike the PVI of Richardson and Wiegand (1977) the soil background reflectance does not need to be

calculated for every candidate green vegetation point. The index is therefore unaffected by differences in soil reflectance making it particularly suitable for mapping green vegetation cover in an area such as northern Kenya where marked variations in soil reflectance occur. The results obtained from an application of the index within the Study Area, are discussed in Chapter 7.

CHAPTER 3

FIELD DATA AND LANDSAT IMAGERY

The first part of the chapter describes the fieldwork methods and the interpretation of air photography for soil and vegetation mapping. The characteristics of Landsat data and image data pre-processing are described in the second part of the chapter.

3.1 INTRODUCTION

The first stage of the project involved the collection of basic data-sets required for the study; including ground data, maps, reports, air photography and Landsat imagery. This chapter describes the methodologies involved in collecting these data and processing them into an interpretable format for analysis.

3.2 GROUND DATA

The collection of ground information about the characteristics of the vegetation and other surface features is an essential part of any remote sensing programme. Ground data is needed primarily to calibrate the sensor by relating recorded radiance values to measured conditions on the ground, and to determine the mapping accuracy attained from a visual interpretation or digital classification of the imagery. The type of ground data required depends upon the objectives of the study and the scale of mapping employed.

3.2.1 Topographic Maps

The 1:100,000 scale topographic maps produced by the UK Directorate of Military Survey for the Survey of Kenya, were compiled from ortho-photo mosaics of 1972 (RAF) air photography. Relief contours, vegetation, drainage, communications, settlements and administrative boundaries are superimposed in colour. The maps proved to be extremely useful for field work planning and were essential for the geometric rectification of the Landsat digital data (sub-section 3.11.1) but are of too small a scale for useful comparisons with Landsat imagery.

3.2.2 IPAL Vegetation Map

The IPAL vegetation map at 1:50,000 scale (Herlocker, 1979) is based upon the interpretation of 1:50,000 scale air photographs supplemented by extensive field checking. Classification of vegetation categories is based upon species dominance, with the most dominant species determining the primary stratum, and secondary and tertiary strata

defining the associated communities. The map provided useful descriptive information (Chapter 1) and could be compared with the Landsat imagery at a reconnaissance level, but the scale proved to be too small for any detailed comparisons within the Study Area.

In addition to the vegetation map a series of reports published by IPAL with reference to the nomadic peoples and their livestock, and containing data on climate, soils and vegetation have provided essential information for the study. These reports are referred to within the text as appropriate.

3.2.3 Panchromatic Air Photography

A stereo set of 40 panchromatic air photographs covering the Kargi study area were obtained from the Royal Air Force. The photography was flown during the dry season in January 1972 at a nominal scale of 1:50,000. Air photography acquired at a date nearer the fieldwork period would have been preferred but the 1972 set represented the latest available photography for this region. It is believed that over a large part of the Study Area the distribution and density of vegetation will not have changed substantially during the period between the acquisition of the photography in 1972 and fieldwork in 1981. Only in the immediate vicinity of Kargi have substantial changes in the density of vegetation cover occurred in recent years, and this was taken into account during air photo interpretation.

A further set of air photographs acquired in 1957 by the RAF at a smaller, 1:80,000 scale were also acquired for the project as a possible means of monitoring change in the density and distribution of vegetation over a longer period. This photography proved to be too small a scale and not of high enough quality to be used for this purpose, and no comparisons were made between the early and later sets of air photography.

3.3 VEGETATION CLASSIFICATION AND MAP

The 1:50,000 scale air photographs were interpreted to produce a vegetation map and later a soil map, of the Study Area. The vegetation classification system adopted was modified from Herlocker (1979) and Gwynne et al, (1966). Three vegetation strata; primary, secondary and tertiary were defined. A primary stratum is controlled by regional climatic conditions whereas a secondary stratum is determined by soil factors. A tertiary stratum covers the specific plant species composition.

Although the scale and quality of the air photography was good enough to allow for differentiation between dwarf shrub and shrub species and between shrub and woodland species, only four primary and three secondary vegetation types could be easily interpreted. A division of the secondary vegetation units into tertiary species associations was not possible from the air photography and was not attempted during interpretation. Relative

differences in plant canopy cover could be readily interpreted from the air photography, and measured quantitatively on the ground during fieldwork or later from dot-grid analysis techniques. The modified classification system for the air photo interpretation presented in Table 3.1, therefore included a vegetation canopy component.

TABLE 3.1 VEGETATION CLASSIFICATION SYSTEM FOR AIR PHOTO INTERPRETATION

Class code	Primary	Secondary	Per cent Canopy Cover	Appearance on Air Photos
1	Barren	Unvegetated	0	Very light tone, smooth texture
2	Dwarf Shrubland	Dwarf Shrubland	0 - 20	Mosaic of patches of dark grey vegetation interspersed with occasional shrub crowns
3	Shrubland	Deciduous with dwarf shrub understorey	0 - 20	Scattered distribution of single dark-toned shrub crowns, usually clustered in groups. Wide areas of bright bare soil clearly visible
4	Shrubland	Deciduous with dwarf shrub understorey	20 - 40	Relatively even distribution of single, dark-toned and evenly spaced shrub crowns
5	Shrubland	Deciduous with dwarf shrub understorey	40 - 60	Very even distribution of closely spaced shrub crowns; dark tone; very little bare soil visible
6	Shrubland	Deciduous with dwarf shrub understorey	60 - 80	Single shrub crowns coalesced into large patches of very dark-toned vegetation cover obscuring soil surface
7	Woodland	Deciduous with dwarf shrub understorey	20 - 40	Separate tree crowns visible. Crown size much larger than for shrub species. Restricted distribution.

Stereo air photo triplets were placed under a Zeiss Interpretoscope and the effective area of overlap was marked on the middle print. This ensures that the whole area is interpreted but avoids possible duplication due to stereo overlap between adjacent photo prints. A magnification factor of between five and ten times was selected to facilitate interpretation. Boundaries were interpreted between vegetation units based upon differences in the appearance of the vegetation on the air photography described in Table 3.1. Primary and secondary vegetation strata could be easily interpreted, as the very different life forms of woodland, shrubland and dwarf shrubland species give these types a distinctive appearance on the air photos. Where changes in the per cent cover of the vegetation canopy also coincided with a change in species type e.g. from *Acacia reficiens* shrubland to *Acacia tortilis* woodland, a well-defined boundary could be interpreted. In many areas, however, particularly for primary shrubland species, changes in per cent cover occur gradually across an environmental gradient, and in these cases the positioning of a boundary between adjacent mapping units had to be generalised.

The separate air-photo interpretations from each stereo-triplet were subsequently compiled into a single vegetation map of the Study Area by precisely superimposing each overlay onto a semi-controlled air-photo mosaic. The details of this procedure are described in Section 3.5. The completed vegetation map is illustrated in Figure 3.1.

3.4 SOIL CLASSIFICATION AND MAP

Soil types were interpreted from the air photography directly on the basis of variations in soil reflectance, and indirectly on the basis of their association with a particular landform or vegetation type. Stereo-triplets were used for the interpretation and the overlays from each triplet were later mosaiced together and compiled into a final soil map as described in Section 3.5. Differences in reflectance between dark lava gravels and bright, sandy-loam soils or saline soils were clearly visible on the air photography, enabling these and other soils to be easily interpreted. Areas of highly permeable, stabilised sand-dunes support only a very sparse cover of dwarf shrubland and the presence of this species indicated a dry, sandy soil. Soils derived from the products of erosion could generally be mapped from their association with a characteristic landform of gently sloping deposits surrounding lava outcrops. Using this kind of direct and indirect evidence six soil types were mapped as shown in Figure 3.2.

Transparent copies of Figures 3.1 and 3.2 are to be found in Appendix B. This is to facilitate comparison between the distribution of vegetation and soils in the Study Area .

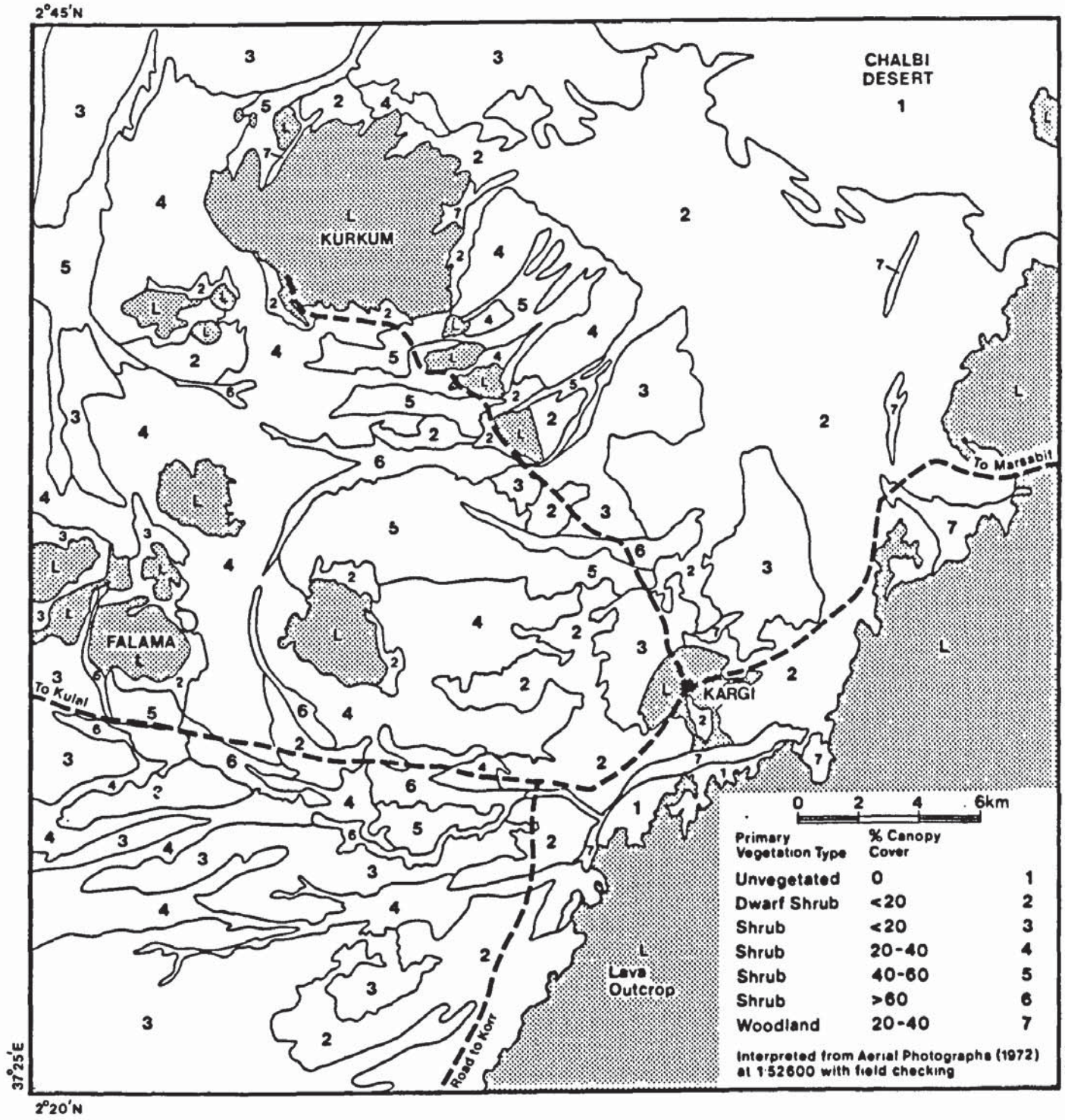

Figure 3.1 Vegetation Map of the Kargi Subscene Derived from Air-Photo Interpretation with Field-Checking

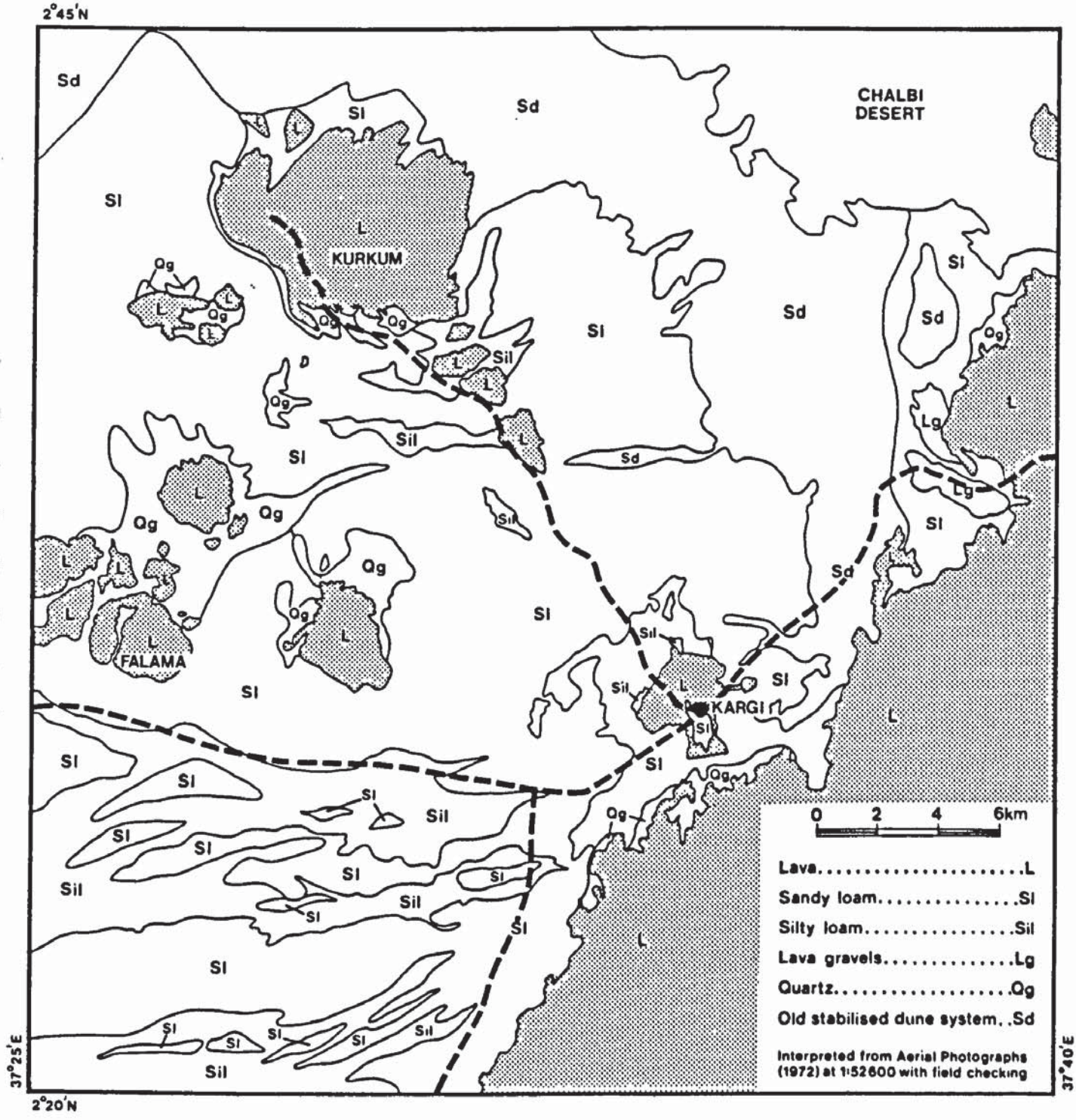

Figure 3.2 Soil Map of the Kargi Subscene Derived from Air-Photo Interpretation with Field-Checking

3.5 AIR PHOTO MOSAIC

To enable the interpreted overlays from individual photo prints to be compiled into vegetation and soil maps for the Study Area, the air photographs were mosaiced together. It was also important that the final vegetation and soil maps could be later registered with the Landsat imagery at the same map projection and scale.

An air photograph is not a true plan representation of the ground due to variations in relief within the photo area, and variations in the tilt, altitude and attitude of the aircraft. For this reason air photographs cannot be mosaiced together into a distortion-free map without reference to a precise coordinate system. The rectification of air photography is usually achieved photogrametrically from ground control points, but this was not possible in the present study. The solution was to mosaic the photographs to the 1:100,000 scale topographical map of the Study Area which had been produced by the Survey of Kenya from rectified ortho-photo maps for the national map series. This required the topographical map to be enlarged to the average 1:52,600 scale, as opposed to the nominal 1:50,000 scale, of the air photography.

A glass scale was used to measure distances between a pair of identifiable features on each photograph and between the same pair of points on the topographical map. The average from ten measurements was 1:52,600, and this figure was taken to be the average scale of the photography covering the Kargi study area. The difference in scale,which varied from 1:51,600 to 1:53,400, was probably due to a change in aircraft altitude between photographs along adjacent flight lines. A grid of one km squares was drawn at the average 1:52,600 scale of the air photography. The boundaries of distinctive features on the topographical maps, which could also be identified on the air photographs, were then transferred visually onto the 1:52,600 scale grid, using the one km spaced grid lines on the topographical maps as a guide. Major features, mostly lava outcrops and distinctive boundaries between soil types, were thereby transferred from the smaller, geometrically true map scale of the topographic map to the larger average scale of the photography.

The photo prints were mosaiced as a simple print 'lay-down' by aligning identifiable features on the air photographs with the same features on the enlarged 1:52,600 scale topographical map. The air photographs were stuck down with a glue that allowed small positional adjustment to be made after the prints had made contact with the map. Some misfit between mosaic and map occurred as a result of small deviations in scale between individual photo prints and the calculated average scale, and some mismatching of boundaries between adjacent prints also occurred. With the mosaic complete the

interpretation overlays for each print could be accurately positioned onto the mosaic, and the vegetation class boundaries compiled into the final vegetation and soil map for the Study Area at 1:52.600 scale. The scale of both maps has been reduced to 1:200,000 to facilitate inclusion in this thesis. The air photo mosaic is reproduced at a reduced scale in Figure 3.3.

3.6 FIELDWORK

A visit was made to northern Kenya in July and August of 1981 to collect ground data. This followed an earlier visit to the Study Area in 1979 (Griffiths, 1980) which had provided adequate general information about the environmental characteristics, conditions, and problems involved in working in a remote area of northern Kenya to be of considerable assistance in planning a more detailed and extended visit in 1981.

The purpose of field sampling vegetation and soil characteristics was to provide quantitative and qualitative data to check the validity of air photo and Landsat interpretation. Two months were spent at Kargi during the dry-season in northern Kenya. Unfortunately it was not possible to be in the field after a wet season when the growing vegetation cover is in green leaf.

Given the rather short time available for fieldwork and the problems of access to remote sites within the Study Area, a non-random sampling strategy proposed by Hellden, (1979) was employed. Sample locations were selected to include the whole range of vegetation types found within the Study Area based upon a stratification of the air photography into a number of classes (Table 3.1). This approach reduces the possibility of under-representing small classes given the small sample of 34 fieldwork sites which were selected to represent the range of vegetation types found within the Study Area. Each site was located in the field using landmarks which could be identified both on the air photography and on the ground. Such landmarks included vehicle tracks, 'luggas', rock outcrops and distinctive clumps of vegetation. At each site a sample quadrat 50 x 50 m in area (0.25 ha) was marked out on the ground and the following parameters recorded:

(a) dominant species type
(b) per cent canopy cover of shrub and dwarf shrub species
(c) per cent cover of herbaceous species
(d) soil surface characteristics and soil Munsell colour

A 35 mm colour photograph was also taken at each field site to record the typical vegetation cover, and referenced with a location number.

Figure 3.3 Air photo mosaic of the Kargi subscene

TABLE 3.2 SOIL COLOUR AND SURFACE CHARACTERISTICS OF EACH FIELD SAMPLE SITE

Site No.	Munsell Colour	Comments
1 - 6	No data	No data
7	NR	Fine white sand
8	NR	White calcareous crust with rough pebbles
9	NR	Dark grey lava pebbles
10	NR	Dark grey lava pebbles
11	7.5 YR 5/6	Silt; hard crust undisturbed by livestock
12	5 YR 5/6	Sandy loam; hard crust undisturbed by livestock
13	7.5 YR 5/6	Silt
14	7.5 YR 5/6	Silt loam with large quartz particles
15	7.5 YR 5/6	Silt; very fine, powdery; crust disturbed by livestock
16	5 YR 5/6	Sandy loam
17	NR	White calcareous pebble surface
18	7.5 YR 5/6	Coarse sand and dark lava gravel
19	7.5 YR 5/6	Silt; dark lava gravel surface
20	7.5 YR 4/4	Silt; dark lava gravel surface; crust disturbed by livestock
21	5 YR	Sand
22	5 YR 5/8	Sand; wind-sorted crust; large quartz particles
23	7.5 YR	Silt-loam; hard crust
24	7.5 YR 5/6	Silt-loam
25	7.5 YR 5/6	Silt-loam
26	5 YR 5/6	Loamy sand
27	5 YR 5/6	Sandy sand
28	5 YR 4/6	Silt-loam; dune formation with hard crust of silt in hollows; sand on ridges
29	7.5 YR 5/6	Sandy loam
30	7.5 YR 6/6	Silt with hard baked crust
31	5 YR 5/6	Sandy loam; crust disturbed by livestock
32	7.5 YR 5/6	Sand with dark lava gravel
33	NR	White lava gravel

NR = Not Recorded

The canopy cover of shrub and dwarf shrub species was estimated by measuring the crown dimension (length and width) of a sample of shrubs within the quadrat and calculating the average crown area. This figure was then multiplied by the total number of plants within the quadrat to give a final per cent cover figure for the species. The per cent cover of herbaceous species was estimated visually according to a scale of cover values.

The method of measuring canopy cover at each sample was time-consuming, thus effectively reducing the number of sites visited in the field. Other workers have used the angle gauge or Bitterlich stick (Cooper, 1957) to make rapid measurements of canopy cover in areas of sparse vegetation, although this method cannot be used to measure low-lying dwarf shrub and herbaceous cover. A combination of the angle gauge for rapid measurement of tree and shrub canopy cover, in combination with the line intercept method (Canfield, 1941) for estimation of dwarf shrub and herbaceous cover would have been a more efficient method of measuring vegetation cover.

However, the results obtained in the field (Appendix C) yielded useful qualitative information about the canopy cover and species composition of vegetation within the Study Area. This information was used to assist in the interpretation of the air photography.

At each site the Munsell colour of the soil (dry) was recorded and the percentage fraction of sand, silt and clay constituents estimated according to a standard soil particle size classification (Munsell, USDA, 1975). Other qualitative aspects of the soil surface including crusting, level of disturbance by livestock, erosional features, plant litter and stoniness were also noted (Table 3.2). The data were useful as a guide to soil type classification during photo interpretation for soil mapping (Section 3.4).

3.7 VEGETATION CANOPY COVER MEASUREMENTS FROM PANCHROMATIC AIR PHOTOGRAPHY

Vegetation canopy cover measurements were taken directly from the air photography to obtain a larger and more representative sample of vegetation cover than could be obtained during fieldwork. These data were then used to quantify the vegetation map into canopy cover classes. The small scale of the photography precluded the use of normal dot grid analysis techniques which are commonly used for measuring plant canopy cover from larger scale air photography (Warren and Dunford, 1983). At small scales the dots obscure detail on the photo-print and prevent the accurate measurement of cover. The solution was to use a 0.5 mm grid containing 100 cells finely etched onto clear perspex, each cell representing a ground area of 25 m x 25 m (0.06 ha).

The canopy cover measurement was made by placing the grid on the air photograph under a Zeiss Interpretoscope at up to 15 times magnification, and visually estimating the cover of woodland and shrubland dwarf species within each of the 100 cells. The cover estimates for each cell were summed and averaged to give a per cent cover figure for the sample point.

The grid was placed at 75 randomly selected areas on the air photo mosaic. To ensure that all vegetation classes were represented in the sampling, a minimum of five sites per vegetation class was specified. Each sample area measured approximately 10 mm x 10 mm (25 ha) on the air photo print. This enabled at least five cover measurements to be made within each sample area. The cover measurements were averaged to reduce the likelihood of a single measurement being affected by purely localised variation in canopy cover.

The shrub and dwarf canopy cover estimates are given in Appendix D and presented as a histogram in Figure 3.4. The majority of the sites (39%) had a canopy cover of between 20-40 per cent, but almost as many (32%) had a canopy cover of less than 20 per cent. The remainder of the sites (29%) had a canopy cover in excess of 40 per cent. These data indicate that shrub vegetation canopy cover within the Study Area is variable, though with a considerable bias towards sites of lower cover.

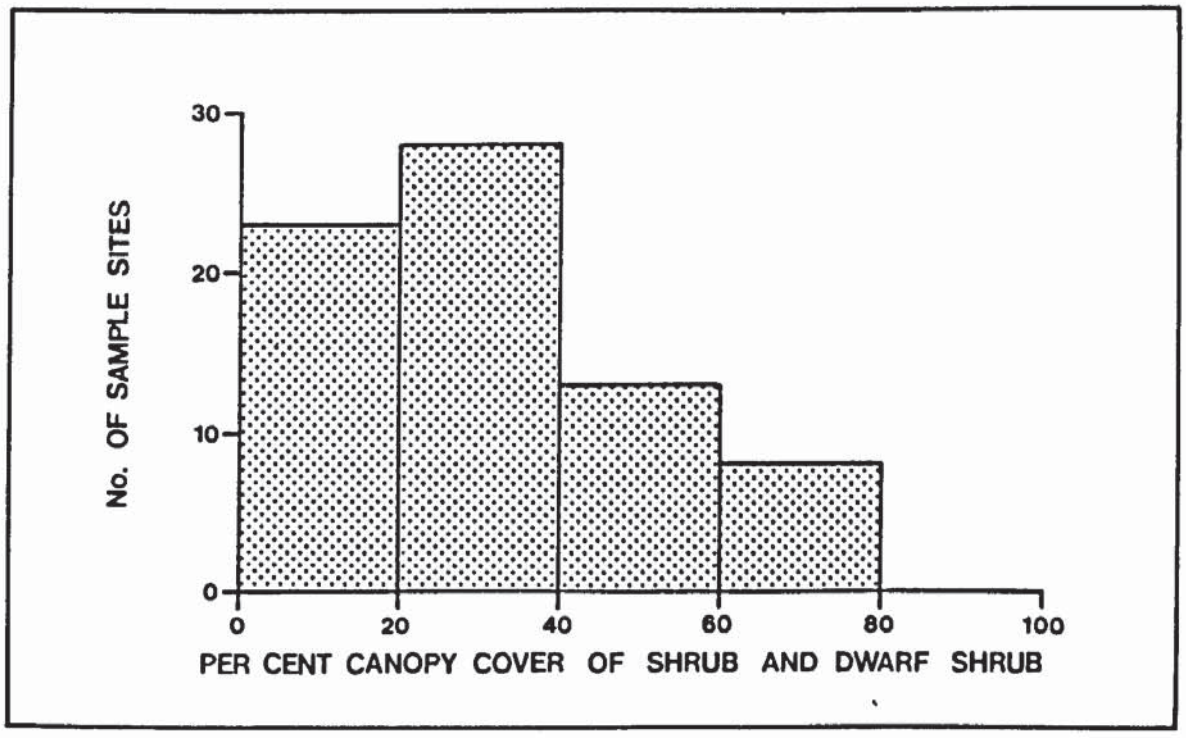

Figure 3.4 Histogram Showing the Relationship between the Number of Air-Photo Sample Sites and the Per Cent Canopy Cover of Shrub and Dwarf Shrub Vegetation

3.8 VERTICAL COLOUR AIR PHOTOGRAPH SURVEY

A hand-held small format (35 mm) camera was used to acquire large scale vertical colour transparencies from a Cessna light aircraft for more detailed information about the vegetation characteristics of the Study Area. The aircraft was flown at a height of 1500 ft (500 m) and maintained by the pilot at this altitude during the survey with the guidance of a radar altimeter. Six transects were flown across the Study Area, each transect being 20 km long and 2 km apart. At a flying speed of 80 kph and an exposure interval of 40 seconds, the distance between successive photographs along the transect was two kilometres. This sampling scheme was designed to give a sample of 60 photographs positioned at the interstices of a 2 km x 2 km grid, covering approximately 400 km^2 or 50 per cent of the Study Area. At the altitude of the aircraft and the focal length of the lens (55 mm) the area covered by each photograph was 218 m x 318 m (7.2 ha). The difference of 100 m between the two area dimensions is due to the aspect ratio (35 mm x 24 mm) of a Kodachrome 64 film colour transparency.

Some problems were encountered with high cross winds which are an almost daily occurrence during the dry-season in this region of northern Kenya. As a result the planned grid system could only be approximated, making it very much more difficult to plot precise flight lines on a map and locate individual photographs on the ground. With this problem in mind a number of oblique photographs of easily identifiable features, particularly lava outcrops, were taken during the survey flight at points along and at the end of each transect line in an attempt to fix the orientation and length of the flight lines on a map. To further assist with photograph location certain distinctive features passing vertically beneath the camera were also photographed e.g. the well at Kargi. Finally, features on some of the photographs could be identified on the panchromatic air photography enabling their positions to be very precisely fixed. Using these various guides it proved possible to plot the flight lines on a flight plan (Figure 3.5). Although every attempt was made to ensure precise positioning of photographs on the ground, it is estimated that positional errors of up to 200 m could have occurred.

The colour air photographs proved to be a valuable source of information about vegetation cover within the Study Area. Furthermore, the extremely low cost of the survey compared to conventional aerial surveys, and the timeliness of the survey, makes this an effective method of data collection in remote areas.

3.9 VEGETATION CANOPY COVER MEASUREMENTS FROM COLOUR AIR PHOTOGRAPHY

An example of one of the colour air photographs is given in Figure 3.6. Areas of bare

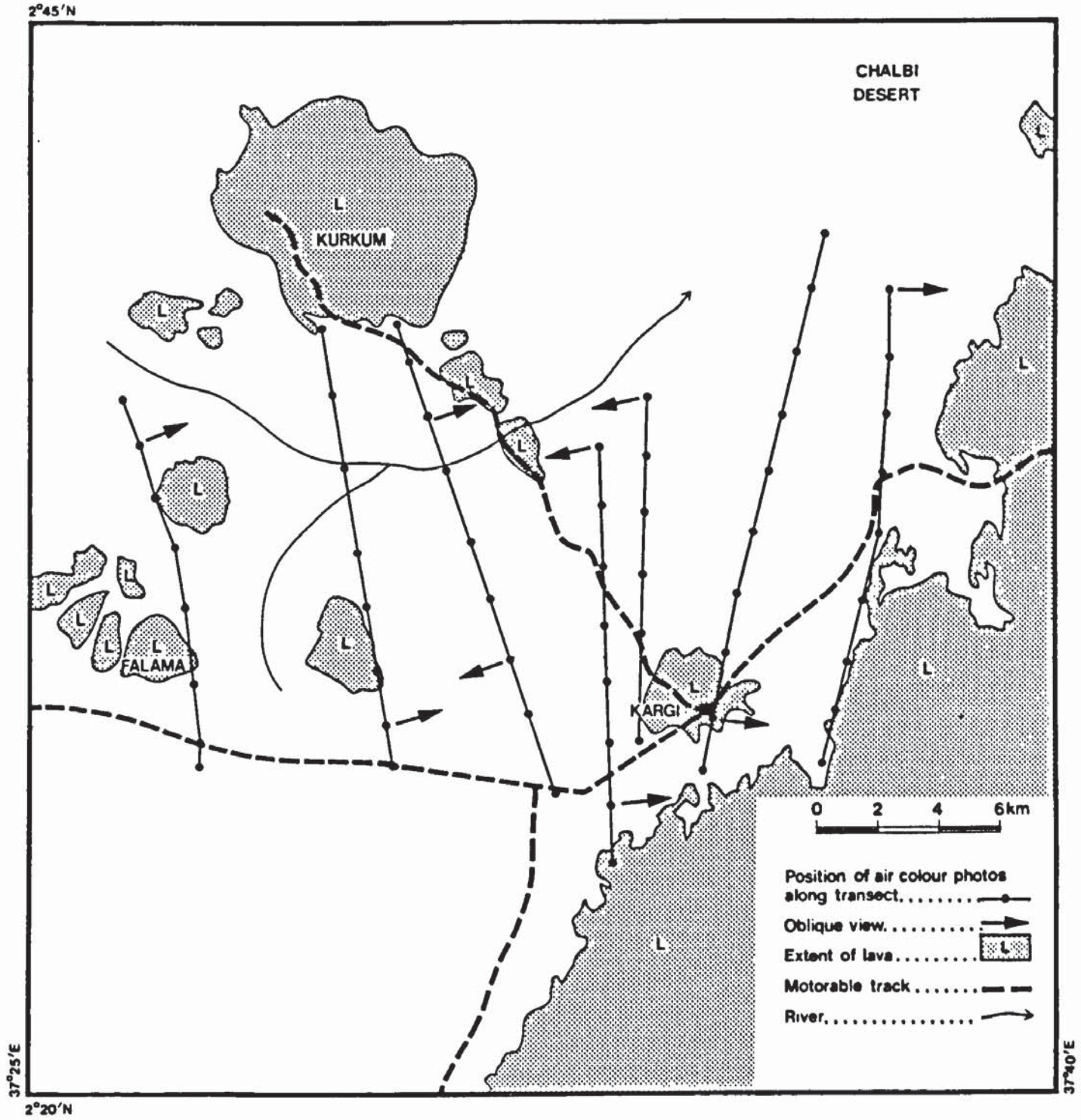

Figure 3.5 Flight Plan for Small-Format Colour Air Photo Survey

soil appear reddish in colour, dwarf shrub and shrub plants give a characteristically rough texture and appear grey in colour, and the ground layer of dry herbaceous species appears yellow. Vegetation types were therefore distinctive enough in colour and texture to be distinguished from the soil background during interpretation.

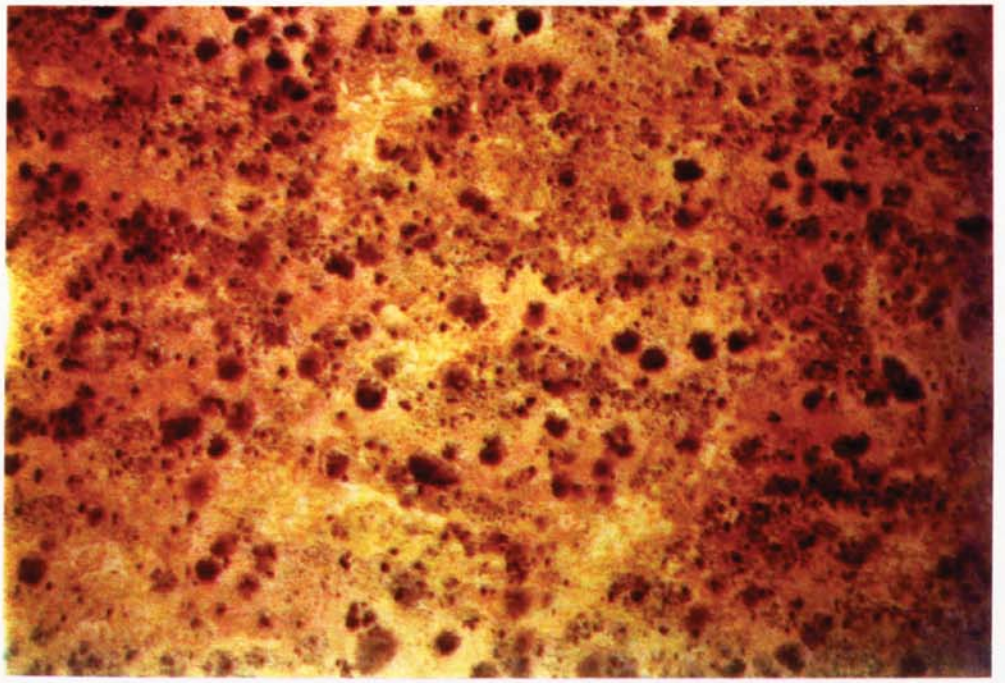

Figure 3.6 An Example of a Small Format Colour Air-Photo

The percentage cover of bare soil, dwarf shrub, shrub and herbaceous vegetation was measured from a selection of 20 of the colour air photographs. Each transparency was projected onto a horizontal ground glass screen mounted on a projection box, and magnified approximately ten times, to a scale of about 1:1000. The projection box, which was constructed in the Civil Engineering Department, University of Aston, uses a mirror angled at 45 degrees to reflect a photographic image from a slide projector onto the horizontal screen at variable scales. A grid, covering a ground area of 0.5 ha at the projected scale and containing 100 evenly spaced and theoretically infinitely small dots, was placed over the projected image. The percentage cover of bare soil, shrub and herbaceous cover was determined by counting the number of dots falling on each cover type according to a method described by Warren and Dunford (1983), and Lamprey (pers. comm.).

The procedure was repeated five times at different positions on each of the projected photographs to give an average figure from five separate measurements in order to reduce possible local variations in canopy cover which were not characteristic of the class as a

whole.

The canopy cover estimates derived from the colour air photography are listed in Table 3.3.

TABLE 3.3 GROUND COVER ESTIMATES MEASURED FROM SMALL FORMAT COLOUR AIR PHOTOGRAPHS

Photograph No.	Mean % cover Bare Soil		Mean % cover Shrub and Dwarf Shrub Species		Mean % cover Herbaceous Species		Total % Cover
1	27.8	(5.8)	21.4	(1.5)	50.8	(5.4)	100
2	27.0	(4.4)	12.8	(3.0)	60.2	(3.0)	100
3	33.6	(4.9)	30.0	(5.6)	36.4	(3.3)	100
4	24.4	(5.8)	58.5	(5.5)	16.8	(4.2)	100
5	35.2	(5.8)	24.0	(5.2)	42.8	(6.6)	100
6	50.6	(3.3)	28.6	(3.7)	20.8	(2.2)	100
7	59.6	(6.9)	25.6	(3.9)	14.8	(3.3)	100
8	31.6	(15.1)	43.8	(7.4	25.6	(7.7)	100
9	41.8	(3.2)	10.0	(1.2)	48.0	(3.2)	100
10	34.0	(4.0)	29.2	(10.6)	36.8	(14.6)	100
11	40.6	(5.1)	17.0	(2.0)	42.4	(5.5)	100
12	45.8	(5.8)	35.4	(1.7)	18.8	(5.4)	100
13	18.2	(1.8)	17.4	(3.3)	64.4	(3.0)	100
14	49.6	(6.9)	31.6	(4.1)	18.8	(9.7)	100
15	36.6	(6.7)	39.8	(3.3)	23.6	(5.0)	100
16	21.3	(3.6)	36.6	(4.5)	42.0	(2.7)	100
17	18.8	(5.4)	30.8	(9.8)	50.4	(12.5)	100
18	63.6	(6.3)	20.6	(2.7)	15.8	(6.2)	100
Mean $\bar{X}$	36.6		28.5		34.9		

Note: Numbers in brackets are mean deviations for n = 5 measurements.

Warren and Dunford (1983) correlated dot-grid cover estimates from large scale air photography of semi-arid shrubs in Arizona, with field measurements of canopy cover. Their trials showed a very high correlation between ground cover measured on the ground and estimates derived by dot-grid analysis from the air photography.

A comparison between the mean canopy cover figures for shrub, dwarf shrub and herbaceous cover given by Lamprey, (1981) with canopy cover estimates obtained from colour air photography within the Study Area, is given in Table 3.4.

TABLE 3.4 A COMPARISON OF VEGETATION CANOPY COVER ESTIMATED FROM AIR PHOTOGRAPHY BY LAMPREY (1981) AND FOR THE STUDY AREA

Location and vegetation class	Shrub per cent cover	Dwarf shrub per cent cover	Herbaceous cover and bare soil
Balesa kulal *Acacia reficiens* shrubland (Lamprey - Site A)	14.5	24.5	61.0
Balesa kulal *Acacia reficiens* shrubland (Lamprey - Site B)	13.75	19.25	67.0
Kargi Study Area		28.5	71.5

The three areas of broadly similar ecological composition show some measure of agreement in canopy cover estimates. Both sets of data were obtained from large scale air photography using the dot grid method for estimating vegetation cover as described.

3.10 LANDSAT DATA OBTAINED FOR THE STUDY AREA

Table 3.5 summarises the Landsat film products and digital data obtained for the Study Area. The operation of the Landsat system and the characteristics of MSS data, are adequately described in the literature (Manual of Remote Sensing, 1983), and further descriptions have not been included in this thesis. Landsat data distributed by the EROS Data Centre (EDC), usually require additional processing to correct for geometric and radiometric sources of error, before the data are in a suitable format for analysis. In addition to a description of the film products and digital data specifically obtained for this study, the preprocessing corrections required and the procedures involved, are outlined in the concluding sections of this chapter.

TABLE 3.5 LANDSAT DIGITAL DATA AND PHOTOGRAPHIC IMAGERY ACQUIRED FOR THE STUDY AREA (Path 181/Row 058)

Date	Scale	Product type[1]
January 1973	1:3.3m	F
January 1976	1:3.3m	F
January 1979	1:3.3m	F
June 1979	1:3.3m	F
January 1973	1.1m	F
January 1979	1.1m	F
June 1979	1.1m	F
January 1973	1:250,000	FCC
January 1976	1:250,000	FCC
June 1979	1:250,000	FCC
January 1973	-	CCT
June 1979	-	CCT

Note: [1] *F = Film*
FCC = False Colour Composite Print
CCT = Computer Compatible Tape

At least two dates were obtained for both digital and film products to enable multi-temporal comparisons to be made between scenes (Table 3.5). The imagery was acquired under dry-season conditions due to thick cloud cover which prevails in northern Kenya during the wet season. Unfortunately this meant that seasonal differences in the rangeland

under wet and dry conditions could not be mapped from the imagery. However, the earliest image date (January 1973) was acquired at the end of the Sudano-Sahel drought (1968-1973) and is therefore representative of extremely dry conditions, whilst the latest cloud-free date (June 1979) was acquired after significant rainfall during the April-May wet season of 1979. East Africa is not within range of a Landsat receiving station, and prior to the launch of the Tracking and Data Relay Satellite (TDRS), data had to be stored by on-board recorder until the satellite passed within range of the Goddard Space Flight Centre (GSFC) receiving station in the United States. This data acquisition system proved to be unsatisfactory as the recorders on-board Landsat 1, 2 and 3 suffered from technical problems and limited mission life. Following the launch of TDRS in 1982, it is understood that Landsat data for East Africa are now acquired more frequently, thus increasing the possibility of obtaining wet-season imagery.

3.10.1 Landsat Film Products Obtained for the Study Area

A number of different film products were obtained for the Study Area, including single waveband black and white negatives and positives at various scales for use in a colour additive viewer, and large scale false colour composite prints for direct visual interpretation. A description of the procedures used in the interpretation of this imagery and the results obtained, are given in Chapter 4.

3.10.2 Landsat Digital Data Obtained for the Study Area

Two Landsat computer compatible tapes (CCT) were obtained from the EROS Data Centre (EDC) for January 1973 and January 1979. Since February 1979 Landsat data have been received by the NASA controlled GSFC ground receiving station and converted into digital form on high-density tapes (HDTs) by the Image Processing Facility (IPF) at the Goddard Space Flight Centre. The HDTs are converted to customer products by the EROS Data Centre Image Processing System (EDIPS). The geometric and radiometric corrections that are applied to the data during EDIPS processing are described in detail by Holkenbrink (1979), in the Landsat Data Users Handbook (USGS, 1979) and various editions of Landsat Data Users Notes.

3.10.3 EDC Processing of Landsat Data

Landsat imagery suffers from inherent systematic and non-systematic sources of geometric error, and does not therefore represent a distortion-free map of the earth's surface.

Systematic sources of geometric error, including earth rotation, variations in space-craft altitude, non-linear mirror sweep velocity, detector to detector sampling delay and

band-to-band offset (Holkenbrink, 1979) are therefore corrected during EDIPS processing. Scan line lengths are equalised, and the image array 'skewed' to compensate for earth rotation beneath the satellite track.

Non-systematic and therefore largely unquantifiable sources of geometric error, which include variations in spacecraft pitch, yaw and attitude, are also corrected for during EDIPS processing. Image data are transformed to a specific map projection, usually Universal Transverse Mercator (UTM) or Hotine Oblique Mercator (HOM), that matches spatial relationships on the earth's surface. The transformation is based upon a digital 'warping' procedure which involves cubic convolution resampling to fit the uncorrected image array to a corrected image array defined by user selected ground control points. During this transformation, pixels are resampled from the nominal 79 m x 56 m to square pixels measuring 56 m x 56 m. Pre-EDIPS Landsat imagery have not been fully corrected and transformed to a specific map projection. The geometric correction applied to the two Landsat scenes obtained for the study are described in sub section 3.11.1.

All Landsat scenes have been radiometrically corrected for temporal variations in sensor gain and offset using data obtained from the satellites internal calibration lamps. A major source of radiometric error in Landsat MSS image data lies in the poor calibration between the six sensors for each band which produces 'striping' in the image. This is caused by a number of factors, but most importantly by mismatch of spectral response between sensors (Slater, 1979). The amplitude of systematic noise introduced by such radiometric errors varies from scene to scene, but can be estimated by an analysis of the separate sensor histograms and corrected for using a histogram equalisation technique (Rothery, 1982). The technique used for destriping the Landsat scenes used in the study is described in sub section 3.11.2.

A further major source of radiometric error in Landsat MSS data is caused by atmospheric effects between sensor and target and between sun and target. The former is an additive effect and adds an extraneous path radiance component to image brightness values, whilst the latter is a multiplicative effect which attenuates radiation arriving at the surface. Such differences in atmospheric conditions can occur within a single scene, between adjacent scenes or between multi-temporal scenes.

Scattering, which is the most significant of these two effects, occurs when radiation is reflected or refracted by particles in the atmosphere which may range in size from molecules of constituent gases to dust particles and large water droplets. Rayleigh scatter is the most common phenomenon and is inversely proportional to the fourth power of the

wavelength (λ^{-4}). Thus, shorter wavelengths are much more affected by scatter than longer wavelengths. Scattering increases scene brightness with a resulting loss of contrast by adding a 'skylight' path radiance term to the recorded signal. The effect of this can be seen from radiance values (DN) sampled in the four Landsat wavebands over deep water (>25m) in Lake Turkana (Table 3.6). Deep water absorbs all incident light and under conditions of no scatter should return zero radiance values. In fact the mean values from 100 pixels for the 1979 scene are 14.2 in MSS 4; 8.9 in MSS 5; 2.9 in MSS 6 and zero in MSS 7. In the 1973 scene the path radiance term is almost double the term for the 1979 scene. A user may order a CCT from EDC and specify an atmospheric correction. The algorithm for atmospheric scatter compensation performs a simple bias on each pixel value. An offset grey level (equal to the amount of haze in the band), is established for each spectral band, and subtracted from each pixel value. No atmospheric scatter correction was applied to the EDIPS scene used in this study, and no correction was applied during preprocessing of the two scenes acquired for the study (Section 3.11). The problem of differences in scene brightness is discussed in Chapter 7.

TABLE 3.6 REFLECTANCE VALUES (DN) IN FOUR LANDSAT WAVEBANDS SAMPLED OVER DEEP WATER IN LAKE TURKANA FOR 1973 AND 1979

June 1979					January 1973			
	MSS4	MSS5	MSS6	MSS7	MSS4	MSS5	MSS6	MSS7
	12	7	1	0	26	14	7	4
	15	8	2	0	25	14	9	4
	13	9	2	0	28	15	9	2
	13	8	2	0	27	14	8	2
	18	11	11	0	31	15	9	2
	17	11	4	0	27	14	9	4
	13	8	1	0				
	14	9	0	0				
	13	9	2	0				
Mean	14.2	8.9	2.9	0	Mean 27.3	14.3	8.3	3.0

The unique orbit of Landsat causes the spacecraft to pass over the same point on the earth at essentially the same local time every 18 days. Even though local time remains the

same, changes in solar elevation angle cause variations in sun illumination and therefore scene brightness. Sun elevation and azimuth angles for a particular scene are contained within the header records of the CCT. The sun elevation angles for the 1973 and 1979 scenes covering the Study Area are almost identical and no correction for differences in sun angle was therefore required:

CCT	Sun Angle	Sun Azimuth
31 January 1973	48°	120°
02 June 1979	048°	059°

3.11 PREPROCESSING OF THE LANDSAT DATA OBTAINED FOR THE STUDY AREA

Despite the first order geometric and radiometric corrections which are applied to Landsat data at the EROS Data Centre, the data usually require additional processing prior to analysis by the user. The processing procedures applied to the two Landsat scenes obtained for the Study Area are described in the following sub-sections.

3.11.1 Geometric Correction of Landsat Data

To enable multi-temporal comparisons to be made between the 1973 and 1979 scenes and for spatial comparisons to be made between both images and map information, it was necessary to transform the two scenes to a common projection.

The first step was to transform the 1979 EDIPS scene to a UTM projection. Initially, 21 evenly distributed GCPs (Ground Control Points) were selected within the Hedad subscene and located on the 1:100 000 scale topographic map. The GCPs are used to define the UTM output matrix to which the uncorrected image matrix is to be fitted. Rock outcrops and other sharply defined features which could be identified on both the Landsat image and map were used as GCPs. The longitude and latitude of each GCP was measured from the topographic map and converted into pixel line and sample coordinates within the subscene. A least-squares fit was then performed between the line and sample coordinates of the output matrix and their corresponding coordinates in the input matrix, to determine the error in pixels between all pairs of GCPs. Two pairs of points which displayed large errors were discarded. The average error, which is indicative of the maximum possible positional error following the transformation, from 19 pairs of GCPs was 1.9 pixels (Table 3.7). An average error of less than one pixel would have been preferable, but due to the problem of locating common points on map and image and measuring longitude and latitude from the small scale maps available, this was not attained. The transformation of the 1979 Landsat scene to a UTM projection was performed using cubic convolution resampling. The sin x/x form of a cubic

convolution function yields more satisfactory results in terms of original image spatial resolution and radiometric fidelity compared to nearest neighbour and bi-linear resampling (Rifman, 1973). A similar procedure was used to warp the 1973 Kargi scene to the 1979 scene, with the corrected 1979 scene defining the output matrix. A pixel positional error of less than one pixel was achieved for this scene to scene multitemporal registration due to the relative ease of choosing common GCPs on the two Landsat scenes.

TABLE 3.7 GEOMETRIC CORRECTION OF IMAGE DATA; RESULTS FROM LEAST SQUARES FIT BETWEEN INPUT AND OUTPUT MATRICES DEFINED BY GCPs

GCP No.	Pixel error
1	1.32
2	1.44
3	0.89
4	1.10
5	1.48
6	0.80
7	3.86
8	0.12
9	4.20
10	5.24
11	3.68
12	0.90
13	1.70
14	2.37
15	0.76
16	1.22
17	0.97
18	2.04
19	1.63
Average Error	1.9

3.11.2 Radiometric Correction of Landsat Data

The radiometric 'sixth-line striping' which is apparent on Landsat imagery, was removed during analysis of the two Landsat scenes using a 'destripe' function in the image analysis system. This technique is a specialised form of spatial filtering, and by averaging the error between the six adjacent scan line considerably improves the appearance of the image.

CHAPTER 4

THE INTERPRETATION OF LANDSAT FALSE COLOUR COMPOSITE IMAGERY

The effectiveness of a visual interpretation of false colour composite imagery for mapping semi-arid vegetation in the Study Area is evaluated.

4.1 INTRODUCTION

Landsat false colour composite imagery has been extensively used for land resource mapping (Dunford et al., 1983), particularly within humid tropical regions where vegetation cover is high. In this chapter a visual interpretation of false colour imagery for mapping semi-arid vegetation of low cover is evaluated within the Study Area.

The advantages of using false colour imagery for land resource mapping are related to its low cost compared with digital data and in the ease of interpretation. The cost of a single Landsat false colour print at 1:250 000 scale from the EROS Data Centre (EDC) is US$ 195 from an existing colour composite negative, compared with US$ 730 for a computer compatible tape (CCT)[1]. The analysis of CCT data also requires the use of a computer-based image analysis system, and specialist knowledge for its operation and in the interpretation of results.

The majority of developing countries in Africa cannot afford the high cost of a digital image analysis system and do not generally have earth resource scientists with training in the digital analysis of Landsat data. By contrast, a Landsat false colour image can be produced optically using relatively low-cost equipment, and can be analysed in the field using easily acquired visual interpretation techniques.

False colour imagery is produced by combining the spectral information in any of the three Landsat wavebands into a single image, and assigning either a blue, green or red filter to each channel. In a standard false colour image, blue is assigned to Landsat MSS4, green to MSS5 and red to MSS7. In this colour filter/waveband combination healthy green vegetation appears red, bare soil blue/green and water black (Lillesand and Kiefer, 1979) to produce an image which is similar in appearance to a colour infra-red air photograph.

1. EDC prices effective February 1st, 1985.

The combining of spectral channels considerably improves the interpretability of an image compared with a single waveband image. The eye can distinguish subtle differences in any of the three visual coordiantes (hue, saturation, intensity) in a multispectral natural, false or pseudocolour image. On a panchromatic image intensity is the only parameter available for discriminating features of interest, and this effectively reduces its information content (Lamar and Merifield, 1973). For this reason the eye is only able to differentiate 16 tones of black and white image, but many more on a colour image.

Two types of Landsat false colour composite imagery were interpreted and compared within the Study Area:

(a) A 1:250 000 scale false colour composite image for June 1979 obtained from the EROS Data Centre (EDC).

(b) Single Landsat waveband positives at 1:1 million scale optically combined into false colour imagery using the I^2S Colour Additive Viewer at Hunting Technical Services Limited.

High quality false colour Landsat scenes for East and Central Africa can now be obtained from the Regional Remote Sensing Facility in Nairobi, but unfortunately it was not possible to obtain such imagery for the Study Area.

4.2 INTERPRETATION OF EROS DATA CENTRE FALSE COLOUR COMPOSITE IMAGERY

The June 1979 EDC false colour image was interpreted according to spectral colour and pattern. The rationale behind the interpretation was based upon the analysis of a colour triangle. This was produced in a digital image analysis system by superimposing three grey scale wedges in blue, green and red at 120 degree orientation to each other. Each grey scale wedge contained 64 brightness (grey) levels. The colour triangle is illustrated in Figure 4.1 with the spectral tones which correspond to vegetation and soil classes on the false colour image marked on the figure. The apex of the colour triangle represents healthy green vegetation with a high MSS7 reflectance (red), whilst the base of the triangle represents different soil types displaying high MSS4 reflectance (blue) and high MSS5 reflectance (green).

The majority of the scene displays a spectral tone similar to the zone marked A on Figure 4.1. In these areas the vegetation cover is too sparse and non-green to give a spectral response which is indicative of healthy, green vegetation.

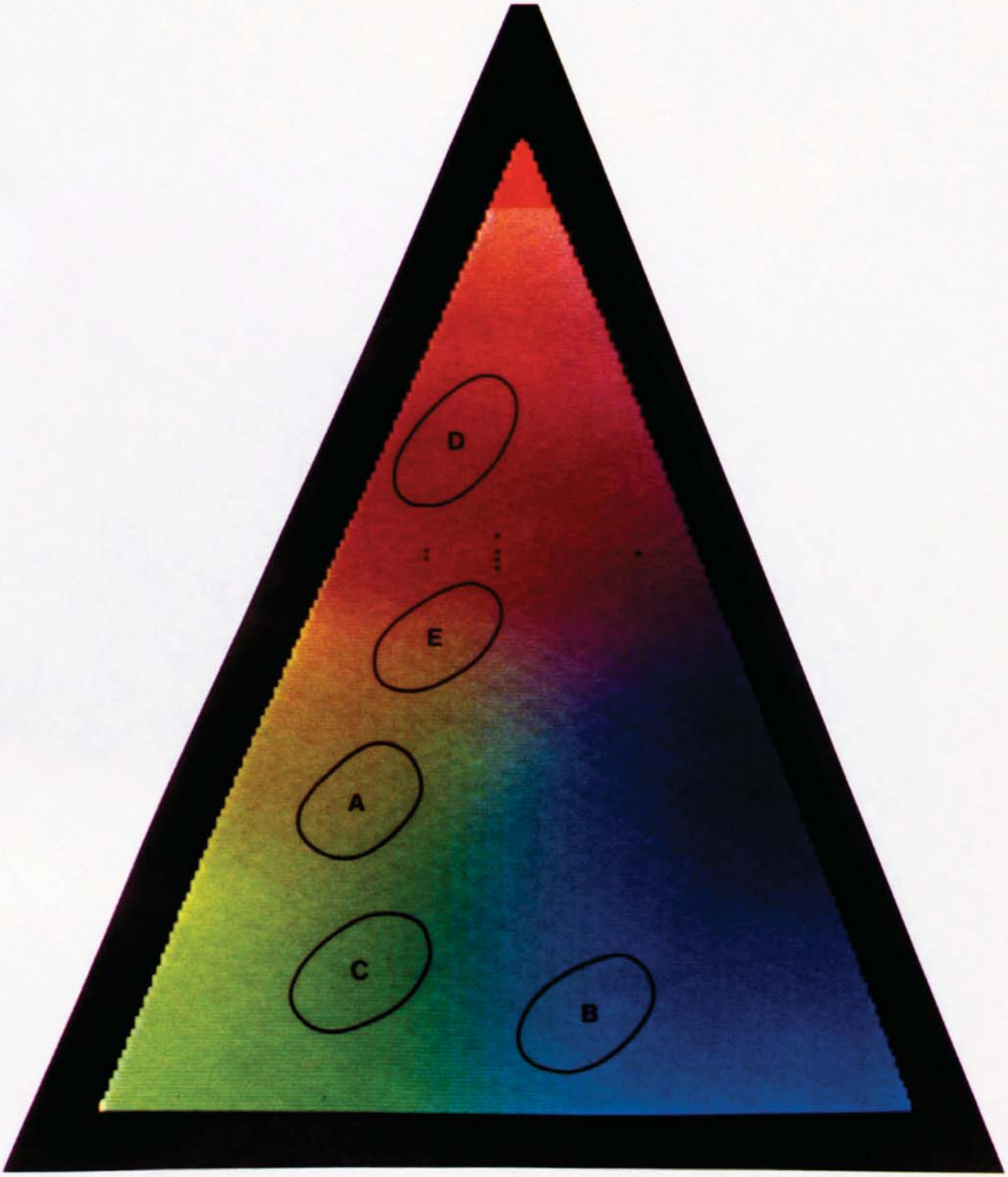

Figure 4.1 The Colour Triangle used to assist in the Interpretation of False Colour Imagery

Some areas of the saline Chalbi desert are distinctively blue in tone on the image and correspond to the zone marked B on the colour triangle. Outcrops of lava appear green and correspond to C on the colour triangle. Isolated patches of bright red tones, which are indicative of a dense, green vegetation canopy, can be seen on the image near the base of lava outcrops where soil moisture content is higher than for other parts of the Study Area. These bright red tones correspond to the zone marked D on the colour triangle. Other more extensive areas of a duller red tone suggesting a green vegatation canopy of lower density can also be seen on the image. These duller red tones correspond to the zone marked E on the colour triangle.

A section of the original EDC false colour image and accompanying interpretation is reproduced in Figure 4.2. Using the colour triangle classification only two vegetation types, green *Acacia tortilis* woodland and dense *Acacia reficiens* shrubland, could be positively identified from the imagery. Mature *Acacia tortilis* and associated *Salvadora persica* trees remain green even during the dry season. *S. persica* is an evergreen whilst *A. tortilis* is able to utilise groundwater at the base of the flood basalts to continue growth during dry conditions. The distribution of these two vegetation classes is shown on the vegetation map (Figure 3.1).

Increased water availability also favours the development of a dense canopy of non-green *Acacia reficiens* shrubland. In some areas this dense vegetation type can only be identified on the basis of pattern because its spectral response is indistinguishable from dark bare soil. Thickets of dense shrubland fringe ephemeral water courses and the resulting linear patterns enable this category to be separated from bare soil of similar spectral tone. In other areas the closed canopy of shrub thicket also masks a bright reflectance from the soil, thus reducing the amplitude of reflectance and producing a marked spectral contrast between the shrub cover and surrounding bright soil.

Apart from dense shrubland and green woodland it appears that the distribution of shrub and dwarf shrub vegetation types which cover the majority of the Study Area, cannot be identified on false colour imagery. The canopy cover of much of the vegetation within the Study Area is too low for the vegetation to be discriminated from bare soil, and not green enough to appear distinctively red.

In a study of ephemeral and perennial rangeland vegetation, with a canopy cover of less than 20 per cent, Bentley et al., (1976) showed that in many cases vegetation classes could be mapped on the basis of their association with soil type. This association between soil type and vegetation community has also been observed by Hellden (1979) in Kenya, and was used by Hunting Technical Services Limited (1974) to map vegetation in the


CHALBI
DESERT
KULAL
LAVA
BALESA
LAVA
SPARSE
SHRUB
COVER
KARGI
HEDAD
MEDIUM SHRUB
COVER
LAVA
Green Acacia woodland
Very dense Acacia shrubland

Figure 4.2 The False Colour Image for the Hedad Study Area with an Interpretation Overlay showing the Distribution of *Acacia* Woodland and dense shrubland (Part of Landsat scene path 181/row 058 - June, 1979)

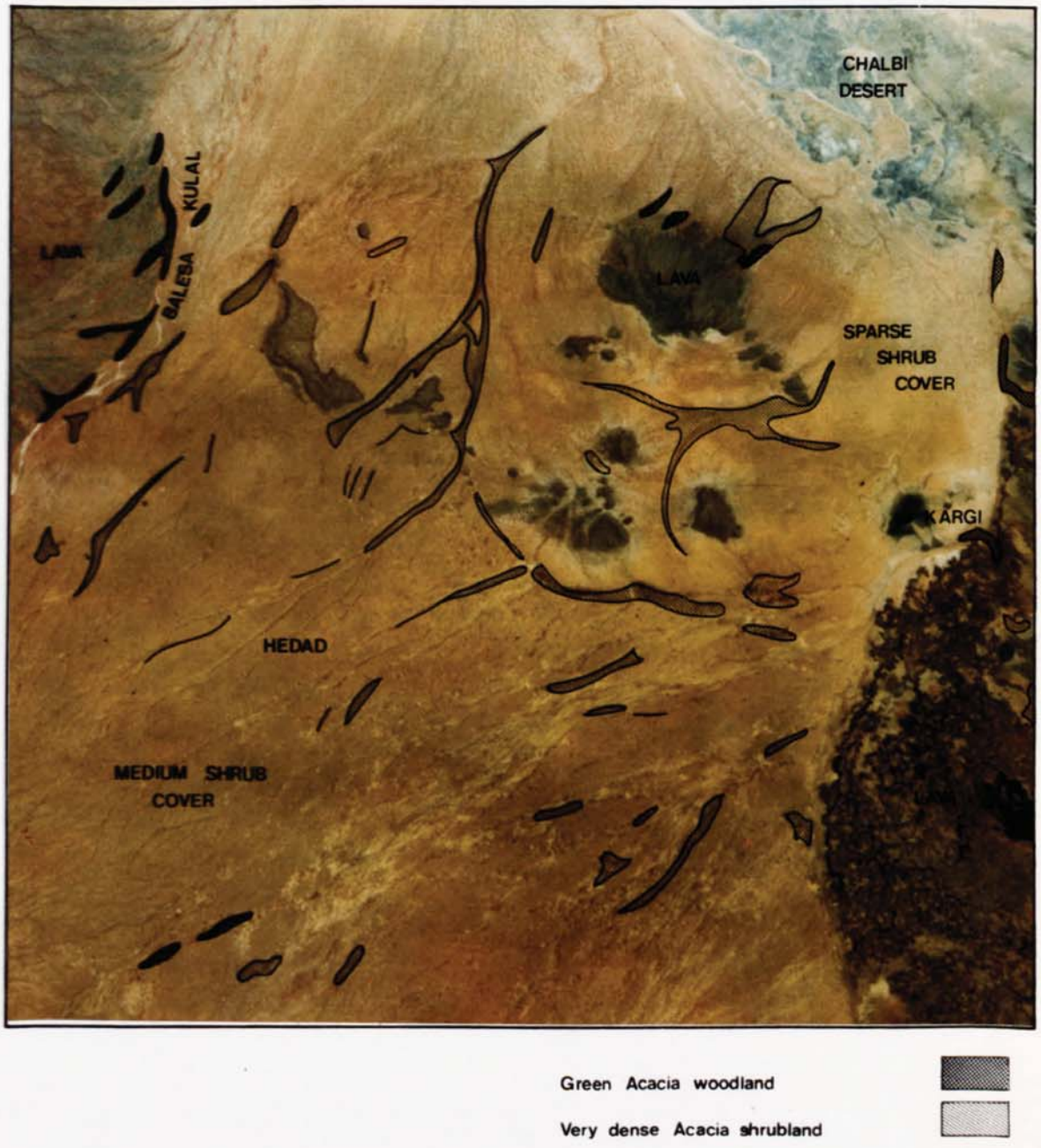

Figure 4.2 The False Colour Image for the Hedad Study Area with an Interpretation Overlay showing the Distribution of *Acacia* Woodland and dense shrubland (Part of Landsat scene path 181/row 058 - June, 1979)

Western Savannah region of the Sudan. Using detailed ground data about the type of vegetation community associated with a particular soil type Hellden, (1979) was able to map forest, woodland, dense bushland, bushland and bush grassland, grassland and riparian vegetation with a reasonable degree of accuracy.

However, Hellden, (1979) observed that a specific vegetation class could appear in completely different colours on the same Landsat false colour image depending upon the soil background reflectance. Mapping of broad vegetation types on the basis of their association with a particular soil type therefore requires very detailed information about the spectral response of soils within a region and the soil types favoured by different plant species.

In order to investigate the possibility of mapping the distribution of vegetation within the Study Area on the basis of its local correspondence with soil type, a visual comparison was made between the soil and vegetation map derived from the air photography (Appendix B).

In an area where water for plant growth is scarce, differences in the permeability of the soil strongly influences the distribution of vegetation types (Herlocker, 1979). In particular sandy soils, because of their high permeability, have less surface run-off than silty soils, thereby allowing water to penetrate deeper into the soil. This gradient of decreasing soil moisture potential occurs within the Study Area where there is a transition from lava-derived clayey soils to sandy-loam soils, and results in a transition from a sparse dwarf shrubland community of short, shallow-rooted plants to a denser and taller shrub community of deeply rooted plants (Noy-Meir, 1974). Other characteristics of the soil in addition to soil moisture properties,also appear to be important determinants of plant cover within the Study Area.

For example, there is a distinctive change in soil type from the paleo-dune soils north of Kargi to the sandy-loam soils covering much of the Study Area, this being associated with a marked change in vegetation from sparse, dwarf shrubland to denser shrubland. In other areas along water courses and in zones of water accumulation, alluvial processes have sorted out the finer silt fraction and redeposited it as a silty-loam soil type supporting a dense shrubland community. At the base of lava outcrops the products of erosion fan outwards to produce a coarse, stony surface which supports only a sparse canopy of vegetation. It appears that there are a number of factors, including soil permeability, geomorphology, drainage and soil parent material which determine the density and species composition of a particular vegetation community. A comparison between the soil and

vegetation maps (Appendix B) suggests that differences in soil type are in some areas associated with a change in the canopy cover and species composition of a vegetation type. In these areas it is possible to identify different vegetation types on the basis of their association with a particular soil type. However, in other areas the lack of association between soil and vegetation suggests that additional factors other than differences in soil type determine the distribution of vegetation within the Study Area.

In an attempt to isolate these factors an interpretation of the Landsat false colour image was compared with the soil map at 1:250 000 scale. Due to a difference in scale between the two maps, the comparison was made with a Zoom Transferscope. This instrument enables a map, image or air photograph of a smaller scale to be transferred to a base map at a larger scale. In this case the smaller scale false colour interpretation was transferred onto the larger scale soil base map. A comparison between the false colour interpretation and soil map clearly shows that not all the spectral variation within the image can be accounted for by mapped differences in soil type.

Siegal and Goetz, (1977) show that for a dry, non-green sage bush vegetation type in Arizona a vegetation canopy as low as 10 per cent can modify soil reflectance, the magnitude of the effect being related to the type of vegetation and the background soil response. McCoy and Watt (1978) show that there is a marked increase in reflectance as vegetation cover decreases and a shift from a typical green vegetation response representing high density cover towards an increasing similarity to the bare soil spectral curve. This concept is explored in further detail in Chapter 5.

A comparison between an interpretation of the false colour image (Figure 4.2) and the vegetation map (Appendix B) shows that the amplitude of soil reflectance is also modified by the vegetation cover within the Study Area. It is argued that variations in vegetation canopy cover are responsible for much of the observed spectral variation on the false colour image. However, it is not possible on the image to identify the difference in spectral tone between bare soil and bare soil modified by a non-green vegetation cover in a region where reflectance is a combined response from both soil and vegetation.

4.3 COLOUR ADDITIVE VIEWER

An attempt was made to evaluate whether different combinations of spectral bands and colour filters could be used to improve discrimination between vegetation types of varying canopy cover and species composition. An I^2S (International Imaging System) colour additive viewer, loaned by Hunting Technical Services Limited, was used to produce various combinations of spectral bands and colour filters; true colour, false colour and

pseudocolour. By registering any combination of three single waveband MSS positives together in the viewer and assigning each waveband to a different colour filter, it is possible to produce a colour composite image which is optimal for vegetation discrimination.

The 1:1 million scale single waveband positives for the whole Landsat scene were used to enable the Study Area to be viewed at an enlarged 1:150 000 scale. Those spectral band/colour filter combination which appeared to be most successful for vegetation discrimination were interpreted and compared with the interpretation from the EDC false colour image (Figure 4.1).

The results obtained from the colour additive viewer were disappointing, despite the enlarged scale (1:150 000) and possibility of changing the waveband to colour filter combination. Less information could be derived from this imagery than from the EDC 1:250 000 scale colour composite, largely because of misregistration between the three separate waveband positives. At this enlarged scale the line mismatch along feature boundaries on the image reduced image interpretability. The EDC false colour image is derived from digitally contrast-stretched image data resulting in a much brighter, more interpretable image than could be obtained from the colour viewer (USGS, 1979).

Other workers (Anderson, 1983; Falconer, pers. comm.) have successfully used optical techniques to enhance Landsat imagery. In terms of brightness and contrast this imagery compares favourably with digitally enhanced false colour imagery and is cheaper to produce.

4.4 SUMMARY

Only two types of vegetation, green *Acacia* woodland and dense non-green shrubland could be accurately mapped from the false colour imagery. The use of false colour imagery for mapping a sparse and generally non-green rangeland vegetation within the Study Area appears to be limited. However, some qualitative insights into the relative difference between the spectral curves for vegetation and soils was obtained from the imagery. Figure 4.3 is a diagrammatic representation of the spectral curves for dark-toned lava, dense shrub, sparse shrub, green vegetation and bright bare soil. Discrimination between bright bare soil and sparse shrub, and between dense shrub and lava is difficult; these categories are differentiated only in terms of the amplitude and not frequency of reflectance. Conversely, green woodland is separable from bare soil in at least one Landsat waveband due to differences in the frequency spectra of these two categories.

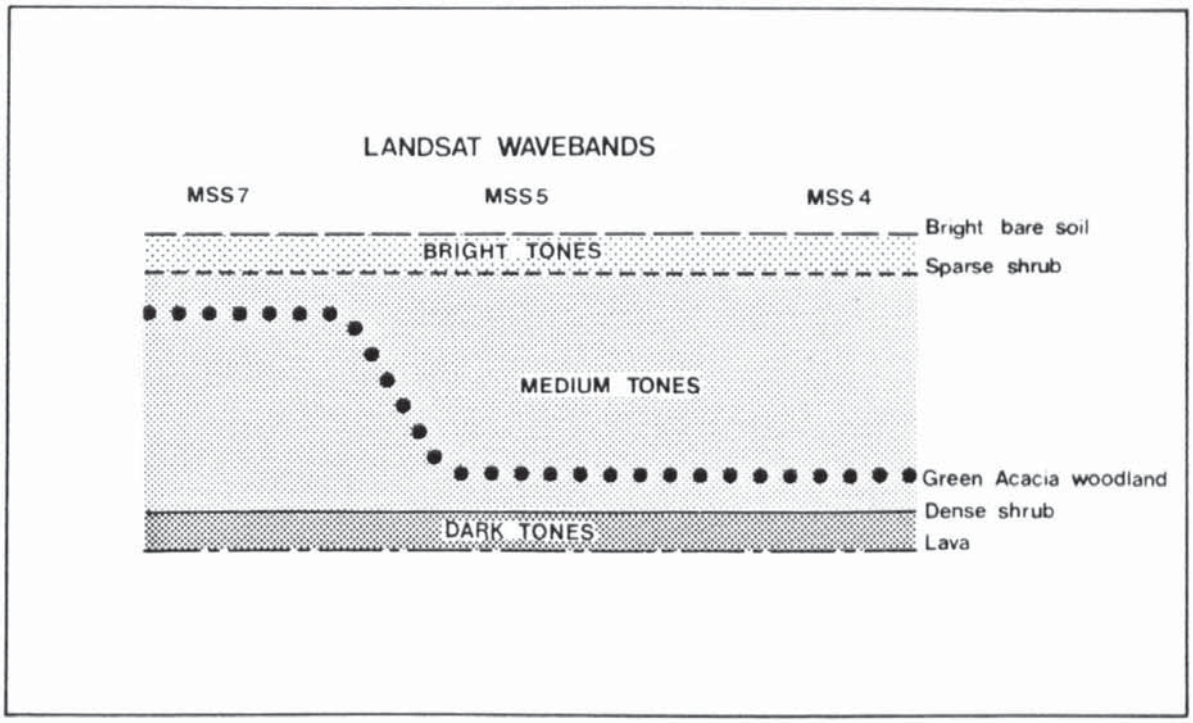

Figure 4.3 A Representation of the Spectral Curves for Lava, Dense Shrub, Sparse Shrub, Woodland and Bare Soil derived from an Analysis of Landsat False Colour Imagery

The results obtained from the visual interpretation of false colour imagery do not satisfactorily meet the objective of the study to map the characteristics of semi-arid vegetation from Landsat satellite data. This will only be achieved by gaining a precise quantitative knowledge of the spectral response of various soil types together with an analysis of the way in which vegetation modifies soil reflectance. A quantitative analysis of the spectral reflectance of bare soil, non-green vegetation and green vegetation is given in Chapter 5.

CHAPTER 5

REFLECTANCE OF SEMI-ARID VEGETATION AND SOILS

The major spectral components of the semi-arid landscape: bare soil, non-green vegetation and green vegetation are analysed and described.

5.1 THE SPECTRAL COMPONENTS OF THE SEMI-ARID LANDSCAPE

Figure 5.1 is an example of a vertical colour air photograph taken during a survey flight across the study area (Chapter 3). The survey was conducted during the dry season. Under these conditions shrub and dwarf species appear in grey on the photograph and grassland appears yellow. Following rain the general appearance of the rangeland from the air is overwhelmingly green as grassland and shrub species commence vigorous growth (H. Lamprey pers, comm.). The sandy-loam soil which is clearly visible between the shrub and dwarf plants, is a distinctively reddish colour.

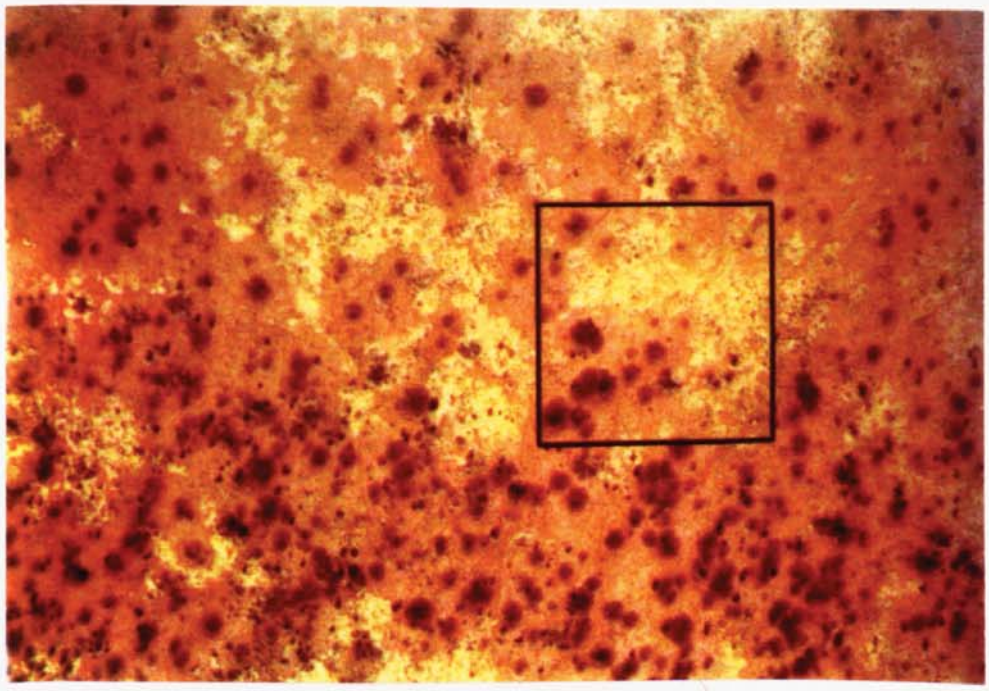

Figure 5.1 An Example of a small format Colour Air Photograph Acquired within the Study Area

The square marked on the photograph represents the area covered by a single Landsat pixel approximately 80 m square. The area covered by the pixel contains a proportion of a soil, a proportion of shrub cover and a proportion of grassland cover. Each of these types will contribute a spectral component of specific amplitude and frequency to the total reflectance from the pixel. In this chapter an attempt is made to determine the spectral contribution of each of these components to total measured reflectance.

5.2 SOIL REFLECTANCE

The 1979 Hedad subscene was dispalyed as a MSS 7/5/4 false colour image on the monitor of an interactive image analysis system. The image data was contrast stretched using an automatic linear stretch function to improve the contrast and brightness of the image. This merely uses a pre-defined ramp stretch in the look-tables (LUTs) of the processor to stretch the image histograms for all three bands to the full 8-bit data range available. Areas of bare soil, which had previously been identified on the air photographs and on the ground during fieldwork, were located on the image. These varied in size from an expanse of bare saline soil in the Chalbi desert to much smaller patches of silty-loam soil. A function on the image analysis system allows the user to place a moving cursor over any pixel within the displayed scene and record the DN (Digital Number) of the pixel in the four Landsat wavebands.

A sample of 40 bare soil pixels (DN) were recorded from the 1979 Hedad subscene and a smaller sample of 20 different bare soil pixels (DN) were sampled from the 1973 Hedad subscene (Appendix E)[1]. Very small areas of bare soil (< 10 pixels) were not included in the sample to avoid possible boundary effects from surrounding vegetated pixels.

The soil spectral curve for the Hedad 1973 and 1979 subscene is presented in Figure 5.2. Both spectral curves display low reflectance in the visible green (MSS4), and a peak of reflectance in the visible red (MSS5) and near infra-red (MSS7). The data given in Table 3.6 indicated that the 1973 scene contained more haze than the 1979 scene, and this results in the higher reflectance from bare soil in 1973 observed on Figure 5.2.

Compared with the sharp peak and valley appearance of the characteristic spectral curve for green leaves (Figure 2.1) the spectral curve for semi-arid soils in northern Kenya displays a much smoother response. The structure of soil, which is composed of mineral and organic matter surrounded by air and water, is much simpler than the complicated physiology of a plant leaf. As a result the interaction between incident sunlight and soil is

1. The size of the soil data sample was arbitrary

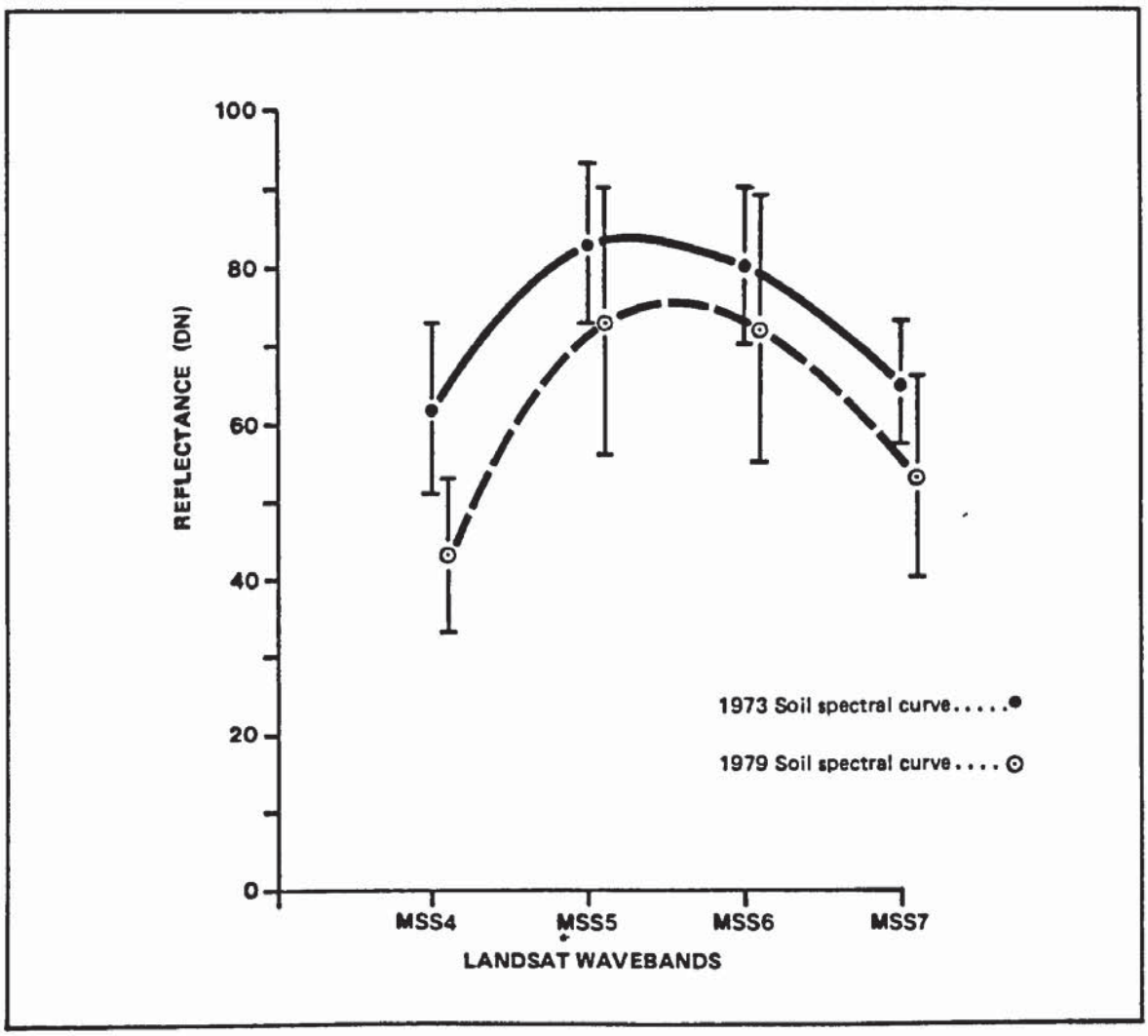

Figure 5.2 Soil Spectral Curves in the Four Landsat Wavebands for 1973 and 1979

very much less complicated than the interaction of sunlight with green leaves (Hoffer, in Swain and Davis, 1978). All sunlight incident upon a soil surface will either be absorbed or reflected from the surface, whilst in the case of a multiple-layered leaf canopy, energy is frequently transmitted and then reflected many times from lower leaf layers in the canopy. Soil reflectance is largely determined by moisture content, organic matter, iron oxide, soil particle size and surface roughness. A wet soil will have a lower reflectance than a dry soil and soil with a high humus and iron oxide content will also display a lower soil reflectance. Smooth textured soils will display a higher reflectance than rough-textured soils, whilst soils with a high proportion of silt and clay particles will have a higher reflectance than coarser, sandy soils. Other factors, including soil parent material, salt content, shadowing and soil disturbance also affect soil reflectantance. Otterman, (1981) suggests that crumbling of the surface in over-grazed areas of the Sinai desert results in a very sharp increase in surface albedo by up to 60 per cent in some areas as measured by Landsat. These and other influences combine in a complex inter-relationship to give the characteristic spectral curve for a particular soil.

No attempt has been made to explain in physical and chemical terms the shape and amplitude of the soil spectral curve for the Study Area. A comparison of the spectral curves for bright sandy-loam soil and dark lava outcrop within the Study Area with soil spectral curves derived for similar soils by Condit, (1970), Bentley et al., (1976), Hielkema, (1980) and Graetz and Gentle (1982), show similarities in functional form; an increase in reflectance with an increase in visible wavelength and a levelling-off or drop in reflectance in the near-infrared wavelengths (Figure 5.3).

The very high reflectance in MSS5 and MSS6 of sandy-loam soil within the Study Area is related to the reddish colour of this soil type clearly visible on Figure 5.1. The ratio of humus to iron oxide is an important determinant of soil reflectance (Manual of Remote Sensing, 1983). For a low ratio, spectral curves have a distinct maximum in the red spectral zone because the iron oxide colour dominates. This appears to be the cause of the anomolously high reflectance in MSS5 and MSS6 of the reddish sandy-loam soils within the Study Area; humus content in a sparsely vegetated region is low and soil iron content is highly oxidised.

The characterisation of soil reflectance properties has shown that in general soil displays a much smoother response than green vegetation with a high correlation in all wavelengths. The correlation coefficient (r) for the 40 bare soil DN values sampled from the 1979 Hedad subscene is high for all waveband combinations, with the highest coefficient (0.96) between the two infrared wavebands (MSS7/5) and the lowest between the

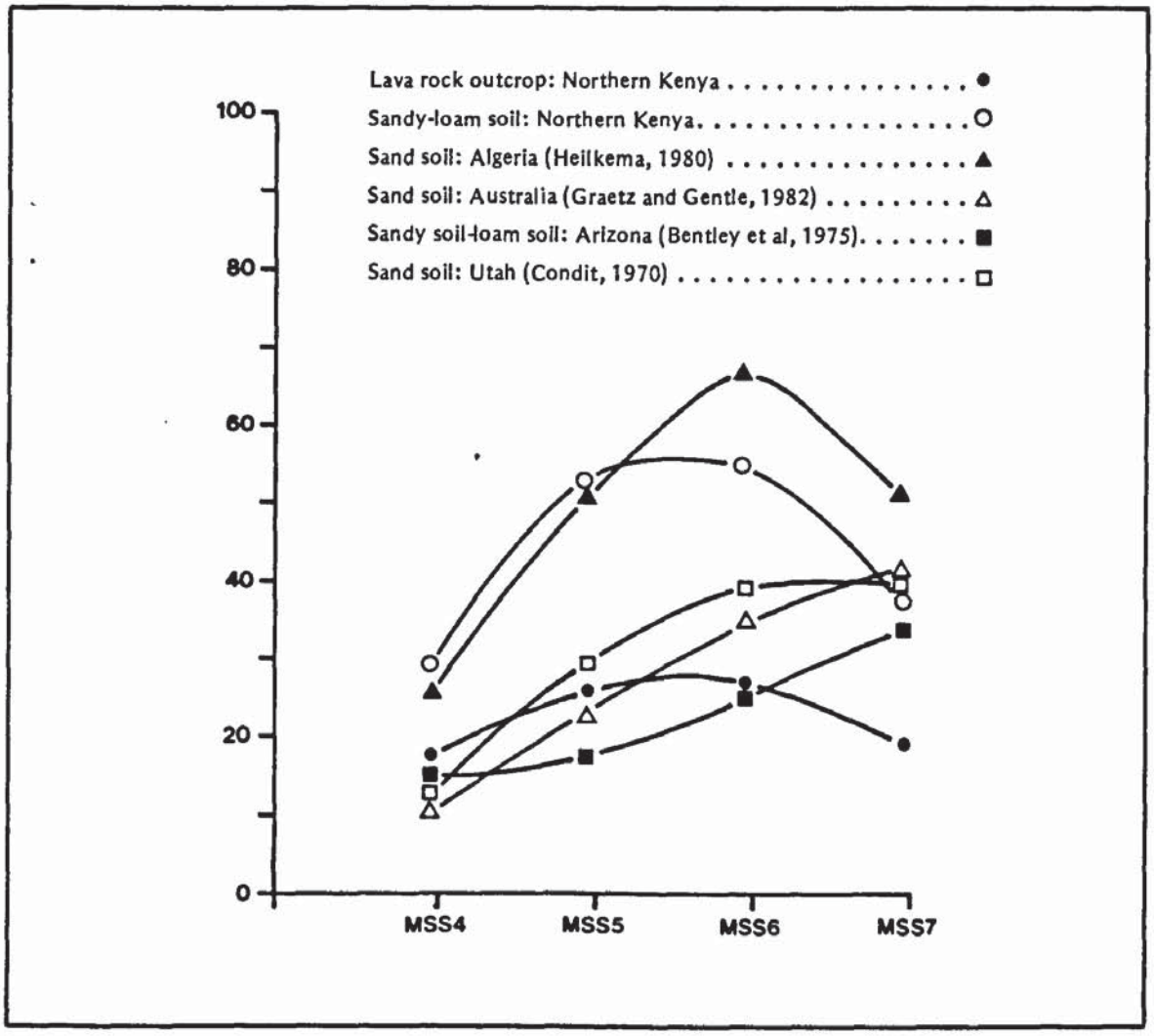

Figure 5.3 A Comparison of the soil spectral curves for the Study Area with soil spectral Curves Reported by Condit (1970) Bentley et al. (1975), Hielkema (1980) and Graetz and Gentle (1982).

near infrared and visible green wavebands (MSS7/4) (Table 5.1).

TABLE 5.1 LINEAR CORRELATIONS IN THE FOUR LANDSAT WAVEBANDS FOR BARE SOIL REFLECTANCE VALUES (DN) SAMPLED FROM THE 1979 HEDAD SUBSCENE

	MSS 4	MSS 5	MSS 6	MSS 7
MSS 4	1.00			
MSS 5	0.80	1.00		
MSS 6	0.72	0.96	1.00	
MSS 7	0.71	0.95	0.96	1.00

In order to show the distribution of bare soil DN values for various linear combinations of Landsat wavebands in the Study Area, scatterplots for all possible waveband combinations were plotted in two dimensional bivariate space and least squares regression lines fitted to the data (Table 5.2). The regression lines for each linear combination of wavebands were calculated from computer programs within the MINITAB statistical package and run on the Harris 500 mini-computer at the University of Aston. Although MINITAB does not contain the wide range of statistical programs available in other more comprehensive statistical packages e.g. SPSS (Statistical Package for the Social Sciences), its ease of use makes it ideal for simple statistical analysis. The data were plotted using the Gino graph plotting routines which are available on the Harris 500 computer and linked to a Calcomp graph plotter. The program used to plot the soil data is given in Appendix H. The scatterplots for four different waveband combinations are presented in Figure 5.4 (a, b, c, d).

The slopes for the linear regression soil lines for the 1979 subscene (Table 5.2) vary from a coefficient of 0.75 for MSS 7/5 and MSS 7/6, to a coefficient of 1.26 for MSS 5/4. These differences in slope coefficients are purely a function of soil reflectance in a particular waveband. The intercept term is small in MSS 7/5 and MSS 7/6 space, with the soil line in these two cases passing through the origin. The distribution of bare soil data in two-dimensional Landsat data space can be statistically described as a straight line. This is shown by the F values associated with each linear regression model in Table 5.3. At the five per cent level of significance ($\propto 0.05$) calculated F values all exceed the critical level. However, the goodness of fit of the linear regression model to the bare soil data measured by the correlation coefficient (R^2) varies considerably depending upon the particular waveband

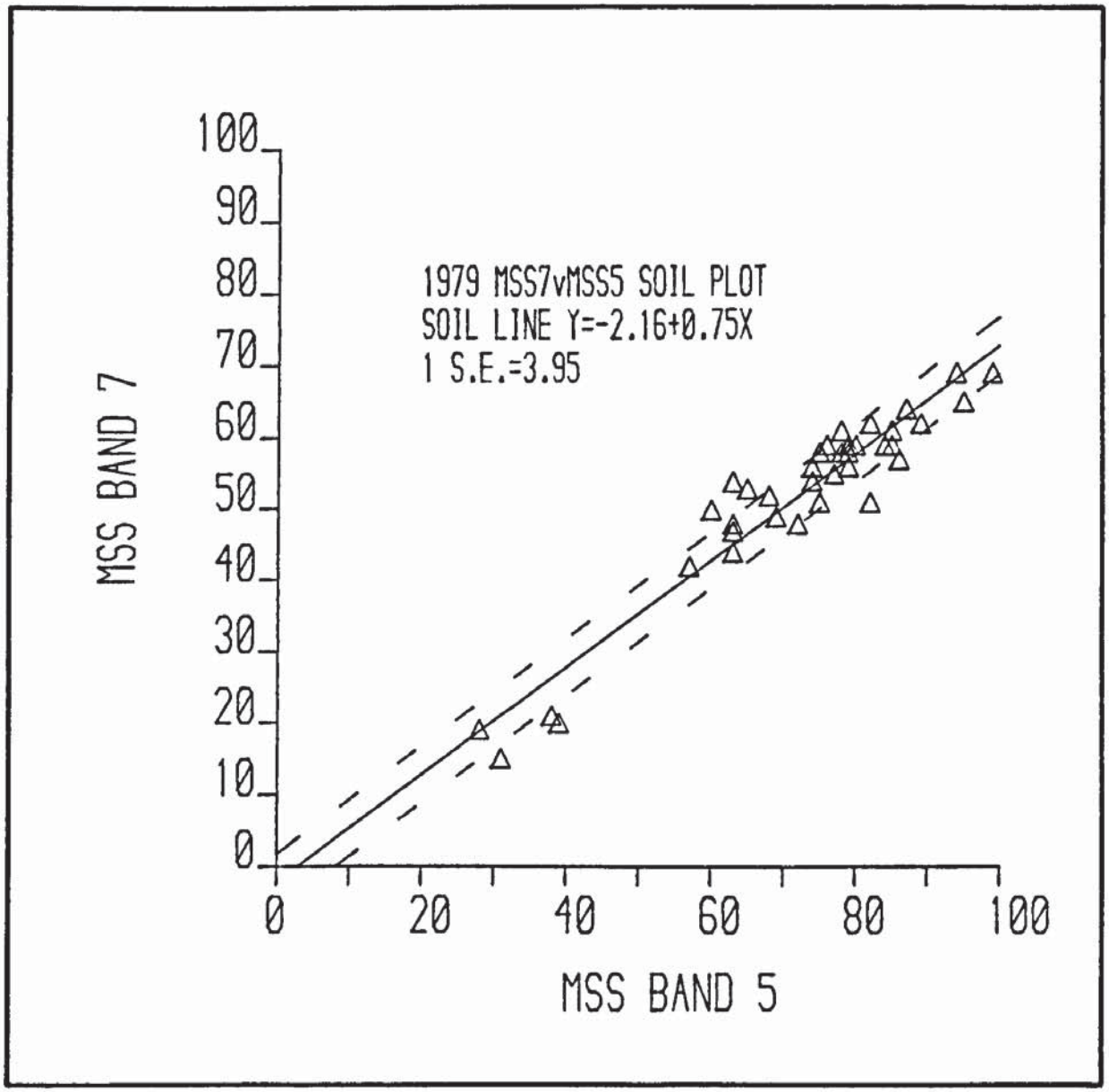

Figure 5.4 (a) The Distribution of Bare Soil Data in MSS7/5 Landsat Space

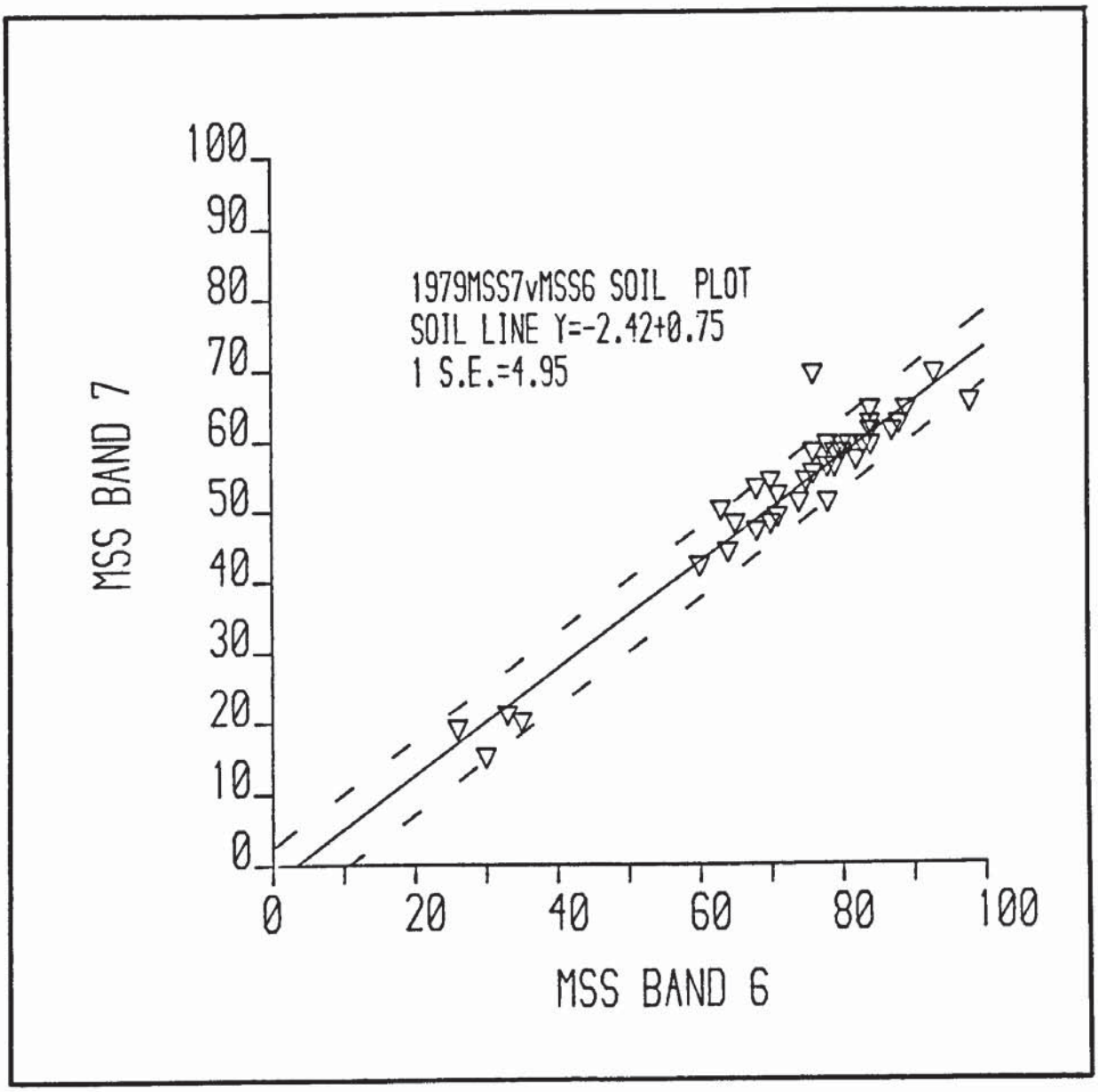

Figure 5.4 (b) The Distribution of Bare Soil Data in MSS7/6 Landsat Space

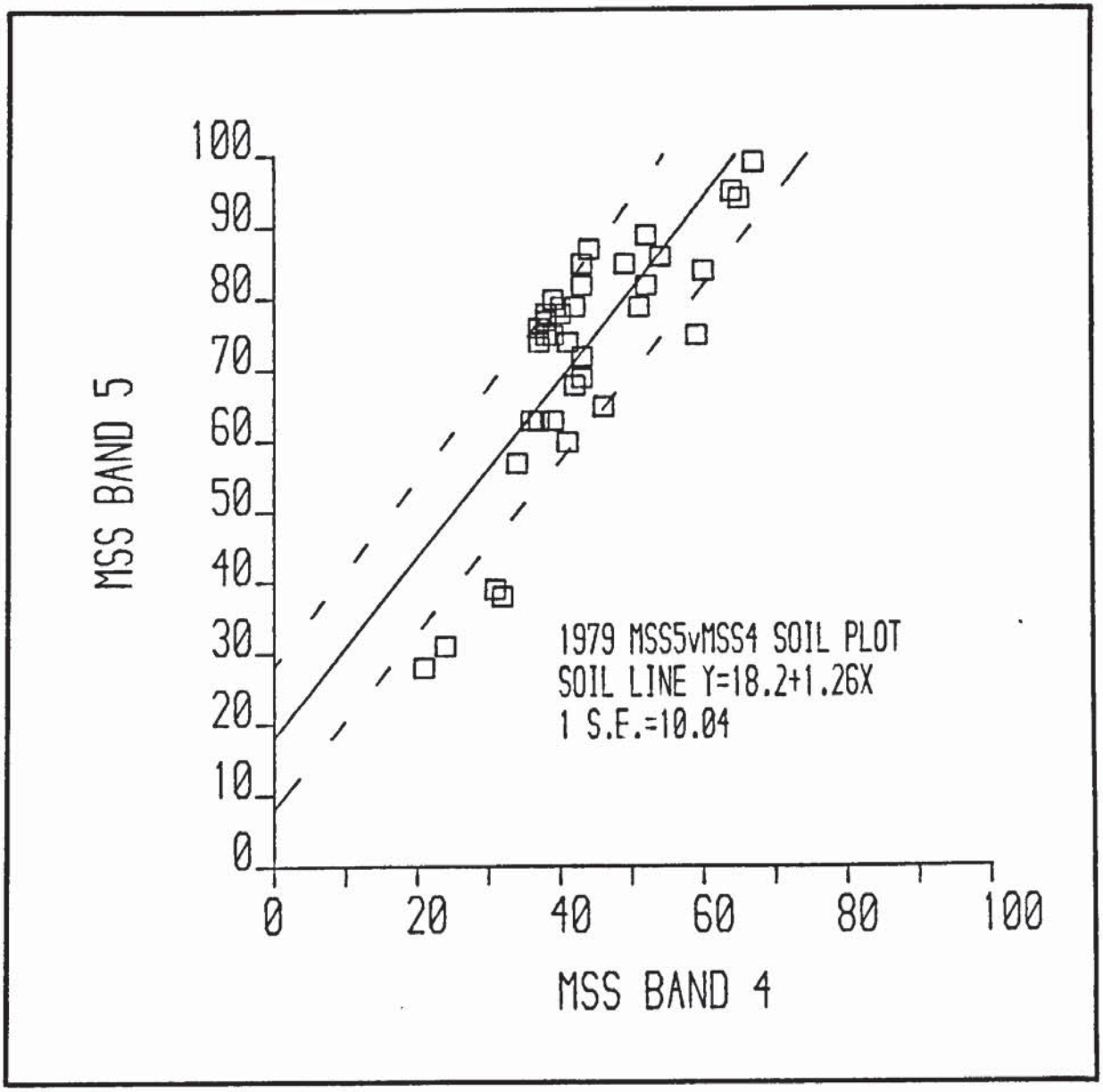

Figure 5.4 (c) The Distribution of Bare Soil Data in MSS5/4 Landsat Space

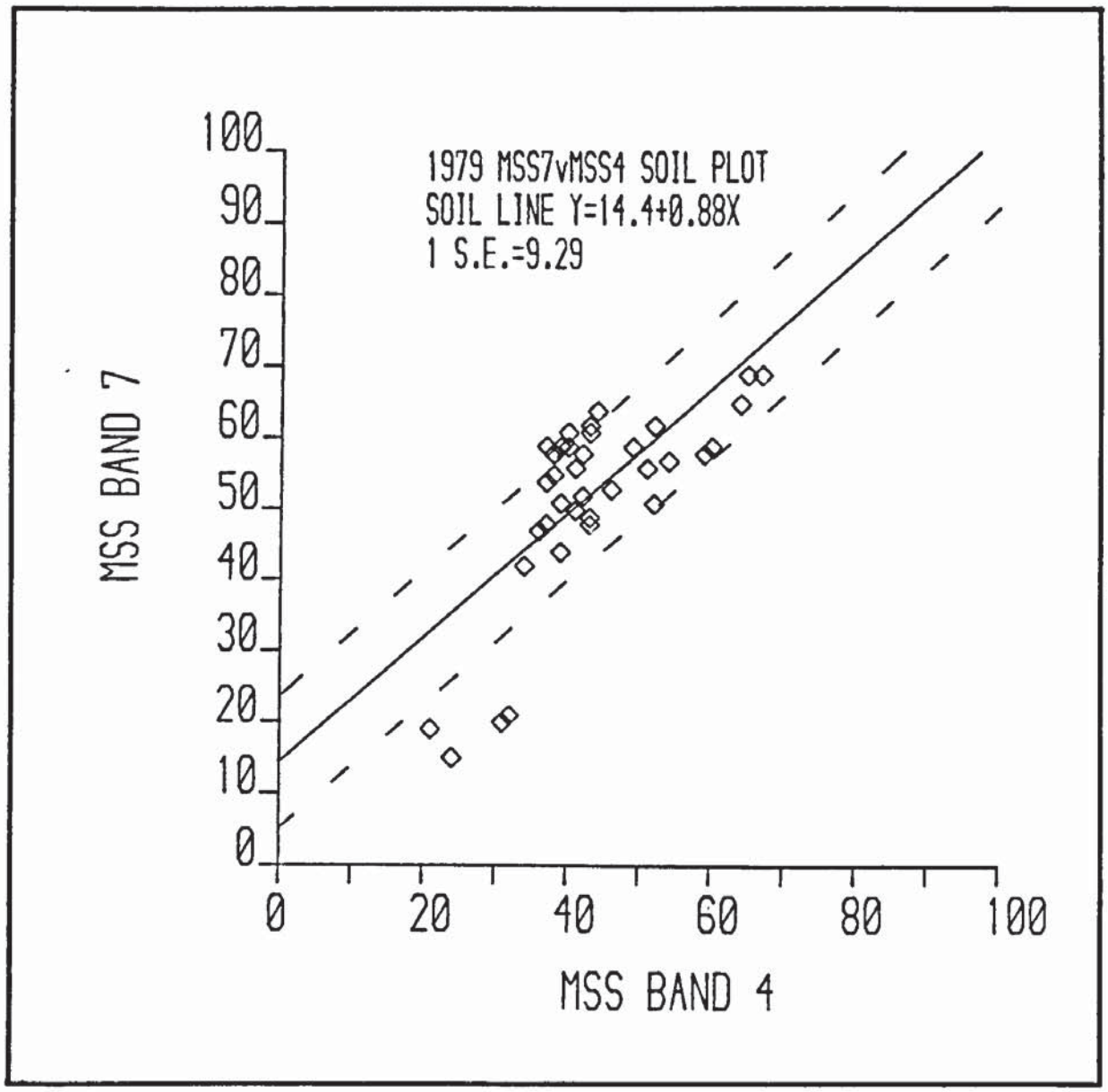

Figure 5.4 (d) The Distribution of Bare Soil Data in MSS7/4 Landsat Space

TABLE 5.2 LINEAR REGRESSION EQUATIONS FOR SAMPLED BARE SOIL DN REFLECTANCE VALUES FOR VARIOUS LINEAR COMBINATIONS OF LANDSAT WAVEBANDS IN 1979 (a) and 1973 (b) (y on x)

Waveband combination (N = 40)	Slope coefficient (y on x)	Intercept value	Standard error of estimate (S.E. of E.)
(a)			
5/4	1.26	18.20	10.04
6/4	1.13	23.90	11.81
7/4	0.88	14.40	9.29
6/5	0.97	2.71	4.77
7/5	0.75	-2.16	3.95
7/6	0.75	-2.42	4.95
(b) (N = 20)			
5/4	0.69	40.0	6.52
6/4	0.54	46.7	8.37
7/4	0.47	36.1	6.13
6/5	0.97	0.28	3.42
7/5	0.74	3.66	2.96
7/6	0.74	5.39	2.40

combination. This problem is examined in more detail in the following section on the analysis of multi-temporal soil lines. This straight line relationship accords very closely with findings by Kauth and Thomas (1976) who described the distribution of unvegetated surfaces as a line of soils in two-dimensional Landsat data space or a plane of soils in multi-channel space (Chapter 2).

5.3 MULTI-TEMPORAL SOIL LINES

Richardson and Wiegand (1977) also found that the intercept of the soil background line differed non-significantly from zero. They showed that the slope and intercept remained constant from one Landsat overpass to another, but argued that further investigations were needed to test conclusively whether the plane of soil shifts significantly

TABLE 5.3 R^2 AND F-VALUES FOR 1979 AND 1973 BARE SOIL LINEAR REGRESSION LINES. CRITICAL VALUE AT 5 PER CENT LEVEL OF SIGNIFICANCE (α 0.05) IS 4.1 FOR 1979 SOIL DATA (DF = 38) AND 4.4 FOR 1973 SOIL DATA (DF = 18)

1979 Waveband combination	R^2 Value	F Value (38 Degrees of Freedom)
MSS 5/4	63.7	69.4
MSS 6/4	50.4	40.6
MSS 7/4	49.7	39.5
MSS 6/5	91.2	439.3
MSS 7/5	90.9	390.5
MSS 7/6	90.9	390.6

1973 Waveband combination	R^2 Value	F Value (38 Degrees of Freedom)
MSS 5/4	55.3	24.5
MSS 6/4	30.3	9.3
MSS 7/4	38.2	12.7
MSS 6/5	89.0	145.2
MSS 7/5	85.5	113.4
MSS 7/6	90.4	181.1

from one study site to another or between dates. Soil line slopes for the 1973 and 1979 subscenes were therefore compared to test whether differences in soil slopes differed significantly between the two dates. Regression equations derived from the bare soil DN values sampled from the 1973 subscene were compared with the regression equations derived from the bare soil DN values sampled from the 1979 subscene (Table 5.2). From Table 5.2 the soil line slope coefficient and intercepts in MSS7/5, MSS7/6 and MSS6/5 are constant between the two dates. This is illustrated for MSS7/5 space in Figure 5.5(a). A special case of the t-statistic commonly used in time series analysis was calculated to test the hypothesis that the MSS 7/5 regression slope in 1973 (b_1) is equal to some pre-defined slope coefficient; in this case the MSS7/5 regression slope in 1979.

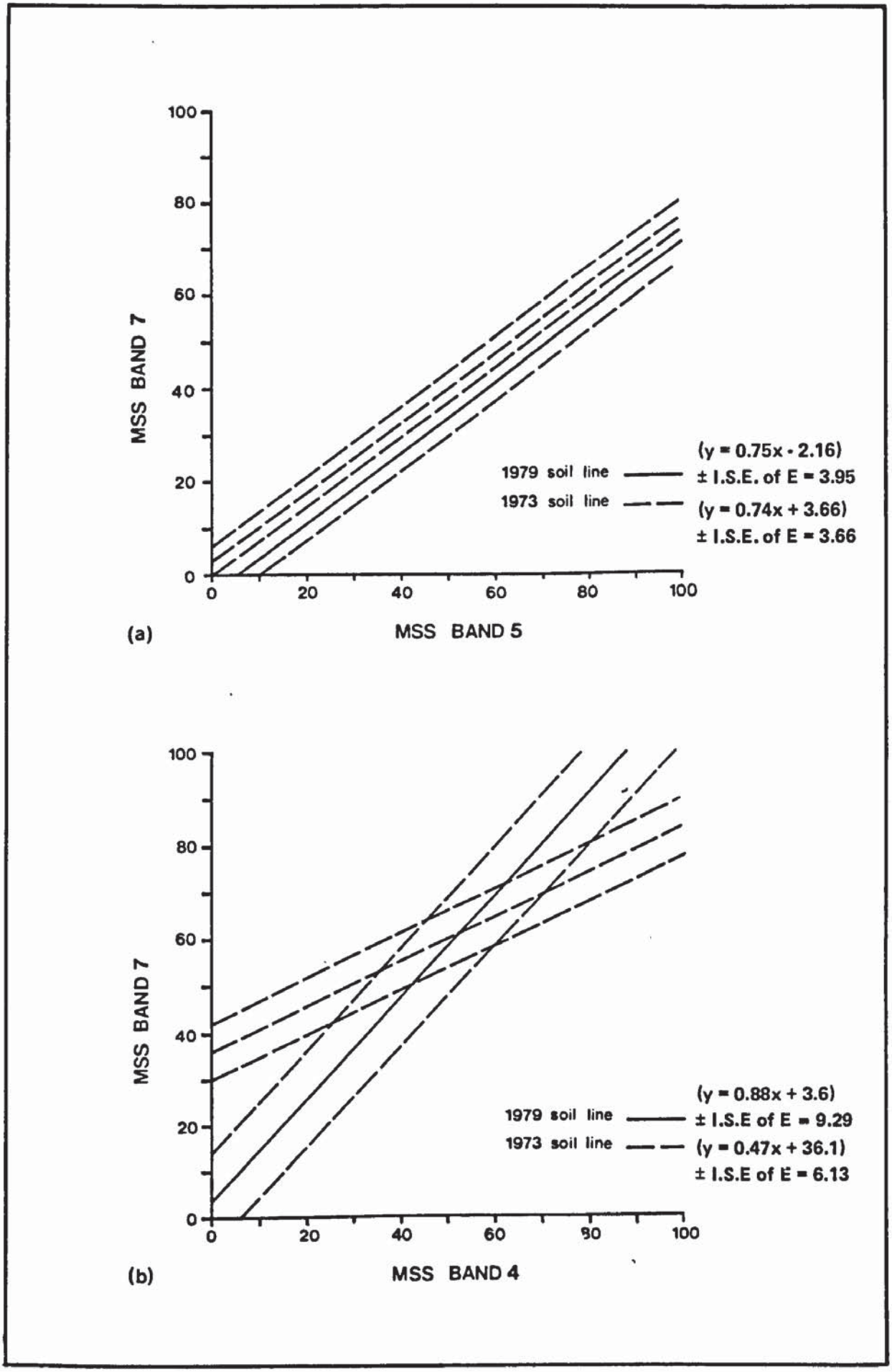

Figure 5.5 Multi-Temporal Soil Lines in MSS7/5 Landsat Space (a) and MSS7/4 Landsat Space (b)

$$t = \frac{b_1 - \beta_1}{\sqrt{MS_D/SS_X}}$$

Where: b_1 is the regression slope coefficient in MSS7/5 space for 1979, β_1 is the regression slope coefficient in MSS7/5 space for 1973, MS_D equals the mean square deviation and SS_X equals the sum of squares.

Calculated t was 0.96 which at the five per cent level of significance (α 0.05) falls within the critical region (t = 1.303); the null hypothesis that there is no difference between the 1973 and 1979 regression slopes cannot be rejected. However, in MSS7/4, MSS6/4 and MSS5/4 Landsat space the slope coefficients in 1979 are approximately twice those in 1973, suggesting a statistical difference in slope for these waveband combinations between the two dates. This is illustrated for MSS7/4 space in Figure 5.5(b). Although at the five per cent (α 0.05) level of significance all soil lines show a statistically significant trend (Table 5.3) the goodness of fit (R^2) is much higher for the MSS7/5, MSS7/6 and MSS6/5 waveband combinations than for all other waveband combinations. For example, in MSS7/6 space for the 1973 subscene the R^2 value is 90.4 i.e. 90.4 per cent of the variance in y can be explained by x, but only 38.2 in MSS7/4 space. These results suggest that the observed differences in slopes between the two dates in MSS7/4, MSS6/4 and MSS5/4 space are a function of a poor fit of the linear regression model to the data distribution, and are not necessarily caused by external environmental factors such as differences in the amount of atmospheric haze or atmospheric transmissivity.

It has so far been assumed that bare soil reflectance data describe a single, highly correlated mean soil line in Landsat MSS space. Doubt has recently been cast on the concept of a mean soil line and Jackson (1983), has shown that the slope of the soil line varies according to the soil type. In a region containing soils of varying reflectance, soil data are therefore distributed within a soils envelope in Landsat feature space. In MSS7/4 bivariate space the soils envelope is wide (Figure 5.4 (d)) and the data display a high S.E. of E. (9.29; Table 5.2) and consequently, a lower inter-band correlation coefficient (0.71; Table 5.1). The linear regression model is a much better fit to the data in MSS7/5 space where variance about the soil line is much lower than for MSS7/4 space. The regression model therefore gives a different slope coefficient for the two dates in MSS7/4 space but not in MSS7/5 space, essentially due to a poor fit of the linear regression model to widely scattered data.

5.4 REFLECTANCE OF NON-GREEN VEGETATION

Non-green vegetation is defined as vegetation which is without green foliage and therefore not actively growing, usually during the dry season. Areas of dense, non-green

predominantly *Acacia reficiens* shrub are found in shallow depressions and along water courses where water supply is plentiful (Chapter 4). Such areas of dense thicket are impenetrable to grazing livestock so that the canopy remains at or generally close to 100 per cent cover (Figure 5.6). This dense bush can be easily identified on the air photography due to its dark tone, and is marked as class 6 on the vegetation map (Figure 3.1). Areas of non-green vegetation cover were identified on a Landsat false colour image of the Kargi subscene and the reflectance values (DN) of this category were sampled in the four Landsat wavebands. A sample of 20 non-green pixels were recorded (Appendix E), to give an average reflectance value in each Landsat waveband (Table 5.4) which could be used to plot a non-green vegetation spectral curve. The shape of the spectral curve for non-green vegetation shows a close resemblance to the shape of the spectral curve for bare soil (Figure 5.8). Both spectral curves display a low MSS4 reflectance, peaking in MSS5 and MSS6 and decreasing in MSS7. However, reflectance from non-green vegetation is markedly lower than for bare soil, with an average value of 28.0 DN in MSS5 for non-green vegetation in contrast to 73.0 DN for bare soil.

TABLE 5.4 THE SAMPLED MEAN REFLECTANCE VALUES (DN) IN THE FOUR LANDSAT WAVEBANDS FOR BRIGHT SOIL, DARK SOIL, A 100 PER CENT COVER OF NON-GREEN VEGETATION AND A 100 PER CENT COVER OF GREEN VEGETATION

Category	MSS Waveband			
	7	6	5	4
Bare bright soil	53.0	73.5	73.0	43.0
Dark bare soil	26.0	35.0	34.0	24.0
Non-green vegetation	27.0	33.0	28.0	19.0
Green vegetation	38.0	47.5	27.0	20.5

Although reflectance of non-green vegetation is very much lower than for the predominantly sandy-loam soil, it nevertheless exerts its own significant reflectance. In

Figure 5.6 **Dense *Acacia reficiens* Shrub cover**

Figure 5.6 the general impression is of a dense thicket of grey coloured vegetation mainly composed of plant stems and branches. Some dry and non-green dwarf shrub leaves can be seen in the foreground. Concurrent with reductions in leaf area are increases in shadow and the area of non-foliage surfaces, including branches, plant litter and bare soil. Other factors also result in both qualitative and quantitative differences in reflectance from non-foliar canopies. Shadows cast by stems and branches reduce reflectance in all wavebands and the presence of plant litter would tend to reduce the area of bare soil visible to the sensor and further lower the reflectance.

The functional forms of the spectral curves for bare soil and non-green vegetation are similar, but the amplitude of reflectance is much higher for bare soil than for non-green vegetation. Non-green vegetation can therefore only be discriminated from bare soil on the basis of differences in amplitude of the reflectance but not on the basis of a difference in spectral frequency. When the vegetation canopy is dense enough to give a lowered reflectance, discrimination between bright soil surfaces and non-green vegetation is possible. However, over the majority of the Study Area canopy cover is low and the amplitude contrast between the reflectance of bare soil and non-green vegetation is correspondingly small. This was demonstrated in Chapter 4 in the interpretation of false colour imagery.

In order to investigate the reflectance characteristics of non-green vegetation of varying canopy cover, DN values were sampled in four Landsat wavebands from six canopy cover classes identified on the vegetation map (Figure 3.1). For each canopy cover class 25 pixels were averaged and the confidence limits about the mean figure calculated at the 95 per cent level (Table 5.5). These data are plotted in Figure 5.7 and show than an increase in canopy cover is associated with a decrease in reflectance as the bright, highly reflective soil surface is masked. The maximum separation between classes occurs in MSS5, a phenomena which has also been observed by other workers (McCoy and Watt, 1973). At low canopy cover (0-20 per cent) vegetation is barely distinguishable from bare soil, and this spectral curve closely resembles the form of the bare soil spectral curve with a marked reflectance peak in the visible green (MSS5) and near-infrared (MSS6) wavelengths. With an increase in non-green vegetation cover the spectral curve begins to flatten as the reflectance from bare soil is obscured by the intervening vegetation. A dense cover of non-green vegetation is therefore highly correlated in all Landsat wavebands.

5.5 REFLECTANCE OF GREEN VEGETATION

The reflectance of the remaining spectral component, green vegetation, was also characterised by sampling the reflectance values of 100 per cent green vegetation cover in the four Landsat wavebands. This proved to be more difficult than for bare soil and non-green vegetation cover because the greenness of vegetation is an ephemeral condition which responds very rapidly to rainfall amount. The Landsat scene was acquired in June 1979 before the commencement of the project. Consequently data for the per cent cover of green vegetation at the date of the Landsat pass could not be collected.

The rate at which shrub, dwarf shrub and grassland species develop new green growth is dependent upon the specific characteristics of the local environment; rainfall amount, the species concerned, the condition of the range at the onset of rain, evapotranspiration rates, the water retentive properties of the soil etc. It is therefore difficult to generalise about the relationship between rainfall amount and vegetation greenness (Le Houeron and Hoste, 1977), but rainfall figures can be used to provide an indirect indication of vegetation greenness.

Although IPAL have made no direct measurements of periods of vegetation growth, it is generally known to be extremely short for semi-arid rangeland species (Gwynne and Pratt, 1977). In a 'normal' year, the long rains in Northern Kenya have finished by mid-May and the growth of plants has commenced, but a month later most plants have ceased active growth and the vegetation cover is beginning to dry. Green vegetation cover is absent from the shrub and grassland species illustrated in Figure 5.1. In a 'normal' year 100 mm of rain falls during the long rains in April and May to give a potential growing period

TABLE 5.5 MEAN PER CENT REFLECTANCE VALUES AND CONFIDENCE LIMITS AT THE 95 PER CENT LEVEL OF SIGNIFICANCE (0.05) FOR SIX VEGETATION CLASSES

Vegetation class and per cent level	MSS 4	MSS 5	MSS 6	MSS 7
Bare soil (0)	50.0 (±3.6)	68.0 (±5.0)	62.0 (±4.0)	40.0 (±4.5)
Dwarf shrub (0 - 20)	48.0 (±2.5)	56.0 (±3.0)	55.0 (±3.0)	30.0 (±1.5)
Shrub (0 - 20)	46.0 (±1.0)	56.0 (±2.0)	53.0 (±2.0)	30.0 (±1.0)
Shrub (20 - 40)	40.0 (±2.0)	46.0 (±2.0)	43.0 (±2.0)	28.0 (±1.0)
Shrub (40 - 60)	38.0 (±2.0)	42.0 (±2.5)	40.0 (±2.0)	25.0 (±1.0)
Shrub (60 - 80)	33.0 (±3.0)	36.0 (±4.5)	34.0 (±3.0)	23.0 (±2.0)

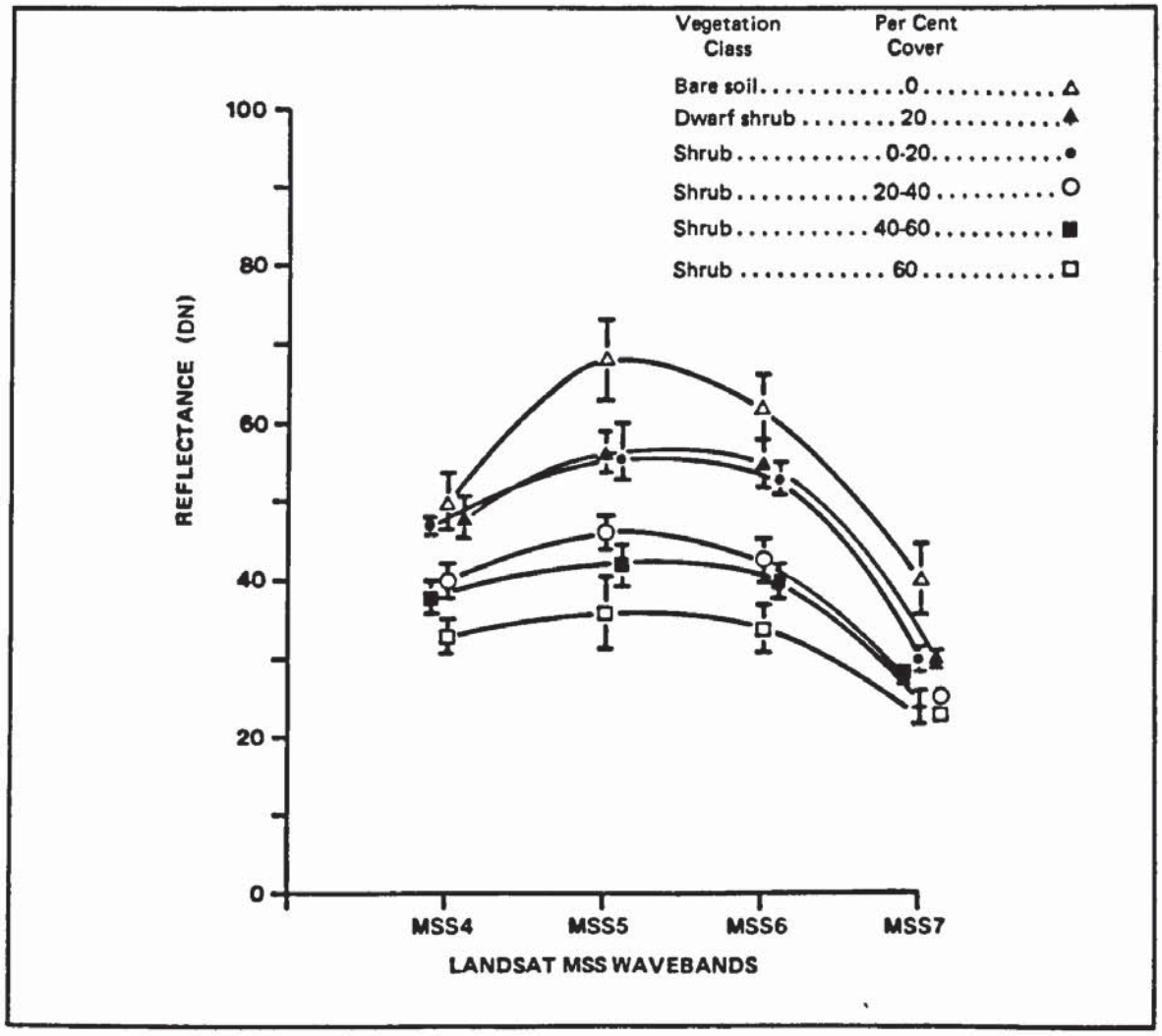

Figure 5.7 The Reflectance in the Four Landsat Wavebands of Non-Green Vegetation of Varying Canopy Cover

of one month and a healthy green vegetation cover. If is it assumed that this 100 mm of rainfall is sufficient to activate and sustain plant growth for one month, then the high rainfall totals in the early part of 1979 (Chapter 1) suggest almost continuous potential for growth until the beginning of May[1]. This would leave approximately one month of drying within the rangeland before the Landsat pass in early June, and the possibility of green cover remaining within the vegetation canopy.

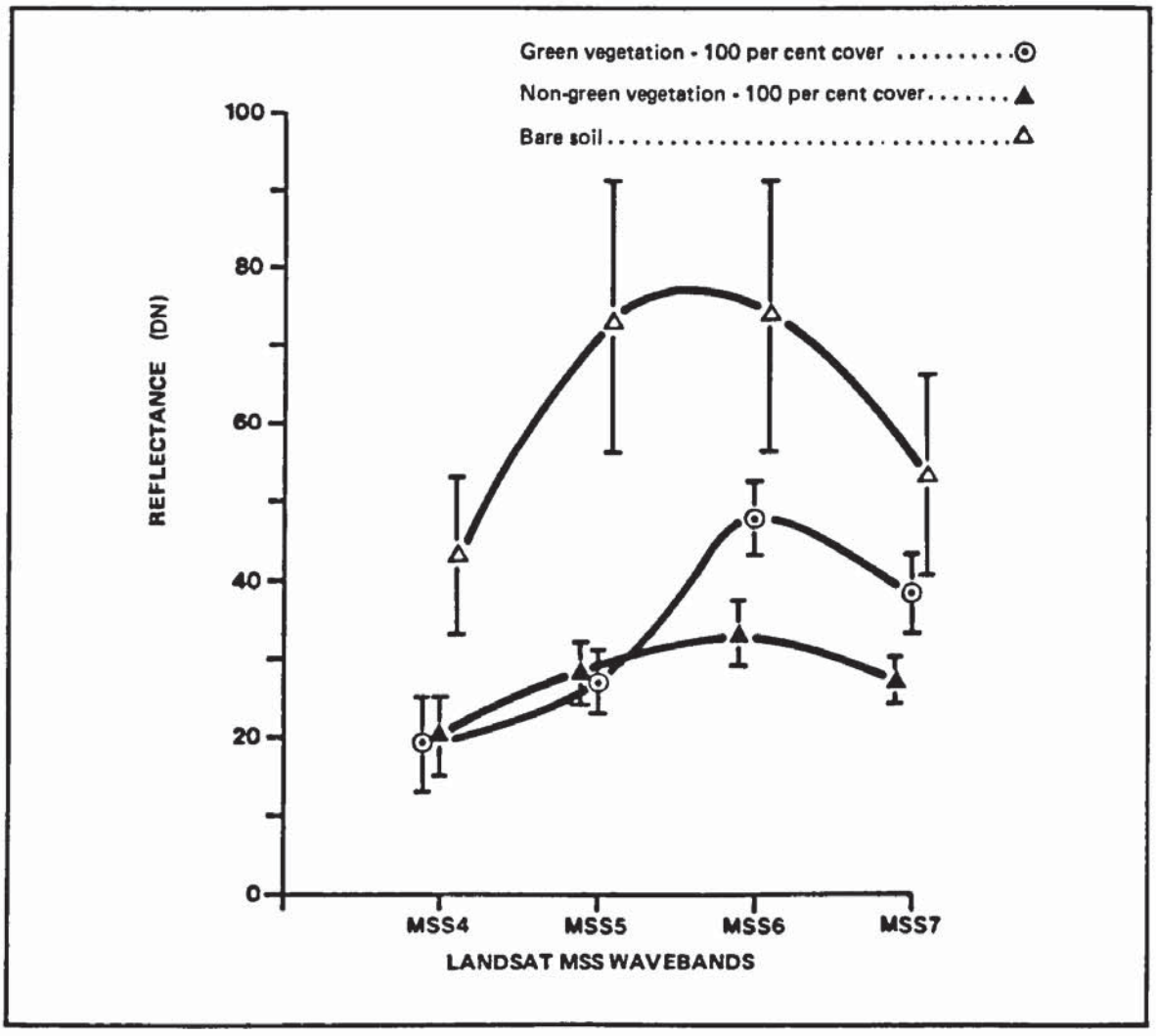

Figure 5.8 A Comparison of the Shape and Amplitude of the Spectral Curves for Bright Bare Soil, Non-Green Vegetation and Green Vegetation Within the Study Area

[1]. The wet season was early in 1979

Areas of green cover were 'searched' for within the display of an enhanced false colour image of the Kargi subscene. Pixels containing a high cover of green vegetation appear red on a standard false colour image (Chapter 4) and the reflectance of 100 of these pixels were sampled in the four Landsat wavebands (Appendix E). From an initial sample of approximately 100 pixels, only those with an MSS 7 - MSS 5 difference of more than or equal to 10 DN values ($\geqq$ 10 DN) were sampled, to improve the probability of sampling a pixel containing a high cover of green vegetation. The final sample only contained 18 green vegetation DN values, which were averaged (Table 5.4) and plotted as a spectral curve (Figure 5.8). The bare soil and non-green spectral curves are also shown on Figure 5.8 for comparison.

The form of the green vegetation spectral curve is similar to the form of the typical spectral curve for a green leaf; low reflectance in the visible wavelengths (MSS 4/5) and high reflectance in the near infra-red wavelengths (MSS 6/7). Reflectance is unexpectedly higher in MSS 6 than MSS 7, almost certainly because the sampled pixels did not contain a 100 per cent cover of green vegetation and included some bare soil with high MSS 6 reflectance. Similarly the dip in the visible red (MSS 5) is less pronounced than predicted theoretically (Woolley, 1971). The inclusion of areas of bare soil, shadow, plant litter and non-green vegetation would tend to smooth out the very sharp peaks and dips of the green leaf spectra. Nevertheless, the green vegetation spectral curve displays a functional form which is clearly differentiated in spectral frequency to the bare soil and non-green vegetation spectral curves, and which shows some resemblance to the typical green leaf spectra shown in Figure 2.1.

CHAPTER 6

A MODEL OF SEMI-ARID VEGETATION REFLECTANCE

A model is proposed which describes the interaction between the major spectral components of the semi-arid landscape, and which accounts for spatial and temporal variations in rangeland vegetation characteristics.

6.1 INTRODUCTION

In the preceding chapter the reflectance of bare soil, non-green vegetation and green vegetation was quantified, enabling the position of each spectral component to be located in the Landsat feature space. A change in the relative proportions of these three components within a pixel will result in a shift in the feature space location of that pixel. The simple model proposed attempts to describe how the magnitude and direction of that shift can be used to indicate soil and vegetation characteristics.

6.2 IMAGE DATA SCATTERPLOTS

Scatter diagrams of one Landsat waveband plotted against another can be used as a qualitative means of analysing the multi-variate structure of image data. Separate scatterplots for different vegetation canopy cover classes and soil types were plotted initially to enable significant gaps and clusters within the distribution as well as its exterior shape to be viewed. These separate plots, which are presented in Appendix F, were later combined into the single scatterplots for MSS7/5(a), 7/4(b), 7/6(c) and 5/4(d) space illustrated in Figure 6.1.

The plots were generated from a systematic sample of pixels in the Kargi subscene. The subscene was smoothed with a median filter using a display function available within the image analysis system. The program takes a box or kernel of user defined dimensions, calculates the median value within the kernel before moving, in increments of one sample, to calculate the median value within the adjacent kernel and so on through the image array. The dimensions of the kernel were specified as 5 x 5 pixels, so that each pixel in the 512 x 512 pixel subscene was replaced by the median value for 25 pixels. To reduce the data-set to a size that could be conveniently manipulated within the Harris 500 computer, the smoothed image array was sub-sampled in the samples (columns) and lines (rows) direction to give a total sample of 40 x 40 pixels (1600), equivalent to 15 per cent of the total pixels within the subscene. The sample and line coordinate of each pixel sample within the filtered

image array was recorded, and the position of each sample point was precisely plotted on the geometrically corrected single channel (MSS 5) image of the Study Area at 1:50,000 scale. The vegetation map, which had previously been compiled from an interpretation of 1:52,600 scale air-photos (Figure 3.1), was superimposed onto the MSS Landsat image at 1:50,000 scale using a Zoom Transferscope to adjust for scale differences. The vegetation species and per cent canopy cover for each of the 1600 sample points was then recorded by observing the vegetation class on the map within which each sample point on the image fell. To ensure that a sample point on the image related to its true ground position on the vegetation map, considerable care was taken to ensure that the image was geometrically transformed to the same UTM projection as the vegetation map. A description of the geometric transformation applied to the image data is given in Chapter 3. In addition, the geometrically transformed image data was sent to the National Remote Sensing Centre (NRSC) to create a film negative of high geometric precision using a digital image writer, from which a 1:50,000 scale enlargement could be produced. The problem of possible misregistration between image and vegetation map was considerably decreased by careful plotting of the larger scale vegetation map onto the smaller scale image base using the Zoom Transferscope to adjust for scale differences and compensate for inherent geometric distortion within the vegetation map.

Each sample was coded with a class number as follows:

Soil and Vegetation Class	Class Number
Bare soil	1
0 - 20 per cent vegetation cover	2
20 - 40 per cent vegetation cover	3
40 - 60 per cent vegetation cover	4
60 - 80 per cent vegetation cover	5
> 80 per cent vegetation cover	6
Lava outcrop	7

The class number assigned to each sample point was input into the computer in the form of a digital array of 40 rows and 40 columns to correspond exactly with the size of the image array (Appendix G). A FORTRAN program incorporating Gino graph-plotting routines was written (Appendix H) to plot scatterplots in MSS7/5 data space for the separate vegetation classes (1-7) (Appendix F), and the combined classes in MSS7/5(a), 7/4(b), 7/6(c) and 5/4(d) Landsat space (Figure 6.1). Enlarged colour versions of these scatterplots are also reproduced in Appendix F.

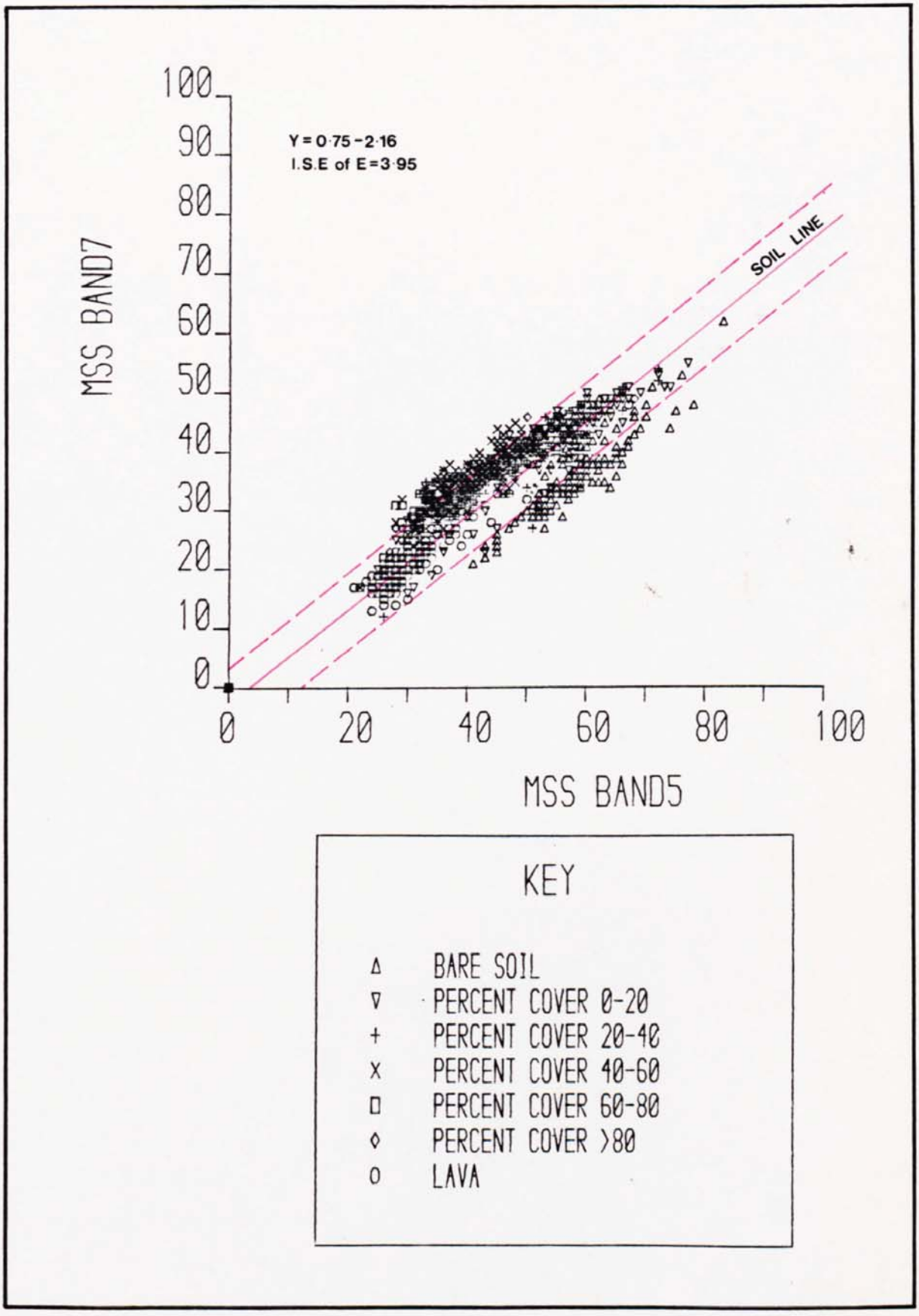

Figure 6.1 (a) The Distribution of Image Data in MSS7/5 Landsat Space

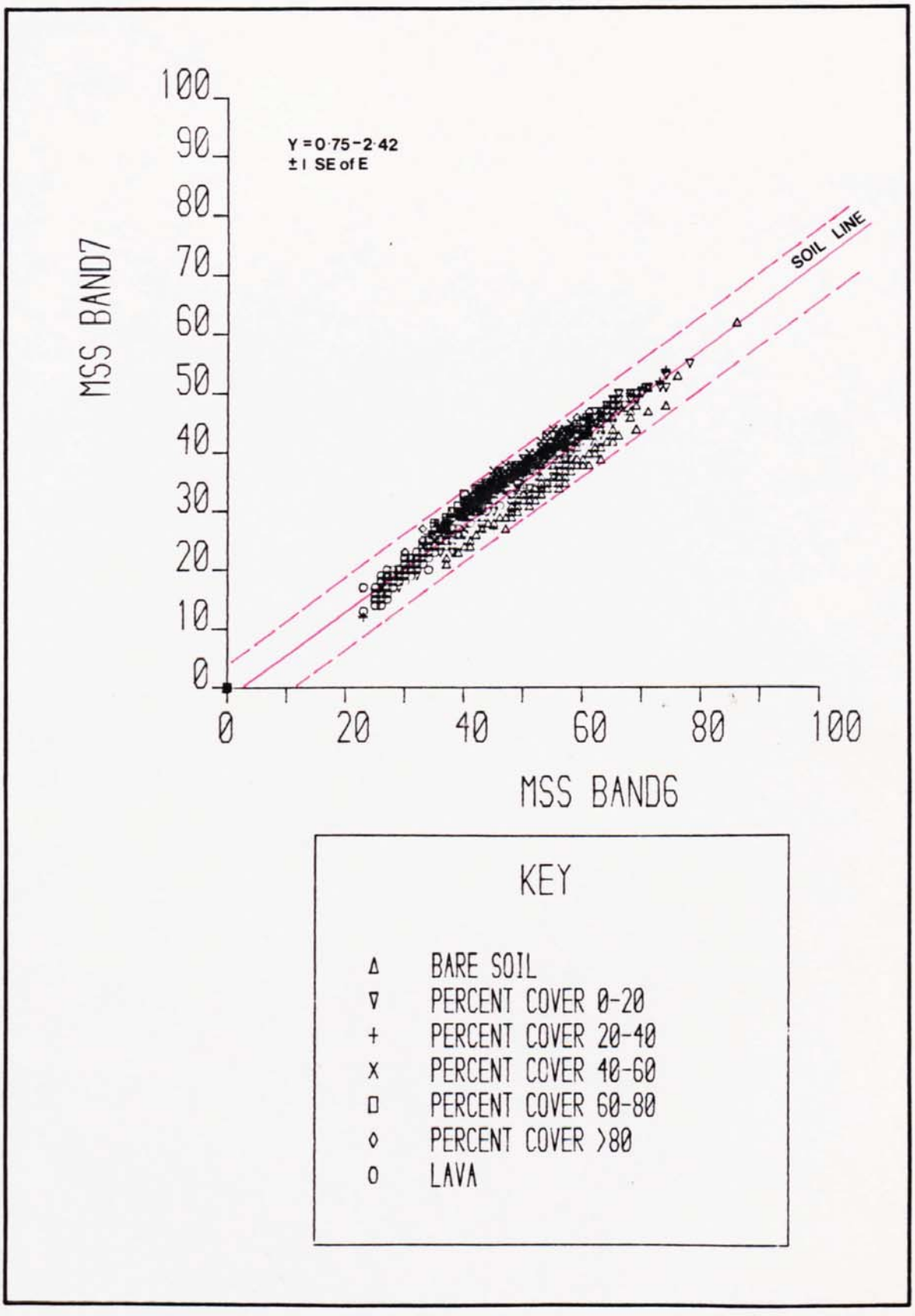

Figure 6.1 (b) The Distribution of Image Data in Landsat MSS7/6 Space

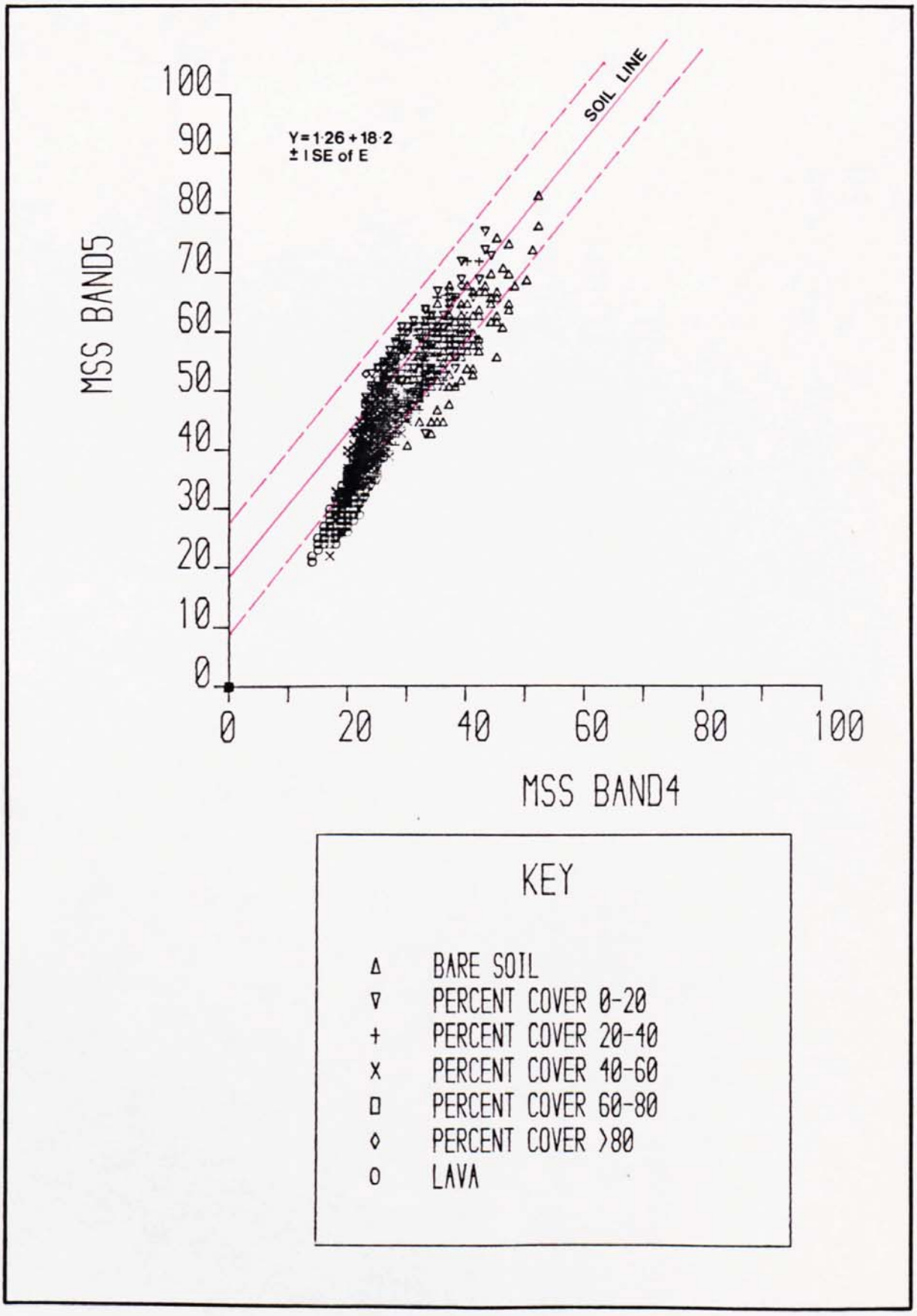

Figure 6.1 (c) The Distribution of Image Data in Landsat MSS5/4 Space

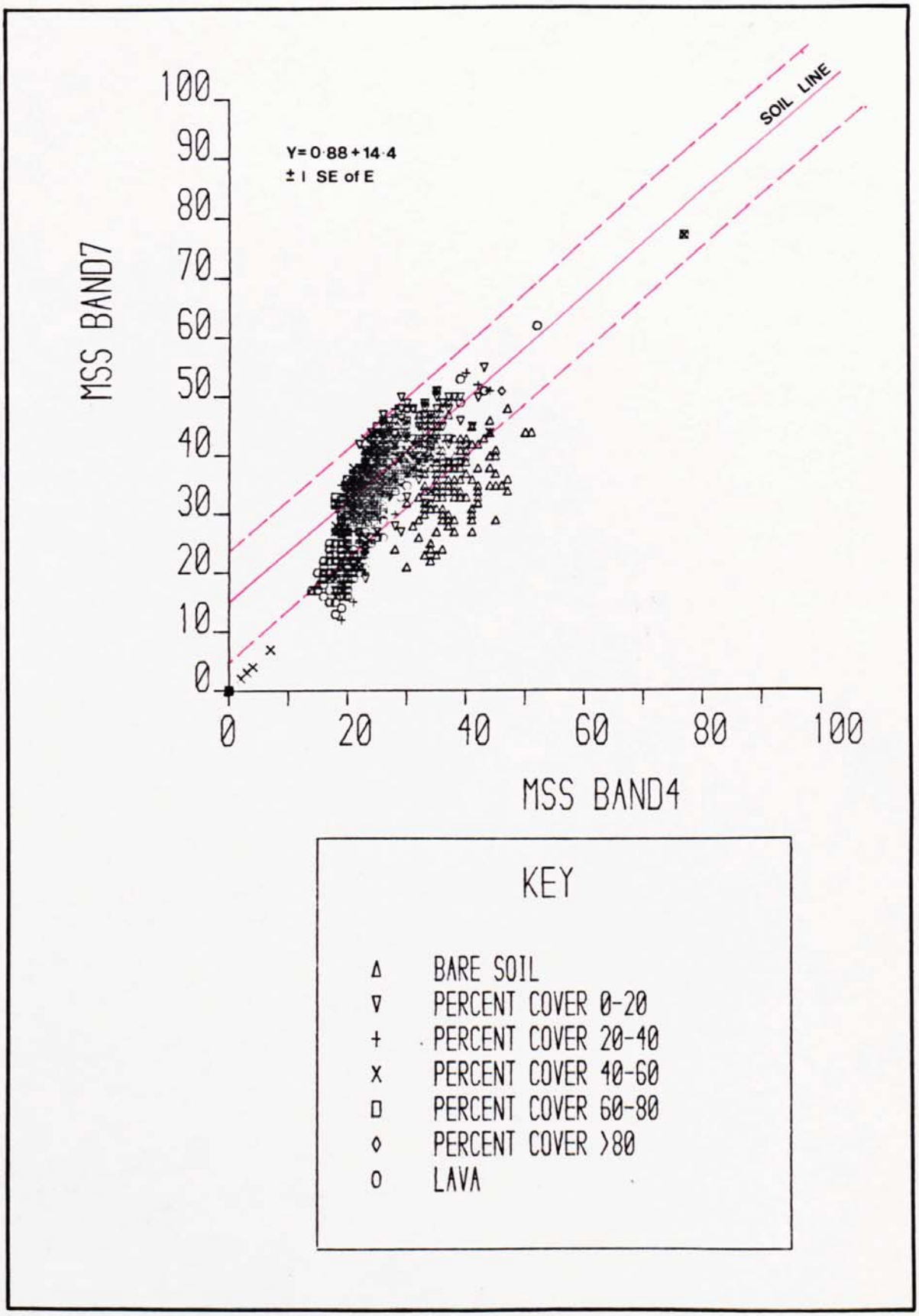

Figure 6.1 (d) The Distribution of Image Data in Landsat MSS7/4 Space

The linear regression soil lines which were previously calculated from a sample of bare soil DN values (Chapter 5) are also plotted on the scatterplots in Figure 6.1, to illustrate the relationship between each distribution and its corresponding soil line. The distribution of data points in Landsat space is generally elliptical, with the long axis of each cluster lying parallel to the soil line. In the two near infrared wavebands (c) and the two visible wavebands (d) all the soil and vegetation data points lie systematically about the soil line in a narrow and highly correlated distribution. The correlation coefficients (r) are 0.94 for MSS7/6 and 0.92 for MSS5/4 (Table 6.1). This high correlation between the two visible and between the two infrared wavebands is typical of the high degree of data redundancy within Landsat data. Tucker (1978), and Misra and Wheeler (1978) have argued that Landsat data is essentially two-dimensional and that only two wavebands; the visible red (MSS5) and near infrared (MSS7) are required for vegetation monitoring. Correlation coefficients for MSS7/5 (0.84) and MSS7/4 (0.69) are much lower, indicating a wider scatter of data points for these waveband combinations.

TABLE 6.1 LINEAR CORRELATIONS IN THE FOUR LANDSAT WAVEBANDS FOR THE DATA PLOTTED IN FIGURE 6.1 (a-d)

	MSS4	MSS5	MSS6	MSS7
MSS4	1.00			
MSS5	0.92	1.00		
MSS6	0.82	0.95	1.00	
MSS7	0.69	0.84	0.94	1.00

A relatively lower correlation between visible and near infrared Landsat wavebands is frequently indicative of the presence of green vegetation (Graetz et al., 1982). It is argued however, that for the Study Area this lower correlation is related to variations in soil reflectance and is not necessarily indicative of green vegetation. It was demonstrated that the linear regression soil line is a poor fit to the data in MSS7/4 space, but a much better fit in MSS7/5 space (Chapter 5). In MSS7/4 space (Figure 6.1 (d)) the majority of vegetated data points lie within 1 standard error of the estimate (± IS.E of E) about the soil line. By contrast in MSS7/5 space (Figure 6.1 (a)), the majority of vegetated pixels lie outside the plotted standard error. It appears that a very much higher variation in soil reflectance in MSS7/4 space 'swamps' a spectral effect from green vegetation which is

apparent in MSS7/5 space due to a much lower variation in soil reflectance. In semi-arid regions therefore, a relatively low correlation coefficient between the infra-red and visible wavebands may be an effect due to variation in soil reflectance which is unrelated to the presence of green vegatation.

An analysis of the location of separate clusters in MSS7/5 data space from Figure 6.1 (a) and Appendix F, reveals that the distribution is comprised of three spectrally overlapping clusters:

(a) bright bare soil and pixels containing a vegetation cover of less than 20 per cent;
(b) dark bare lava outcrop;
(c) pixels containing more than 20 per cent vegetation cover.

The majority of vegetated pixels (classes 2 - 6) lie above the plotted soil line. Conversely, pixels comprised of bright bare soil (Class 1) or containing a very sparse cover of vegetation (Class 2), and pixels comprised of dark bare lave outcrop (Class 7), are arranged almost symmetrically about the soil line. There is a distinct gap in the distribution between the bright sandy-loam soils (Class 1) and the darker lava and lava derived gravels and clay soils (Class 2), although the general trend remains elliptical, with bright bare soil at the upper end of the distribution and dark bare soil at its lower end. Although the more densely vegetated pixels (Classes 2 - 6) display a considerable amount of spectral overlap and do not form distinct clusters in the feature space, two significant trends within the distribution are apparent.

(1) An increase in vegetation canopy cover is associated with movement down the soil line towards the area of dark soils (Class 7);
(2) Movement away from the soil line is associated with an increase in canopy cover up to 60 per cent (Class 5), and a return movement to the soil line is associated with a vegetation cover of more than 60 per cent (Class 6).

The interaction between these two movements; both along and away from the soil line with changes in vegetation canopy cover, produces the convex shape of the distribution in MSS7/5 space. This convexity can be clearly seen in the scatterplot (Figure 6.2) showing the distribution of all pixels within the Kargi subscene in MSS7/5 space. The plot has been contoured and subsequently coloured using a density slicing technique, with each colour representing the frequency of occurrence of each plotted point enabling the structure of the distribution to be analysed in addition to its exterior shape.

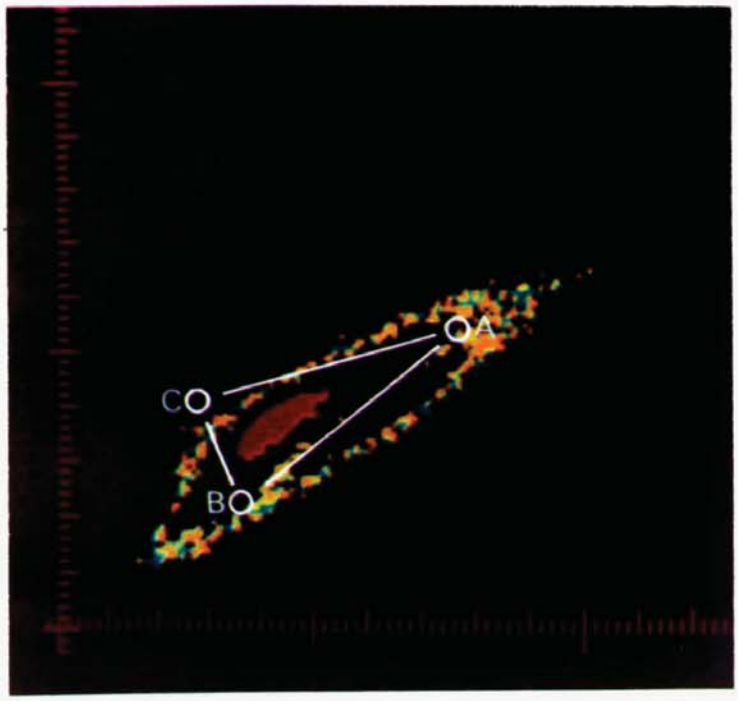

Figure 6.2 The MSS7/5 Scatterplot for Image Data Within the Kargi Subscene

The convexity of the distribution demonstrates the concept of a dual movement within the distribution; simultaneously down the soil line and away from the soil line with an increase in non-green vegetation and green vegetation cover respectively. The bare soil point (A), non-green vegetation point (B) and green vegetation point (C) (Chapter 5, Table 5.4) have been superimposed on the MSS7/5 scatterplot in Figure 6.2 to show the correspondence between the distribution of image data within the Kargi subscene and the established feature space locations of the major spectral components of the semi-arid landscape. The correspondence is extremely good and demonstrates the triangular nature of the distribution defined by a line of soils (A,B) and the maximum green point (C).

Compared with the markedly triangular form of MSS7/5 Landsat data space for soil and vegetation observed by other workers (Graetz and Gentle, 1982), the distribution of image data for northern Kenya illustrated in Figure 6.2 is much flatter and does not converge to a single green vegetation point at the apex. Figure 6.3 is taken from Graetz and Gentle, (1982) and shows the characteristically triangular distribution of points in MSS7/5 Landsat data space for bare soil, shadow, non-green shrubs, plant litter and green ephermerals for semi-arid vegetation in Central Australia. The bare soil, shadow, non-green vegetation and plant litter form the base of the triangle along a 'cover line', whilst reflectance data for green

ephemerals form the sharp apex of the triangle. It appears that at the date of the Landsat pass in northern Kenya the amount of green vegetation within the rangeland was low, and this gives the smoother distribution observed in Figure 6.2.

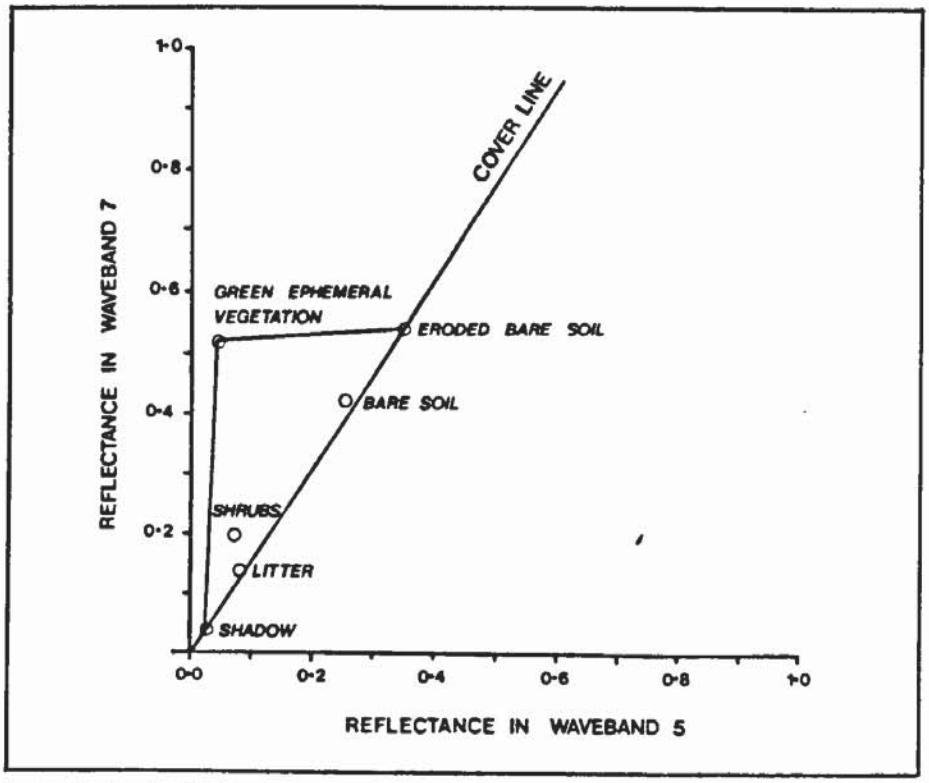

Source:Graetz et al,1982

Figure 6.3 The Reflectance in the Near Infrared (MSS7) and Visible Red (MSS5) Wavelengths of Various Cover Components for Semi-Arid Shrubland Vegetation in Central Australia

The analysis of the structure of the data distribution for all Landsat waveband combinations has shown that the effect of green vegetation reflectance is most pronounced in MSS7/5 data space, but is 'swamped' by background soil reflectance in all other visible/near infrared waveband combinations. In the two visible wavebands (MSS5/4) and the two near infrared wavebands, the (MSS7/6) spectral effect of green vegetation is not apparent. In these two distributions, data points cluster close to the soil line in an elongated ellipsoid and do not display the triangular structure associated with a green vegetation spectral effect. The analysis has also demonstrated that the proportion of bare soil, non-green vegetation and green vegetation within a pixel defines its locations within the triangular data space. In Section 6.3 a model is proposed which attempts to explain the mechanism whereby pixels simultaneously move down and away from the soil line with an increase in non-green and green vegetation cover respectively.

6.3 A MODEL OF SEMI-ARID VEGETATION REFLECTANCE

At the spatial resolution of the Landsat MSS scanner, total reflectance from a sparsely vegetated surface is equal to the addition of reflectance from all components within a pixel

(Bentley et al., 1975; Siegal and Goetz, 1977). This can be expressed:

$$R_j = \sum_{i=1}^{n} p_i \cdot r_{i,j}$$

Where R is the reflectance in waveband j, p is the fraction of the scene of component i, and $r_{i,j}$ is the reflectance of component i in waveband j. For sparsely vegetated surfaces vegetation cover is the most important determinant of R, unlike the situation for densely vegetated surfaces where biomass is more important (Graetz and Gentle, 1982).

It was demonstrated in Section 6.2 that an increase in vegetation cover results in a simple, linear movement down the soil line towards the origin. In effect the soil line becomes a 'cover-line' from the point of bright bare soil and zero vegetation at the upper end of the line to a closed canopy of 100 per cent non-green vegetation at the lower end of the line. The concept of the 'cover-line' is described in Griffiths, (1983) and is similar to the 'cover-line' described by Graetz and Gentle (1982). Graetz and Gentle, (1982) refers to a line which passes from the point of eroded bare soil through the area of non-green shrubs and plant litter to the point of shadow. 'Cover' in this context is a qualitative term used to describe the type of surface, i.e. plant litter, bare soil, etc, and is not therefore a qualitative measure of vegetation density. The simple, two-component 'cover-line' is a useful means of describing the relationship between two of the spectral components in the semi-arid landscape; bare soil and non-green vegetation. However, with the addition of spectrally dissimilar green vegetation cover, a more detailed model is required to describe the interaction between all three spectral components.

The balance of green to non-green vegetation within the rangeland is continuously changing in response to rainfall amount. Unfortunately, data on the greenness of different vegetation species, shrubs, dwarf shrub and grassland, could not be obtained for the date of the Landsat pass in June 1979. There are various techniques for measuring vegetation greenness, including leaf area index (LAI), weight of green biomass and the use of a ground radiometer to calculate the ratio of infra-red to visible red wavelength light (Curran, 1980).

In the absence of such data, the ground cover estimates made from the vertical colour air-photos have been used to establish a crude indication of green vegetation cover for the date of the Landsat scene acquisition. From the canopy cover estimates given in Chapter 3 (Table 3.3), there is a roughly inverse relationship between vegetation cover and bare soil; an increase in vegetation cover is associated with a decrease in soil cover from 0-100 per

cent. Assuming that the vegetation cover is 100 per cent green at the end of the rains, this green vegetation will gradually senesce and become non-green as the dry season advances, until zero per cent vegetation is green and the balance between non-green and green is reversed. From these approximate relationships a set of figures can be derived which summarise the relationship between the per cent cover of bare soil, non-green and green vegetation (Table 6.2). It has not been possible to relate green cover to species composition, or to verify the assumption that the vegetation cover will be 100 per cent green at the end of the wet season. Such additional information would have provided useful refinements to the model, but it is not essential for an illustration of the general principles.

TABLE 6.2 THE RELATIONSHIP BETWEEN THE PER CENT COVER OF BARE SOIL, NON-GREEN VEGETATION AND GREEN VEGETATION

Point No.	Per cent cover of green vegetation	Per cent cover of non-green vegetation	Per cent cover of bare soil
1	90	0	10
2	75	5	20
3	60	10	30
4	45	15	40
5	30	20	50
6	15	25	60
7	0	30	70

The position of a pixel containing known proportions of bare soil, non-green and green vegetation cover, can be plotted within the Landsat data space using the method of vector addition. The dimensions of the data space have been plotted and are shown in Figure 6.4, using the mean reflectance values for bare soil, non-green vegetation and green vegetation (Chapter 5, Table 5.4). The percentage figures for the varying proportions of bare soil, non-green and green vegetation represent distances along the three vectors, X, Y and Z. The three vectors represent the slopes and lengths of the lines joining the mean points for the three spectral components to the origin. This is equivalent to the distance between 100 per cent reflectance from bare soil, non-green and green vegetation cover to zero reflectance at the origin. The data in Table 6.2 have been plotted in Figure 6.4 using the vector addition method. The coordinate position of point 2 is equivalent to a distance of 20 per cent along the bare soil vector (X), plus five per cent along the non-green vegetation vector (Y), plus 75 per cent along the green vegetation vector (Z). The remaining six points

have been plotted in a similar fashion on Figure 6.4.

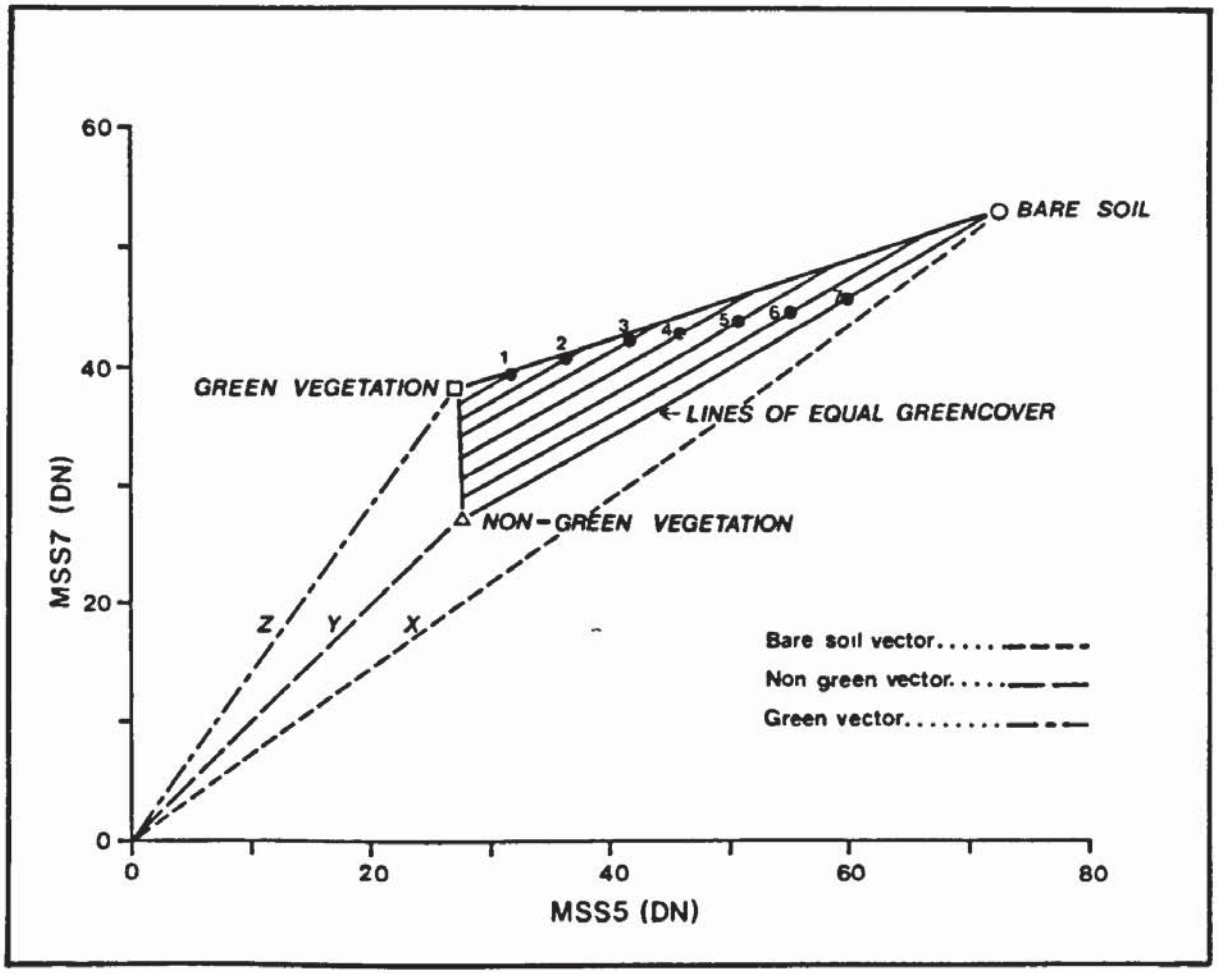

Figure 6.4 The Three Component Model of Semi-Arid Vegetation Reflectance

From the model, lines of equal green cover lie parallel to the soil line. Irrespective of the relative proportions of non-green and green vegetation and the reflectance of bare soil, a pixel containing 60 per cent green vegetation will lie along the 60 per cent greenness cover line. In this manner the data space enclosed by the bare soil, non-green and green vegetation points is 'filled-in' by pixels of varying soil background reflectance and a varying ratio of green to non-green vegetation cover. This process produces the convex shape of the data distribution illustrated in Figure 6.2.

The trajectory of a pixel for a given soil background reflectance to 100 per cent green cover is not a perfectly straight line; thus lines of equal green cover are only approximately equidistant from each other. This is due to the fact that the non-green vegetation vector has a different slope to the bare soil vector; bare soil and non-green

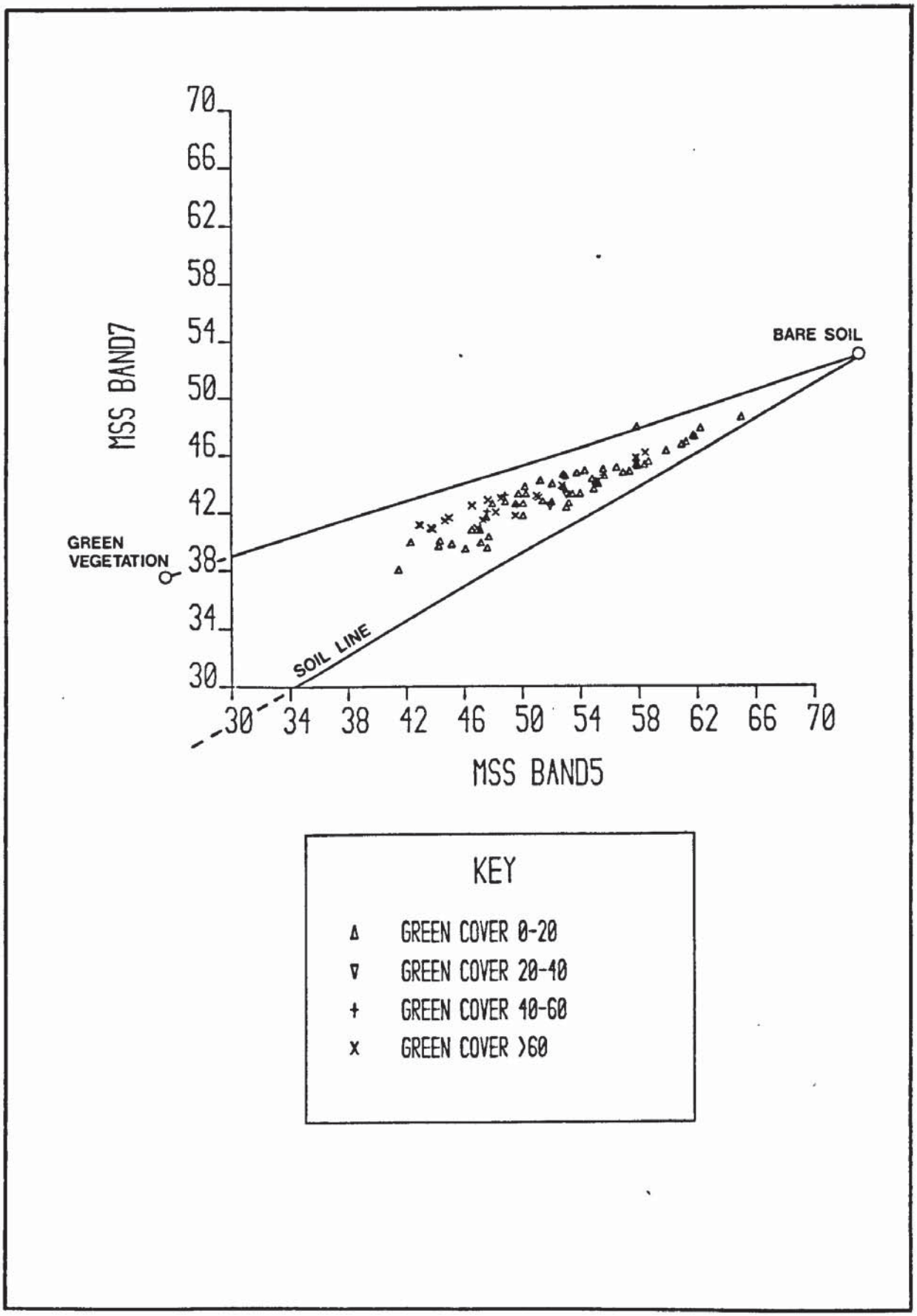

Figure 6.5 Green vegetation of Varying Canopy Cover Plotted in MSS7/5 Landsat Space According to the Principles of the Three-Component Model of Vegetation Reflectance

vegetation are not spectrally identical. It was argued in Chapter 5 that this was a result of selecting a sample of non-green vegetation which inadvertently contained some green vegetation. For the purposes of the model and for the development of a perpendicular index of green vegetation amount it is assumed that lines of equal green cover lie parallel to the soil line at equidistant intervals. Thus the distance from the soil line to the maximum green vegetation point defines a per cent green cover scale.

In order to test the model a FORTRAN program (Appendix H) was used to plot 100 pixels within the MSS7/5 space defined by the triangular data distribution. Using the method of vector addition the coordinate position of each pixel could be calculated from its percentage proportion of bare soil, non-green and green vegetation. The per cent cover of bare soil, non-green and green vegetation within each pixel was measured from the vertical colour air-photos using dot grid analysis techniques (Chapter 3). An assumption was made that herbaceous cover represented green vegetation. From the large per cent cover of herbaceous, mostly grassland, within the rangeland (Chapter 3, Table 3.3), it is reasonable to assume that this vegetation type would contribute a major proportion to the greenness component.

The shape of the resulting distribution (Figure 6.5) is similar to the shape of the distribution for the image data within the Kargi subscene illustrated in Figure 6.2. In particular, points of high green cover lie at the maximum distance from the soil line in a cluster near the mean green point (C). Points of low green cover lie close to the soil line and are distributed along it between the bright bare soil point (A) and non-green vegetation point (B). This is an effect due to varying soil reflectance and vegetation canopy cover and is responsible for the 'filling-in' process described above which accounts for the observed convexity of the distribution for vegetated surfaces in the Study Area.

CHAPTER 7

IMAGE PROCESSING

The images resulting from the application of various digital processing techniques for mapping semi-arid vegetation within the Study Area are presented and evaluated.

7.1 INTRODUCTION

In this chapter the model of semi-arid vegetation reflectance described in Chapter 6, is used as the basis for the development of a vegetation index to map the characteristics of the vegetation cover within the Study Area. The approach has been to compare the results obtained from more conventional techniques, such as multispectral classification and principal components analysis, with the vegetation index.

Interactive and Central Processing Unit (CPU) processing of the image data was undertaken on separate occasions using image processing equipment at the following Institutions:

(a) Hunting Technical Services Limited - International Imaging Systems (I^2S) image analysis system.
(b) National Remote Sensing Centre (NRSC), Farnborough - IDP 3000 and GEMS image analysis systems.
(c) Natural Environment Research Council (NERC) - International Imaging Systems (I^2S) image analysis system.

7.2 MULTISPECTRAL CLASSIFICATION

The principles relating to the multispectral classification of image data were discussed in Chapter 2. The result of a supervised maximum likelihood classification applied to the Kargi subscene is shown in Figure 7.1. The image has been median filtered to give a more generalised and interpretable result, and coloured to enhance differences between classes. MSS wavebands 4, 5 and 7 were used in the classification, and 12 initial classes were defined during the training stage on the basis of the range of spectral tones displayed by the false colour image.

The training set confusion matrix (Table 7.1) indicates the degree of misclassification between the 12 original classes. For example, 90.7 per cent of pixels contained in Class I

Figure 7.1 **Multispectral Classification of the Kargi Subscene**

have been classified as Class 11, indicating spectral confusion between dark lava and dense shrub cover. Additionally, some gravel soil surfaces (Class 7) have been spectrally confused with saline soils in the Chalbi desert (Class 4) and with sandy soils (Class 5). The number of original classes was therefore reduced from 12 to 7 as indicated in Table 7.2.

The spectral confusion between classes was due to the difficulty of defining training areas of homogeneous spectral response in an area of variable vegetation and soil reflectance. In semi-arid regions, boundaries between different land cover types are frequently indistinct with, for example, a change in the density or species composition of different vegetation associations occurring as a gradual transition. Furthermore, in an area of sparse vegetation cover differences in soil reflectance are more pronounced than in an area where the soil surface is largely masked by a vegetation canopy. For these reasons the enhanced false colour image of the Kargi subscene displays a very wide range of spectral tones. In fact the statistics for the training areas show a high standard deviation about the mean vector for each class, indicating overlapping clusters in the Landsat feature space (Table 7.3). The solution to this problem was to select training areas to represent the full range of spectral tones displayed by the false colour image, and subsequently to amalgamate classes which, on the basis of fieldwork, appeared to represent significant land cover features within the scene (Table 7.2).

TABLE 7.1 TRAINING SET CONFUSION MATRIX SHOWING THE DEGREE OF MISCLASSIFICATION BETWEEN LAND COVER CLASSES

Class No.	1	2	3	4	5	6	7	8	9	10	11	12
1	.000	.093									.907	
2		.934	.004								.062	
3			.996				.004					
4				.000	.001		.988		.007	.004		
5					.608		.388	.004				
6						.903		.073	.013	.011		
7					.003		.971	.011	.016			
8						.043	.006	.919	.030	.002		
9						.015	.072	.055	.784	.075		
10						.008	.001	.002	.039	.742	.013	.195
11		.003								.008	.978	.011
12						.020				.130		.850

TABLE 7.2 THE AMALGAMATION OF CLASSIFIED SOIL AND VEGETATION UNITS WITHIN THE KARGI SUBSCENE

Original class No.	Class name	New class No.	New class name	Colour on image
1	Lava outcrop (1)	1	Lava	Grey
2	Lava outcrop (2)			
3	Saline soils (1)	2	Bare soils	Brown
4	Saline soils (2)			
5	Bright sand			
6	Sandy-loam			
7	Gravel surfaces			
8	Shrub 1 (sparse cover)	3	Shrub 1 (sparse cover)	Blue
9	Shrub 2 (open cover)	4	Shrub 2 (open cover)	Dark green
10	Shrub 3 (medium cover)	5	Shrub 3 (medium cover)	Light green
11	Shrub 4 (dense cover)	6	Shrub 4 (dense cover)	Purple
12	Woodland	7	Woodland	Red

TABLE 7.3 MEAN VECTORS AND STANDARD DEVIATIONS FOR TRAINING AREAS

	Mean Vectors			Standard Deviations		
Class No.	MSS 7	MSS 5	MSS 4	MSS 7	MSS 5	MSS 4
1	2.2	7.1	8.5	8.03	12.18	13.77
2	5.5	37.9	62.1	9.73	17.76	21.33
3	7.9	101.5	192.4	14.67	23.46	32.78
4	160.8	192.3	219.0	24.36	28.68	26.03
5	246.3	254.3	250.3	12.22	2.43	10.68
6	200.8	163.4	136.8	17.98	17.13	08.17
7	169.9	198.5	223.5	33.07	35.78	28.83
8	191.1	196.7	150.1	19.58	21.63	22.67
9	140.2	141.5	138.8	16.68	16.35	16.48
10	119.4	97.9	98.7	17.53	15.98	18.29
11	37.1	29.1	29.0	23.21	27.02	22.77
12	101.0	16.0	42.0	17.09	19.63	20.47

A similar approach would have been to apply an unsupervised cluster analysis to the image data, specifying a high number of original classes to represent the full range of spectral tones, and then amalgamating those classes into significant features. The advantage of cluster analysis is that the problems associated with selected training areas are eliminated. However, the minimum distance to means algorithm employed by this technique is not as sensitive to cluster variance within the feature space as the maximum-likelihood classifier, thus introducing the possibility of greater spectral confusion.

A comparison between the classified image and the vegetation map (Appendix B) indicates that only two out of the five vegetation classes on the image correspond to mapped vegetation units and can be positively identified as vegetation, green *Acacia* woodland and dense shrub. The canopy cover of the three remaining classes; medium, open and sparse shrub appears to be too low for these classes to be discriminated from the background soil reflectance. Areas of green *Acacia* woodland/bushland have been successfully classified on the basis of a distinctive spectral response from a green vegetation canopy. Other areas of dense, non-green bushland have also been successfully classified. In these areas the vegetation canopy masks the background soil reflectance and results in a very strong spectral contrast between the dense bush cover and the surrounding bright-toned soil surface.

A computer-assisted classification of the Kargi subscene produced no additonal information about the characteristics of the vegetation cover than could be obtained from a visual interpretation of the false colour imagery. The classifier was unable to discriminate vegetation of low canopy cover and was unsuccessful as a means of displaying variation in green vegetation cover. Multispectral classification techniques have been used successfully for the rapid and precise classification of large areas into different land cover types where the contrast between spectrally homogeneous units is well defined. In these areas, for example the humid tropical regions of high vegetation cover, features form separable clusters in the Landsat feature space allowing for their successful classification. The advantage of the computer-assisted classifier in such areas is related to the ability of the classifier to assign individual pixels to a particular class which gives a more precise result than can be achieved from a visual interpretation of the image.

Most of the vegetation cover in the Study Area however, is too sparse and spectrally indistinguishable from bare soil to be successfully classified, and a more sensitive technique was therefore required.

7.3 PRINCIPAL COMPONENTS ANALYSIS

Principal components analysis (PCA) was used initially to examine the multi-channel structure of Landsat data, with a view to exploring the potential of this technique for vegetation mapping within the Study Area.

A principal components transformation is completely determined by the choice of the sample set on which the covariance matrix will be computed (Mulder and Donker, 1976). Eigenvalues and eigenvectors were therefore calculated separately for the whole scene containing a mixture of bare soil, green vegetation, non-green vegetation, plant litter and shadow; and for a sample of the scene containing only bare soil. In this way the differences between the distribution in multi-dimensional space for bare soil alone, and for bare soil covered by a vegetation canopy were analysed. The eigenvectors, sometimes called loadings, of the two distributions are presented in Table 7.4 and graphically represented in Figure 7.2 for bare soil, and in Figure 7.3 for the whole scene.

Figure 7.2 illustrates the way in which the four MSS wavebands for the bare soil data have been transformed into the first principal component (PC_1). It is a pixel-wise subtraction of the intensities of MSS wavebands 4 and 5, and an addition of the intensities of MSS wavebands 6 and 7. The bipolar component shown by the negative and positive loadings on the first component for bare soil is mainly the differenc between the two highly correlated visible wavebands (MSS 4 and 5) and the two highly correlated near infra-red

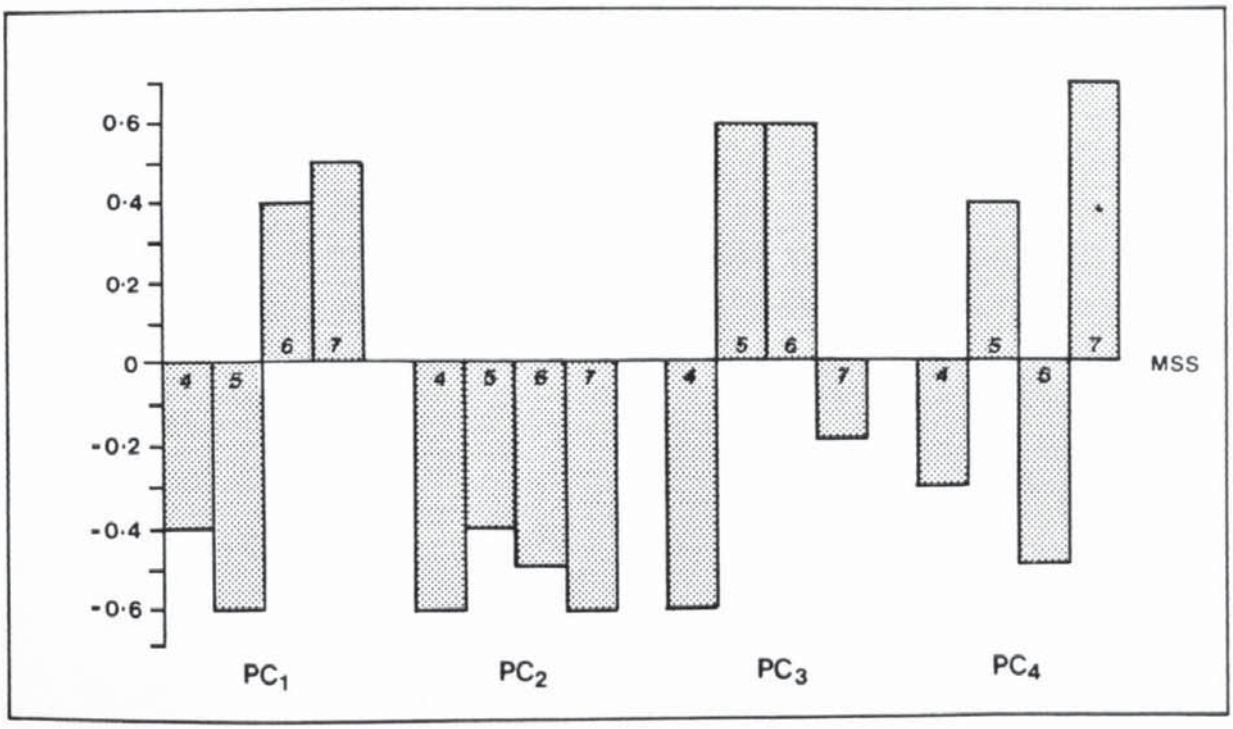

Figure 7.2 Principal Component (PC) Loadings for Bare Soil

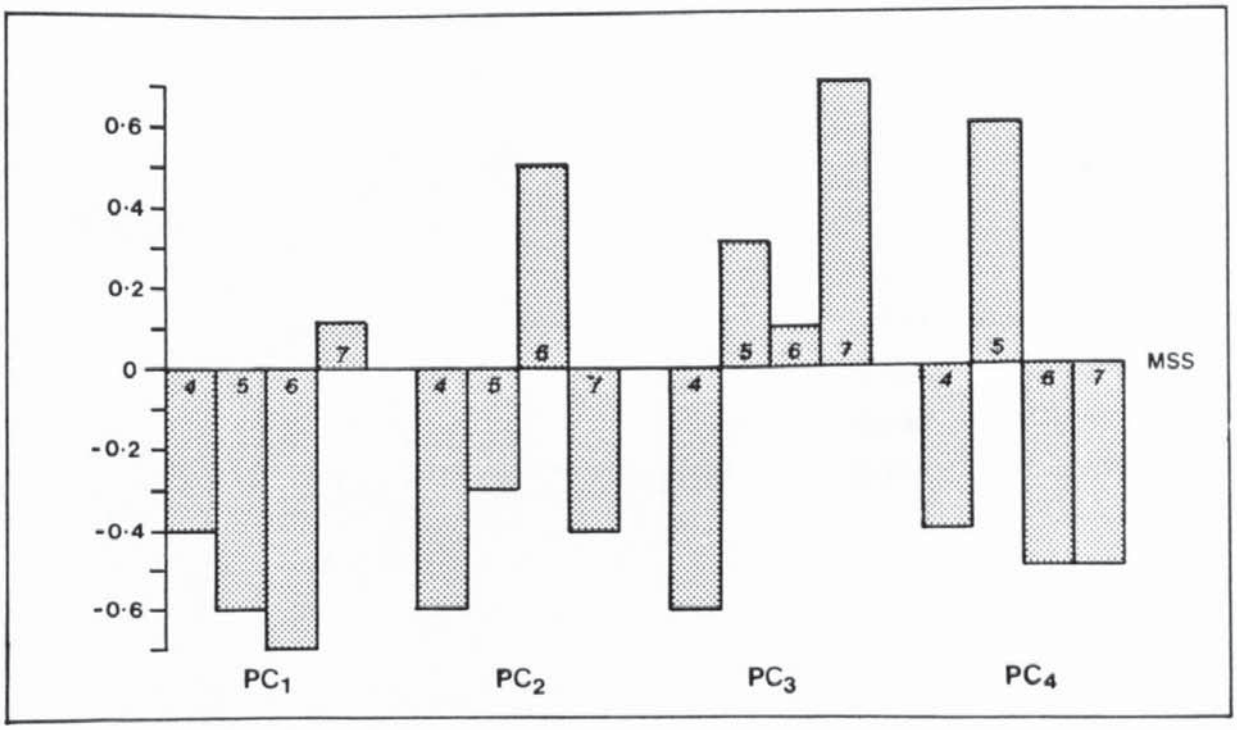

Figure 7.3 Principal Component (PC) Loadings for Bare Soil Covered with Vegetation

TABLE 7.4 EIGENVECTORS AND EIGENVALUES FOR BARE SOIL DATA (a) AND FOR BARE SOIL COVERED WITH VEGETATION (b)

(a) Bare soil

	PC1	PC2	PC3	PC4
Eigenvalue	373.98	24.74	4.46	2.03
Variance	92.2	6.1	1.1	0.5
Cumulative Variance	92.2	98.3	99.4	100.00
Amplitude	19.34	4.97	2.11	1.42
Eigenvectors	-0.372	-0.619	0.437	0.535
	-0.645	-0.359	-0.476	-0.475
	-0.574	-0.561	0.558	-0.205
	-0.338	-0.413	-0.518	0.667

(b) Bare soil and vegetation

	PC1	PC2	PC3	PC4
Eigenvalue	70.0	2.33	1.66	1.2
Variance	92.8	3.1	2.1	1.6
Cumulative variance	92.8	95.9	98.0	99.6
Amplitude	8.37	1.53	1.29	1.1
Eigenvectors	-0.374	-0.630	-0.564	-0.378
	-0.637	-0.298	0.336	0.625
	-0.659	0.553	0.146	-0.487
	0.735	-0.455	0.739	-0.477

wavebands (MSS 6 and 7). Principal component two (PC_2) is a subtraction of the intensities in all four Landsat wavebands and represents the high correlation between all pairs of channels shown by the correlation matrix (Table 7.5 (a)) for the bare soil reflectance data. The third component (PC_3) is the difference between MSS wavebands 4 and 7 and MSS wavebands 5 and 6, whilst the fourth component (PC_4) is the difference between MSS wavebands 4 and 6 and MSS wavebands 5 and 7.

TABLE 7.5 LINEAR CORRELATION IN THE FOUR LANDSAT WAVEBANDS FOR REFLECTANCE OF BARE SOIL (a) AND FOR REFLECTANCE OF BARE SOIL COVERED WITH VEGETATION (b)

	MSS Waveband			
(a) Bare soil				
	MSS 4	MSS 5	MSS 6	MSS 7
MSS 4	1.00			
MSS 5	0.90	1.00		
MSS 6	0.87	0.93	1.00	
MSS 7	0.80	0.87	0.89	1.00
(b) Whole scene				
	MSS 4	MSS 5	MSS 6	MSS 7
MSS 4	1.00			
MSS 5	0.92	1.00		
MSS 6	0.82	0.95	1.00	
MSS 7	0.69	0.84	0.94	1.00

A pattern also emerges from an analysis of the eigenvectors for data from the whole scene (Figure 7.3). The first principal component is a pixel-wise subtraction of the pixel intensities in MSS wavebands 4, 5 and 6 and an addition of pixel intensities in MSS 7. The second principal component is a subtraction of the pixel intensities in MSS wavebands 4, 5 and 7 and an addition of pixel intensities in MSS 7.

The differences between the eigenvectors and eigenvalues for bare soil and for the whole scene, indicate that the addition of a vegetation canopy considerably modifies the shape and orientation of the transformed bare soil distribution in multi-dimensional space. From Table 7.4 the amplitudes of the eigenvalues describe a distribution for both bare soil data and for bare soil covered with vegetation which is essentially an elongated ellipsoid in

which the first principal component accounts for more than 92 per cent of the total variance in the data-set. However this basic similarity in shape belies important differences between the two distributions. In PC_2 for example, the amplitude of the bare soil distribution is roughly three and a half times greater than the amplitude of the distribution for data within the whole scene (Table 7.4). Thus, in three-dimensional space the distribution for bare soil is long and thin ('cigar-shaped'), whilst the distribution for a vegetated surface is wider and gently domed ('saucer-shaped').

7.3.1 Physical Interpretation of Principal Components

Principal components analysis has provided useful insights into the dimensionality of the image data, but so far very little information about the physical interpretation of the components with respect to land cover types. In particular it is not known which characteristic of the vegetation cover define the new set of spectral axes, or which component this characteristic is most closely associated with. Other workers (Allen and Richards, 1983; Mulder and Donker, 1976) have found that the first component, which accounts for maximum variance in the data-set, is related to soils, whilst the second component, orthogonal to the first, is related to green plant development. This idea accords with the model of vegetation reflectance described in Chapter 6; a triangular MSS 7/5 data space defined by a bare soil baseline and green vegetation at the apex of the triangle. However, an examination of the principal component images suggests that the relationship between components and land cover types in this semi-arid region of northern Kenya is not straightforward.

A principal component image is generated by projecting the image data of a scene onto a new set of spectral axes, such that each component is associated with a principal component image (Chapter 2). This is achieved by the transformation:

$$Y^{n}_{1_i} = X_{1i} + X_{2i} + X_{3i} + X_{4i} + Xni \qquad [1]$$

which projects the ith pixel onto n principal axes, multiplying the observed values of X_1 to X_n by the corresponding elements of the eigenvectors for each component.

The PC_1 image (Figure 7.4 (a)), which is equivalent to a negative of a single Landsat channel, is essentially a brightness image and displays variations in the intensity of different land cover features. Brightness is related to both soil reflectance and vegetation canopy cover (Chapter 5). The PC_1 image is therefore a map of variations in soil reflectance and vegetation cover within the Kargi subscene.

(a)

PC_1

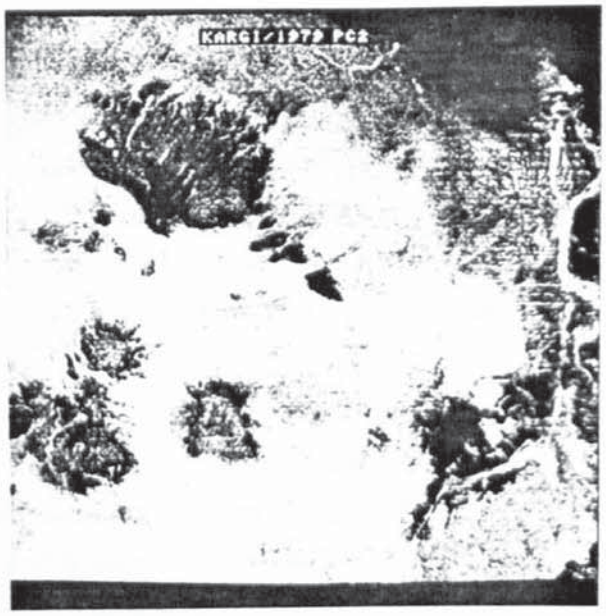

(b)

PC_2

(c)

PC_3

(d)

PC_4

Figure 7.4 Principal Component Images of the Kargi Subscene, PC_1 (a), PC_2 (b), PC_3 (c) and PC_4 (d)

In the PC_2 image (Figure 7.4 (b)) green vegetation is brighter than both bare soil and non-green vegetation and can therefore be discriminated in this component. PC_2 is orthogonal to PC_1 and, theoretically, represents a measure of vegetation greenness parallel to the soil line or brightness plane. The PC_2 image was median-filtered and density-sliced to create an image displaying five green cover classes in contrasting colours (Figure 7.5). On the basis of fieldwork, areas known to be bare soil were assigned to one class and the remainder of the PC2 intensity range was divided equally into four green cover classes (Table 7.6).

The eigenvalues (Table 7.4) showed that the distribution of bare soil spectra do not describe a single dimensionless line in multi-dimensional space, but are enclosed by a data envelope having width as well as length. This means that bare soil contributes variance to PC_2 in addition to PC_1, such that bare soil also contains a greenness component. Hence the first class with the lowest intensity in the PC_2 greenness image represents bare soil.

As well as differnt land cover types contributing to the variance in different principal components, different land cover types also contribute equal variance within the same component. Areas of green vegetation and bright bare soil are both displayed in dark tones on the PC_3 image (Figure 7.4 (c)). In this component therefore, green vegetation cannot be discriminated from bright bare soil. PC_3 is weighted towards MSS 7, hence green vegetation with a high reflectance in the near-infrared and bright bare soil also with a high near-infrared reflectance, are spectrally indistinguishable in the PC_3 image.

The results from an analysis of the separate component images therefore shows that:

(a) More than one cover type contributes to the variance in a single component;
(b) Different cover types contribute the same amount of variance in a single component.

These two points are summarised in Table 7.7. The intensity of the four different cover types in each component; bright bare soil, dark bare soil, non-green and green vegetation have been classified as low, medium or high. This simple classification corresponds to the projected scores of each cover types in the three separate components. Principal component four (PC_4) illustrated in Figure 7.4 (d), has not been included in this analysis as it contains no useful land cover information. The small per cent variance contributed to this component (Table 7.4) is essentially radiometric striping caused by sensor mismatch. From Table 7.7 it can be seen that non-green and green vegetation cannot be differentiated in PC_1; bright soil and dark soil cannot be differentiated in PC_2 and bright soil and green

Figure 7.5 A Density-Slice of the PC_2 Image for the Kargi Subscene

TABLE 7.6 SOIL AND VEGETATION CLASSES FOR THE PC_2 GREENNESS IMAGE OF THE KARGI SUBSCENE

Class No.	Class name	Colour on image
1	Bright/dark bare soil	Grey
2	Shrub (low green cover)	Light blue
3	Shrub (medium green cover)	Green
4	Shrub (high green cover)	Red
5	Woodland (very high green cover)	Cyan

vegetation cannot be differentiated in PC_3. Likewise, bright bare soil contributes roughly equal variance in PC_1, PC_2 and PC_3; dark soil contributes equal variance in PC_1 and PC_3 and non-green vegetation contributes equal variance in PC_1 and PC_2. Only green vegetation contributes a different amount of variance to each component and is therefore separable in all three components.

It was argued in the three-component model presented in Chapter 6, that a pixel contained a spectral mix of bare soil, non-green vegetation and green vegetation. In two-dimensional space the location of a pixel was therefore determined by the outer dimensions of a triangular data space whose vertices were represented by a 100 per cent cover of bare soil, non-green and green vegetation. According to the diagram (Figure 7.6), which defines a soils plane of two components (PC_1 and PC_3) and a green vegetation plane of two components (PC_1 and PC_2) these two planes are orthogonal to each other with PC_1 forming the intersection. Thus a pixel can be resolved onto only one component (point 1 on Figure 7.6) i.e. along the major axis PC_1; onto two components i.e. on the plane of soils defined by PC_1 and PC_3 (point 2), or on the plane of vegetation defined by PC_1 and PC_2 (point 3). Finally a pixel could be resolved onto all three components (PC_1, PC_2 and PC_3) i.e. within the triangular wedge between the plane of soils and the plane of vegetation (point 4).

In models of green vegetation reflectance bare soil is normally represented by a single straight, dimensionless line in multi-dimensional space along which variations in the amplitude, but not the frequency of the spectra occur. Green vegetation develops perpendicularly outwards from this straight line in the second component and the data structure is assumed to be essentially two-dimensional with the first two components commonly accounting for 98 per cent of the total variance in the data-set. In this situation a pixel containing a mixture of green vegetation and bare soil would therefore simply be projected onto the vegetation plane. Recently the idea of a single dimensionless soil line has been discredited and the concept of an 'envelope' of soils that describes variance both along and orthogonal to the major axis, has been introduced. Jackson, (1983) demonstrated how differences in soil moisture content for soils of mineralogically varying composition produced significant spectral frequency shifts in a sample of soils. There is some evidence to suggest that reflectance from soils within the Study Area varies both in amplitude and frequency. This is most clearly expressed by the considerable variations in colour of bare soil on a false colour image of the study area; saline soils in the Chalbi desert appear blue whilst sandy-loam soils appear green. It is hypothesised that the small percentage variance contributed by PC_3 is due to slight changes in the frequency spectra of bare soil within the

TABLE 7.7 SPECTRAL CONFUSION BETWEEN AND WITHIN THE FIRST THREE PRINCIPAL COMPONENTS

Within components	Between components: PC_1	PC_2	PC_3
Bright bare soil	L	L	L
Dark bare soil	H	L	H
Non-green vegetation	M	M	H
Green vegetation	M	H	L

L = Low intensity

M = Medium intensity

H = High intensity

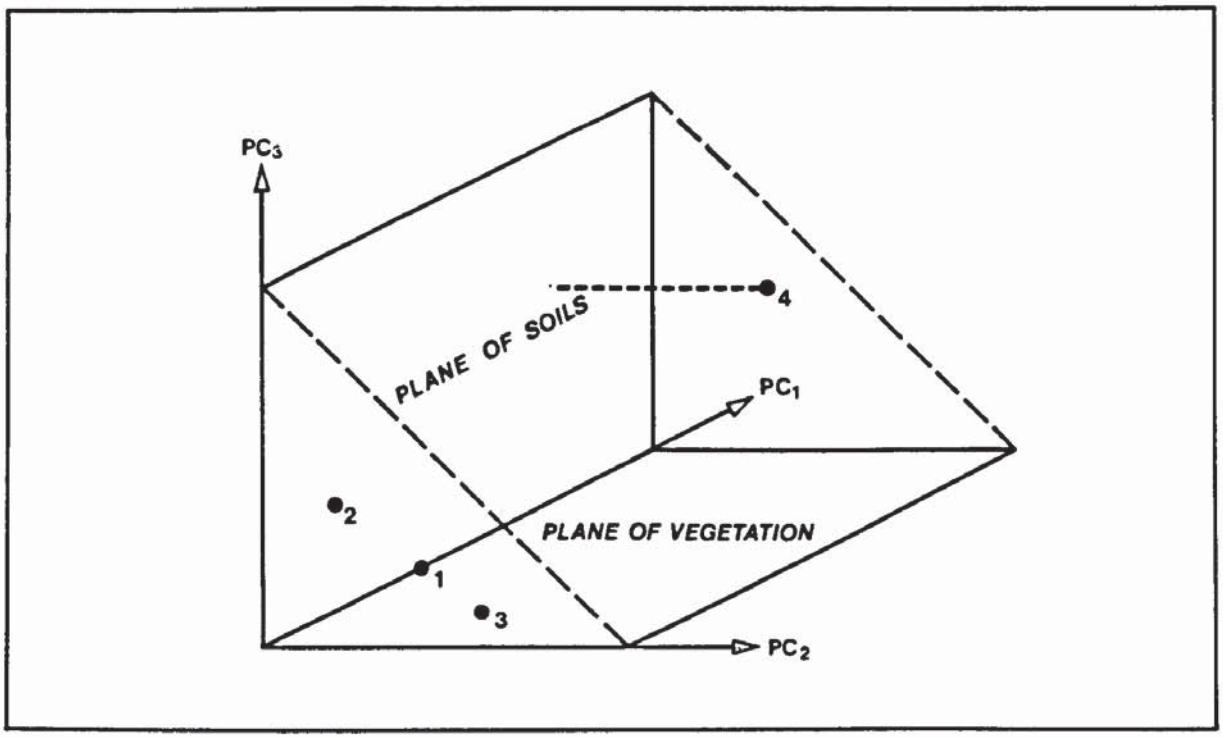

Figure 7.6 The Plane of Soils and the Plane of Vegetation Defined by the First Three Principal Components

Study Area. As a result, soil is represented by a plane of soils defined by PC_1 and PC_3, and not a single line represented by PC_1 alone. In general therefore, pixels containing green vegetation and growing on soils which vary both in amplitude and frequency will be resolved onto all three components simultaneously and lie within the wedge-shaped space illustrated in Figure 7.6.

The ability to discriminate land cover features in separate component images will depend upon differences in intensity between features. Spectral confusion between land cover types can potentially be reduced by combining the spectral information in all three components and producing a colour-coded image (Figure 7.7). The concept is analogous to combining multi-spectral channels in a false colour image, but with the additional advantage of a rotation of spectral axes. In the colour-coded feature space pixels that lie precisely on a principal component will appear red in PC_1, green in PC_2 and blue in PC_3. Pixels which are defined by two components and are located on a plane will be differentiated by varying hues; dark bare soil which is enhanced in PC_1 and PC_3 will be a mixture of red and blue and will appear in magenta on the colour-coded principal components image. Pixels which lie in the wedge-shaped space between the soil and vegetation planes will be a mixture of PC_1, PC_2 and PC_3 (red, green and blue) and will be differentiated in terms of saturation or whiteness:

Figure 7.7 Colour-coded Composite Image of $PC_{1/2/3}$ for the Kargi Subscene

SINGLE COMPONENT	PLANE DEFINED BY TWO COMPONENTS	SPACE DEFINED BY THREE COMPONENTS
Intensity	Hue	Saturation
PC_1 - Red	$PC_1 + PC_2$ - Yellow	
PC_2 - Green	$PC_1 + PC_3$ - Magenta	$PC_1 + PC_2 + PC_3$ - Brightness
PC_3 - Blue	$PC_2 + PC_3$ - Cyan	

Accordingly, in the colour-coded principal components image different land cover types will appear in the colours indicated by Table 7.8.

The colour-coded principal components image is a more effective means of differentiating between land cover types than any of the single component images. However, the image is difficult to interpret into physically significant land cover types. Many of the subtle differences in colour on the image are probably related to variations in soil mineral content and other soil related factors which it is wished to suppress rather than enhance.

TABLE 7.8 COLOUR CODE FOR MULTI-COMPONENT IMAGE

Class name	Image colour
Saline soils	Red
Sandy-loam soils	Green/Cyan
Bright sand soils	Blue
Dark soils/lava	Magenta
Non-green vegetation (sparse cover)	Cyan
Non-green vegetation (dense cover)	Yellow
Green vegetation (dense cover)	Bright green

This is due to the fact that the transformation defines a new set of spectral axes which may have no basis for the physical interpretation of land cover features. Statistical procedures such as principal components analysis are therefore well suited for analysing large areas where little a priori knowledge of soils and vegetation is available, but a more refined technique is required which enables particular land cover features to be associated with specific components.

7.4 VEGETATION INDICES

Kauth and Thomas (1976) proposed a transformation that used the four Landsat MSS bands in linear combinations to produce four indices; brightness, greenness, yellowness and non-such (Chapter 2). The transformation is calculated using the Gramm-Schmidt process (Freiberger, 1960) to obtain four orthogonal linear combinations of the four Landsat wavebands. From a Landsat image Kauth and Thomas (1976) selected clusters of pixels which they indentified as soil, and other clusters which they identified as vegetation, and calculated the appropriate units vectors which form the coefficients for the transformation. In this way the transformation is constrained such that the rotation defines a new set of spectral axes which form physically significant indices in n-dimensional space.

The bright soil, dark soil and green vegetation reflectance points (Table 5.4) were used to define the transformed spectral axes using the Gramm-Schmidt orthogonalisation procedure described in Section 2.5.2. A BASIC computer program (Appendix H) was written to calculate the brightness and greenness coefficients of these spectral components in multi-dimensional Landsat space. For comparative purposes, the brightness and greenness coefficients for ten different waveband combinations were calculated (Table 7.9).

The coefficients were used to plot a sample of bare soil pixels and green vegetation pixels onto the transformed spectral axes in MSS 7/6/5/4 space (Figure 7.8) and in MSS 7/5 space (Figure 7.9). These two waveband combinations were chosen to compare the differences between the distributions in two-dimensional MSS 7/5 space and in four-dimensional MSS 7/6/5/4 space. In the two-dimensional case the distribution of bare soil and green vegetation in the brightness/greenness plane, is equivalent to a simple rotation of the original spectral axes as indicated in Figure 7.9.

To make an accurate comparison between different waveband combinations or between multi-temporal imagery for the same waveband combination, a correction must be made to account for differences in soil line intercept values. In n-space the soil line will not usually pass through the origin and greenness will not therefore be zero for bare soil. From Table 7.10 the greenness of bright bare soil is -1.89 in MSS 7/6/5/4 space and 2.58 in MSS7/5 space. The correction is a simple subtraction of the greenness values for bare soil from the greenness values for green vegetation. An average soil greenness value has been used to calculate the correction factor, based upon the assumption that the reflectance of the majority of soils within the study area will give a reflectance which is close to this average figure.

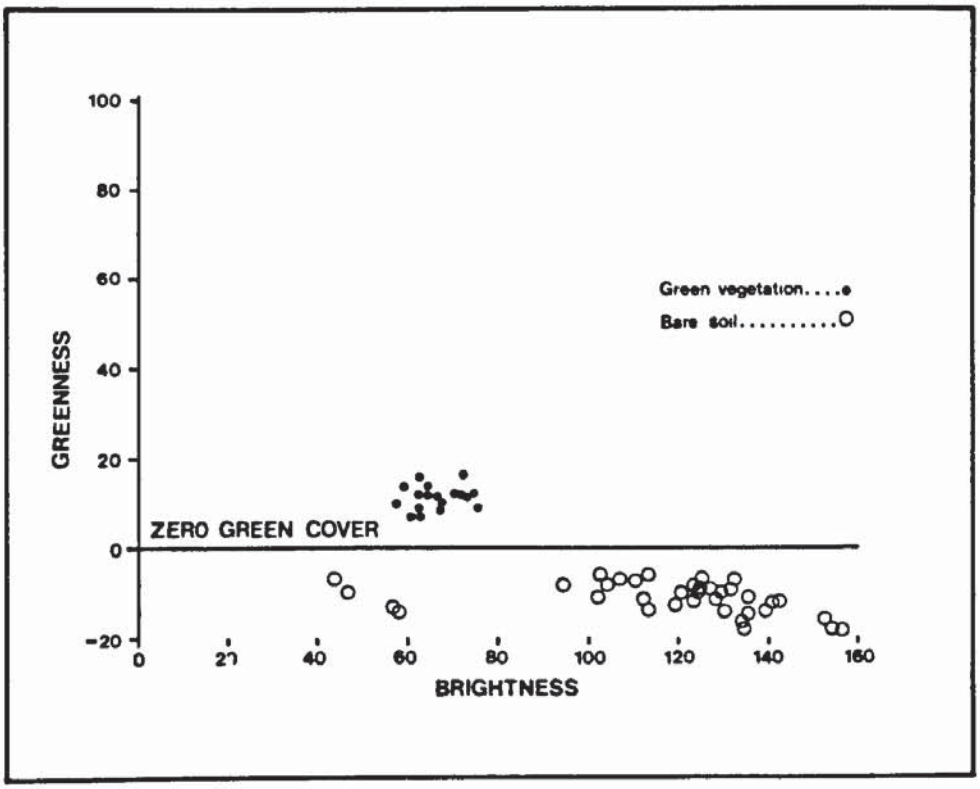

Figure 7.8 The Distribution of Bare Soil and Green Vegetation in Transformed MSS 7/6/5/4 Brightness/greenness Space

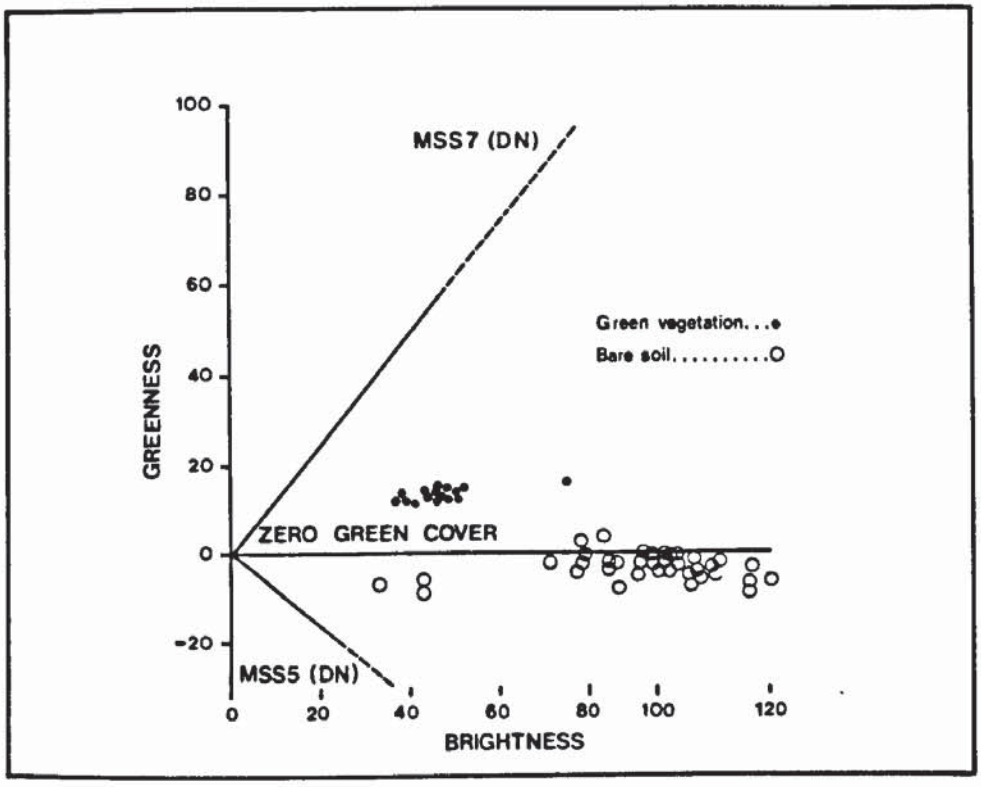

Figure 7.9 The Distribution of Bare Soil and Green Vegetation in transformed MSS 7/5 Brightness/greenness Space

TABLE 7.9 BRIGHTNESS AND GREENNESS COEFFICIENTS OF SPECTRAL COMPONENTS CALCULATED FROM THE GRAMM-SCHMIDT ORTHOGONALISATION PROCEDURE

Waveband combination		Brightness coefficients	Greenness coefficients
1	MSS 7/6/5/4	0.42	0.51
		0.60	0.45
		0.61	-0.64
		0.30	-0.35
2	MSS 7/5/4	0.53	0.83
		0.76	-0.48
		0.37	-0.28
3	MSS 7/6/5	0.44	0.49
		0.62	0.39
		0.64	-0.78
4	MSS 7/5	0.57	0.82
		0.82	-0.56
5	MSS 7/6/4	0.62	0.35
		0.65	0.32
		0.44	-0.88
6	MSS 6/5/4	0.66	0.74
		0.68	-0.58
		0.33	-0.32
7	MSS 7/4	0.82	0.53
		0.57	-0.84
8	MSS 6/5	0.70	0.73
		0.72	-0.68
9	MSS 6/4	0.89	0.44
		0.45	-0.90
10	MSS 5/4	0.90	0.36
		0.44	-0.93

TABLE 7.10 CALCULATED GREENNESS VALUES FOR BRIGHT BARE SOIL, DARK BARE SOIL, NON-GREEN VEGETATION AND GREEN VEGETATION IN MSS 7/6/5/4 SPACE (a) AND MSS 7/5 SPACE (b)

(a) MSS 7/6/5/4 space

	Greenness value
Bright bare soil	-1.89
Dark bare soil	4.37
Non-green vegetation	-1.15
Green vegetation	16.5

(b) MSS 7/5 space

Bright bare soil	2.58
Dark bare soil	7.02
Non-green vegetation	6.2
Green vegetation	16.04

TABLE 7.11 CORRECTED GREENNESS VALUES

	Waveband Combination	Average Greenness value of bare soil point	Greenness value of maximum green vegetation point	Corrected greenness value
1	MSS 7/6/5/4	-1.89	16.25	18.14
2	MSS 7/5/4	-3.09	12.98	16.07
3	MSS 7/6/5	-2.50	15.89	18.39
4	MSS 7/5	2.58	16.04	13.46
5	MSS 6/5/4	-2.08	12.72	14.80
6	MSS 7/6/4	4.07	10.74	6.67
7	MSS 7/4	-8.03	3.34	11.37
8	MSS 6/5	3.65	15.95	12.30
9	MSS 6/4	-6.58	2.68	9.26
10	MSS 5/4	-13.70	-8.88	4.82

The corrected values for the ten waveband combinations show that the corrected greenness range is highest in four-dimensional MSS 7/6/5/4 space, and lowest in two-dimensional MSS 5/4 space.

The total greenness range from the mean soil line to the point of maximum green vegetation indicates which combination of wavebands is optimal for discriminating green vegetation from bare soil for the majority of soil types found within the study area. However, in developing a technique for monitoring green vegetation productivity which could be applied within a wide range of environments, it is clearly important to determine to what extent variations in the width of the soil envelopes affect the green cover limit i.e. the per cent cover below which green vegetation cannot be discriminated from bare soil.

The width of the soil envelope in four-dimensional MSS 7/6/5/4 space (Figure 7.8) is greater than in two-dimensional MSS 7/5 space (Figure 7.9). This is believed to be due to the inclusion of MSS 4 in the four-dimensional transformation.

It was demonstrated in Chapter 5 that soil data in MSS 7/4 space were widely scattered about a linear regression line which was a relatively poor-fit to the data compared with other waveband combinations. The green cover limit is therefore determined by two factors; the total dynamic range of greenness and the width of the soil envelope.

Both these factors can be incorporated into an index of the true green cover range for different waveband combinations. The threshold below which green vegetation cannot be discriminated from bare soil is equal to the width of the soil envelope in the greenness direction (Gb), divided by the total greenness range (Gr). The green vegetation threshold (GVT) can be expressed:

$$GVT = \frac{Gb}{Gr} \times 100 \text{ (per cent)} \qquad [2]$$

It is assumed in the results presented in Table 7.12 that the maximum green vegatation point represents 100 per cent cover of green vegetation and that the greenness range is equivalent to a per cent green cover scale. In practice this assumption could not be verified in the field, a problem which is discussed in more detail in the concluding chapter.

The GVT results presented in Table 7.12 show that when both factors, the total greenness range and the width of the soil envelope are taken into account, two wavebands (MSS 7/5) are equally as effective as four wavebands in discriminating green vegetation from bare soil. The results represent the worst case in that the total width of the soil envelope is influenced by those few soil points which lie outside the main data cluster in brightness/greenness space (Figure 7.8 and Figure 7.9). Statistical linear regression analysis could be used to define the width of the soil envelope at specified confidence limits, but this was not undertaken in the present study. However, if the greenness of the mean soil line in two-dimensional MSS 7/5 space is used to define the limit below which green vegetation cannot be discriminated from bare soil (Figure 7.9), then for the majority of soil types within the study area, green vegetation cannot be discriminated from bare soil at less than 20 per cent cover.

The results show that a technique for mapping green vegetation based upon a linear combination of two wavebands in the visible red (MSS 5) and the near-infrared (MSS 7) is as effective for mapping green vegetation cover as four wavebands. On the basis of these findings a two-dimensional vegetation index was developed for mapping green vegetation cover, and applied within the study area.

TABLE 7.12 THE GREEN VEGETATION THRESHOLD (GVT) VALUES IN FOUR-DIMENSIONAL MSS7/6/5/4 SPACE AND TWO-DIMENSIONAL MSS 7/5 SPACE

Waveband combination	Greenness range (Gr)	Width of soil envelope (Gb)	GVT (%) (Gb/Gr)
MSS7/6/5/4	16.25	7.50	46
MSS7/5	16.04	5.0	31

7.5 TWO-DIMENSIONAL VEGETATION INDICES

A perpendicular vegetation index[1] (PVI) was developed on the basis of the model of vegetation reflectance described in Chapter 6. In that model it was demonstrated that lines of equal green cover lie parallel to the soil line, hence a measure of green vegetation cover is equal to perpendicular distance from the soil line. The vegetation index,which was described in Chapter 3,uses analytical geometry to measure distance along the soil line:

1. The PVI referred to in this thesis should not be confused with the PVI of Richardson and Wiegand (1977).

$$S_d = MSS\ 5 \cos\theta + MSS\ 7 \sin\theta \quad [3]$$

and distance along a green vegetation line perpendicular to the soil line;

$$G_d = MSS\ 7 \cos\theta - MSS\ 5 \sin\theta \quad [4]$$

where S_d is distance along the soil line, G_d is perpendicular distance along the green vegetation line and θ is the angle between the soil line and the x axis (MSS 5). The values of sin θ (0.58) and cos θ (0.81) can be found from the equation for the soil line in MSS 7/5 space ($y = 0.75x - 2.16c$).

Equation [3] was used to generate a brightness image for the Kargi subscene.

This image is a weighted transformation of MSS 5 and MSS 7 and is similar in appearance to the PCI image (Section 7.3). The brightness image shown in Figure 7.10 has been contrast enhanced and clearly displays differences in brightness along the 'cover line' from shadow and non-green vegetation to bright bare soil. Density-slicing was used to divide the brightness range into two unvegetated classes and four vegetated classes (Figure 7.11). This division of the brightness range into soil and vegetation classes was only possible on the basis of field information about the distribution of bare soil within the Study Area. Once these areas had been identified and assigned to a range of brightness values at the upper and lower ends of the range, equal divisions of the remaining brightness range represent per cent canopy cover classes as indicated in Table 7.13. This assumes that soil reflectance is uniform and that the relationship between brightness and vegetation canopy cover is perfectly linear. The findings discussed in Chapter 5 showed that for a uniform soil reflectance, an increase in vegetation canopy cover is associated with a decrease in reflectance, but a detailed analysis of the form of this relationship, was not undertaken. It is clear from a comparison between the brightness image and the soil and vegetation maps (Appendix B) that areas of dense bushland can be accurately mapped from the image, but at lower canopy cover differences in soil reflectance dominate the brightness values. Thus dense shrub cover (Class 2) and medium shrub cover (Class 3) can be discriminated from bare soil, but at a canopy of less than about 50 per cent, differences in soil reflectance reduce the accuracy with which open shrub cover (Class 4) and sparse shrub cover (Class 5) can be positively identified.

Figure 7.10 The Brightness Image for the Kargi Subscene

Figure 7.11 A Density-slice of the Brightness Image for the Kargi Subscene into Soil and Vegetation Canopy Cover Classes

TABLE 7.13 SOIL AND VEGETATION CLASSES FOR THE BRIGHTNESS IMAGE OF THE KARGI SUBSCENE

Class No.	Class name	Colour on image	Per cent canopy cover
1	Dark bare soil/lava	Grey	0
2	Shrub (dense cover)	Light blue	75 - 100
3	Shrub (medium cover)	Dark blue	50 - 75
4	Shrub (open cover)	Green	25 - 50
5	Shrub (sparse cover)	Dark green	0 - 25
6	Bright bare soil	Red	0

A greenness image of the Kargi subscene was generated using Equation [4] and is illustrated in Figure 7.12. This image is a weighted subtraction of MSS 5 from MSS 7 and represents distance along a 'green cover line' perpendicular to the soil line. The distance between the mean soil line and the maximum green point is equivalent to a linear scale ranging from zero green cover to 100 per cent green cover. This was demonstrated in the three-component model (Chapter 6), enabling the greenness range to be divided into equal green cover classes. The greenness image was therefore density-sliced to give two bare soil classes and six green cover classes, and coloured to enhance the contrast between units (Figure 7.13).

The bare soil class incorporates the width of the soil envelope in the greenness direction and is equal, according to the results discussed in Section 7.4, to approximately 15 - 20 per cent of the total greenness range. The remaining six green cover classes therefore represent equal divisions of the greenness range from 15 per cent cover to 100 per cent cover, as shown in Table 7.14. The area of each class in hectares and as a percentage of the total area is also given.

7.6 GREEN VEGETATION COVER MAP

The greenness image (Figure 7.13) was used to compile a map of the distribution of green cover classes within the Kargi subscene at 1:200,000 scale (Figure 7.14 and Appendix B). This scale is compatible with the scale of the soil and vegetation maps, enabling comparisons to be made between all three maps.

Figure 7.12 The Greenness Image for the Kargi Subscene

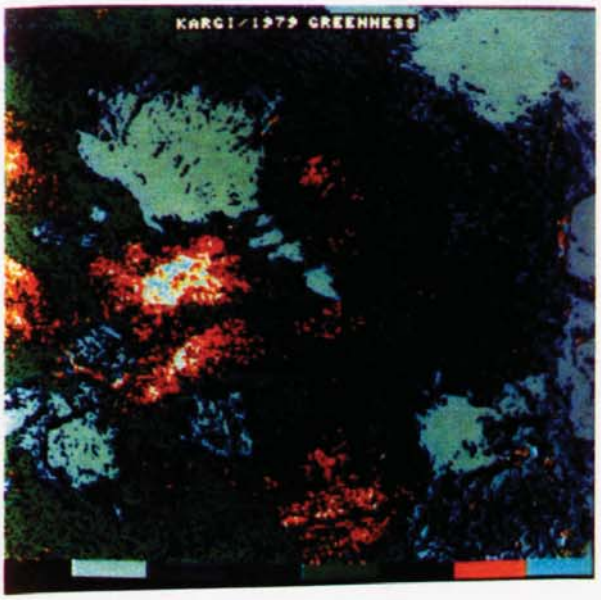

Figure 7.13 A Density-slice of the Greenness Image for the Kargi Subscene Into Green Cover Classes

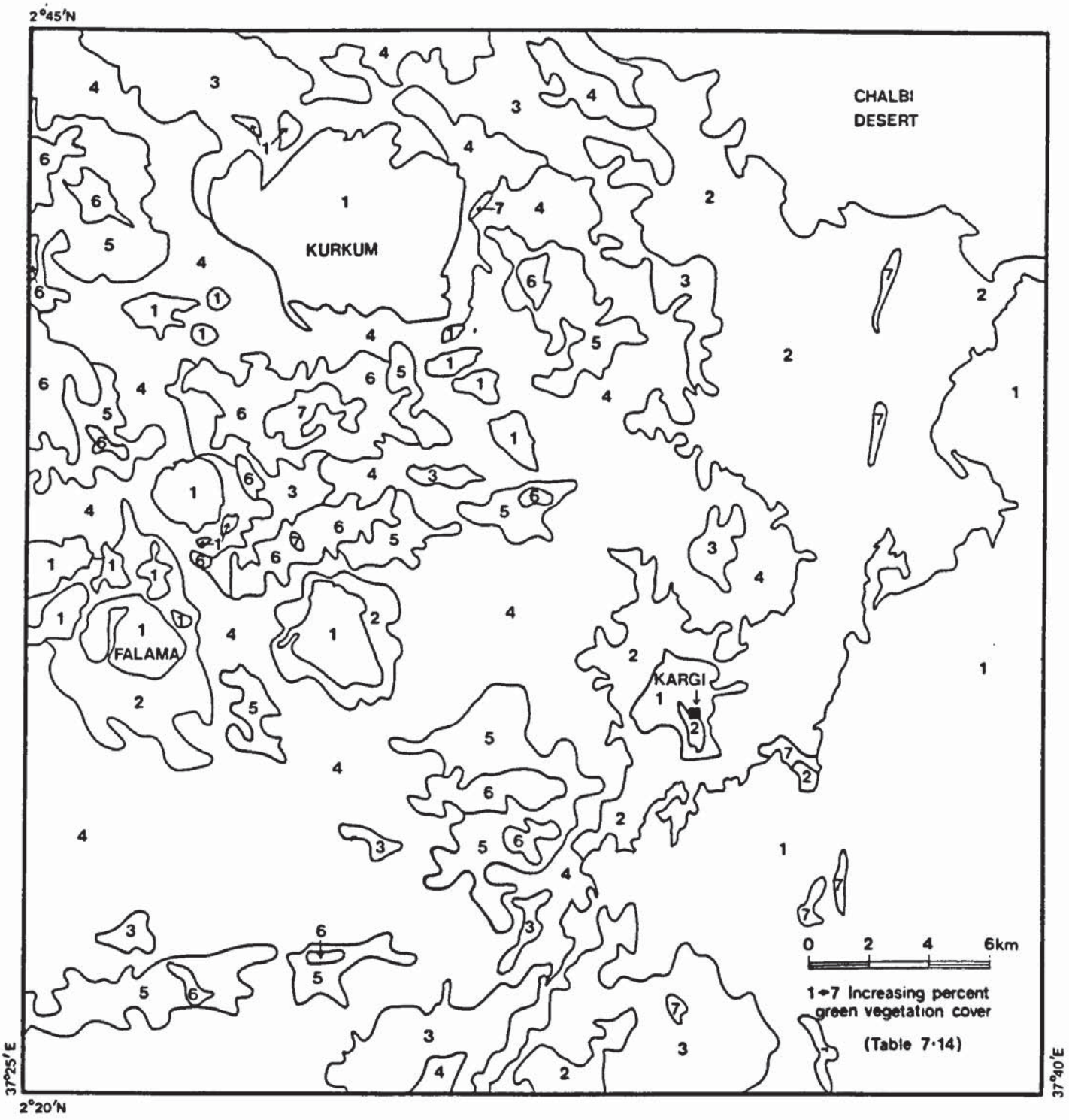

Figure 7.14 The Green Cover Map Showing Relative Differences in Green Vegetation Cover Within the Kargi Subscene

TABLE 7.14 A DIVISION OF THE GREENNESS IMAGE FOR THE KARGI SUBSCENE INTO SEVEN GREEN COVER CLASSES AND THE AREA IN PER CENT COVER AND HECTARES OF EACH CLASS

Class No.	Approximate per cent green cover	Colour on image	Per cent area	Hectares
1	Zero	Grey	20	16442
2	Zero	Light blue	12	9865
3	15 - 30	Dark blue	15	12331
4	30 - 45	Light green	18	14797
5	45 - 60	Dark green	18	14797
6	60 - 75	Red	12	9865
7	>75	Cyan	5	4110
		TOTAL	100	82208[1]

[1] The Kargi subscene is 512 x 512 pixels (EDIPS pixels are 56 m x 56 m) to give a total area of 82208 ha.

7.6.1 A Comparison Between the Green Cover Map and the Soil and Vegetation Maps

From a comparison of the green cover map derived from the greenness image and the map of vegetation canopy cover, there appears to be only minimal correspondence between the greenness classes and vegetation canopy cover. The correspondence occurs where there is a marked change in the species composition or density of the vegetation cover, e.g. in areas of green *Acacia* woodland, very dense shrubland and sparse dwarf shrubland.

At intermediate greenness levels there is no apparent relationship between vegetation canopy cover and green cover, suggesting that in these areas the herbaceous layer is an important component of the greenness cover. Without field data obtained specifically at the date of image acquisition it is not possible to determine the relative proportions of herbaceous ground cover and canopy cover which contribute to measured greenness values. However, measurements of vegetation canopy cover from large scale aerial photography (Chapter 3) and from Lamprey (1981) show that herbaceous cover is a major component of the vegetation cover. It is believed that during growth post-rains, green herbaceous cover would make a significant contribution to greenness values.

A comparison between the green cover map and the soil map shows that the PVI is unaffected by variations in soil reflectance, except where a difference in green cover also coincides with a change in soil type. This occurs at the boundary between the zero green

cover classes i.e. bare soil/lava (Class 1 and 2 on the green cover map) and all other green cover classes. Silty-loam soils support a dense canopy of vegetation, and for this soil type a green cover class also coincides with a soil boundary. In all other areas, mapped differences in green cover do not coincide with soil boundaries, positive evidence that the PVI is independent of variations in soil reflectance. Some doubt has recently been cast upon the independence of orthogonal greenness measures from variations in soil brightness (Heute et al., 1985). This problem is discussed in more detail in the concluding Chapter (8) of this thesis.

7.7 MULTI-TEMPORAL GREENNESS IMAGES

The encouraging results obtained from the application of the PVI within the Kargi subscene, suggested that the effectiveness of the technique for monitoring changes in the distribution of green cover should be evaluated, and that the technique should be extended to a larger area.

It can be deduced from Figure 2.6 that if the slope of the soil line changes, the orthogonal distance to the maximum green vegatation point will also change. Constant soil line slopes are therefore a pre-condition for calculating a multi-temporal greenness index. The slopes of the soil lines for soil data sampled from the 1973 scene and the 1979 scene were shown to be statistically identical in Chapter 5, with soil lines passing through the origin. As a result the greenness values for the two Hedad subscenes can be compared directly without the need to equalise soil line slopes. In circumstances where the slopes of multi-temporal soil lines vary, possibly due to atmospheric effects, the soil lines should be rotated to the same slope coefficient using a method described by Hielkema (1980).

Scatter caused by haze will tend to increase scene brightness and move the soil line laterally in the feature space, thus introducing a high intercept term. However, unlike a radio technique the PVI is uninfluenced by differences in intercept between multi-temporal soil lines and the effects of scatter can be disregarded. Graetz and Gentle (1982) demonstrated that the dynamic range of the data measured in MSS DN along the cover-line from the point of shadow to the bare soil point, was 2.6 times greater under high sun illumination in mid-summer than in mid-winter. Under winter radiance conditions, Graetz and Gentle (1982) concluded that the Landsat data would be much less capable of resolving changes in plant cover than image data acquired in summer. The dynamic range of greenness would be similarly affected by differences in sun illumination and would be lower under low sun illumination. This was not a problem for a multi-temporal comparison of the January 1973 and June 1979 scenes. Sun angle is the same at the equator for the winter solstice (January) and the summer solstice (June).

The 1973 Hedad subscene was registered to the geometrically corrected 1979 Hedad subscene using cubic convolution resampling (Subsection 3.11.1). Greenness images for the 1973 and 1979 Hedad subscenes were generated from Equation [4] and density-sliced using the same values in each case (Figures 7.15 and 7.16).The per cent area and hectares in each class were computed using a function in the image analysis system. The results are given in Table 7.15.

TABLE 7.15 THE PER CENT COVER AND HECTARES FOR EACH GREENNESS CLASS IN THE 1973 HEDAD SUBSCENE (a) AND THE 1979 HEDAD SUBSCENE (b)

(a) 1973 subscene

Class No.	Class name (per cent green cover)	Per cent area	Hectares
1	Bare soil	24	68 516
2	Non-green vegetation	12	34 258
3	Green vegetation (15 - 30)	18	31 387
4	Green vegetation (30 - 45)	22	62 806
5	Green vegetation (45 - 60)	16	45 675
6	Green vegetation (60 - 75)	6	17 129
7	Green vegetation > 75	2	5 710
	TOTAL	100	285 481

(b) 1979 subscene

Class No.	Class name (per cent green cover)	Per cent area	Hectares
1	Bare soil	26	74 225
2	Non-green vegetation	13	37 113
3	Green vegetation (15 - 30)	20	57 096
4	Green vegetation (30 - 45)	22	62 806
5	Green vegetation (45 - 60)	14	39 967
6	Green vegetation (60 - 75)	4	11 419
7	Green vegetation > 75	1	2 855
	TOTAL	100	285 481

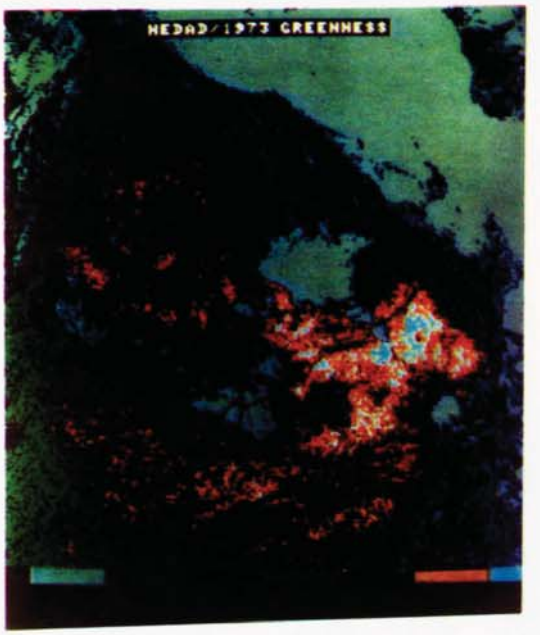

Figure 7.15 A Density-slice of the Greenness Image for the 1973 Hedad Subscene into Green Cover Classes

Figure 7.16 A Density-slice of the Greenness Image for the 1979 Hedad Subscene into Green Cover Classes

Bare soil and non-green vegetation account for approximately 25 per cent of the Hedad subscene in both years. The largest green cover class is between 30 - 45 per cent cover in both 1973 and 1979, and the smallest green cover class is between 75 and 100 per cent in both 1973 and 1979. The small differences in the area of each green cover class presented in Table 7.15 belies a marked change in the distribution of green cover classes between the two dates. This is clearly shown by comparing the 1973 greenness image for the Hedad subscene (Figure 7.15) with the 1979 greenness image for the same subscene (Figure 7.16). Particularly noticeable is the absence of green vegetation cover surrounding the settlement of Kargi in 1979 compared with 1973. This period coincided with a very large increase in the settled population and in the numbers of livestock, resulting in overgrazing and a general destruction of the surrounding vegetation cover (Chapter 1). A further difference between the two images is the absence of green vegetation within woodland areas along the base of the Kulal and Marsabit lava in the 1973 image, an effect possibly due to the drought conditions prevailing at this time.

Changes in the distribution of green cover classes between 1973 and 1979 are also displayed in the greenness 'difference' images which show:

1. The change in the distribution of the two highest green cover classes (6 and 7) (Figure 7.17).

2. the change in the distribution of the two middle green cover classes (4 and 5) (Figure 7.18).

The two greenness 'difference' images were generated by overlaying the selected green cover classes on the 1973 image with the selected green cover classes on the 1979 image, and adding the two images using a CPU function in the image analysis system. In Figure 7.17 green therefore represents green cover in 1979, red represents green cover in 1973 and blue represents green cover in both 1973 and 1979. Figure 7.17 shows a marked shift in the distribution of the two highest green cover classes over the period, with very little correspondence between the two dates. The change in the greenness of the linear woodland areas along the base of the Marsabit lava and fringing the Balesa Kulal river, is also clearly visible on the greenness 'difference' image, the woodland appearing green in 1979 but mostly non-green in 1973. A similar marked shift in the distribution of the two medium green cover classes is also displayed (Figure 7.18) although for these larger classes there is a much greater degree of overlap between green cover classes for the two dates. Greenness 'difference' images are an effective means of enhancing changes in the distribution of green cover within the Hedad subscene, and potentially could be used to monitor seasonal variations in green cover in response to rainfall and grazing pressure.

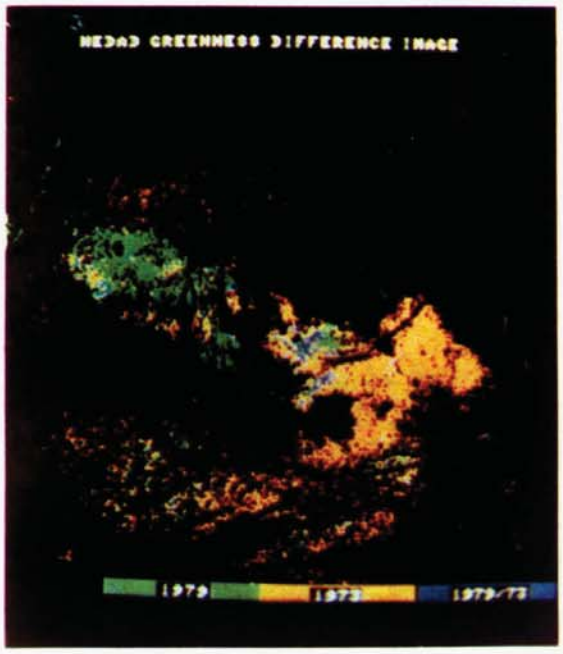

Figure 7.17 The Greenness 'Difference' Image Showing the Marked Change in the Distribution of the Two Maximum Green Cover Classes Between 1973 and 1979

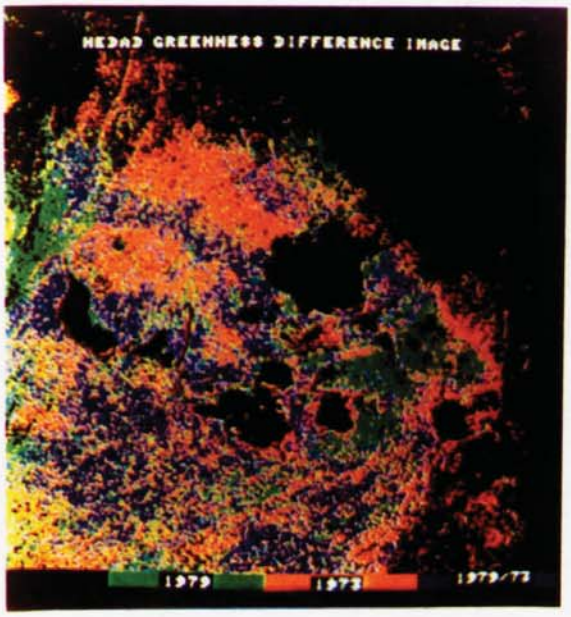

Figure 7.18 The Greenness 'Difference' Image Showing the Marked Change in the Distribution of the Two Medium Green Cover Classes Between 1973 and 1979

CHAPTER 8

DISCUSSION OF RESULTS AND CONCLUSIONS

The main conclusions from the study are presented and the problems associated with the practical application of the methodology for range resource mapping are discussed.

8.1 INTRODUCTION

The objectives of the study were formulated within the context of a widespread concern about the causes and consequences of desertification in many Sudano-Sahelian countries of Africa. Since the commencement of the study in 1981 a number of African countries, particularly Sudan, Chad and Ethiopia, have experienced a series of extremely dry years and in these countries large areas are now suffering from desertification. Soil erosion caused by overgrazing and overcropping at a time of continuing low rainfall is reducing the capacity of the land to sustain a rapidly increasing human population.

Tolba (1985) states that the worst effects of the drought could have been avoided if the solutions to halt desertification proposed by the UN Conference on Desertification (UN, 1976) had been implemented by the governments of those countries worst affected. The continuous monitoring of rangeland resources was seen as an essential part of the development and long term management of range resources for the benefit and welfare of pastoralists and others who are dependent upon rangeland vegetation for building materials and fuelwood, and most importantly for livestock grazing.

8.2 DISCUSSION OF RESULTS

The approach throughout the study has been to develop a technique for mapping the characteristics of rangeland vegetation that could be applied within other environmentally similar regions of Africa. This has involved a comparison of field data and air photography with various types of Landsat false colour and digitally processed imagery. A model of the reflectance of the major spectral components of the semi-arid landscape was established and used as a theoretical basis for the digital processing of Landsat data. The effectiveness of a number of different techniques, including the visual interpretation of Landsat false colour imagery, multi-spectral classification, principal components analysis and orthogonal measures of green vegetation, were evaluated.

The disappointing results obtained from an interpretation of the Landsat false colour

imagery (Chapter 4) indicated that at the spatial resolution of the MSS scanner, the sparse nature of the semi-arid vegetation cover presented particular problems in discriminating vegetation from the background soil reflectance. Only vegetation with a dense canopy cover and a high proportion of green foliage could be positively identified on the imagery, suggesting that in semi-arid regions the density and greenness of the vegetation cover are important factors in the identification of rangeland vegetation from Landsat MSS imagery. Green *Acacia* woodland with a high near-infrared (MSS7) reflectance could be identified, and so also could a dense cover of non-green vegetation. The majority of the Study Area however, is covered with a much sparser and largely non-green cover of shrub and dwarf shrub vegetation and comprises the most important grazing resource within the Study Area. It was therefore important to determine the nature of the limitations imposed by the sparse nature of the non-green vegetation cover and by the marked variations in soil reflectance, in mapping semi-arid vegetation from Landsat imagery within this region.

Although false colour imagery has been successfully used for mapping broad ecological zones in semi-arid areas (HTS, 1985), the limitations of visual interpretation techniques for rangeland vegetation mapping quickly became apparent. It was argued in Chapter 4 that further progress would only be made by careful characterisation of the spectral response of various soil types, together with an analysis of the way in which soil reflectance is modified by vegetation of varying canopy cover and greenness.

This was achieved by establishing a simple model of semi-arid vegetation reflectance based upon the spectral properties of bare soil, non-green and green vegetation recorded by the MSS scanner (Chapter 5). The development of the model suffered from lack of adequate field information about actual conditions on the ground at the time of scene acquisition, in particular about the greenness of the vegetation cover. A possible future approach would be to sample radiometrically the reflectance of the major spectral components of the semi-arid landscape to coincide with the date of scene acquisition. This was not possible in the present study due to the interval between image acquisition in June, 1979 and fieldwork in the summer of 1981.

Despite the limitations of the model the careful analysis of the spectral properties of bare soil, non-green and green vegetation based upon an examination of reflectance data for various two-dimensional combinations of Landsat wavebands (Chapter 6), provided the basis upon which to design a digital technique for mapping vegetation characteristics. The model demonstrated that lines of equal green cover lie parallel to the soil line, and that variations in vegetation canopy cover resulted in movement along that soil line. It was assumed that the spectral components were mixed in an additive way to give the characteristic triangular

shape to the data distribution observed in two-dimensional MSS7/5 Landsat space. A largely theoretical approach was adopted because of the real difficulties involved in testing empirically in the field the analytical techniques, including multi-spectral classification, principal components analysis and various ratio and orthogonal measures of vegetation greenness, that have been developed in recent years. A detailed comparison of the effectiveness of these different techniques would have required an extensive fieldwork programme in which detailed data on the relationship between vegetation density, species type, plant biomass at different growth stages and vegetation greenness for different soil backgrounds and varying rainfall/grazing conditions, would need to be related to MSS reflectance within selected sample sites.

In Chapter 7 a number of conventional image processing techniques, which have been applied successfully for vegetation mapping in a wide range of environments, were initially tested within the Study Area. The reasoning behind their application was to assess whether the results obtained from these more conventional techniques satisfactorily met the objectives set for the study and, if not, whether alternative techniques specifically developed for the Study Area would give improved results. Multi-spectral classification of image data failed to discriminate variations in green vegetation cover, or to separate non-green vegetation from the background soil reflectance. A major problem with multi-spectral classification was in defining training areas in a region of highly variable spectral response and subsequently to assign classes to specific land cover types. Although training areas were selected for the classification on the basis of varying spectral tones displayed by the false colour imagery, it was demonstrated in Chapter 4 that an interpretation of spectral tones into land cover types could not be achieved with any degree of certainty. A similar problem was encountered during a principal components transformation of image data. Experience from other areas has shown that the first principal component is associated with variations in soil brightness, and that the second principal component, orthogonal to the first, is associated with green plant development. A comparison of the second component image with soil and vegetation maps of the study area combined with an analysis of the structure of soil and vegetation reflectance data in transformed space, indicated that in practice the relationship between principal components and land cover types is not a simple one. In the Study Area, it appeared that variations in soil spectral frequency were enhanced by the transformation, whilst the vegetation spectra were suppressed. A more sensitive indicator of vegetation characteristics was therefore required, and in developing such a technique a number of key problems were identified.

1 Soil Brightness Effects

Elvidge and Lyon (1984) examined the effectiveness of several vegetation indices in

arid regions of high soil variability and found that differences in soil brightness affect ratio values, such that darker soil substrates result in higher greenness values under constant vegetation amounts. The model of vegetation reflectance proposed in Chapter 6 established that lines of equal green cover lie parallel to the soil line and therefore do not coincide with the non-parallel nature of lines of equal ratio value. For this reason an orthogonal measure of vegetation greenness appeared to provide a more effective technique for discriminating vegetation than a ratio technique, and further analysis of ratio techniques was therefore not undertaken.

However, for the perpendicular vegetation index (PVI) to remain valid, greenness lines of constant vegetation amount must remain parallel to the soil line. Recent results obtained by Huete et al. (1985), based upon an investigation of the reflectance of cotton crops at various levels of vegetation density growing on different soil types show that differences in greenness values from dark to bright soil backgrounds become greater with increasing vegetation density up to 60 per cent cover (Figure 8.1) Huete et al. (1985) argued that the observed non-parallel nature of individual greenness lines suggest that soil and vegetation spectral behaviour are somehow correlated and dependent upon each other. Thus the soil background spectral response may be dependent upon the transmittance or scattering properties of the overlying canopy. Allen and Richardson (1968), demonstrated how near infrared radiation can be transmitted through eight layers of leaves. Transmission of near infrared (MSS7) radiation through a canopy without a corresponding penetration of visible red (MSS5) radiation, may account for the brightness effect observed by Huete et al., (1985). As soil background becomes brighter, much more of the vegetation-transmitted near infrared radiation is reflected upwards towards the sensor in relation to non-transmitted red light.

The three-component model presented in Chapter 6 assumed simple, additive mixing of the three spectral components within the semi-arid landscape; bare soil, non-green vegetation and green vegetation. This assumption is based upon the premise that in semi-arid regions vegetation cover is the primary determinant of reflectance, not biomass (Graetz and Gentle, 1982; Otterman, 1981). In semi-arid regions therefore the effect of differential transmission of near infrared and visible red light within a multi-layered vegetation canopy is minimised and the soil brightness effect on the greenness measure is reduced. In fact Huete et al. (1985) demonstrates that the combined soil spectral and brightness effects were minimal at low vegetation densities, and that orthogonal greenness measures may be particularly useful in normalising soil reflectance in areas of low vegetation canopy.

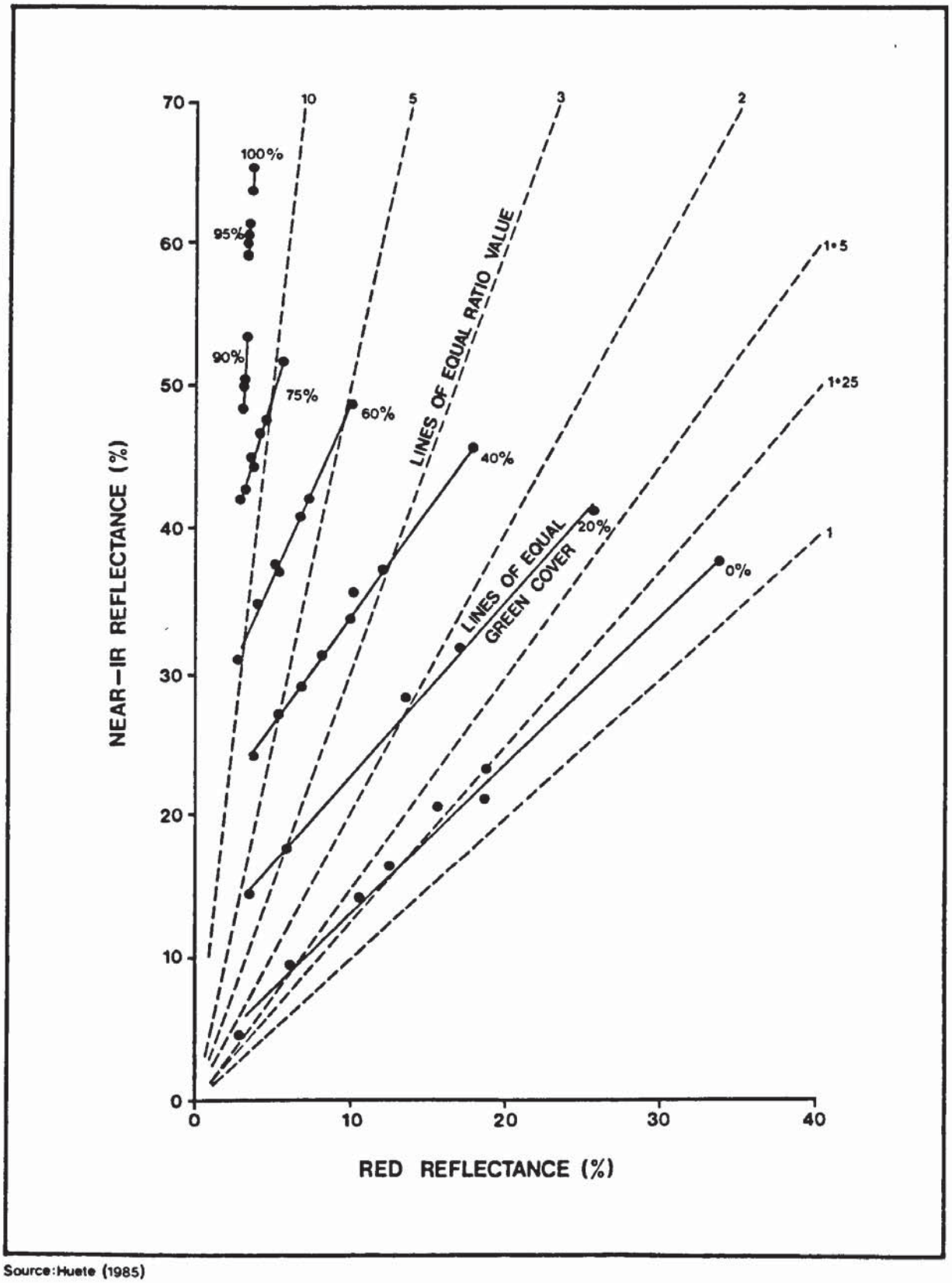

Source: Huete (1985)

Figure 8.1 Distribution of Composite Spectra in Two-Dimensional MSS7/MSS5 Space as a Function of Per Cent Canopy Cover

The effect of soil brightness differences were also a serious constraint to the accurate mapping of variations in vegetation canopy cover. The problem was encountered during a visual interpretation of the false colour imagery (Chapter 4) when it was observed that at low vegetation densities it was difficult to distinguish between a combined spectral response from soil and from vegetation

A possible solution to the problem of mapping differences in vegetation canopy cover within an area of varying soil brightness is to base the anslysis on information about the distribution of different soil types. Separate measures of canopy cover could then be derived for soils of varying brightness based upon an analysis of a single waveband Landsat image.

2 Soil Frequency Effects

The performance of a vegetation index can be assessed by the magnitude of soil-induced greenness changes caused byvariations in soil background reflectance for constant vegetation amounts (Huete et al., 1985). For example, Jackson et al., (1983) found the PVI of Richardson and Wiegand (1977) to be sensitive to soil moisture condition on a uniform soil surface, whilst Huete et al., (1985) found the PVI to be sensitive to both soil moisture condition and soil type. Although the PVI developed for the study is largely unaffected by differences in soil brightness i.e. movement along the soil line, it is affected by differences in soil colour i.e. scatter about the soil line. These spectral frequency effects, which are believed to be due to variations in soil mineral content, are the soil induced greenness changes referred to by Huete et al., (1985) and should be minimised for optimal discrimination of green vegetation from bare soil. This can only be achieved by selecting the appropriate combination of Landsat wavebands for which the width of the soil envelope is at a minimum and the greenness range is at a maximum (Chapter 7).

It was demonstrated in Chapter 7 that the dynamic range of greenness is highest in four-dimensional space, (Table 7. 9), but that the noise presented by bare soil deviations about the soil line were much higher in four-dimensions than in two. Thus the added problem due to soil variations in the greenness direction diminished the usefulness of the higher dynamic range of greenness in four wavebands. This does not necessarily imply that four, or in the case of the Landsat 5 Thematic Mapper (TM), seven wavebands, are less useful for monitoring vegetation, only that for certain soil types and conditions the inclusion of some channels may enhance non-vegetative spectral components more than spectra from the vegetation.

There are thus two conflicting objectives; to select a combination of wavebands in which soil deviations in the greenness direction are at a minimum, whilst maintaining the dynamic range of greenness at a maximum. A comparison of ten wavebands combinations in brightness/greenness space based upon a transformation calculated from the Gramm-Schmidt orthogonalisation procedure, showed that in MSS7/5 space a reasonable compromise between these two objectives could be achieved. However, it is clear that soil frequency effects reduce the effectiveness of the index by reducing the total greenness range. In the future, more accurate estimates of green cover would be obtained by deriving separate greenness indices for individual soil types within the overall soil envelope.

3 The Green Cover Scale

It has been assumed that the sampled maximum green vegetation point represents a 100 per cent cover of green vegetation. In the absence of detailed field information about the greenness of the vegetation canopy at the date of image acquisition, the reflectance of green vegetation had to be sampled directly from the Landsat CCT. In order to divide the greenness range into percentages it is critical that the maximum green vegetation point does in fact correspond to a 100 per cent cover of green vegetation. Without field verification of the proportion of green vegetation within pixels sampled to define the maximum green vegetation point, the index cannot be properly calibrated. The importance of field sampling at a date close to the time of image acquisition is again emphasised, in this case to provide adequate calibration data for the vegetation index.

8.3 CONCLUSIONS

It is accepted that the index that was developed for mapping green vegetation cover within the Study Area suffers from a number of unresolved problems, and that its application as a practical means of monitoring rangeland vegetation resources is as yet untested. However, in theoretical terms the vegetation index, which is a modification of a simple orthogonal greenness measure, is optimal for monitoring range resources within a region of semi-arid vegetation in Northern Kenya and could potentially be used in other, environmentally similar regions of Africa.

The index was based upon a modification of the PVI developed by Richardson and Wiegand (1977). The modification was necessary to ensure that, unlike the PVI of Richardson and Wiegand (1977), the effect of variations in soil brightness was minimised. Two Landsat wavebands, the visible red (MSS5) and near infrared (MSS7) were found to be optimal for mapping green vegetation cover, but only one waveband (MSS5) was required for mapping variations in vegetation canopy cover. The use of digital techniques enabled the mapping to be achieved with greater precision than could be achieved from a visual interpretation of false colour imagery. In addition, digital processing of the Landsat

data enabled thematic maps of range resources covering extensive areas at different dates to be processed and compared, thus providing a basis for the continuous monitoring of rangeland vegetation.

8.4 RECOMMENDATIONS FOR FUTURE WORK

In a paper summarising the results from the IPAL (Integrated Project for Arid Lands) Pilot Project, Lusigi and Glaser, (1984) make a number of recommendations for the future management of range resources within the IPAL Study Area. Part of the management plan involves the introduction of planned watering points, with controls on water availability to assist in the dispersal of livestock into previously unpastured areas. Based upon the availability of these additional water resources the distribution of livestock would be controlled depending upon the carrying capacity of designated range units at the end of each growing season. IPAL propose to designate and evaluate the condition of range units based upon estimates of forage production calculated from each seasons rainfall figures, coupled with verification of the forage estimates from aerial and ground survey.

Within this programme of monitoring range conditions, the potential benefits of Landsat imagery for range resource mapping could be realised in two ways:

(a) In the designation of range units. The designation of units would be based upon a stratification of the image into regions of varying rangeland productivity. The use of multi-temporal imagery would be an important element in identifying those areas which are constantly productive, and those areas which are rarely productive;

(b) In deriving estimates of forage production within each designated range unit and monitoring the changing productivity of each unit over time.

Using figures given by Lamprey (1981) the following outline methodology is proposed for translating measures of per cent green cover derived from the Landsat imagery into estimates of forage production. Based upon aerial survey and fieldwork for typical *Acacia reficiens* shrub cover in the Hedad, Lamprey (1981) established the relationship between the biomass of green foliage and per cent cover for shrub, dwarf shrub and herbaceous species (Table 8.1).

From Table 8.2, 15 to 30 per cent of the vegetation canopy in Class 3 contains green vegetation; in Class 4 between 30 and 45 per cent of the canopy contains green vegetation and so on to Class 7 in which more than 75 per cent of the canopy contains green

TABLE 8.1 ESTIMATES OF GREEN BIOMASS FOR DIFFERENT VEGETATION SPECIES BASED UPON FIGURES GIVEN BY LAMPREY (1981)

Species	Per cent cover	Biomass kg ha^{-1}
Tree/shrub	14	73
Dwarf shrub	10	20
Herbaceous, including annual and perennial grassland	62	370
(Bare soil	14	zero)

TABLE 8.2 THE AREA IN PER CENT AREA AND HECTARES FOR GREEN COVER CLASSES DERIVED FROM THE GREENNESS IMAGE OF THE 1979 HEDAD SUBSCENE

Class No.	Class name and per cent green cover	Percent area	Ha
1	Bare soil - zero	26	74 225
2	Bare soil - zero	13	37 113
3	Green vegetation - 15 - 30	20	57 096
4	Green vegetation - 30 - 45	22	62 806
5	Green vegetation - 45 - 60	14	39 967
6	Green vegetation - 60 - 75	4	11 419
7	Green vegetation - > 75	1	2 855
	TOTAL	100	285 481

vegetation. Thus, for a region of uniform canopy cover, in green cover Class 3 between 15 and 30 per cent of the shrub cover is green, between 15 and 30 per cent of the dwarf shrub cover is green and between 15 and 30 per cent of the herbaceous cover is green. Total biomass per hectare can be calculated by determing the proportion of green cover in each class for the species type and multiplying by the biomass figure per hectare for that species (Table 8.3). Thus, for tree/shrub species at a typical 14 per cent canopy cover, in green cover Class 3 between 15 and 30 per cent of the canopy is green, i.e. between 2 and 4 per cent of the total canopy contains green foliage. At 14 per cent cover of tree/shrub cover biomass is equal to 20 kg ha^{-1}, and at between 2 and 4 per cent this is equal to between 1.5 and 3.0 kg ha^{-1}. From Table 8.2, green cover Class 3 covers 57 096 ha of the Hedad subscene, which multiplied by the biomass figure for this class gives between 77 080 - 154 161 kg of green biomass.

The figures given are only crude estimates of green biomass partly due to the limitations of the vegetation index discussed above, but also because of the assumptions which have been made in calculating the biomass figures. Firstly, due to lack of data it has had to be assumed that vegetation canopy within the Hedad subscene is uniform. Under a uniform canopy differences in the greenness of the vegetation canopy are caused by differences in vegetation productivity. In a semi-arid region of northern Kenya rainfall amount is likely to be the most important determinant of vegetation productivity (Le Houerou and Hoste, 1977), but grazing pressure and soil type may also be important in restricted areas. However, there exist quite marked differences in vegetation canopy cover within the Hedad subscene as indicated by the vegetation map (Figure 3.1). It is believed that differences in green cover will be associated with differences in canopy cover. Green biomass figures for vegetation of varying canopy cover are therefore required to provide information about the complex relationship between canopy cover, rainfall and vegetation greenness.

Secondly, it has been assumed that different species contribute equally to the measured greenness value in proportion to their cover. In other words, a 20 per cent cover of tree foliage contributes an equal greenness component to a 20 per cent cover of herbaceous foliage. A careful characterisation of the reflectance properties of the green foliage of different vegetation species at different growth stages is required to determine the varying contribution of different species to measured greenness.

The calculations involved in estimating vegetation productivity within the Hedad subscene have provided an insight into the problems of deriving practical benefits from the applications of Landsat imagery for range resource mapping in semi-arid regions. Future

TABLE 8.3 ESTIMATED GREEN BIOMASS DERIVED FROM 1979 HEDAD GREENNESS IMAGE

	Relationship between biomass and per cent vegetation cover											Estimate of total biomass within each vegetation cover class				
Species Type	Typical per cent cover for species	Green cover Class 1	Biomass kg ha^{-1}	Green cover Class 2	Biomass kg ha^{-1}	Green cover Class 3	Biomass kg ha^{-1}	Green cover Class 4	Biomass kg ha^{-1}	Green cover Class 5	Biomass kg ha^{-1}	Biomass kg ha^{-1} Class 1	Biomass kg ha^{-1} Class 2	Biomass kg ha^{-1} Class 3	Biomass kg ha^{-1} Class 4	Biomass kg ha^{-1} Class 5
Tree/shrub	14	2.0-4.0	1.5-3.0	4.0-6.0	3.0-4.5	6.0-8.0	4.5-6.0	8.0-10.0	6.0-7.5	10.0-12.0	7.5-9.0	85 644-171 288	188 418-282 627	179 851-239 802	68 514-85 642	96 412-115 696
Dwarf shrub	10	1.5-3.0	0.3-0.6	3.0-4.5	0.6-0.9	4.5-6.0	0.9-1.2	6.0-7.5	1.2-1.5	7.5-9.0	1.5-1.8	17 129-342 576	37 684-56 325	35 970-47 96-	13 703-17 128	19 282-23 139
Herbaceous	62	9.0-18.0	2.4-4.8	18.0-27.0	4.8-9.6	27.0-36.0	9.6-19.2	36.0-45.0	19.2-38.4	45.0-54.0	38.4-76.8	137 030-274 061	301 469-602 938	383 683-767 366	219 245-438 490	493 632-987 264

monitoring programmes will need to be closely linked to the collection of biomass data in the field if the potential benefits of Landsat imagery and other types of remotely sensed imagery, for example data form the Advanced Very High Resolution Radiometer (AVHRR), are to be fully realised.

REFERENCES

Allan, J.A., and T.S. Richards, 1983. Remote sensing for identifying low density vegetation cover in semi-arid coastal north-west Egypt. *Proceedings of the Ninth Annual Conference of the Remote Sensing Society.* Silsoe College, UK., pp. 69-79.

Allen, W.A., and A.J. Richardson, 1968. Interaction of light with a plant canopy. *Optical Society of America,* Vol. 58, pp. 1023-1031.

Anderson, R.L., 1983. *Photogrammetric Engineering and Remote Sensing,* Vol. 44, Front Cover.

Bentley, R.G., B.C. Salmon-Drexler, W.J. Bonner, and R.K. Vincent, 1976. *A Landsat Study of ephemeral and perennial rangeland vegetation and soils.* Bureau of Land Management, Denver, Colorado. p. 234.

Canfield, R.H., 1941. Applied line interception method in sampling range vegetation. *Journal of Forestry,* Vol. 39, pp. 388-394.

Carneggie, D.M., and S.D. DeGloria, 1973. Monitoring California's forage resources using ERTS-1 and supporting aircraft data. *Proceedings of the Symposium on Significant Results Obtained from Earth Resources Technology Satellite-1.* Vol. 1, Section A, pp. 91-95. Goddard Space Flight Center, Maryland.

Colwell, J.E., 1974. Grass canopy bidirectional spectral reflectance. *Proceedings of the Tenth International Symposium on Remote Sensing of the Enviornment.* pp. 1061 - 1085. Ann Arbor, Michigan.

Condit, H.R., 1970. The spectral reflectance of American soils. *Photogrammetric Engineering and Remote Sensing,* Vol. 36, pp. 955-966.

Cooper, C.F., 1957. The variable plot method for estimating shrub density. *Journal of Range Management,* Vol. 10, pp. 111-115.

Crist, E.P., and R.C. Cicone, 1984. Application of the tasseled cap concept to simulated thematic mapper data. *Photogrammetric Engineering and Remote Sensing,* Vol. 50, pp. 343-352.

Curran, P., 1980. Multispectral remote sensing of vegetation amount. *Progress in Physical Geography,* Vol. 4, pp. 316-341.

Deering, D.W., 1978. *Rangeland reflectance characteristics measured by aircraft and spacecraft sensors.* Ph.D. thesis, Texas A and M University, p. 338.

Dodson, R.G., 1963. *Geology of the South Horr Area.* Ministry of Natural Resources, Geological Survey of Kenya. Report No. 60, p. 53.

Dolan, R., 1980. Migration patterns in the Rendille, 1923-1978. *Proceedings of a Scientific Seminar,* Nairobi. IPAL Technical Report A-3, pp. 124-131.

Dunford, C., D.A. Mouat, M. Norton-Griffiths, and D.M. Slaymaker, 1983. Remote sensing for rural development planning in Africa, *ITC Journal,* Vol. 2, pp. 99-109.

Edwards, K.A., C.R. Field, and I.G.G. Hogg, 1979. *A preliminary analysis of climatological data from the Marabit District of northern Kenya.* IPAL Technical Report B-1, p. 44.

Elvidge, C.D., and R.J.P. Lyon, 1984. *Influence of substrate albedo on vegetation indices employing red and near-infrared.* Seminar on Remote Sensing for Geological Mapping, IUGS-UNESCO Programme on Geological Applications of Remote Sensing, France, p. 11.

Freiberger, W.F., Ed., 1960. *The International Directory of Applied Mathematics.* Van Nostrand, Princeton, N.J., p. 412.

Gates, D.M., H.J. Keegan, J.C. Schelter, and V.R. Weidner, 1965. Spectral properties of plants. *Applied Optics,* Vol. 4, pp. 11-20.

Gates, D.M., 1970. *Physical and physiological properties of plants.* Remote Sensing, National Academy of Science, Washington D.C., pp. 224-252.

Gausman, H.W., R.R. Rodriguez, and A.J. Richardson, 1976. Infinite reflectance of dead compared with live vegetation. *Agronomy Journal,* Vol. 68, pp. 295-296.

Gausman, H.W., 1977. Reflectance of leaf components. *Remote Sensing of Environment,* Vol. 6, pp. 1-9.

Gonzalez, R.C., and P. Wintz, 1977. *Digital Image Processing.* Addison-Wesley, Mass. p. 431.

Graetz, R.D., and M.R. Gentle, 1982. The relationship between reflectance in the Landsat wavebands and the composition of an Australian semi-arid shrub rangeland. *Photogrammetric Engineering and Remote Sensing,* Vol. 48, pp. 1721-1730.

Griffiths, G.H., 1980. *The Detection of Overgrazing Surrounding the Water-hole at Kargi, Northern Kenya using Landsat Satellite Imagery.* Unpublished thesis, Cambridge University Library, 50 p.

Griffiths, G.H., and W.G. Collins, 1983. Mapping the greenness of semi-arid rangeland vegetation in northern Kenya from Landsat data. *Proceedings of the Ninth Annual Conference of the Remote Sensing Society,* Silsoe College, Beds., pp. 108-122.

Gwynne, M.D., P.J. Greenway, and D.J. Pratt, 1966. Classification of East African Vegetation. *Journal of Applied Ecology,* Vol. 3, pp. 369-385.

Gwynne, M.D., and D.J. Pratt, 1977. *Rangeland Management and Ecology in East Africa.* Hodder and Stoughton. p. 310.

Hellden, U., 1979. *A test of Landsat 2 imagery and digital data for thematic mapping, illustrated by an environmental study in northern Kenya.* University of Lund, Sweden. p. 63.

Herlocker, D., 1979. *Vegetation of Southwestern Marsabit District, Kenya.* IPAL Technical Report D-1, p. 68.

Hielkema, J., 1980. *Remote sensing techniques and methodologies for monitoring ecological conditions for desert locust population development.* FAO/USAID Final Technical Report Phase 1, p.

Holkenbrink, P.F., 1979. *Manual on Characteristics of Landsat Computer-Compatible Tapes Produced by the EROS Data Centre Digital Image Processing System.* p. 64.

Huete, A.R., R.D. Jackson, and D.F. Post, 1985. Spectral response of a plant canopy with different soil backgrounds. *Remote Sensing of Environment,* Vol. 17, pp. 37-53.

Hunting Technical Services Limited, 1974. *Southern Darfur Land Use Planning Survey,* Annex 1, Soil and Vegetation, Government of Sudan. p. 26.

Hunting Technical Services Limited, 1985. *Mapping Land Use Change from Landsat Satellite Imagery: Results of a Pilot Study in Southern Darfur.* p. 40.

Jackson, R.D., 1983. Spectral indices in n-space. *Remote Sensing of Environment,* Vol. 13, pp. 409-421.

Jackson, R.D., P.N. Slater, and P.J. Pinter, 1983. Discrimination of growth and water stress in wheat by various vegetation indices through clear and turbid atmospheres. *Remote Sensing of Environment,* Vol. 13, pp. 187-208.

Jordan, C.F., 1969. Derivation of leaf area index from quality of light on the forest floor, *Ecology,* Vol. 50, pp. 663-666.

Kauth, R.J., and G.S. Thomas, 1976. The tasselled-cap; a graphic description of the spectral temporal development of agricultural crops as seen by Landsat. *Proceedings of the Symposium of Remotely Sensed Data, Purdue University, Indiana,* pp. 4B41-4B51.

Knipling, E.B., 1970. Physical and physiological basis for the reflectance of visible and near-infrared radiation from vegetation. *Remote Sensing of Environment,* Vol. 1, pp. 155-159.

Lamar, J., and P. Merifield, 1973. Pseudocolour transformation of ERTS Imagery. *Symposium on Significant Results Obtained from Earth Resources Technology Satellite - 1.* Vol. 1, Section A, pp. 1187-1198. Goddard Space Flight Center, Maryland.

Lamprey, H.F., 1978. The Integrated Project on Arid Lands (IPAL). *Nature and Resources,* Vol. 14, pp. 2-11.

Lamprey, H.F., 1981. *IPAL Woodland Ecology Programme,* Unpublished Report, p. 50.

Le Houerou, H.N., and C.H. Hoste, 1977. Rangeland production and annual rainfall relations in the Mediterranean Basin and in the Africa Sahelo-Sudanian. *Journal of Range Management.* Vol. 30, pp. 18-89.

Lillesand, T.M., and R.W. Kiefer, 1979. *Remote Sensing and Image Interpretation,* Wiley, p. 612.

Lusigi, W.J., 1981. *Combatting desertification and rehabilitating degraded production systems in northern Kenya.* IPAL Technical Report A-4, p. 141.

Lusigi, W.J., and G. Glaser, 1984. Desertification and nomadism : a pilot approach in eastern Africa. *Swara,* pp. 21-31.

Manual of Remote Sensing, 1983. Vol. II, pp. 2111-2162, American Society of Photogrammetry.

Maxwell, E.L., 1976. Multivariate system analysis of multispectral imagery, *Photogrammetric Engineering and Remote Sensing,* Vol. 42, pp. 1173-1186.

McCoy, R.M., and R.G. Watt, 1978. Mapping vegetation with low cover from Landsat data. *Proceedings of American Society of Photogrammetry,* Alberquerque, New Mexico,

Misra, P.N., and S.G. Wheeler, 1978. Crop classification with Landsat multi-spectral scanner data. *Pattern Recognition,* Vol. 12, pp. 1-13.

Mulder, N.J., and N.H.W. Donker, 1976. Analysis of MSS digital imagery with the aid of principal component transform. *ITC Journal.* 1977-3, pp. 434-466.

Musk, L.F., 1983. Outlook - changeable, *Geographical Magazine.* Vol. 25, pp. 532-3.

Noy-Meir, I., 1974. Multi-variate analysis of the semi-arid vegetation in southeastern Australia, II. Vegetation catenae and environmental gradients. *Australian Journal of Botany,* Vol. 22, pp. 115-140.

Otterman, J., and R.S. Fraser, 1976. Earth-atmosphere system and surface reflectivities in arid regions from Landsat multispectral scanner measurements. *Remote Sensing of Environment,* Vol. 5, pp. 247-266.

Otterman, J., 1981. Satellite and field studies of man's impact on the surface in arid regions. *Tellus,* Vol. 33, pp. 68-77.

Pearson, R.L., and L.D. Miller, 1972. Remote sensing of standing crop biomass for estimation of the productivity of short grass prairie. *Proceedings of the Eighth International Symposium on Remote Sensing of the Environment,* pp. 1355-1384, Ann Arbor, Michigan.

Perry, C.R., and L.F. Lautenschlager, 1984. Functional equivalence of spectral vegetation indices. *Remote Sensing of Environment,* Vol. 14, pp. 169-182.

Pratt, W.K., 1977. *Digital Image Processing,* Wiley, New York,

Randel, B.A., 1970. *Geology of the Laisamis Area,* Ministry of Natural Resources, Geological Survey of Kenya, Report No. 84, p. 24.

Rapp, A., 1978. *A Review of Desertization in Africa - water, vegetation and man.* University of Lund, Sweden, p.

Richardson, A.J., and C.L. Wiegand, 1977. Distinguishing vegetation from soil background information. *Photogrammetric Engineering and Remote Sensing,* Vol. 43, pp. 1541-1552.

Rifman, S.S., 1973. Digital rectification of ERTS multispectral imagery. *Symposium on Significant Results Obtained from Earth Resources Technology Satellite -1,* vol. 1, Section A, pp. 1131-1142, Goddard Space Flight Center, Maryland.

Rothery, D.A., 1982. *The Evaluation of the Wuqbah Block and the Application of Remote Sensing in the Oman Ophiolite.* Ph.D. thesis, Open University, p. 414.

Rouse, J.W., R.H. Haas, J.A. Schell, D.W. Deering, and J.C. Harlan, 1974. *Monitoring the vernal advancement and retrogradation (greenwave effect) of natural vegetation.* NASA/GFSC Type III, Final Report, Greenbelt, Maryland, p. 371.

Siegal, B.S., and A.F.H. Goetz, 1977. Effect of vegetation on rock and soil type discrimination. *Photogrammetric Engineering and Remote Sensing,* Vol. 43, pp. 191-196.

Slater, P.N., 1979. A re-examination of the Landsat MSS. *Photogrammetric Engineering and Remote Sensing,* Vol. 45, pp. 1479-1485.

Smith, J.A., and R.E. Oliver, 1972. Plant canopy models for simulating composite scene spectral radiance in the 0.4-1.05 μm region. *Proceedings Eighth International Symposium on Remote Sensing of Environment,* pp. 133-1353. Ann Arbor, Michigan.

Suits, G.H., 1972. The calculation of the directional reflectance of a vegetation canopy. *Remote Sensing of Environment,* Vol. 2, pp. 175-182.

Swain, P.H., and S.M. Davis (Eds.), 1978. *Remote Sensing : The Quantitative Approach.* McGraw Hill, New York, p. 396.

Tolba, M.K., 1984. Desertification is stoppable. *Arid Lands Newsletter,* Vol. 21, pp.2-7.

Tucker, C.J., 1977. Asymptotic nature of grass canopy spectral reflectance. *Applied Optics,* Vol. 16, pp. 1151-1157.

Tucker, C.J., 1976. Sensor design for monitoring vegetation canopies. *Photogrammetric Engineering and Remote Sensing,* Vol. 42, pp. 1399-1410.

Tucker, C.J., 1978. A comparison of satellite sensor bands for monitoring vegetation. *Photogrammetric Engineering and Remote Sensing,* Vol. 44, pp. 1369-1380.

United Nations, 1976. *Desertification : Its Causes and Consequences.* Pergamon, p.454

U.S.D.A., 1975. *Munsell Soil Colour Charts,* U.S.D.A., 18, Soil Survey Manual.

U.S.G.S., 1979. *Landsat Data Users Handbook,* (Revised edition).

Vinogradov, B.W., 1969. Remote sensing of the arid zone vegetation in the visible spectrum for studying the productivity. *Proceedings Sixth International Symposium on Remote Sensing of Environment,* pp. 1237-1250. Ann Arbor, Michigan.

Walther, D., and D. Herlocker, 1981. *Indicators of environmental degradation and range conditions in the Korr area of southwestern Marsabit District, Kenya.* International Workshop on Strategies for Developing the Resources of the Arid and Semi-Arid Areas of Kenya, Nairobi, p. 10.

Warren, P.L., and C. Dunford, 1983. Vegetation sampling with large-scale aerial photography. *Remote Sensing Newsletter,* University of Arizona, p. 6.

Woolley, J.T., 1971. Reflectance and transmittance of light by leaves. *Plant Physiology,* Vol. 47, pp. 656-662.

GLOSSARY OF ACRONYMS

BASIC	Beginners All-purpose Symbolic Instruction Code
CCT	Computer Compatible Tape
CPM	Central Processing Unit
DN	Digital Number
EDC	EROS Data Centre
EDIPS	EROS Data Centre Image Processing System
ERTS	Earth Resources Technology Satellite
FORTRAN	Formula Translator
GCP	Ground Control Point
GSFC	Goddard Space Flight Centre
HDT	High Density Tape
HTS	Hunting Technical Services
IPAL	Integrated Project for Arid Lands
IPF	Image Processing Facility
LAI	Leaf Area Index
LUT	Look-up Tables
MAB	Man and Biosphere Programme
NASA	National Aeronautics and Space Administration
NERC	Natural Environment Research Council
NRSC	National Remote Sensing Centre
PVI	Perpendicular Vegetation Index
SPSS	Statistical Package for the Social Sciences
TDRS	Tracking and Data Relay Satellite
UNEP	United Nations Environment Programme
UNESCO	United Nations Educational, Scientific and Cultural Organisation.

APPENDIX A

PLANT SPECIES

COMMONLY OCCURRING PLANT SPECIES FOUND WITHIN THE STUDY AREA WITH THEIR RENDILLE NAMES

Woodland Species	Rendille Name
Acacia tortilis	Bahar
Salvadora persica	Haya
Balanites aegyptiaca	Kulum
Shrubland Species	
Acacia reficiens	Khasah
Acacia senegal	Hadhadh
Acacia horrida	Gomor
Euphorbia cuneata	Andika
Commiphora	-
Dwarf Shrubland Species	
Duosperma eremophilum	Yabah
Indigofera spinosa	Khoro
Indigofera cliffordiana	Hanhanis
Baleria proxima	Suchah
Herbaceous Species	
Cenchrus cilaris	Ballah
Aristida mutabilis	Ririma
Aristida adscencionis	Maad
Blepharis linariifolia	-

APPENDIX B

VEGETATION/SOIL MAP OVERLAYS

PAGE

NUMBERING

AS ORIGINAL

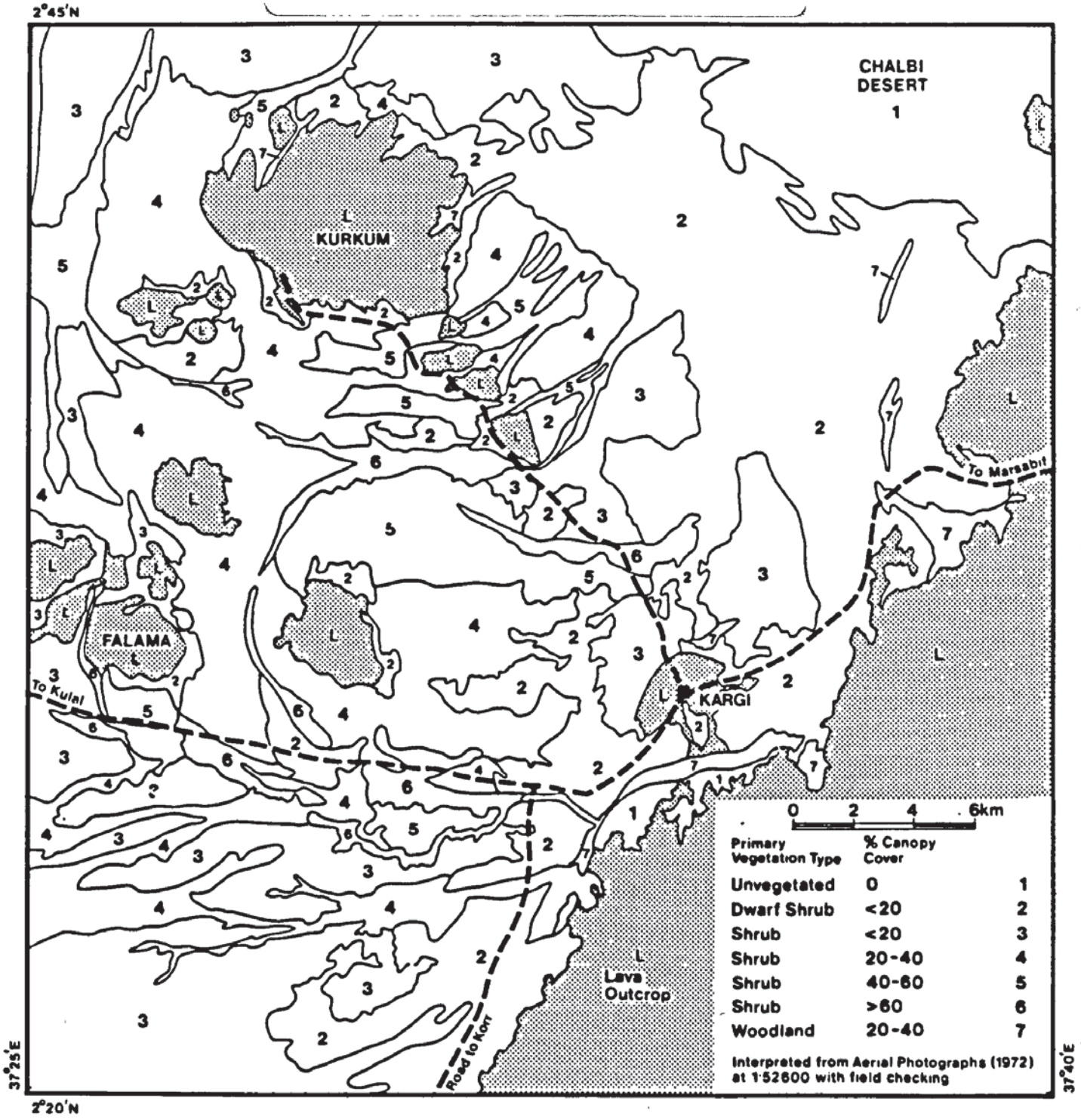

Figure 3.1 Vegetation Map of the Kargi Subscene Derived from Air-Photo Interpretation with Field-Checking

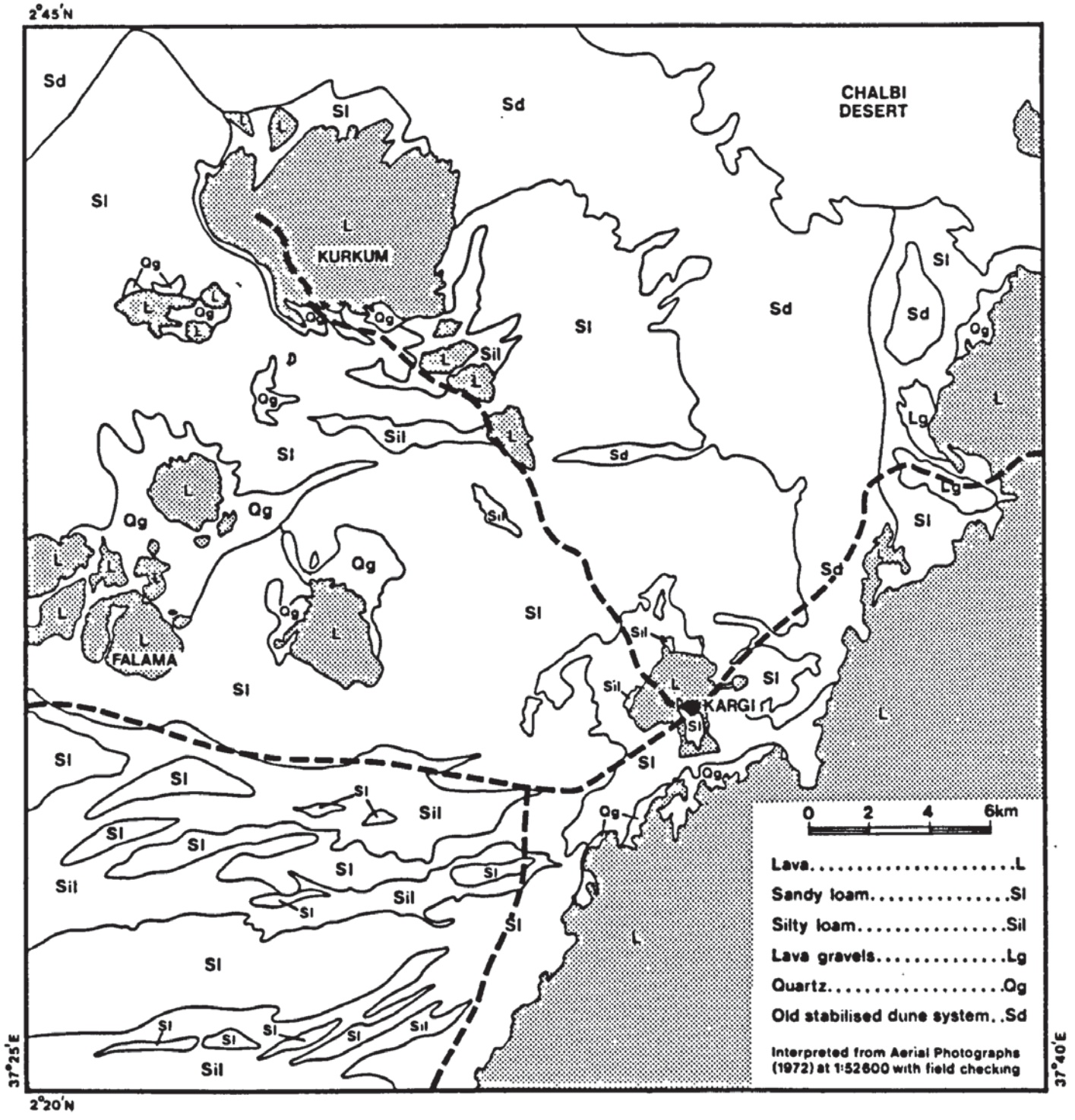

G.H.GRIFFITHS Ph.D. MAY 1985

MAPPING RANGELAND VEGETATION IN NORTHERN KENYA FROM LANDSAT DATA

Figure 3.2 Soil Map of the Kargi Subscene Derived from Air-Photo Interpretation with Field-Checking

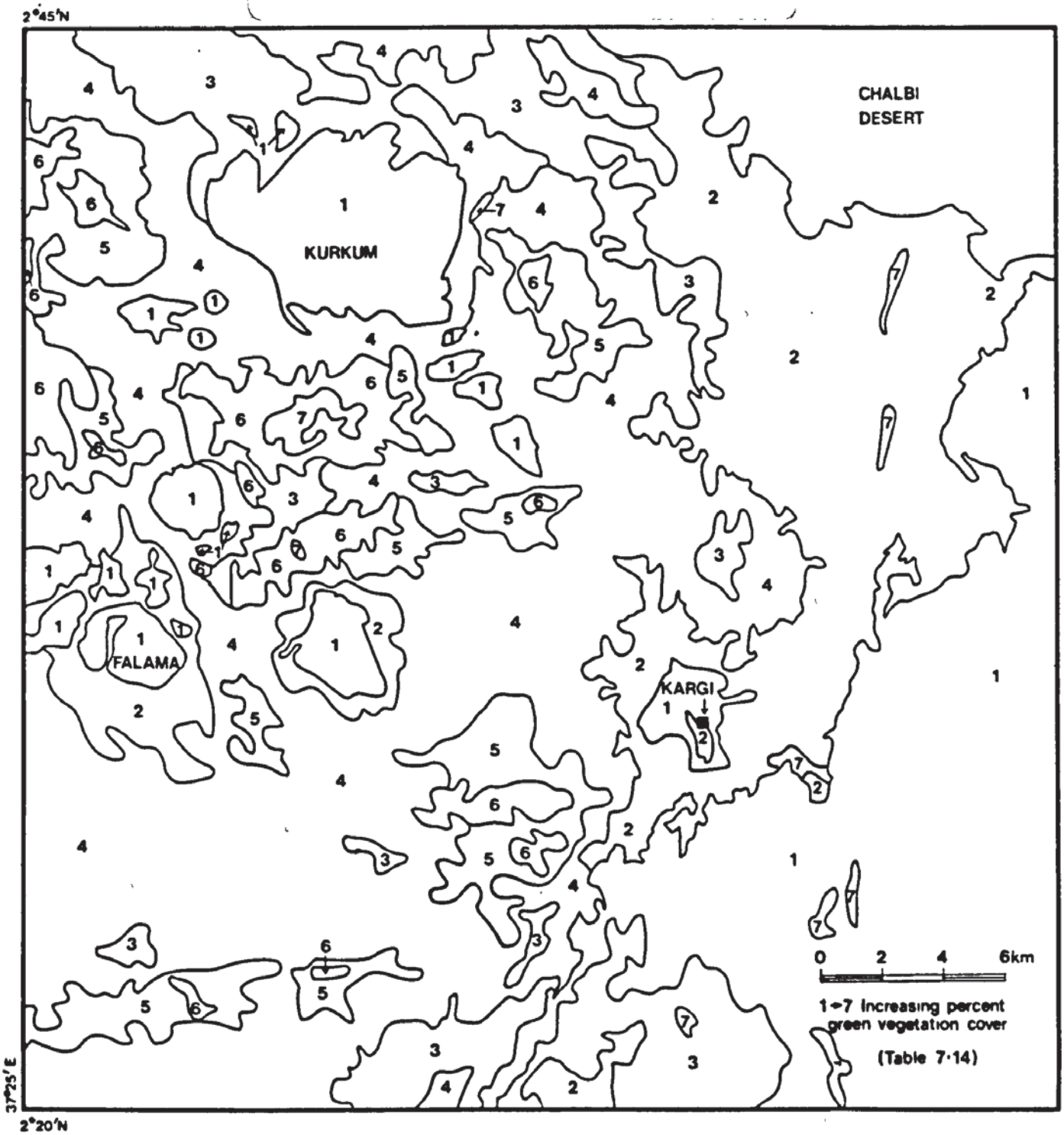

Figure 7.14 The Green Cover Map Showing Relative Differences in Green Vegetation Cover Within the Kargi Subscene

APPENDIX C

VEGETATION CANOPY

VEGETATION CANOPY COVER FIELD SAMPLING RESULTS

SITE NO (50 x 50m) QUADRAT	DRAWF SHRUB % COVER	NUMBER PLANTS/ QUADRAT	DENSITY (m^2)	SHRUB % COVER	NUMBER PLANTS	DENSITY (m^2)	COMMENTS	VEG CLASS
1	0.5	425	0.17	-	-	-	Shrub absent	2
2	-	-	-	30.0	55	0.02		4
3	-	-	-	-	-	-	Grassland	-
4	8.5	20	0.001	-	-	-		2
5	-	-	-	-	-	-	Grassland	-
6	-	-	-	17.0	55	0.01	Shrub	3
7	-	-	-	55.5	52	0.01	Woodland	7
8	-	-	-	4.0	87	0.03	Woodland	7
9	2.0	312	0.12	5.0	-	-		2
10	2.0	156	0.06	8.0	25	0.01	Lava - very sparse cover	2
10a	6.0	359	0.14	1.0	-	-	Impenetrable bush	2
11	-	-	-	780.0	-	-	Impenetrable bush	6
12	13.0	400	0.16	24.0	46	0.02		2
13	81.0	375	0.15	60.0	162	0.06		
14	40.0	75000	2.0	1.0	-	-	Very sparse; well grazed	2
15	5.0	32	0.12	20.0	25	0.01	Woodland	5
16	41.0	-	-	-	-	-	Shrub absent; well grazed	5
17	-	-	-	-	-	-	Vegetation absent	1
18	-	-	-	-	-	-	Grassland	-
19	9.5	1250	0.5	-	-	-	Shrub absent; well grazed	2
20	0.5	62.5	0.02	29.5	15	0.006	Woodland	7
21	25.0	3000	1.2	12.0	100	0.04		4
22	18.0	3000	1.2	7.5	30	0.01		4
23	22.5	3500	1.4	1	-	-		4
24	10.0	937	0.4	8.0	36	0.01		2
25	16.0	75000	2.0	-	-	-		2
26	4.5	625	0.25	40.0	30	0.01		5
27	4.0	625	0.25	-	-	-		2
28	26.0	1250	0.5	14.0	194	0.01		4

Continued

SITE NO (50 x 50m) QUADRAT	DWARF SHRUB % COVER	NUMBER PLANTS/ QUADRAT	DENSITY (m^2)	SHRUB % COVER	NUMBER PLANTS	DENSITY (m^2)	COMMENTS	VEG CLASS
29	18.5	3500	1.4	-	-	-	Shrub absent	2
30	-	-	-	-	-	-	Vegetation absent	
31	9.0	3500	1.25	11.0	25	0.01		4
32	4.0	2500	0.9	-	-	-	Shrub absent	2
33	-	-	-	-	-	-	Vegetation absent	1

APPENDIX D

PER CENT SHRUB AND DWARF SHRUB CANOPY

PERCENT SHRUB AND DWARF SHRUB CANOPY COVER
MEASURED FROM PANCHROMATIC AIR PHOTOGRAPHS

AIR PHOTO NUMBER	SAMPLE POINT	PERCENT CANOPY COVER (Average 5 measurements)
0123	1	44
"	2	3.4
	3	39
	4	280
	5	32
	6	13
0129	1	18.8
	2	5.2
	3	33
	4	29
0027	1	35.2
	2	1
	3	24.6
	4	10.2
	5	22.7
	6	84
	7	33
	8	33
	9	9.5
	10	26
0131	1	28
	2	9
	3	29
	4	6
	5	26
	6	17
	7	64
	1	58
	2	38
	3	31
	4	74.8

Continued

AIR PHOTO NUMBER	SAMPLE POINT	PERCENT CANOPY COVER (Average 5 measurements)
0131	5	14
	6	28
	7	27
	8	61
	9	41
	10	59
	11	45
	12	30
0130	1	75
	2	47.3
	3	29
	4	14
	5	87
	6	1
0125	1	1
	2	16
0085	1	19
	2	18.5
0137	1	1
	2	8
	3	81
0087	1	9
	2	39
0023	1	1
	2	33
	3	30.8
	4	36.5
	5	47
	6	45
	7	25

Continued

AIR PHOTO NUMBER	SAMPLE POINT	PERCENT CANOPY COVER (Average 5 measurements)
0023	8	10
	9	31
	10	68
	11	45
0021	1	13
	2	54
	3	24
	4	12
0081	1	11
0135	1	30
	2	32
	3	47
	4	10

APPENDIX E

SAMPLED SOIL AND VEGETATION REFLECTANCE

1. SOIL REFLECTANCE VALUES (DN) IN FOUR LANDSAT WAVEBANDS SAMPLED FROM THE JUNE 1979 HEDAD SUBSCENE

	MSS 4	MSS 5	MSS 6	MSS 7
	44	87	84	64
	37	76	78	59
	38	75	76	58
	54	86	82	57
	37	63	65	48
	43	85	87	61
	43	82	84	62
	42	79	80	58
	43	69	71	49
	34	57	60	42
	39	80	80	59
	65	94	93	69
	46	65	68	53
	49	85	84	59
	40	78	84	61
	39	63	64	44
	60	84	81	59
	51	79	79	56
	39	75	79	58
	37	63	70	54
	41	60	63	50
	32	38	33	21
	32	89	88	62
	44	87	89	64
	37	74	75	54
	67	99	76	69
	64	95	98	65
	40	79	83	59
	41	74	79	56
	38	77	76	55
	38	78	80	58
	36	63	68	47
	42	68	71	52
	39	75	74	51
	31	39	35	20
	24	31	30	15
	21	28	26	19
	64	95	98	65
	43	72	70	48
MEAN	43.15	73.20	73.47	52.77
STANDARD	10.34	16.65	16.78	13.09

2. BARE SOIL REFLECTANCE VALUES (DN) IN FOUR LANDSAT WAVEBANDS SAMPLED FROM THE JANUARY 1973 HEDAD SUBSCENE

	MSS 4	MSS 5	MSS 6	MSS 7[1]
	60	89	88	70
	48	75	74	58
	52	76	75	60
	78	92	90	70
	53	66	64	48
	58	87	85	66
	58	83	86	70
	61	88	87	72
	57	84	83	66
	64	89	85	68
	59	84	81	66
	86	105	95	78
	58	66	64	54
	63	85	81	62
	63	91	96	76
	54	65	59	52
	86	96	84	70
	68	82	78	68
	52	76	73	60
	51	75	74	62
MEAN	61.4	82.7	79.7	64.8
STANDARD DEVIATION	10.7	10.4	10.1	7.8

[1] MSS7 DN values have been doubled to correct for smaller dynamic range in this waveband (0-63) compared with dynamic range of 0-127 for MSS 4, 5 and 6 for 1973 pre-EDIPS scene.

3. REFLECTANCE (DN) IN FOUR LANDSAT WAVEBANDS OF A 100 PER CENT COVER OF GREEN VEGETATION SAMPLED FROM THE JUNE 1979 HEDAD SUBSCENE

	MSS 7	MSS 6	MSS 5	MSS 4
	39	39	29	23
	39	40	28	20
	39	37	29	22
	40	54	30	23
	39	47	29	22
	40	54	30	24
	39	54	28	23
	37	49	27	21
	40	51	28	22
	42	51	30	22
	45	49	35	24
	44	41	32	23
	32	43	22	20
	32	50	22	20
	33	47	21	19
	36	48	21	17
	35	51	23	20
	35	49	25	20
MEAN	38.10	47.44	27.17	20.28
STANDARD DEVIATION	3.74	5.3	4.00	5.39

4. REFLECTANCE (DN) IN FOUR LANDSAT WAVEBANDS OF A 100 PER CENT COVER OF NON-GREEN VEGETATION SAMPLED FROM THE JUNE 1979 HEDAD SUBSCENE

	MSS 7	MSS 6	MSS 5	MSS 5
	28	32	27	21
	29	32	30	21
	26	37	26	20
	28	33	27	20
	28	34	30	20
	27	37	28	20
	27	32	26	19
	27	31	27	20
	25	32	27	19
	25	33	25	20
	26	33	30	33
	30	38	31	20
	33	41	36	22
	23	27	20	17
	25	30	23	18
	27	31	31	20
	23	29	23	16
	23	29	22	18
	26	29	28	18
	32	42	36	23
MEAN	26.9	33.1	27.65	19.25
STANDARD DEVIATION	2.71	4.02	4.14	5.67

APPENDIX F

SCATTER PLOTS

CONTAINS PULLOUTS

KEY

△	BARE SOIL
▽	PERCENT COVER 0-20
+	PERCENT COVER 20-40
X	PERCENT COVER 40-60
□	PERCENT COVER 60-80
◇	PERCENT COVER >80
O	LAVA

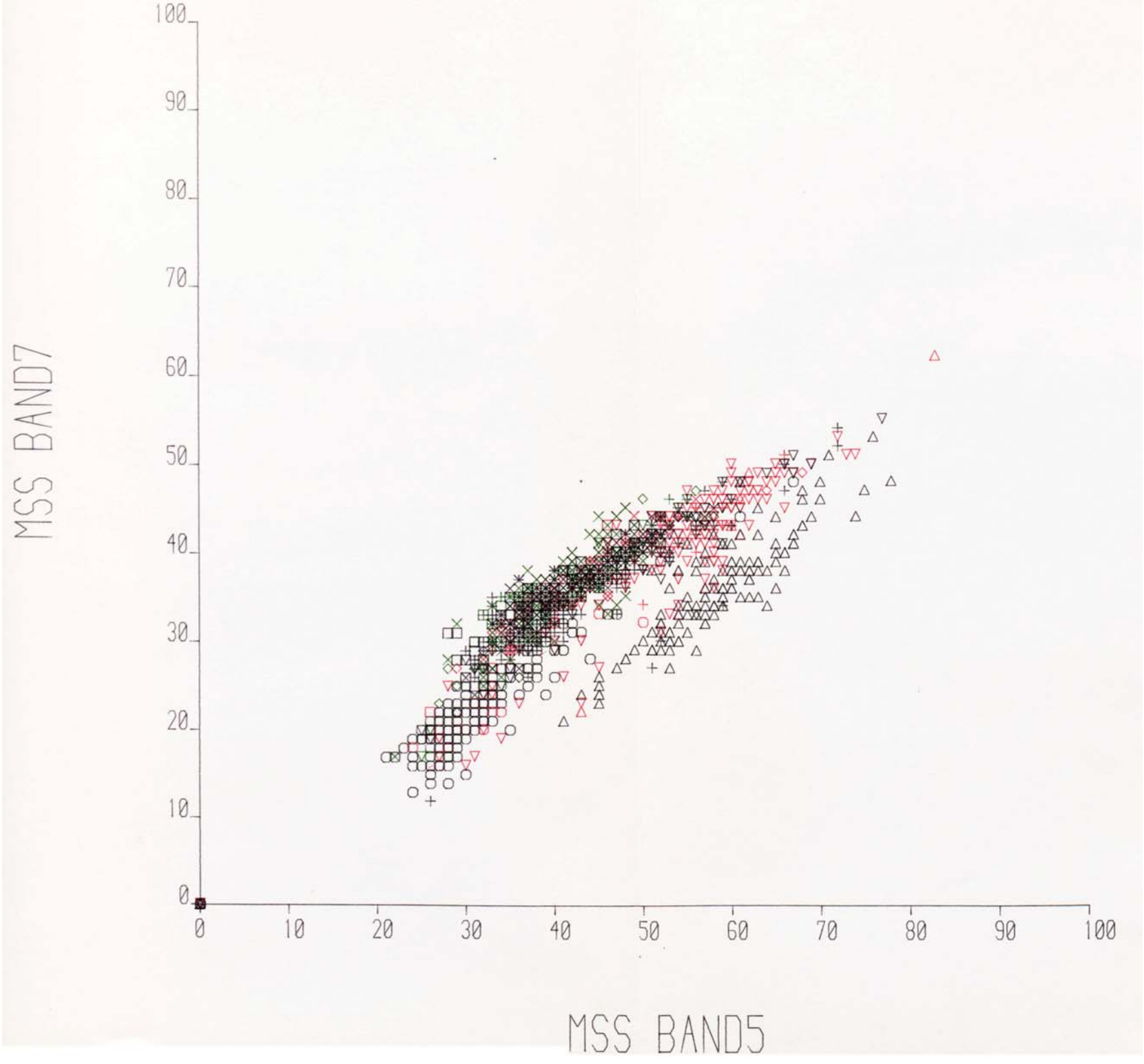
MSS BAND7
MSS BAND5
0
10
20
30
40
50
60
70
80
90
100

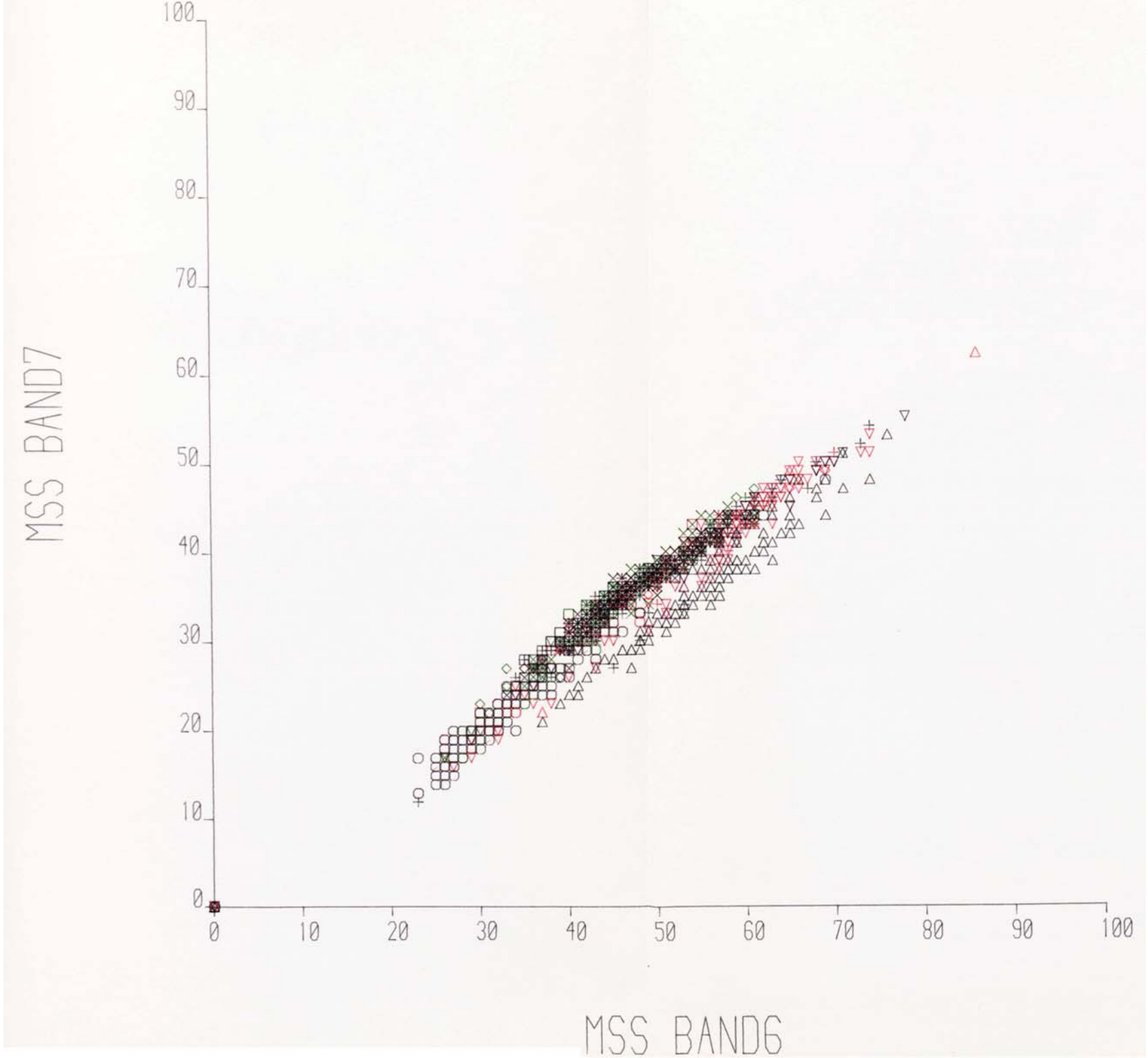
MSS BAND7
MSS BAND6
0
10
20
30
40
50
60
70
80
90
100

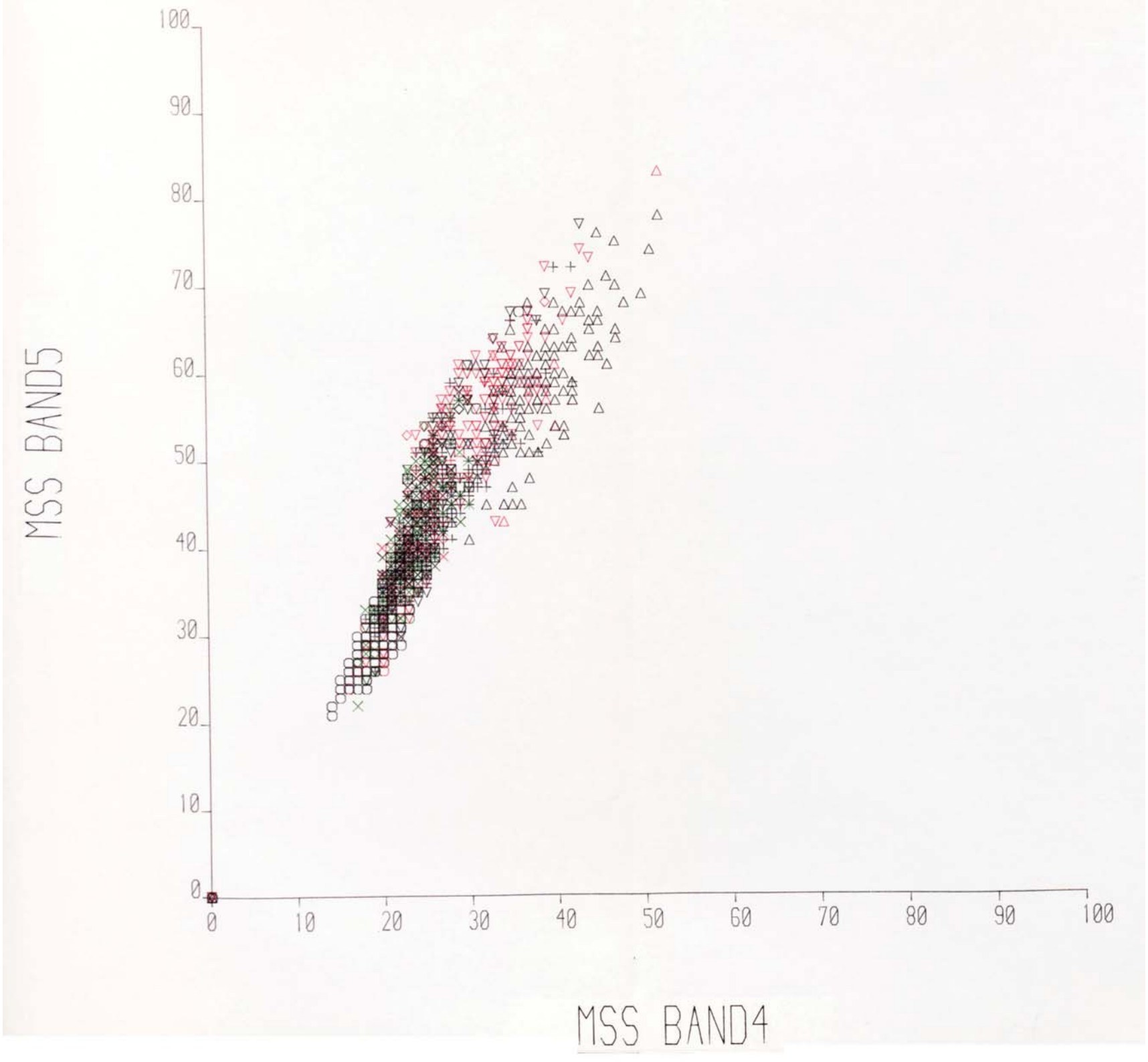
MSS BAND5
MSS BAND4
0
10
20
30
40
50
60
70
80
90
100

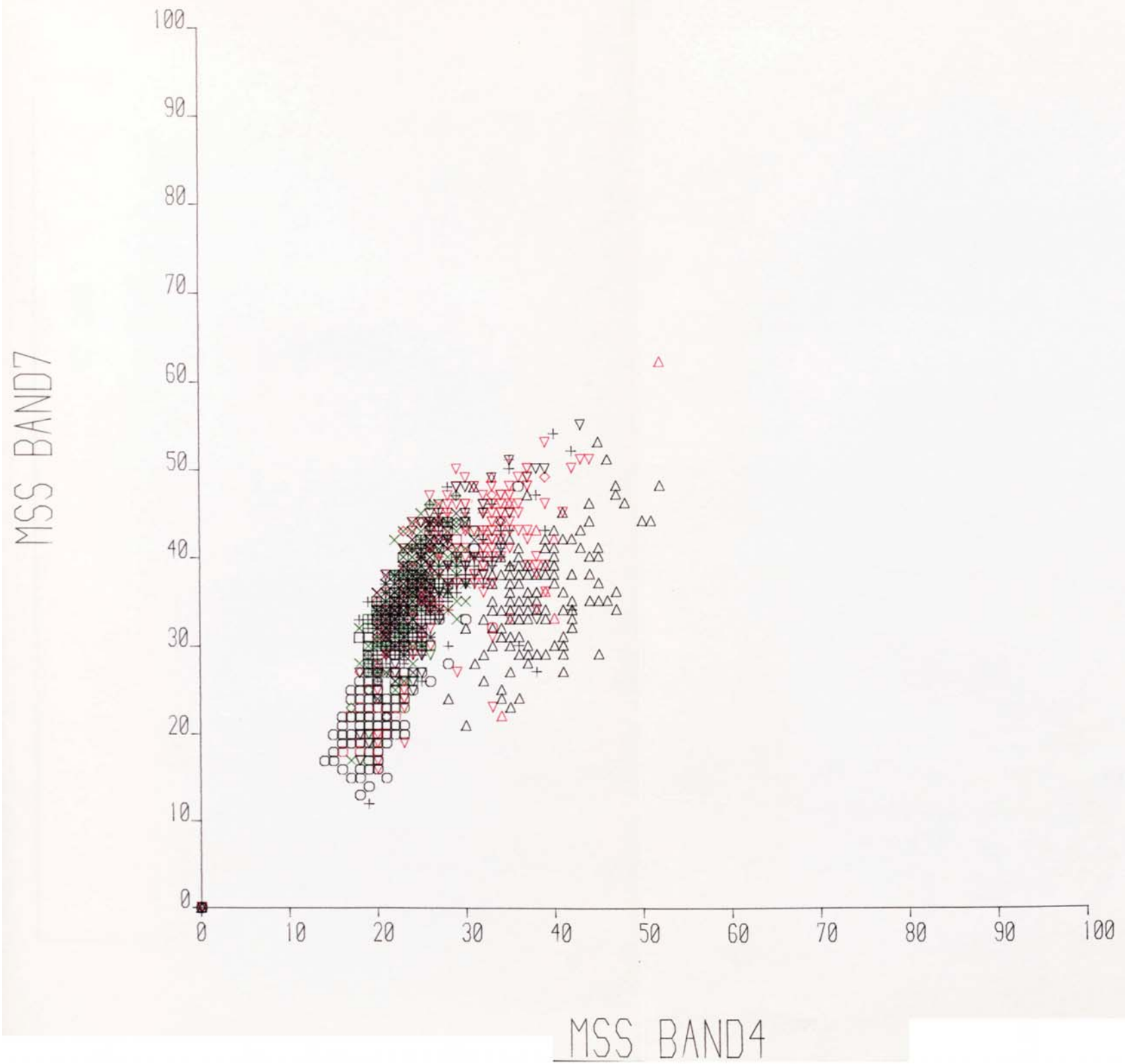
MSS BAND7
100
90
80
70
60
50
40
30
20
10
0
0
10
20
30
40
50
60
70
80
90
100
MSS BAND4

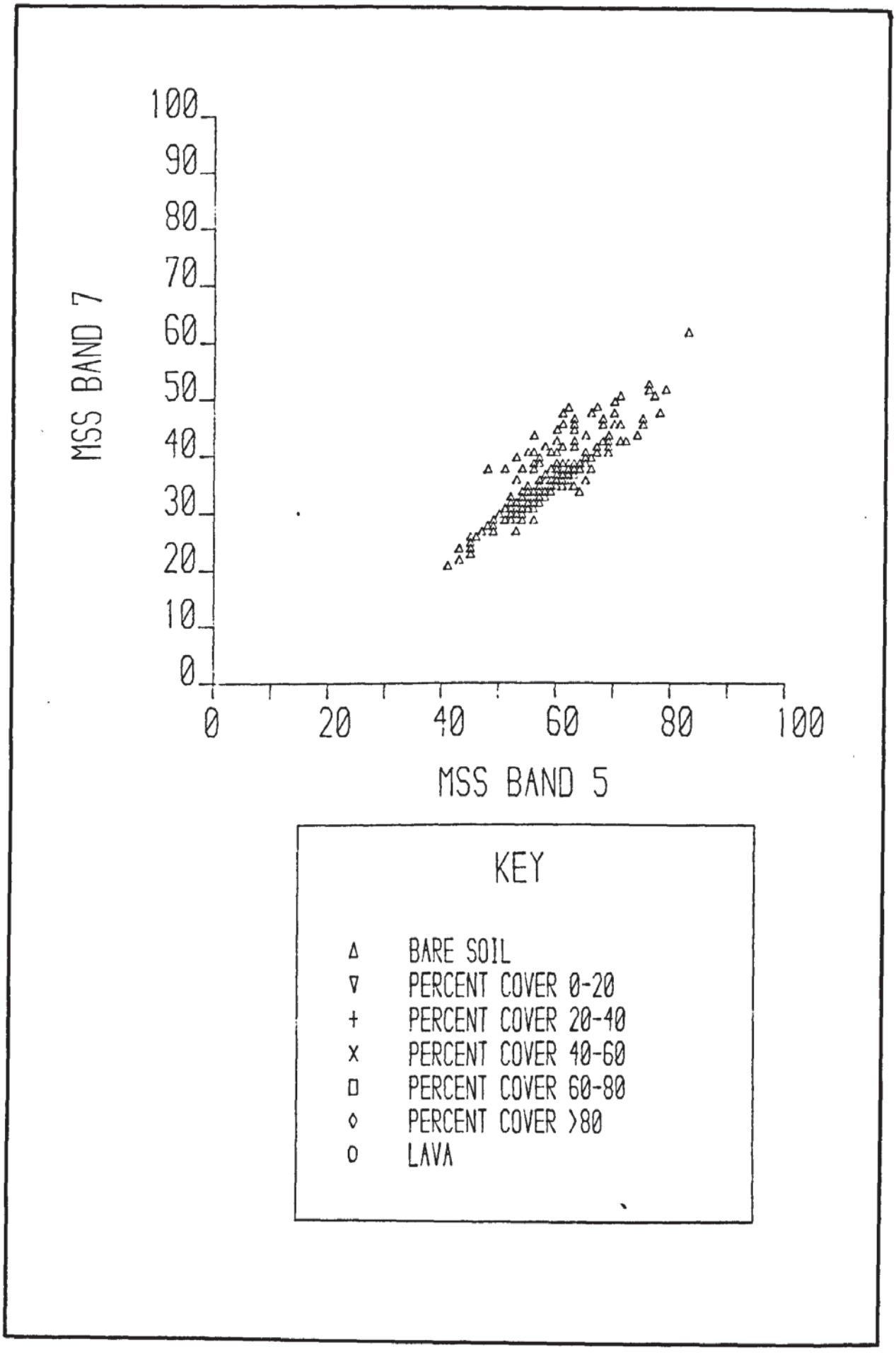
MSS BAND 7
100
90
80
70
60
50
40
30
20
10
0
0
20
40
60
80
100
MSS BAND 5
KEY
BARE SOIL
PERCENT COVER 0-20
PERCENT COVER 20-40
PERCENT COVER 40-60
PERCENT COVER 60-80
PERCENT COVER >80
LAVA

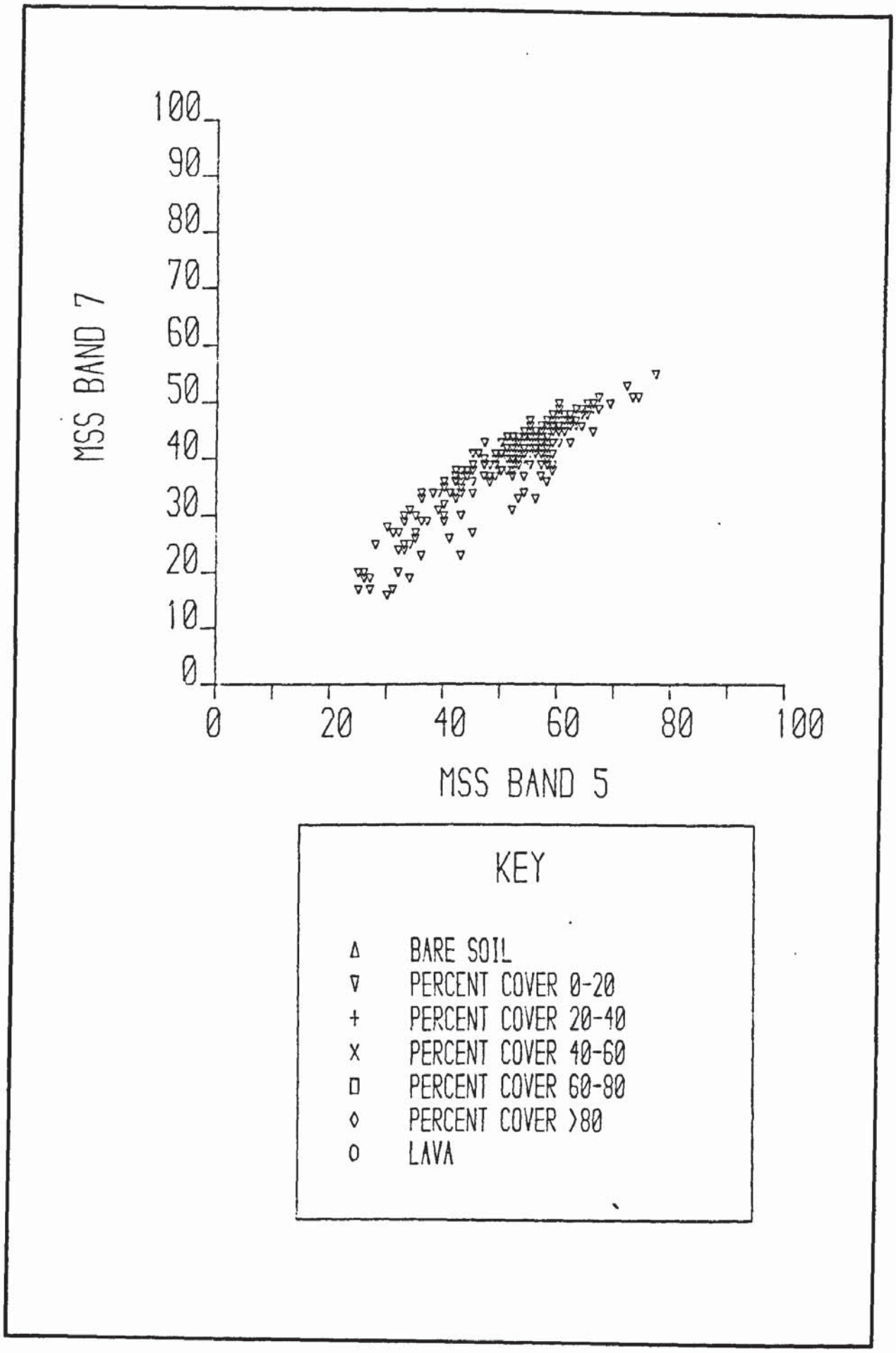
MSS BAND 7
100
90
80
70
60
50
40
30
20
10
0
0
20
40
60
80
100
MSS BAND 5
KEY
BARE SOIL
PERCENT COVER 0-20
PERCENT COVER 20-40
PERCENT COVER 40-60
PERCENT COVER 60-80
PERCENT COVER >80
LAVA

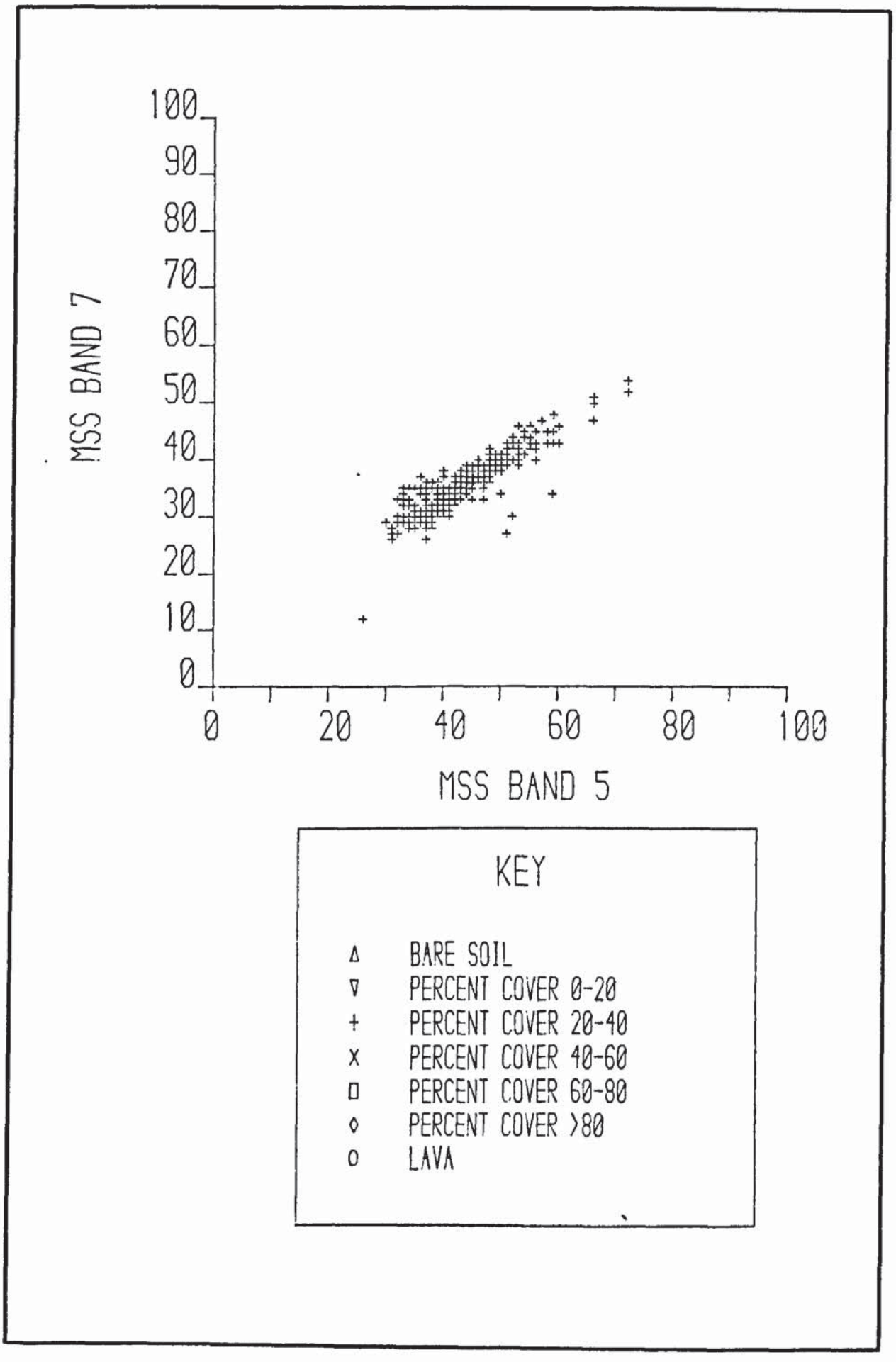
MSS BAND 7
100
90
80
70
60
50
40
30
20
10
0
0
20
40
60
80
100
MSS BAND 5
KEY
BARE SOIL
PERCENT COVER 0-20
PERCENT COVER 20-40
PERCENT COVER 40-60
PERCENT COVER 60-80
PERCENT COVER >80
LAVA

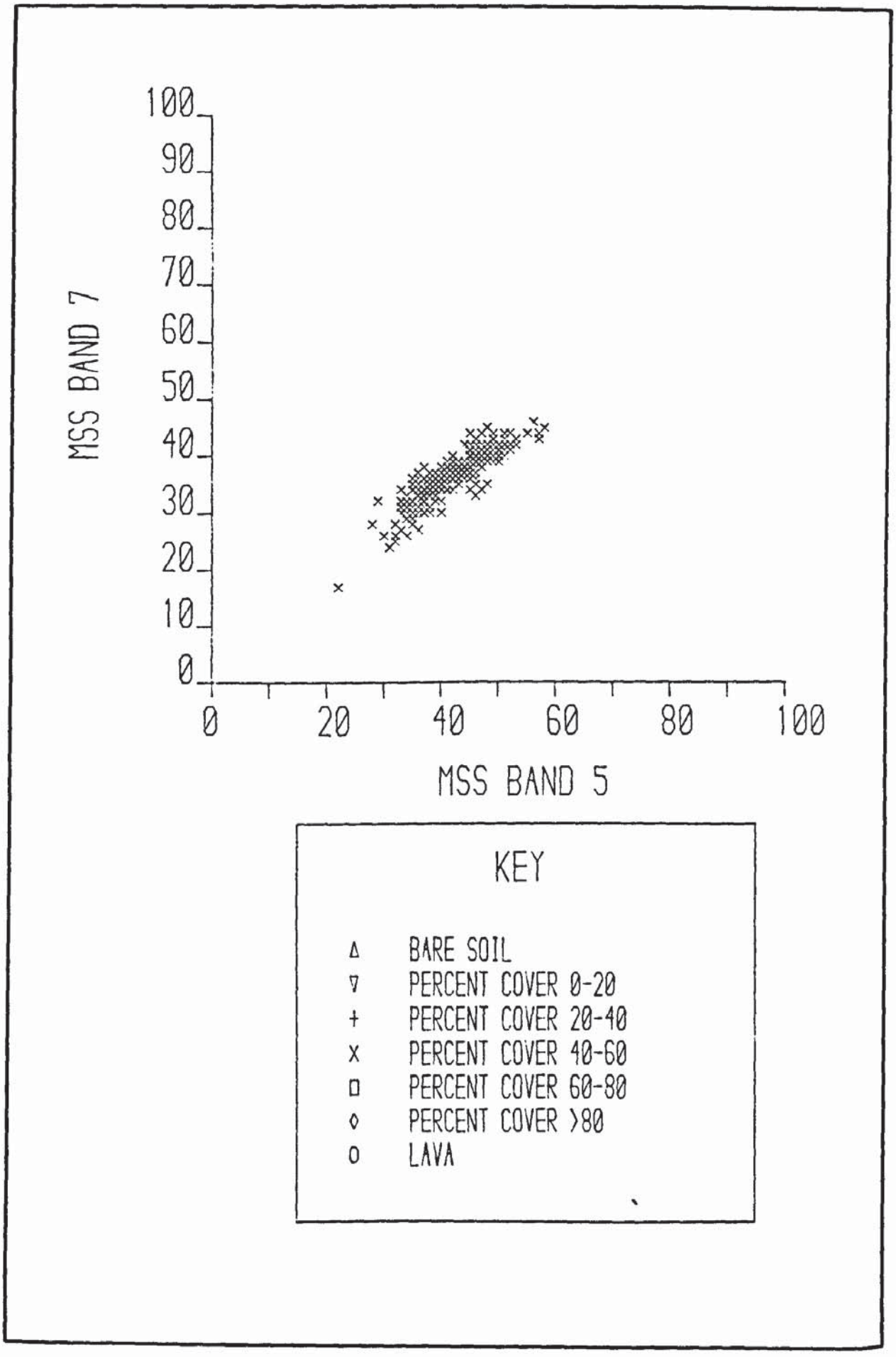
MSS BAND 7
100
90
80
70
60
50
40
30
20
10
0
0
20
40
60
80
100
MSS BAND 5
KEY
BARE SOIL
PERCENT COVER 0-20
PERCENT COVER 20-40
PERCENT COVER 40-60
PERCENT COVER 60-80
PERCENT COVER >80
LAVA

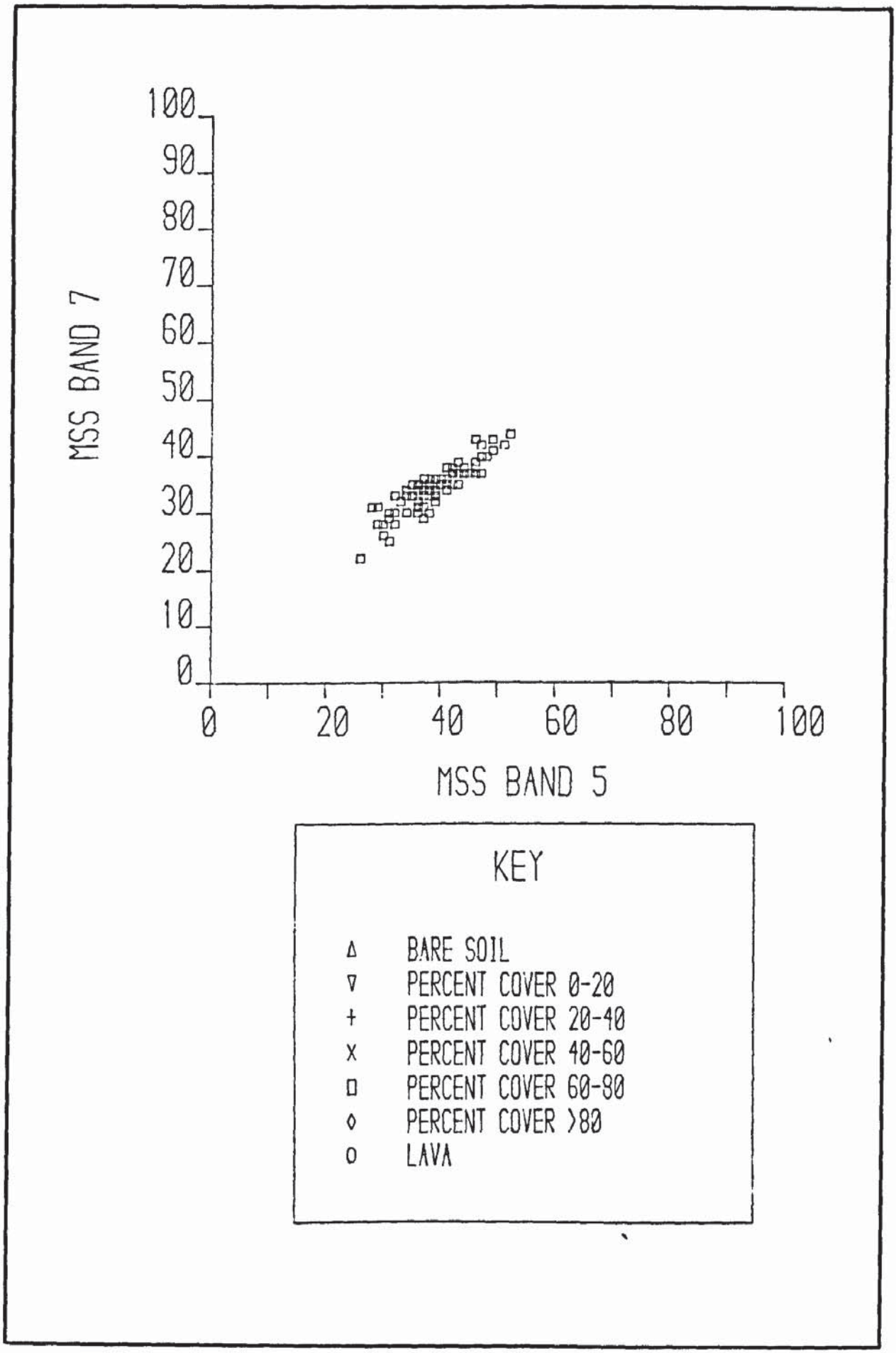
MSS BAND 7
100
90
80
70
60
50
40
30
20
10
0
0
20
40
60
80
100
MSS BAND 5
KEY
BARE SOIL
PERCENT COVER 0-20
PERCENT COVER 20-40
PERCENT COVER 40-60
PERCENT COVER 60-80
PERCENT COVER >80
LAVA

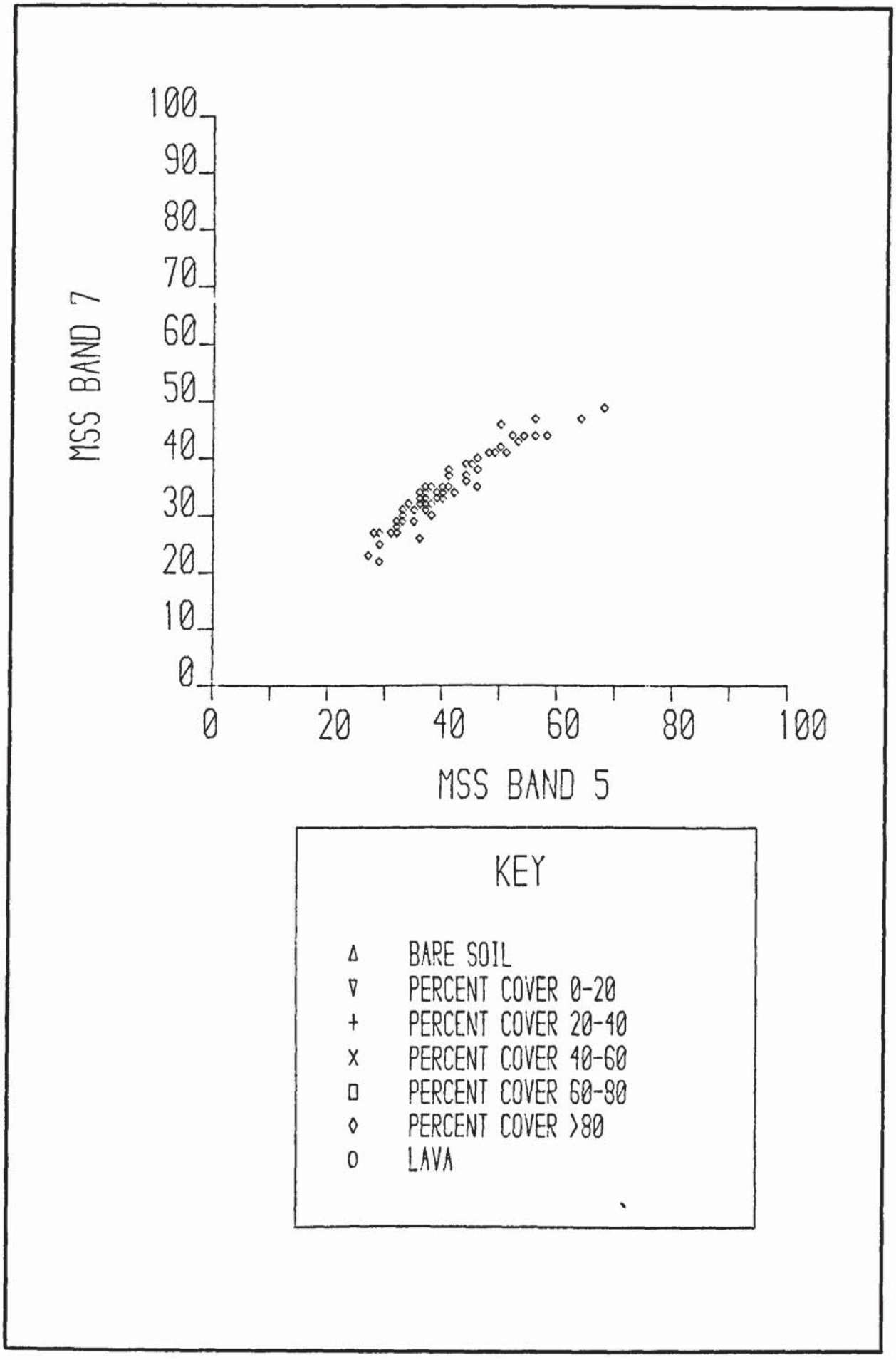
MSS BAND 7
100
90
80
70
60
50
40
30
20
10
0
0
20
40
60
80
100
MSS BAND 5
KEY
BARE SOIL
PERCENT COVER 0-20
PERCENT COVER 20-40
PERCENT COVER 40-60
PERCENT COVER 60-80
PERCENT COVER >80
LAVA

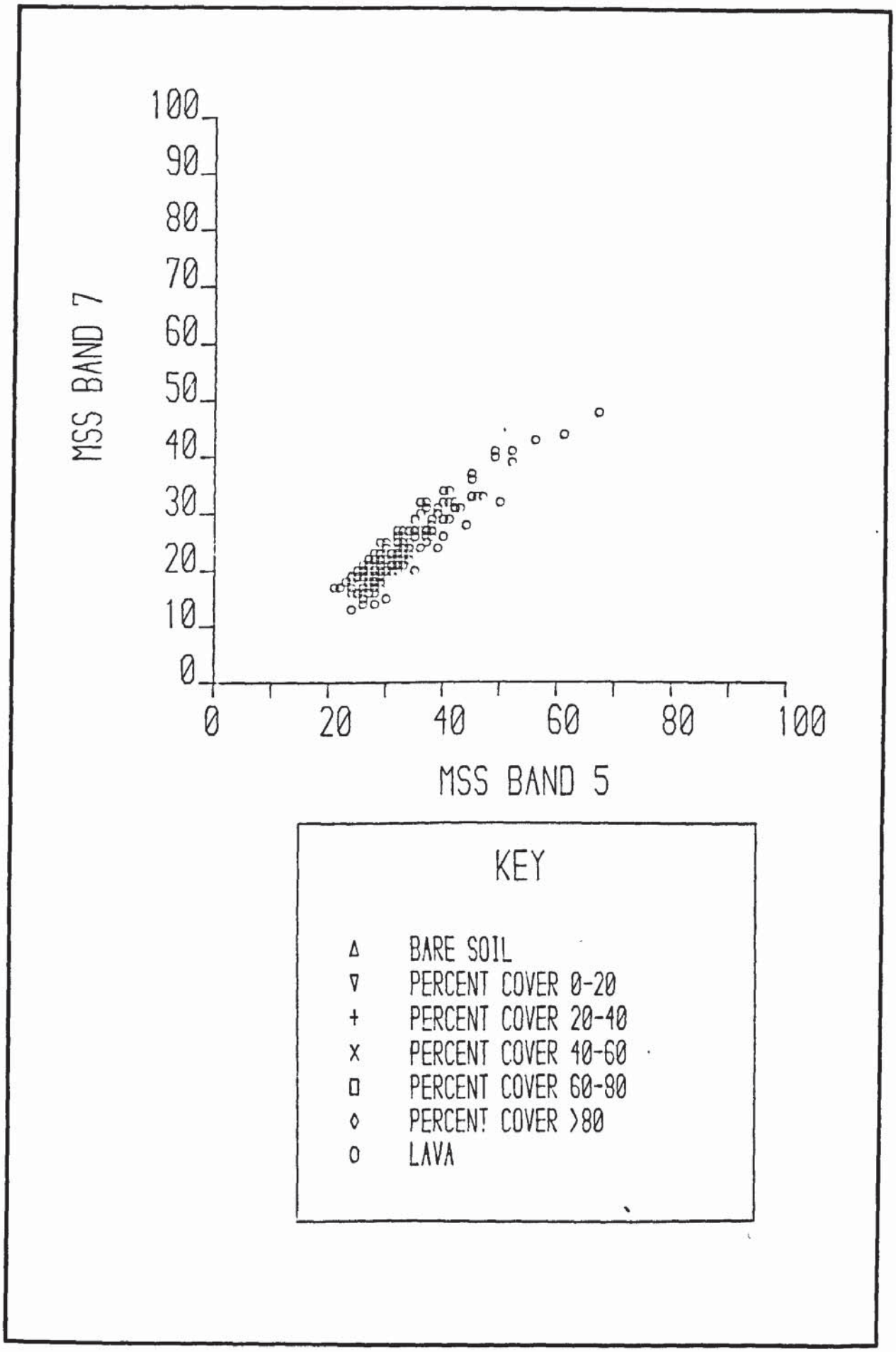
MSS BAND 7
100
90
80
70
60
50
40
30
20
10
0
0
20
40
60
80
100
MSS BAND 5
KEY
BARE SOIL
PERCENT COVER 0-20
PERCENT COVER 20-40
PERCENT COVER 40-60
PERCENT COVER 60-80
PERCENT COVER >80
LAVA

APPENDIX G

ARRAY OF SOIL AND VEGETATION CLASS CODES

ARRAY OF SOIL AND VEGETATION CLASS CODES

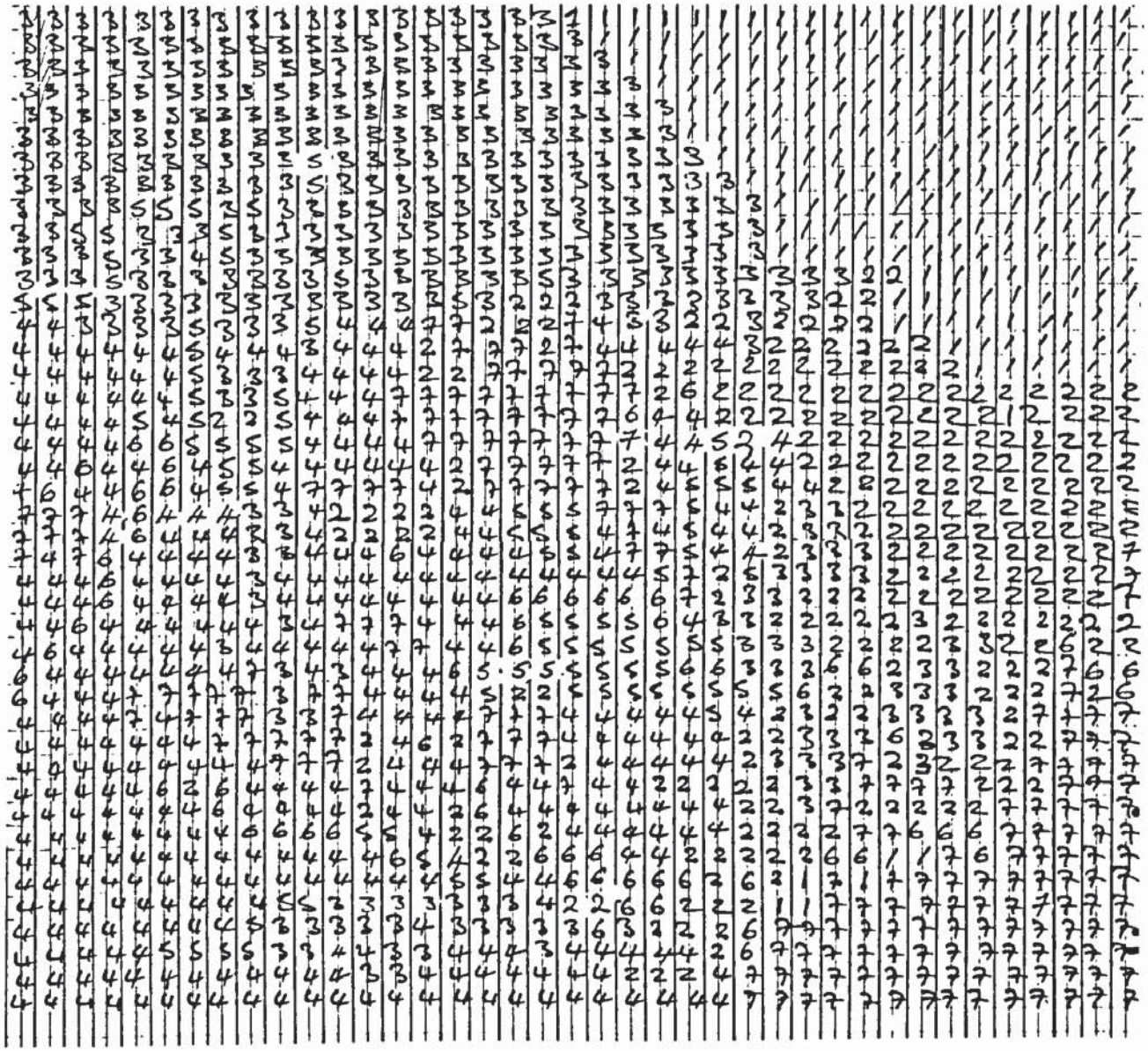

Each sample was coded with a class number as follows:

Soil and Vegetation Class	Class Number
Bare soil	1
0 - 20 per cent vegetation cover	2
20 - 40 per cent vegetation cover	3
40 - 60 per cent vegetation cover	4
60 - 80 per cent vegetation cover	5
> 80 per cent vegetation cover	6
Lava outcrop	7

APPENDIX H

COMPUTER PROGRAMS

1. PROGRAM TO PLOT SOIL DATA IN LANDSAT FEATURE SPACE

```
C       KARGI79 SOIL POINTS PLOT
C       SPLT7975
        COMMON/GINO12/IREAD, IPLT
        INTEGER X
        REAL A(40), B(40), C(40), D(40)
        DO 10 I=1, 40
        READ(12, 20) A(I), B(I), C(I), D(I)
 10     CONTINUE
        WRITE(10, 50)
        READ(10, 40)X
 40     FORMAT(I1)
 50     FORMAT(' INPUT SYMBOL')
 20     FORMAT(4F5. 1)
        CALL GINO
        IF(IPLT. EQ. 1) CALL UNITS(0. 5)
        CALL SHIFT2(50. 0, 50. 0)
        CALL AXIPOS(0, 0. 0, 0. 0, 100. 0, 1)
        CALL AXIPOS(0, 0 0, 0. 0, 100. 0, 2)
        CALL AXISCA(3, 10, 0. 0, 100. 0, 1)
        CALL AXISCA(3, 10, 0. 0, 100. 0, 2)
        CALL AXIDRA(1, 1, 1)
        CALL AXIDRA(-1, -1, 2)
C       LABEL AXES
        CALL CHASIZ(3. 0, 5 0)
        CALL MOVTO2(40. 0, -20. 0)
        CALL CHAHOL(12HMSS BAND 5*. )
        CALL MOVTO2(-20. 0, 40. 0)
        CALL CHAANG(90. 0)
        CALL CHAHOL(12HMSS BAND 7*. )
        CALL CHAANG(0. 0)
        CALL CHASIZ(4. 0, 4. 0)
C       DRAW SOIL PLOT
        DO 30 I=1, 40
        CALL GRAMOV(B(I), D(I))
        CALL SYMBOL(X)
30      CONTINUE
C       DRAW REGRESSION LINE
        CALL MOVTO2(2. 87, 0. 0)
        CALL LINTO2(100. 0, 72. 84)
C       DRAW UPPER S. E.
        CALL DASHED(1, 10. 0, 3. 0, 2. 0)
        CALL MOVTO2(0. 0, 1. 81)
        CALL LINTO2(100. 0, 76. 79)
C       DRAW LOWER S E.
        CALL MOVTO2(8 17, 0. 0)
        CALL LINTO2(100 0, 68. 89)
C       LABEL GRAPH
        CALL CHASIZ(2. 0, 4. 0)
        CALL MOVTO2(20. 0, 80. 0)
        CALL CHAHOL(26H1979 MSS7vMSS5 SOIL PLOT*. )
        CALL MOVTO2(20 0, 74. 0)
        CALL CHAHOL(25HSOIL LINE Y=-2. 16+0. 75X*. )
        CALL MOVTO2(20. 0, 68. 0)
        CALL CHAHOL(13H1 S. E. =3. 95*. )
        CALL DEVEND
        STOP
        END
```

2. PROGRAM TO PLOT SOIL AND VEGETATION DATA IN LANDSAT FEATURE SPACE

```
C.      KARGI7S GROUUND DATA SCATTERPLOTS
C       COVEG75
        COMMON/GINO12/IREAD, IPLT
        INTEGER X, Y, Z, P, C
        DIMENSION X(39, 43), Y(39, 43), Z(39, 43)
        DO  10  I=1, 43
        READ (12, 20) (X(I, J), J=1, 39)
        READ (14, 20) (Y(I, J), J=1, 39)
        READ (16, 40) (Z(I, J), J=1, 39)
 10     CONTINUE
 20     FORMAT (39I3)
 40     FORMAT (39I2)
        CALL  GINO
        IF(IPLT. EQ. 4)CALL UNITS(2. 0)
        CALL SHIFT2(150. 0, 150. 0)
        CALL AXIPOS(0, 0. 0, 0. 0, 120. 0, 1)
        CALL AXIPOS(0, 0 0, 0. 0, 120. 0, 2)
        CALL AXISCA(3, 10, 0. 0, 100. 0, 1)
        CALL AXISCA(3, 10, 0. 0, 100. 0, 2)
        CALL AXIDRA(1, 1, 1)
        CALL AXIDRA(-1, -1, 2)
C       LABEL AXES
        CALL CHASIZ(3. 0, 5. 0)
        CALL MOVTO2(50. 0, -20. 0)
        CALL CHAHOL (11HMSS BAND5*. )
        CALL MOVTO2(-20. 0, 50. 0)
        CALL CHAANG(90. 0)
        CALL CHAHOL (11HMSS BAND7*. )
        CALL CHAANG(0. 0)
        CALL CHASIZ(2. 0, 2. 0)
        DO 30 J=1, 39
        DO 30 I=1, 43
        IF(Z(J, I). EQ. 1)C=1
        IF(Z(J, I). EQ. 2)C=2
        IF(Z(J, I). EQ. 3)C=5
        IF(Z(J, I). EQ. 4)C=7
        IF(Z(J, I). EQ. 5)C=1
        IF(Z(J, I). EQ 6)C=2
        IF(Z(J, I). EQ. 7)C=5
        IF(Z(J, I). EQ. 1)P=1
        IF(Z(J, 1). EQ 2)P=2
        IF(Z(J, I). EQ. 3)P=3
        IF(Z(J, I). EQ. 4)P=4
        IF(Z(J, I) EQ. 5)P=5
        IF(Z(J, I). EQ. 6)P=6
        IF(Z(J, I). EQ. 7)P=7
        X1=FLOAT(X(J, I))
        Y1=FLOAT(Y(J, I))
        CALL  GRAMOV(X1, Y1)
        CALL SYMBOL(P)
        CALL PENSEL (C, 0. 0, 0)
 30     CONTINUE
        CALL SHIFT2(15 0, -95 0)
        CALL MOVTO2(0. 0, 0. 0)
        CALL LINTO2(0. 0, 70. 0)
        CALL LINTO2(80 0, 70. 0)
        CALL LINTO2(80 0, 0. 0)
        CALL LINTO2(0. 0, 0 00)
        CALL MOVTO2(35. 0, 60 0)
        CALL CHASIZ(3. 0, 5. 0)
        CALL CHAHOL(5HKEY*. )
        CALL CHASIZ(2 0, 4. 0)
        CALL MOVTO2(10. 0, 48. 0)
        CALL  PENSEL(1, 0. 0, 0)
        CALL SYMBOL (1)
        CALL MOVTO2(20. 0, 46. 0)
        CALL CHAHOL(11HBARE SOIL*. )
        CALL MOVTO2(10. 0, 42. 0)
        CALL PENSEL(2, 0. 0, 0)
        CALL SYMBOL(2)
        CALL MOVTO2(20 0, 40. 0)
        CALL CHAHOL(20HPERCENT COVER 0-20*. )
        CALL MOVTO2(10. 0, 36. 0)
        CALL PENSEL(5, 0. 0, 0)
        CALL SYMBOL(3)
        CALL MOVTO2(20. 0, 34. 0)
        CALL CHAHOL(21HPERCENT COVER 20-40*. )
        CALL MOVTO2(10. 0, 30. 0)
        CALL PENSEL(7, 0. 0, 0)
        CALL SYMBOL(4)
        CALL MOVTO2(20. 0, 28. 0)
        CALL CHAHOL(21HPERCENT COVER 40-60*. )
        CALL MOVTO2(10. 0, 24. 0)
        CALL PENSEL(1, 0. 0, 0)
        CALL SYMBOL(5)
        CALL MOVTO2(20. 0, 22. 0)
        CALL CHAHOL(21HPERCENT COVER 60-80*. )
        CALL MOVTO2(10. 0, 18. 0)
        CALL PENSEL(2, 0. 0, 0)
        CALL SYMBOL(6)
        CALL MOVTO2(20. 0, 16. 0)
        CALL CHAHOL(19HPERCENT COVER >80*. )
        CALL MOVTO2(10. 0, 12. 0)
        CALL PENSEL(5, 0. 0, 0)
        CALL SYMBOL(7)
        CALL MOVTO2(20 0, 10. 0)
        CALL CHAHOL(6HLAVA*. )
        CALL DEVEND
        STOP
        END
```

3. PROGRAM TO PLOT SOIL AND VEGETATION DATA IN THREE-COMPONENT MODEL

```
C       PROGRAMME TO PLOT COVER POINTS IN 3-COMPONENT SYSTEM
C       COMPLOT2
        COMMON/GINO12/IREAD, IPLT
        INTEGER P
        REAL A, B, C, D, E, F, S(88), N(88), G(88), X(88), Y(88)
C       INPUT END-POINT REFLECTANCE #7 DN
        A=52 8
        B=35. 6
        C=39 5
C       INPUT END-POINT REFLECTANCE #5 DN
        D=73. 2
        E=41. 4
        F=36 5
C       READ COVER DATA AND CALCULATE COORDINATE POSITIONS
        DO  10 I=1, 88
        READ(12, 40) S(I), N(I), G(I)
        X(I)=(D*S(I)/100)+(E*N(I)/100)+(F*G(I)/100)
        Y(I)=(A*S(I)/100)+(B*N(I)/100)+(C*G(I)/100)
        WRITE(14, 40) X(I), Y(I), S(I)
 10     CONTINUE
 40     FORMAT(3F5 1)
        CALL GINO
        IF (IPLT EQ 1) CALL UNITS (0. 5)
        CALL SHIFT2(150. 0, 150. 0)
        CALL AXIPOS(0, 0. 0, 0. 0, 120. 0, 1)
        CALL AXIPOS(0, 0. 0, 0. 0, 120. 0, 2)
        CALL AXISCA(3, 10, 30. 0, 70. 0, 1)
        CALL AXISCA(3, 10, 30. 0, 70. 0, 2)
        CALL AXIDRA(1, 1, 1)
        CALL AXIDRA(-1, -1, 2)
C       LABEL AXES
        CALL CHASIZ(3. 0, 5 0)
        CALL MOVTO2(50 0, -20. 0)
        CALL CHAHOL(11HMSS BAND5*. )
        CALL MOVTO2(-20. 0, 50. 0)
        CALL CHAANG(90 0)
        CALL CHAHOL(11HMSS BAND7*. )
        CALL CHAANG(0. 0)
        CALL CHASIZ(2. 0, 2. 0)
        DO 80 I=1, 88
        IF(G(I). LT. 20)P=1
        IF(G(I). EQ. 20. AND. G(I). LT. 40)P=2
        IF(G(I). EQ 40. AND. G(I). LT. 60)P=3
        IF(G(I). GE. 60)P=4
        CALL GRAMOV(X(I), Y(I))
        CALL SYMBOL(P)
 80     CONTINUE
        CALL SHIFT2(15. 0, -90. 0)
        CALL MOVTO2(0. 0, 0. 0)
        CALL LINTO2(0. 0, 60. 0)
        CALL LINTO2(80. 0, 60. 0)
        CALL LINTO2(80 0, 0. 0)
        CALL LINTO2(0. 0, 0. 0)
        CALL MOVTO2(35. 0, 50 0)
        CALL CHASIZ(3. 0, 5. 0)
        CALL CHAHOL.(5HKEY*. )
        CALL CHASIZ(2. 0, 4. 0)
        CALL MOVTO2(10. 0, 40. 0)
        CALL SYMBOL(1)
        CALL MOVTO2(20 0, 38. 0)
        CALL CHAHOL(18HGREEN COVER 0-20*. )
        CALL MOVTO2(10 0, 32. 0)
        CALL SYMBOL(2)
        CALL MOVTO2(20. 0, 30. 0)
        CALL CHAHOL(19HGREEN COVER 20-40*. )
        CALL MOVTO2(10. 0, 24. 0)
        CALL SYMBOL(3)
        CALL MOVTO2(20. 0, 22. 0)
        CALL CHAHOL(19HGREEN COVER 40-60*. )
        CALL MOVTO2(10 0, 16. 0)
        CALL SYMBOL(4)
        CALL MOVTO2(20. 0, 14. 0)
        CALL CHAHOL(17HGREEN COVER >60*. )
        CALL DEVEND
        STOP
        END
```

4. PROGRAM TO CALCULATE BRIGHTNESS AND GREENNESS COEFFICIENTS

```
10 REM Programme to calculate brightness/greenness coefficients
20 DEFINT I-N
30 DIM IBAND(10),IBRIGHT(10),IDARK(10),IGREEN(10),B(10),V(10),G(10),D(10),ID(10)
40 PRINT "Brightness coefficients"
50 INPUT "How many bands",NBAND
60 PRINT "Specify bands"
70 FOR I=1 TO NBAND
80     PRINT "BAND
90    PRINT "Band no.",I
100    INPUT IBAND(I)
110 NEXT I
120 PRINT "Now input values for bright soil point"
130 FOR I=1 TO NBAND
140    IB=IBAND(I)
150     PRINT "Band no.",IB
160     INPUT IBRIGHT(I)
170 NEXT I
180 PRINT "Input values for dark soil point"
190 FOR I=1 TO NBAND
200    IB=IBAND(I)
210     PRINT "Band no.",IB
220     INPUT IDARK(I)
230 NEXT I
240 PRINT "Input values for green vegetation point"
250 FOR I=1 TO NBAND
260    IB=IBAND(I)
270     PRINT "Band no.",IB
280     INPUT IGREEN(I)
290 NEXT I
300 SUMSQ=0
310 FOR I=1 TO NBAND
320     B(I)=IBRIGHT(I)-IDARK(I)
330     SUMSQ=SUMSQ+B(I)*B(I)
340 NEXT I
350 BIGB=SQR(SUMSQ)
360 LPRINT "Brightness coefficients"
370 FOR I=1 TO NBAND
380     B(I)=B(I)/BIGB
385 LPRINT "Band",IBAND(I),B(I)
390 NEXT I
400 PRINT "Calculate greenness coefficients"
410 FOR I=1 TO NBAND
420     V(I)=IGREEN(I)-IDARK(I)
430 NEXT I
440 D=0
450 FOR I=1 TO NBAND
460     ID(I)=V(I)*B(I)
470     D=D+ID(I)
480 NEXT I
490 SUMSQ1=0
500 FOR I=1 TO NBAND
510     G(I)=V(I)-(D*B(I))
520     SUMSQ1=SUMSQ1+G(I)*G(I)
530 NEXT I
540 BIGG=SQR(SUMSQ1)
550 LPRINT
560 LPRINT
570 LPRINT "Greenness coefficients"
580 FOR I=1 TO NBAND
590     G(I)=G(I)/BIGG
600 LPRINT "Band",IBAND(I),G(I)
610 NEXT I
620 END
```

APPENDIX I

CALCULATION OF VEGETATION INDEX

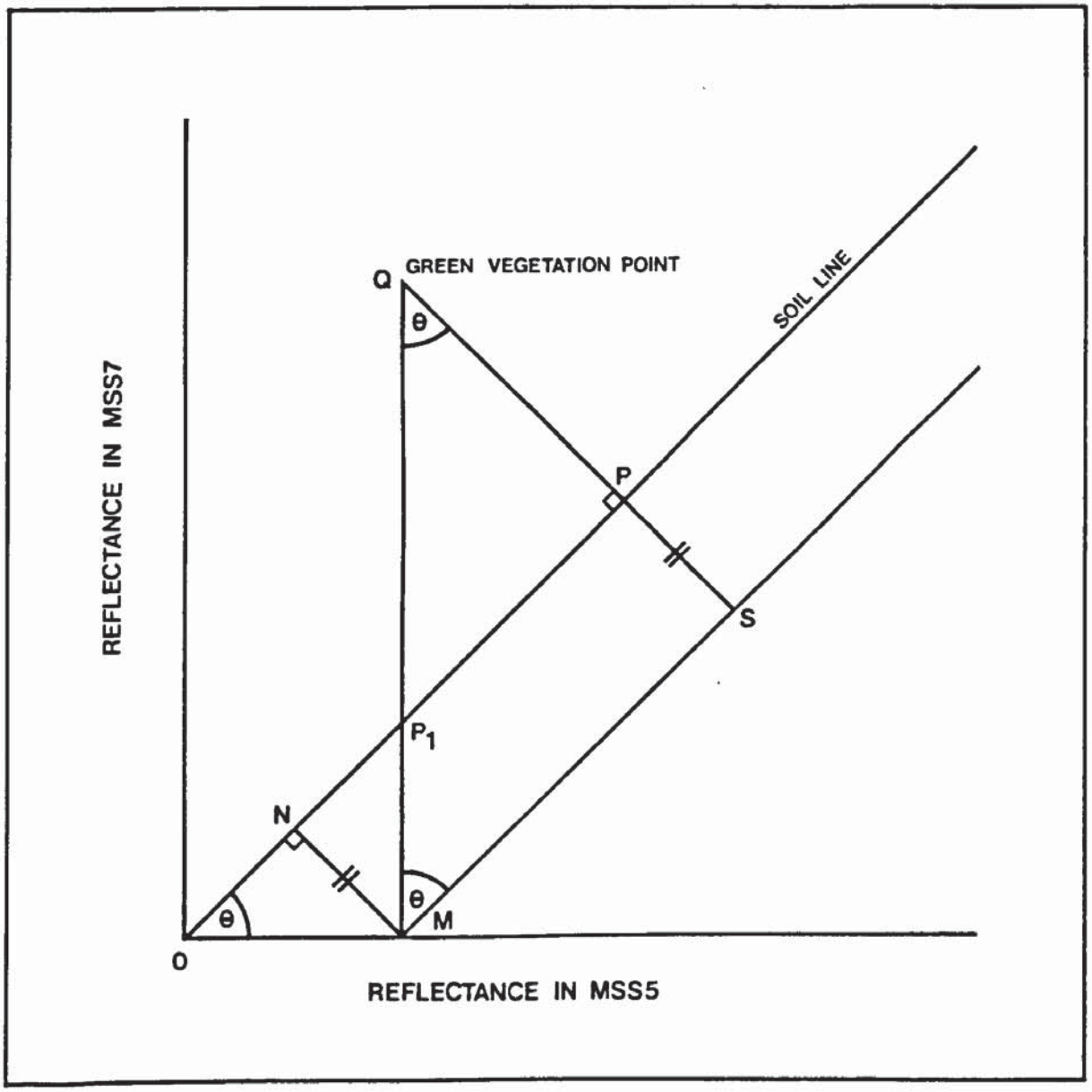

QM = MSS7
OM = MSS5

1) Perpendicular distance from soil line to green vegetation point (QP)

$QS = QM \cos\theta$
$NM = OM \sin\theta$
$NM = PS$
$QP = QS - PS$ (perpendicular distance)

$\therefore \quad QP = QM \cos\theta - OM \sin\theta$

$\therefore$ Perpendicular vegetation index (PVI) = $MSS7 \cos\theta - MSS5 \sin\theta$

2) Cover line index (O, P_1)

$OM = MSS5 \cos\theta$
$NP_1 = MSS7 \sin\theta$

$\therefore \quad OP_1 = OM \cos\theta + NP_1 \sin\theta$

$\therefore$ Cover line index = $MSS5 \cos\theta + MSS7 \sin\theta$